HW-77609

727765

R

HANFORD RADIOLOGICAL SCIENCES RESEARCH AND DEVELOPMENT ANNUAL REPORT FOR 1962

STAFF MEMBERS
OF PHYSICS AND INSTRUMENTS LABORATORY
CHEMICAL LABORATORY
JANUARY THROUGH DECEMBER 1962
EDITED BY
C. C. GAMERTSFELDER AND J. K. GREEN

JANUARY 1963

HANFORD LABORATORIES

HANFORD ATOMIC PRODUCTS OPERATION
RICHLAND, WASHINGTON

GENERAL ELECTRIC

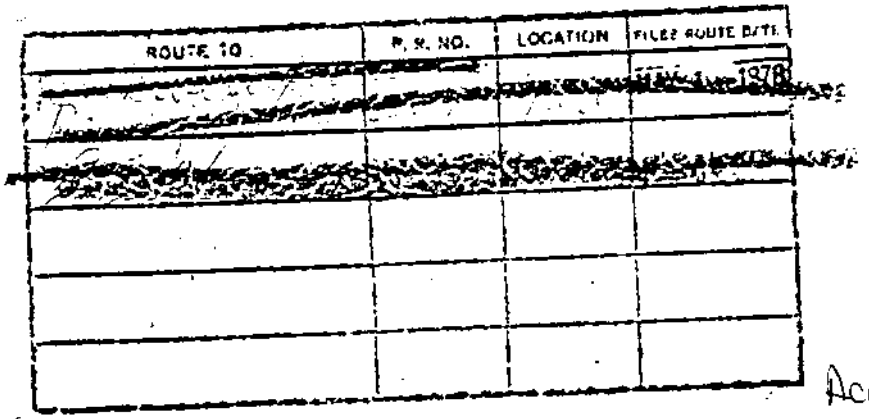

LEGAL NOTICE

This report was prepared as an account of Government sponsored work. Neither the United States, nor the Commission, nor any person acting on behalf of the Commission:

A. Makes any warranty or representation, expressed or implied, with respect to the accuracy, completeness, or usefulness of the information contained in this report, or that the use of any information, apparatus, method, or process disclosed in this report may not infringe privately owned rights; or

B. Assumes any liabilities with respect to the use of, or for damages resulting from the use of any information, apparatus, method, or process disclosed in this report.

As used in the above, "person acting on behalf of the Commission" includes any employee or contractor of the Commission, or employee of such contractor, to the extent that such employee or contractor of the Commission, or employee of such contractor prepares, disseminates, or provides access to, any information pursuant to his employment or contract with the Commission, or his employment with such contractor.

AEC-GE RICHLAND, WASH.

HW-77609

UC-48, Biology and Medicine
(TID-4500, 22nd Ed.)

HANFORD RADIOLOGICAL SCIENCES RESEARCH AND DEVELOPMENT ANNUAL REPORT FOR 1962

By

Staff Members of
Physics and Instruments Laboratory
Chemical Laboratory

Hanford Laboratories

Edited by

C. C. Gamertsfelder and J. K. Green

January through December 1962

HANFORD ATOMIC PRODUCTS OPERATION
RICHLAND, WASHINGTON

Work performed under Contract No. AT(45-1)-1350 between the Atomic Energy Commission and General Electric Company

Printed by/for the U. S. Atomic Energy Commission

Printed in USA. Price $4.00 Available from the

Office of Technical Services
Department of Commerce
Washington 25, D. C.

TABLE OF CONTENTS

TABLE OF CONTENTS (Contd.)

TABLE OF CONTENTS (Contd.)

TABLE OF CONTENTS (Contd.)

TABLE OF CONTENTS (Contd.)

TABLE OF CONTENTS (Contd.)

TABLE OF CONTENTS (Contd.)

TABLE OF CONTENTS (Contd.)

TABLE OF CONTENTS (Contd.)

HANFORD RADIOLOGICAL SCIENCES RESEARCH AND DEVELOPMENT ANNUAL REPORT FOR 1962

ATMOSPHERIC PHYSICS

Atmospheric Diffusion, Deposition, and Transport - C. L. Simpson, C. E. Elderkin, J. J. Fuquay, P. W. Nickola, M. F. Scoggins, and W. T. Hinds

Atmospheric diffusion and transport studies during the past year emphasized both analysis of data collected in 1960 through 1962 and the continuation of field experiments over the Hanford Diffusion grids. Detailed analysis of the "30 Series" tests performed at Hanford in 1960-61 and tests performed with the same experimental technique at Cape Canaveral and Vandenberg Air Force Base in 1961-1962 demonstrated effects of climatic regimes and terrain on diffusion results. It was found that, for both off-site areas, tests performed in the winter, and particularly on winter nights, resulted in the narrowest plumes. The large scale pressure gradients associated with frontal weather control the flow in the wintertime, producing a persistent wind direction, and, consequently, the narrowest plumes. In the summer, the flow was controlled by the small scale sea breeze circulation where local changes and irregularities caused large variations in wind direction, giving the widest plumes observed. At both Cape Canaveral and Vandenberg, the sea breeze prevailed in the summer and frontal weather was dominant in the winter. When the seasonal and diurnal effects were accounted for, plume widths for the two off-site areas were in good agreement and Hanford "30 Series" tests, conducted primarily in the summertime, gave curves of plume widths vs. distance from the source comparing well with the group of off-site summer data.

The effect of terrain was most noticeable at Vandenberg where one diffusion grid was constructed over a hillside-river-valley complex cut by a number of deep gullies. The widest plumes were produced there at night when the summer sea breeze diminished and flow around the terrain features became more pronounced. This situation also resulted in extreme curvature of the plume trajectories. The possibility

of similar terrain and circulation effects on the plume width and trajectories at Hanford was suggested by the off-site results.

The normalized peak exposures for all three test sites show a dominant gross thermal stability dependence. When this stability dependence is accounted for, the results for the three sites show good agreement. The range of stabilities covered by these tests, particularly the Hanford "30 Series", is much broader than that of the previous Hanford Green Glow tests conducted only at night where no obvious stability dependence was noted. The relationship between dosage and stability was more clearly demonstrated through the crosswind integrated dosages calculated for the "30 Series" tests. The effect of lateral diffusion in reducing the dosage was thus removed and a more detailed dependence on stability for each test was shown. The lack of agreement between the crosswind integrated form of Sutton's diffusion model and the experimental values plotted vs. distance is considered to result from deposition on the ground of the diffusing material, which is not accounted for in the mathematical model.

The experimental diffusion program at Hanford continued during the last half of 1962 with a series of ground releases designed to relate diffusion measurements out to 12.8 km to detailed wind structure, terrain, and length of release effects. Two additional ground releases were made over cheat grass fields, continuing the investigations begun in 1961 of the direct measurement of deposition on the surface. Another series of experiments provided the diffusion patterns at the surface, resulting from a continuous release at 185 ft. Dosage measurements were made on 9 arcs extending to a distance of 1600 m from the source. The data from the recent Hanford tests have been reduced and preliminary analyses have been made. More complete analyses will be the subject of future reports.

Research in problems of atmospheric diffusion, transport and deposition has advanced in two areas of interest. First, the data that has been collected during the period 1960-62 at Hanford, Washington; Cape Canaveral, Florida; and Vandenberg Air Force Base, California, have been summarized in considerable detail. This summary points up the differences and similarities between the diffusion at these three testing sites and helps define the factors that cause variations in diffusion results. It is significant that the results from the Air Force sites are very valuable in interpreting the diffusion measurements at the Hanford site. Results from the off-site tests have been particularly

pertinent to Hanford problems in demonstrating the effects of vegetation, terrain, diurnal, and seasonal variations, forming a basis for further analysis of the Hanford data gathered to date and for modification of the Hanford experimental design.

The second area of progress has been the continuation of the experimental field program at Hanford. Emphasis was given to the measurement of ground level dose resulting from a release at 185 ft under a regime of unstable atmospheric conditions in one series of experiments, the horizontal cloud growth from a ground source and its relation to the spectrum of wind directions in a second group of tests, and the measurement of the deposition of particulates over a grass surface to a distance of 200 m in a third group.

Table 1.1 summarizes the 275 experiments that have been completed since 1958 and will be frequently referred to in this report. The Green Glow program was reviewed in the 1960 issue of this report and "30 Series" (Phase I) was the topic of the 1961 report. The combined "30 Series" and the remaining tests listed in Table 1.1 will be discussed in this report.

The "30 Series" was a group of experiments designed to investigate diffusion, transport, and deposition of a plume out to 3200 m from the source of the tracer material released near the ground. This series was an extension of the earlier 1959 test series, utilizing the Hanford fluorescent tracer technology reviewed in the 1960 report and References 1.1 and 1.2. While the Green Glow tests were conducted in only slightly to moderately stable atmospheric conditions, the "30 Series" were obtained over all stabilities from typical nighttime conditions to those found on a summer afternoon. Additional samplers were added to the grid for a more detailed definition of the vertical mass distribution near the ground. The outer two arcs, at 12.8 km and 25.6 km, were not used in the first two phases of the "30 Series" tests, but the 12.8 km arc was reactivated for the

TABLE 1.1

SUMMARY OF EXPERIMENTS

Program Name	Time of Program	Location of Experiments	Number of Experiments
Green Glow	6/18/59 - 9/3/59	Hanford, Wash.	28
"30 Series"			
Phase I	2/8/60 - 10/18/60	Hanford, Wash.	17
Phase II	1/18/61 - 2/28/62	Hanford, Wash.	15
Phase III	7/22/62 - 8/2/62	Hanford, Wash.	9
Ocean Breeze			
Phase I	5/15/61 - 6/18/61	Cape Canaveral, Fla.	23
Phase II	1/11/62 - 2/3/62	Cape Canaveral, Fla.	27
Phase III	3/10/62 - 3/31/62	Cape Canaveral, Fla.	26
Dry Gulch			
Phase I	6/6/61 - 8/3/61	Vandenberg AFB, Cal.	52
Phase II	2/5/62 - 3/30/62	Vandenberg AFB, Cal.	27
Phase III	5/28/62 - 6/30/62	Vandenberg AFB, Cal.	30
Elevated Source			
Phase I	11/18/60 - 11/9/62	Hanford, Wash.	18
Cheat Grass		Hanford, Wash.	3

third phase to investigate the influences of terrain, length of emission, and the relation of the growth of the plume to the variability of the wind. During stable conditions when the plume was contained within the vertical extent of the towers, the deposition on the ground and vegetation was calculated from mass flux considerations. The amount deposited is equivalent to the depletion of the plume determined by integrating the mass of material passing through successive downwind cross-sectional areas. This technique has been described in the 1961 issue of this report and Reference 1.3.

The following description of the Hanford grid and the area over which it extends is essential to understanding the differences in the Hanford and off-site tests, which will be discussed. The detailed description of the Hanford grid has previously been reported and is also found in Reference 1.1. The grid for Phases 1 and 2 of the "30 Series" is located on terrain characterized as gently rolling, which is rather densely covered with vegetation typical of a semiarid region. There are areas within the grid, however, which contain rugged features exhibiting sharp rises and recesses. Although these areas comprise only a small portion of the total grid, off-site studies indicate that the diffusion might very well be affected by the protuberances through the creation of mechanical turbulence or by some systematic deviation from the dominant air flow.

Horizontal and vertical air samples were obtained along arcs at 200, 800, 1600, and 3200 m from the point of emission. Samplers were located 1.5 m above the ground along the arcs and sufficiently spaced to define the cross-section of the plume. In addition to the ground sampling, a network of poles and towers was located at 5 points, 8 degrees apart, on each of the four arcs. Fifteen to eighteen samplers were mounted on each pole or tower, the top level increasing from 27 m on the 200-m arc to 62 m on the 1600- and 3200-m arcs. All samplers were activated before the release of the zinc sulfide tracer from near the ground. The release was continued for 1/2 hr and the samples were removed after the plume had traversed the grid.

A major consideration in the Hanford grid design was the nature of air flow over the region. The orientation of the grid was based on climatological expectancies which show the dominant influence of a mountain-valley wind regime. Northwesterly winds, resulting from differential heating or cooling of the Cascade-Eastern Washington valley complex, prevail over the Hanford area and are markedly different in origin from the land-sea wind regime of the off-site testing areas.

Off-site work was introduced during 1961 and 1962, when the Atmospheric Physics Operation was contracted by the Air Force to perform atmospheric diffusion tests at Cape Canaveral and Vandenberg Air Force Base. The development of advanced missile systems has created a potential pollution problem at these sites from accidental release of toxic fuels. The results of the diffusion experiments along with measurements of average wind speed, average wind direction, and variability of wind direction, and vertical differences of temperature, formed the basis of a computer controlled pollution hazard prediction and display system. The system is to be used by the Air Force at these sites in scheduling missile fueling and launching operations.

The diffusion data collected at Cape Canaveral and Vandenberg are useful in defining the immediate pollution problem at those sites and in demonstrating the influence of terrain, vegetation, and seasonal and diurnal changes in meteorological conditions on diffusion as determined by the Hanford tracer technique. Furthermore, comparisons of the off-site data with the diffusion data collected at Hanford can help clarify these effects as they apply specifically to Hanford and can suggest future experimentation where it is necessary in complete understanding of these influences.

The three locations encompass a wide variety of terrain and vegetation cover. Cape Canaveral is characterized by relatively flat terrain with occasional 20-30 ft sand dunes and bunkers covered primarily by dense palmetto growth about 3 ft high with some areas covered by other tropical vegetation up to 20 ft high.

Extremes in terrain are found at Vandenberg, and required that two diffusion grids be constructed. One diffusion grid, the B course, extended over a broad, very flat mesa on which the airstrip is located. The other diffusion grid, the D course, extended from the edge of the mesa at an elevation of about 300 ft down into the adjoining Santa Inez River valley at sea level and, on one arc, rising again on the other side of the valley, onto Pt. Arguello at an elevation of 350 ft. In addition to the hill-valley complex, the terrain on portions of the D course was very rough with a few deep gullies cutting through the arcs on which the sampling equipment was located. Deep gullies also cut into the edge of the mesa over which the B course extended. The entire area was covered by relatively sparse brush 1 to 4 ft high. In addition, there were a few lines of tall eucalyptus trees across the B diffusion grid. These terrain and vegetation features had a noticeable effect on the diffusion results and will be discussed later.

The testing at Cape Canaveral and Vandenberg was conducted in three phases at each site so that both summer and winter climatic regimes were encountered. In the summertime, at both sites, a strong sea breeze circulation predominated throughout the day and well into the late evening. During the winter tests at both sites, the large scale pressure gradient controlled the flow with a superimposed weak sea breeze having a lesser effect.

The sampling grids at both Cape Canaveral and Vandenberg were oriented to allow testing in the prevalent on-shore sea breeze condition. At Cape Canaveral, the course consisted of 3 arcs concentric about the same source point at radii of 1.21, 2.41, and 4.83 km. The first two arcs covered more than 180 degrees azimuth oriented to test in northerly, easterly, and southeasterly winds. The third arc covered only about 80 degrees of azimuth to be used with the northerly winds occurring frequently only in the winter season.

At Vandenberg, the B grid consisted of two arcs extending over almost 90 degrees of azimuth at 2.30 km and 6.57 km concentric about its source point on the mesa. The D grid consisted of 3 arcs at distances of 0.85 km, 1.50 km, and 4.72 km from the second source point. The first two arcs covered 120 degrees of azimuth and the third arc, 70 degrees of azimuth. Both courses were oriented to catch the prevailing northwesterly winds. The sample spacing at both Cape Canaveral and Vandenberg was from 1 to 2 degrees of azimuth providing a dense network of measurements adequately outlining the crosswind distributions. The samples at Vandenberg were taken at a height of 1.5 m as are the ground samples at Hanford; at Cape Canaveral the primary samples were at a height of 4.6 m to reach above the high dense vegetation that covered part of the diffusion grid. Widely spaced supplementary samples were also included at 1.5 m on the Cape Canaveral grid. Both off-site programs followed Hanford's test procedures and called for a 1/2 hr generation period.

Turning now to the results of the diffusion tests carried out at the three sites described above, the horizontal spread of the plume, characterized by the standard deviation of the crosswind plume distribution as a function of distance, is first considered. The horizontal growth of a plume is influenced by such factors as the variability or gustiness of the wind, the thermal stability, the magnitude of the vertical wind direction shear, and the characteristics of the terrain. These factors produce a wide range of observed plume width results and have been discussed in detail by Pasquill [1.4] and Barad and Fuquay. [1.5] Figure 1.1 shows the Hanford average plume growth for the "30 Series" where the ordinate, σ_y, is the standard deviation of the crosswind dosage distribution. Data from Field Tests 34 and 57 show the variety of results that can be expected. Not only does the magnitude of σ_y at a given distance, x, deviate considerably from the mean, but the rate at which the plume grows can also be affected.

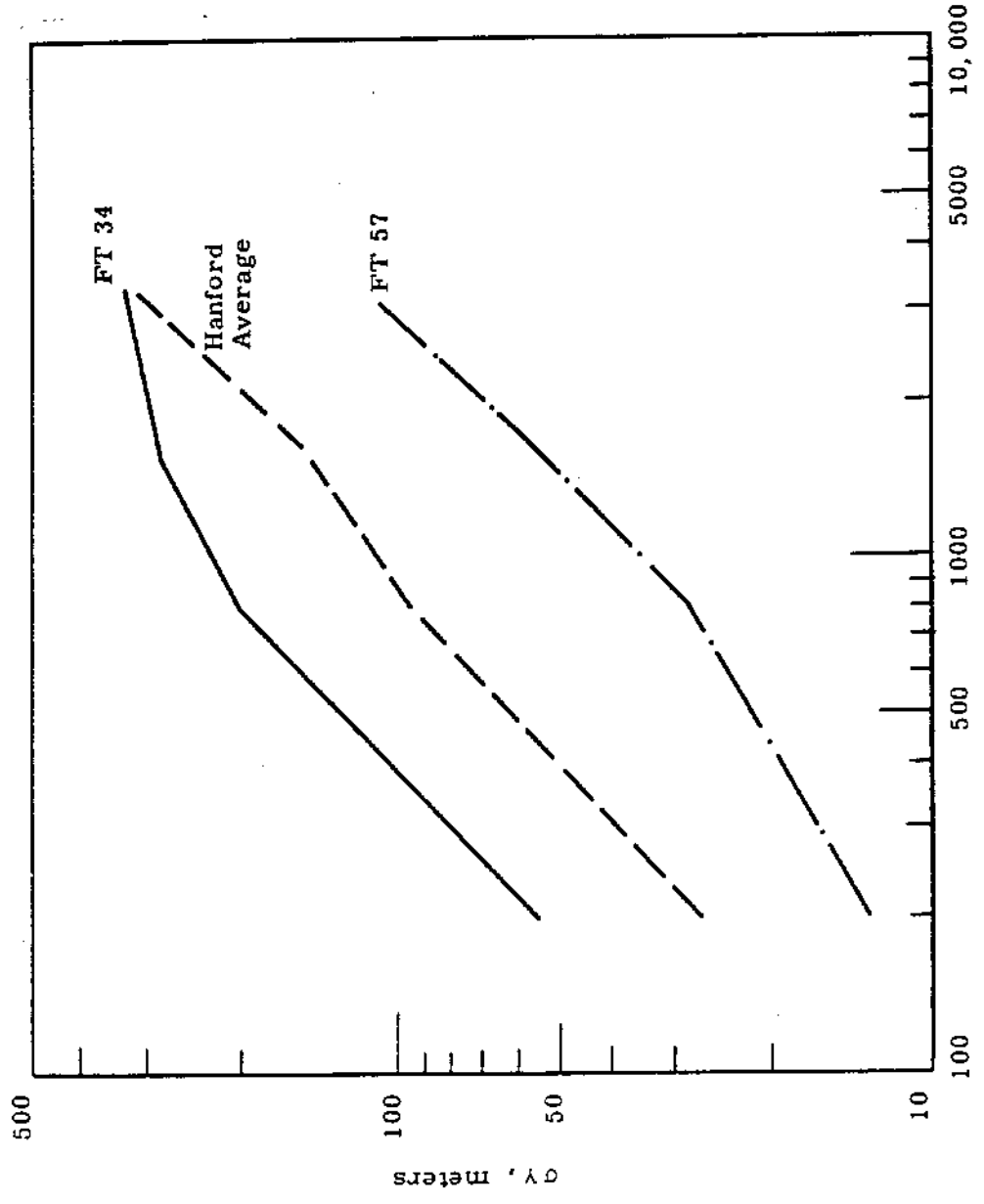

FIGURE 1.1

Standard Deviation of Arcwise Dosage Distributions Versus Distance from the Source for Hanford "30 Series" Tests

One method of dividing the wide range of results into groups with narrower ranges is by classifying the tests by the degree of wind direction variability noted. An example of such a consideration has been given in the 1961 issue of this report for the growth of a plume where the winds exhibit trend (slow but persistent variations of the wind direction during the emission) and no trend (a relatively persistent direction throughout the emission). Regression lines fitted to date for the Green Glow and "30 Series" (Phase I) for these two classifications yield an obvious separation of the results. Factors such as gustiness, stability, shear, and terrain are not only significant in bringing about the variations from the average conditions in the data at any site, but are also reflected in the differences found between the average plume widths determined for night, day, and seasons. This is the sense in which these variations are discussed in this report.

The most significant feature in the comparison of the average plume widths, at the three sites, when the seasonal and diurnal effects have been accounted for, is their similarity. This is particularly evident in the data obtained at Cape Canaveral and Vandenberg where sea to land flow regimes were similar. These data are shown in Figure 1.2 where the standard deviation of the cross-wind mass distribution is represented on the ordinate and distance, x, on the abscissa. The narrowest plumes were observed in the winter at Cape Canaveral and Vandenberg when the wind flow was controlled primarily by the large scale pressure gradient, which was relatively constant in time giving a persistent direction. This was typical frontal-type weather as contrasted to the sea breeze circulation resulting from land-sea temperature differences, dominant in the summertime. In the daytime, in winter, a weak sea-breeze circulation was superimposed on the gradient flow which contributed to greater variations in the wind direction and subsequently caused somewhat wider average plumes. In the summertime, however, the flow results entirely from the sea breeze circulation caused by sea-land temperature differences where small scale local conditions produce nonpersistent winds, leading to much wider plumes.

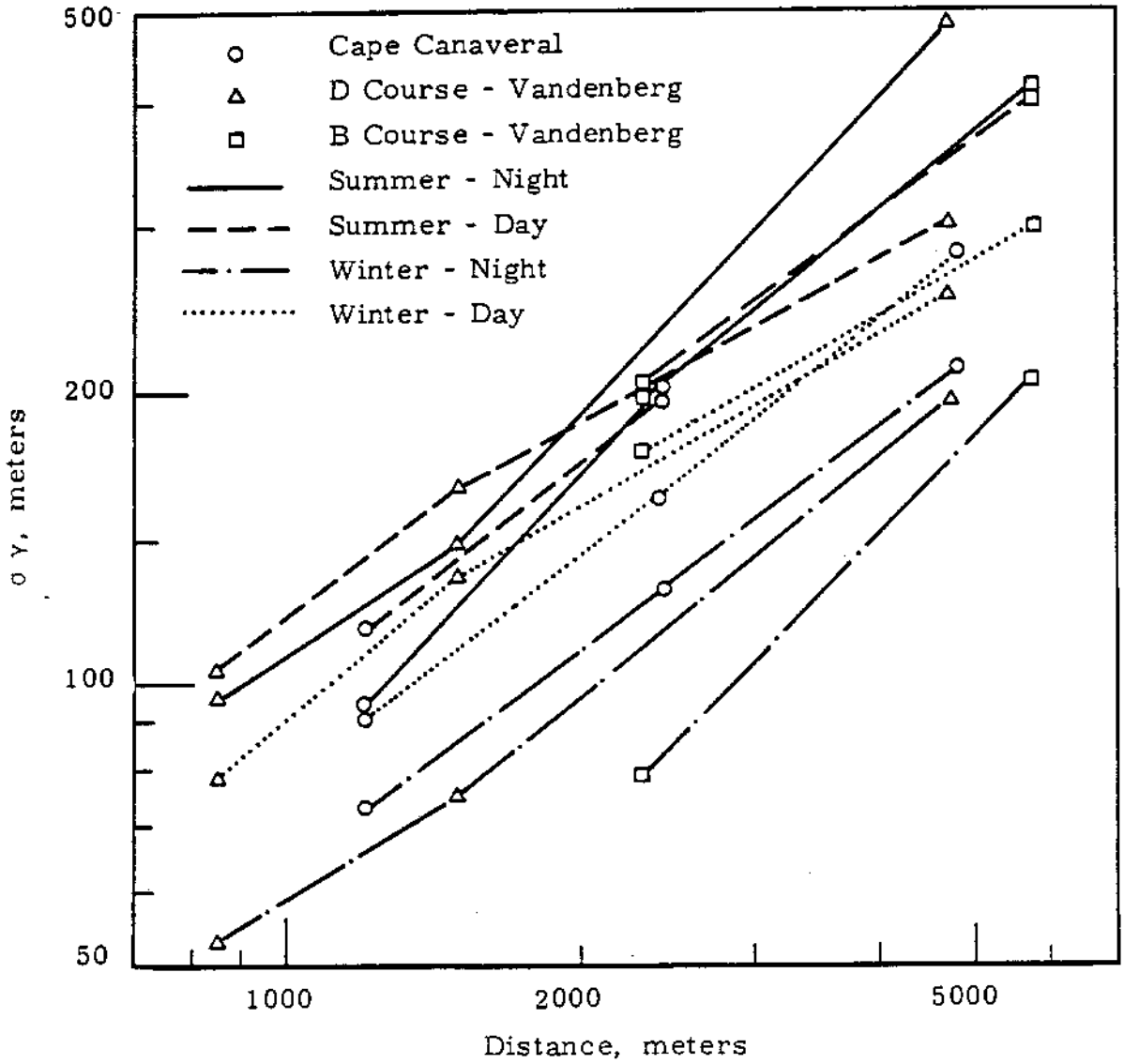

FIGURE 1.2

Standard Deviation of Arcwise Dosage Distributions
Versus Distance from the Source for Off-site Tests

It should be noted that, in the summer, diffusion over the B-course at Vandenberg (flat terrain) and at Canaveral where the terrain is similar produced plumes with widths that are nearly equal where measurements were made at the same distance from the source. Allowing for a reasonable extrapolation, summertime emissions at Canaveral and those over the level areas of Vandenberg spread horizontally to the same degree regardless of whether the release was made at night or day. However, over the rough terrain of the D course at Vandenberg, the increase of plume widths at greater distances is noted with the nighttime releases. The effect of the terrain on the Vandenberg D course is to cause increased variability in the winds at night as the sea breeze diminishes and the flow around terrain features becomes more pronounced with increasing atmospheric stability. The conditions produced the widest plumes observed at either Canaveral or Vandenberg.

At Hanford, the nighttime releases in the summer resulted in widths which agree with the group of off-site results obtained in that season, as shown in Figure 1.3. At the greatest distance from the source, the Hanford data approach the extreme values noted at night on the Vandenberg D course, suggesting that effects of terrain might also require further investigation at Hanford. The plume width data for the Hanford daytime emissions represent tests over all periods of the year and exhibit no significant differences from those data obtained during the summer night. The off-site data suggest that research at Hanford be extended to obtain measurements of the plume width for the winter nights where the off-site results showed the narrow plumes.

The large scale effects of topography in deviating the plume trajectory in the summer stable cases are shown in Figure 1.4. A summer night and day run are shown for each course, demonstrating that over the flat terrain little deviation takes place in either day or night. (An apparent deviation for the day run is caused by reduced exposures on the north end of Arc 2, where lines of eucalyptus trees shielded the sampling equipment.) However, in the daytime over the rough terrain, the plume follows a straight line flowing over prominent

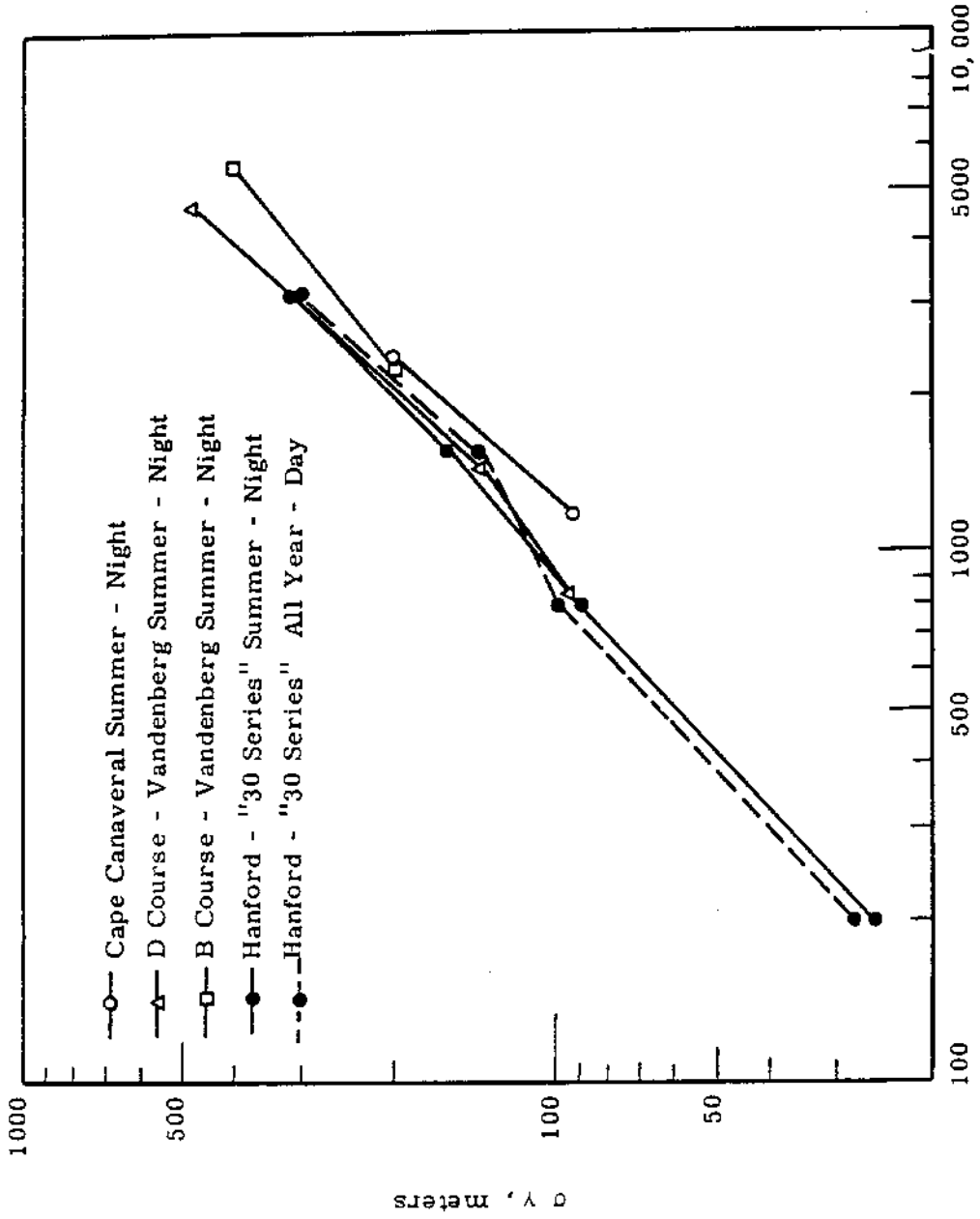

FIGURE 1.3

Standard Deviation of Arcwise Dosage Distributions
Versus Distance Comparison of Hanford and Off-site Results

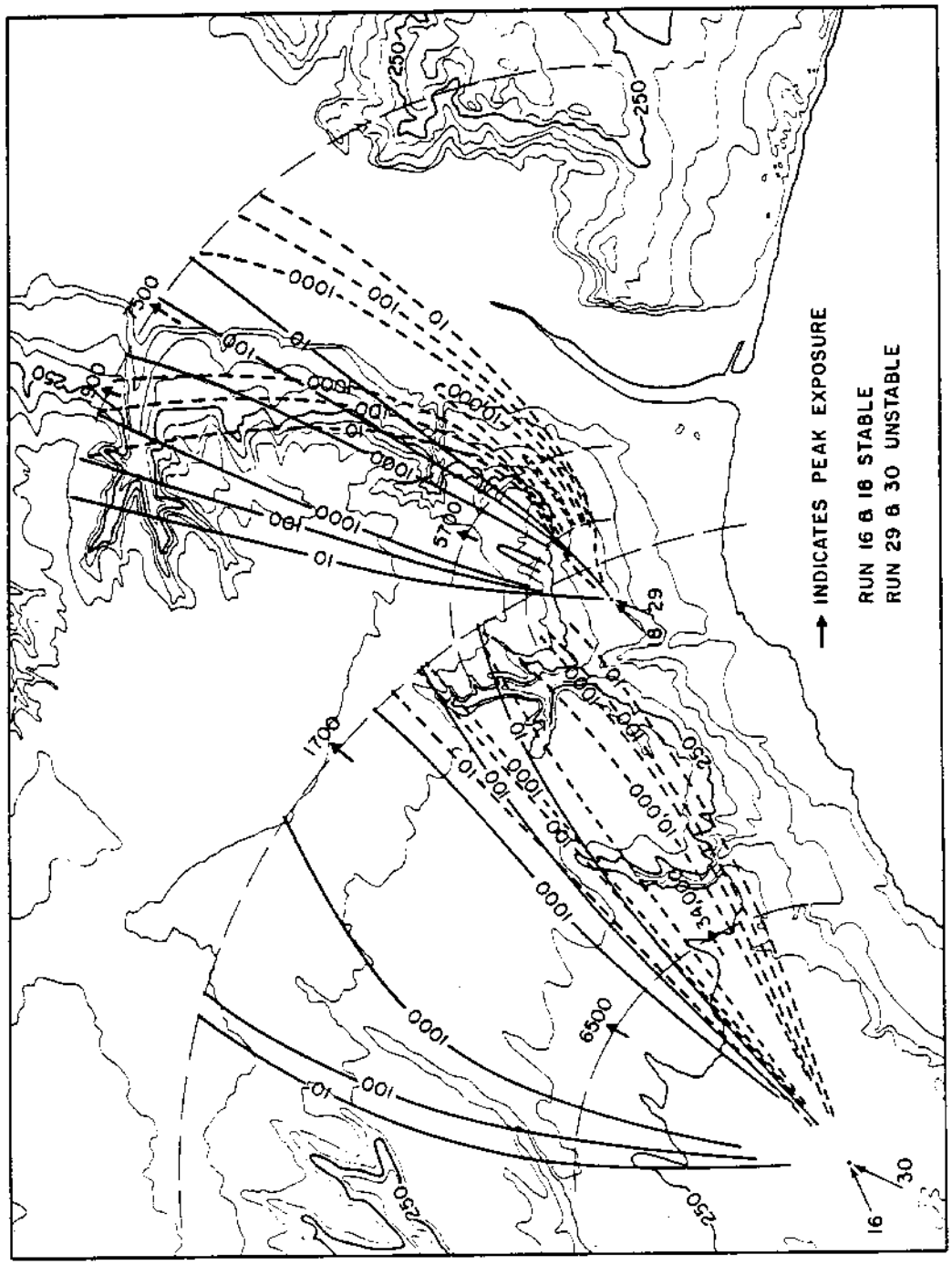

FIGURE 1.4
Effects of Ground Contours on Diffusion Patterns
(Vandenberg Air Force Base)

terrain features while at night there is an extreme curvature of the plume trajectory as it is deviated around these same terrain features. In winter when the large scale pressure gradient was the controlling feature during both day and night, this effect of terrain on trajectory was not observed even in the most stable atmospheric conditions.

Figure 1.5 shows the dependence of the normalized peak exposure on distance. The peak exposure, E_p, was the highest exposure observed on any particular arc and the source strength, Q_T (Mass), is the amount of tracer material released during a test. The dominant role that atmospheric stability has in affecting the level of E_p / Q_T is quite evident for all sites with the highest level of E_p / Q_T being observed at night when the atmosphere is most stable.

The agreement of data is excellent for the Hanford night, the Cape Canaveral night, and the Vandenberg B-course winter night runs. These tests were obtained during the most stable conditions over relatively flat terrain. Departing from these data were those obtained at night during the winter on the Vandenberg D-course. The atmospheric stability associated with these tests was not much different than that which characterized the B-course runs in the same period, yet the exposures were 0.7 of those obtained at comparable distances on the B-course. There are two possibilities accounting for this difference in peak exposures: (1) the measured lateral spread of the plume over the B-course was much less than that of the D-course in these experiments, and therefore should yield higher exposures; and (2) the effect of the rougher terrain of the D-course would act to produce not only the greater lateral mixing observed, but also enhanced vertical mixing.

The tests which were conducted in unstable daytime conditions show fair agreement between the three sites. The Hanford day, Cape Canaveral summer day, and all the Vandenberg day tests fall in this group, but the Cape Canaveral winter-day series is the exception, showing considerably

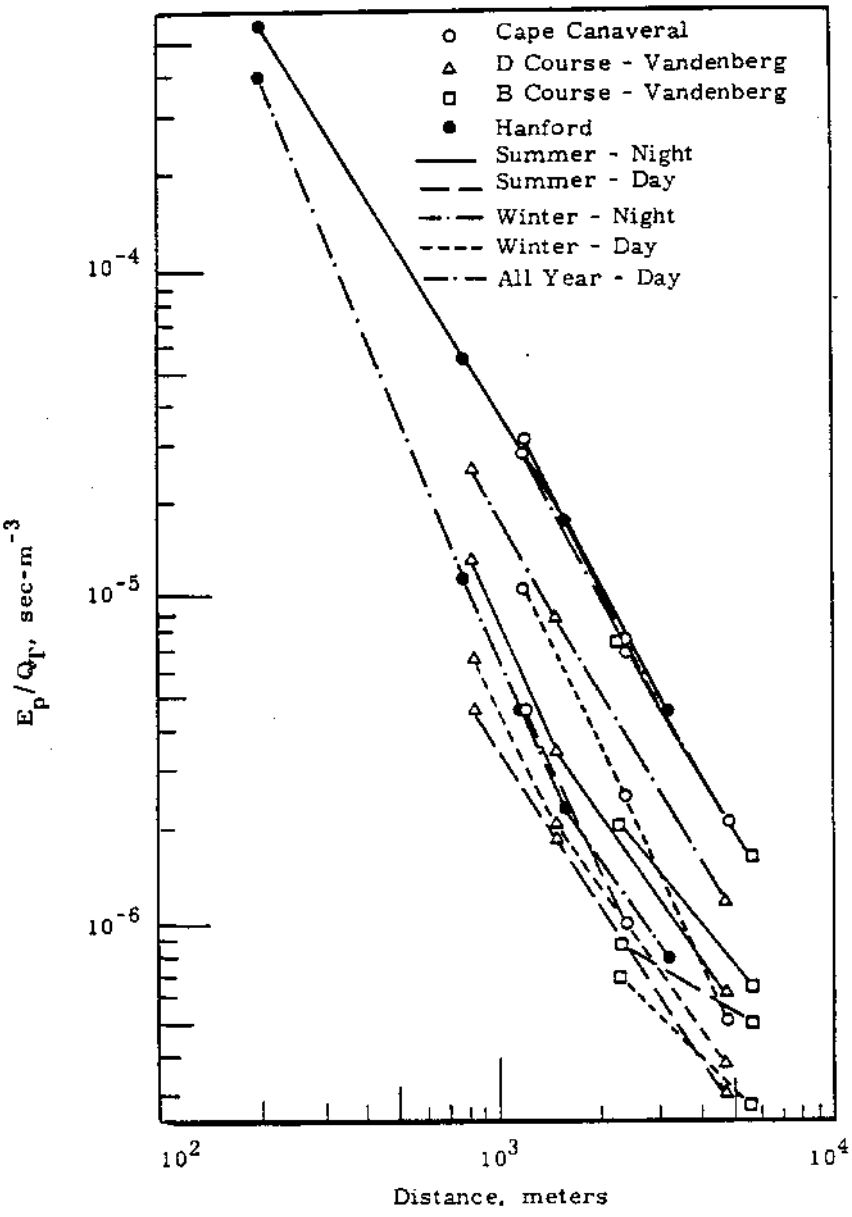

FIGURE 1.5

Normalized Maximum Dosage Versus Distance from the Source

higher exposures. There are again two reasons suggested for this departure, although the evidence by no means precludes further investigation. First, the average horizontal growth of the plume was smaller than all the other daytime tests, and second, the vertical mixing produced by thermal convection was considerable reduced in the winter series.

The decrease of E_p / Q_T with distance for the Vandenberg summer daytime runs on the B-course is much less than is indicated by any other data. These tests were obtained when a thin unstable layer extending to only a few feet above the Earth's surface developed beneath the slightly stable air moving onshore from the ocean. The tracer was released at a height of about 3 m into the stable layer, which acted to retard the downward motion of the particles, leading to low exposure values at distances not far from the source and including the first arc.

Further from the ocean, as the air modification proceeded, the unstable layer became more developed extending deeper into the stable layer, and eventually the unstable layer depth exceeded the height of the plume. The plume was then thoroughly mixed through the layer and the tracer particles were "fumigated" down to the samplers of the furthest arc in concentrations considerably over that which would be expected through the extrapolation of the close-in data. In a few instances, exposures measured on the second arc were actually higher than those on the first arc as shown in Figure 1.6.

Between the stable and unstable groups of data are the two series obtained at Vandenberg during the summer at night. The atmosphere in these tests was near neutral so the exposure estimates falling between those of stable and unstable tests were expected.

The effect that thermal stability has on the level of exposure was studied in more detail with each of the individual Hanford tests. Representative results are shown graphically in Figure 1.7. The ordinate in the figure is the cross-wind integrated exposure normalized by the source

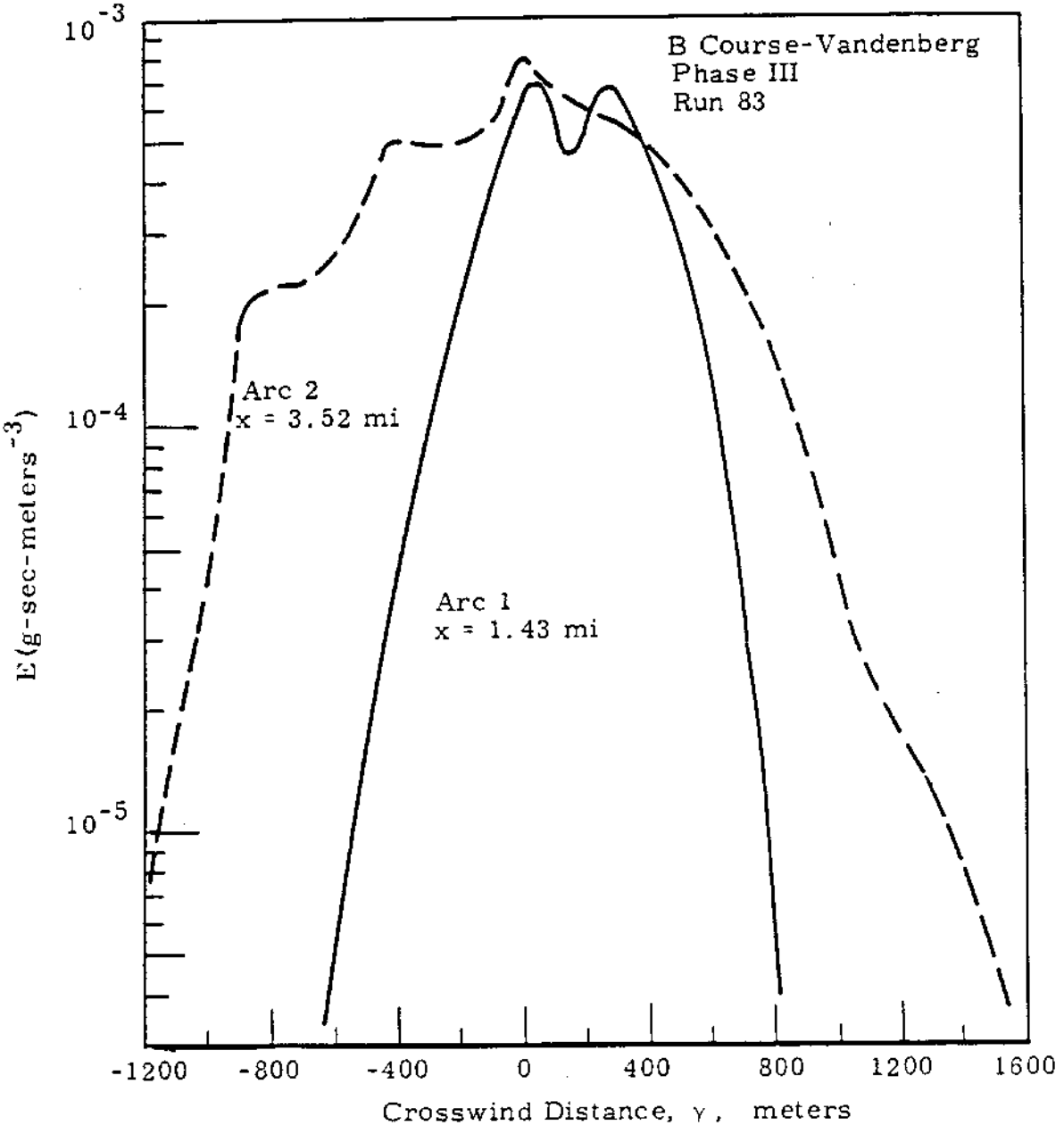

FIGURE 1.6

Crosswind Dosage Distributions Demonstrating Plume Ducting

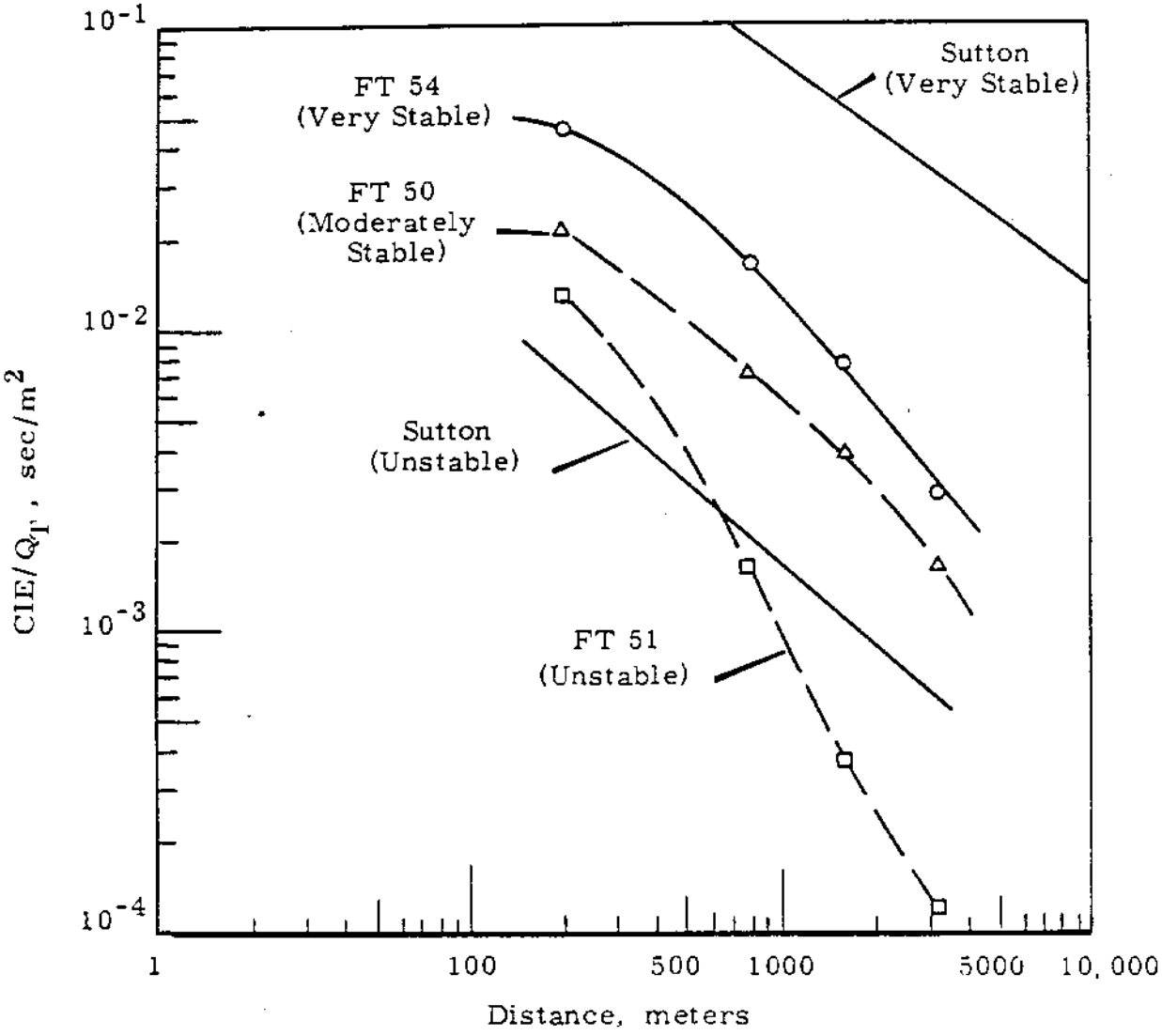

FIGURE 1.7

Normalized Crosswind Integrated Dosage
Versus
Distance from the Source

strength, CIE/Q_T, defined as

$$CIE = \int_{-\infty}^{+\infty} E \, dy.$$

Integrating Sutton's diffusion model,

$$CIE = \frac{Q_T}{\sqrt{\pi}\,\bar{u}\;C_z\;x^{\frac{2-n}{2}}} \quad \exp \quad \frac{-h^2}{C_z^{\,2}\;x^{2-n}},$$

where Q_T is the amount of material released, $\bar{u}$ is the mean wind speed, h is the height of release, x and y are the usual coordinates, and C_z and n are diffusion parameters whose values depend on the ambient meteorological conditions. The principal advantage in using this form of the equation is that the variable effect of lateral diffusion has been removed by the integration so that the change of CIE with distance, x, results only from the vertical depletion of material (i.e., vertical dispersion and deposition) which is most dependent on thermal stability. The Sutton curve in Figure 1.7 assumes $\bar{u}$ = 2 mps, C_z = 0.02, and n = 0.5, which are reasonable values for stable nighttime conditions. Out of the 23 Hanford tests used in the analysis, three "typical" curves representing diffusion in very stable, moderately stable, and unstable atmospheric conditions are shown. Actually, any of the 23 tests could have been used since grouping within stability classifications was excellent and all curves within the same stability classification exhibited the same general shape. Whereas the Sutton model predicts that the CIE/Q_T decreases approximately as a power law with a slope of -0.75 for distances beyond about 500 m, the experimental data show a more rapid rate of decrease with distance, which is not approximated by a power law. The depletion of material through deposition is suspected as the cause of this departure from the Sutton curve, and investigations are continuing in this study. The dependence

of the magnitude and the decrease with distance of the CIE/Q_T on the thermal stability is quite evident. At 200 m, the estimate of CIE/Q_T for the unstable case is four times smaller than the very stable and less than two times smaller than the moderately stable case. But, at 3000 m, the unstable case estimate of the CIE/Q_T is 30 times smaller than the very stable case and about 10 times smaller than the moderately stable case estimate. Investigations are continuing into the basic mechanisms causing these effects and the ultimate development of a prediction model.

In 1962, 13 experiments were conducted to further investigate diffusion and deposition from a ground source. The reduction of these data is nearly complete and analyses will follow. The design of the earlier "30 Series" experiment was modified and extended to allow a more detailed examination of the effects of terrain, time of emission, and variability of wind direction.

The diffusion experiments were mostly obtained during the summer at night. A plume was generated for periods from 1/2 to 3-1/2 hr, and detailed measurements of wind direction and speed were obtained at eight levels from near the ground to 400 ft on the Hanford Meteorology Tower. Air samples were made at all arcs out to 3200 m and during four of the tests, the additional 12.8 km arc was reactivated. Data from these tests will be examined to compare with earlier experiments and will be used in connection with detailed wind trace analysis.

Two of the 13 experiments were conducted to measure the deposition of tracer material released near the ground on natural cheat grass out to 200 m from the source. The experimental design was described in the 1961 issue of this report as were the results of the first experiment of this type which was obtained that year. A few minor changes in the technique were made to facilitate the mechanics of testing, and a more detailed calibration technique was employed which accounts for problems of dust in those samples taken near the ground.

The last group of diffusion experiments, performed during the fall of 1962, consisted of 10 elevated releases from a 185-ft source on the Hanford Meteorological Tower. The release time ranged from 15 min to 1 hr and exposure measurements were made at ground level (1.5 m) on 9 arcs at radial distances from the source of 100 to 1600 m. These tests were carried out in a wide variety of wind speeds and atmospheric stabilities ranging from neutral to very unstable. Together with eight similar experiments performed over this course in 1961, these tests comprise the first complete series of elevated source experiments utilizing the Hanford tracer technique. The data from this series were processed through the plant IBM-electronic computer and preliminary analyses were made.

The expected increase in exposure value with increasing distance was noted, rising to a maximum and then decreasing at greater distances. The distance to the maximum axial exposure was observed to be a function of the wind speed and, in the strongest winds, this distance approached the limits of the sampling grid. It was also noted in many of the tests that beyond the maximum the decrease in exposure was more rapid than anticipated from Sutton's theoretical model for an elevated release.

To investigate the details of the decrease in exposure with distance, it was found necessary to both expand the diffusion sampling grid in azimuth to allow testing with a wind direction where lighter winds are more prevalent and to extend the grid to a distance of 3200 m. This enlargement of the grid should be completed for the second series of elevated release tests to begin early in 1963.

Precipitation Scavenging Processes - R. J. Engelmann and J. J. Fuquay

Problems attendant with the determination of the scavenging efficiency, such as anisokinetic sampling error, droplet evaporation, and particulate wettability are treated. A peak scavenging efficiency is reported to occur at a raindrop diameter of about 0.4 mm, as previously observed by Kinzer and Cobb. The explanation for this deviation from Langmuir's theory is believed to lie in the characteristics of the wakes of different size drops. The results of this research affect washout predictions.

In the 1961 submission for this report, a method was described for obtaining precipitation scavenging efficiencies utilizing the special raindrop sampler developed at Hanford. Results of pilot experiments had indicated a peak collection efficiency at a raindrop diameter less than 0.8 mm. Scavenging efficiencies with respect to particle size appeared to be less than those predicted by Langmuir,[1.6] but similar to previous measurements by McCully, et al.[1.7] Results of preliminary experiments suggested a rapid increase in scavenging efficiency with particle size to values in excess of 1.0. The scavenging research conducted by Atmospheric Physics Operation of Hanford Laboratories during 1962 has been primarily concerned with two areas:

(1) Improvement of the accuracy of determination of scavenging efficiency with respect to particle size

(2) Confirmation of the higher scavenging efficiency of the smaller raindrop.

Following pilot test determination that experiments in natural conditions could be successfully employed to determine the scavenging by rain of a range of particle sizes, a systematic study was made of the uncertainties in the field and laboratory measurements required.

Using the temperature depression calculations of an evaporating water droplet as given by Best,[1.8] computations were made showing that the evaporation of a raindrop during an experiment was small. Since the

zinc sulfide tracer at release is suspended in tiny droplets, which evaporate to leave particlulates, calculations were also made to establish the relative humidity values required for evaporation of the water before its arrival at the scavenging site downwind. Even though evaporation appears to be complete, it is probable that there is always at least a molecular layer of water on the particles, as inferred from studies in surface chemistry.[1.9, 1.10] This would mean that these zinc sulfide particles are wettable and may possess a higher retention after contact with a passing raindrop then non-wettable particles.

The importance of wettability in scavenging is not established, although it has been discussed by Pemberton[1.11] and McCully, et al.[1.7] McCully explained the difference in the scavenging of zinc sulfide 2210 and 2330* by a difference in the wettability of the two tracers, and used contact angles of water on discs made of the tracers to characterize their wettabilities.[1.12] Recent tests in Hanford Laboratories showed that these tracers have about the same wettability, as concluded from their deviations from the Stokes' settling velocities in water. In addition, these two tracers have the same base materials, impurities and colors. This was considered sufficient evidence of similarity to warrant blending the two tracers to obtain a third with a broad size distribution--especially designed for the scavenging studies.

Calculation of the scavenging efficiency requires the measurement of both the material that has been scavenged, and the concentration of material in the path of the precipitation element. The former is obtained directly from the drop images obtained with the Hanford rain samplers. The latter requires knowledge of air-sampling system's efficiency with respect to particle sizes. The air sampling system normally draws air through the intake opening at a lower velocity than that of the wind, causing the streamlines of the flow to diverge and turn as they approach the filter. This anisokinetic sampling error biases the sample toward large particle sizes. Laboratory

---

* U. S. Radium Corporation, manufacturer. 2210 and 2330 have geometrical mean diameters of about 3 and 15 μ, respectively.

and field experiments were started to evaluate this error over a range of wind speeds and particle sizes to permit correction of the air sample data for the anisokinetic bias.

The scavenging power of a particular raindrop size on particulate material below rain cloud level is the product of the drop cross-sectional area, its scavenging efficiency, and its frequency of passage through the particulate laden air. The importance of the small drop portion of the raindrop spectrum is shown in Figure 1.8. This graph gives the percentage of the total cross-sectional area of all the rain that was contributed by drops below a given diameter in two Hanford rains. For instance, 50% of the scavenging area at 1116 PST was provided by drops smaller than 0.8 mm. The curves in Figure 1.8 are for light rains characteristic of this semi-arid region of Eastern Washington.[1.13] Small drops apparently outnumber large ones in heavier rains, too (for instance, see references 1.14, 1.15).

Results of tests conducted at Hanford this past year using artificial rain and zinc sulfide particles have shown that the efficiency of a 0.40 mm diameter drop was 1.6 times that of a 0.82 mm drop, and the efficiency of a 0.36 mm drop was 1.5 times that of a 0.64 mm drop. (These results are not affected by anisokinetic errors.) The 1961 pilot test in natural rain had indicated that the ratios were 1.8 and 1.4, with a peak efficiency at 0.45 mm diameter. Kinzer and Cobb[1.16], in their laboratory experiments had found the ratios 1.4 and 1.1 with a peak efficiency at about 0.4 mm, when their drop was scavenging smaller water droplets, rather than particles. The ratios expected using an interpolation between potential and viscous flow, as predicted by Langmuir,[1.6] are less than one (the actual values depend upon the density and size of the scavenged material) with a rather flat maximum in efficiency for drops larger than 1.2 mm.

There appears to be both a theoretical and physical basis for the higher scavenging efficiency of smaller drops. Pearcey and Hill[1.17] used the Oseen approximation to linearize the equations of motion and obtain the

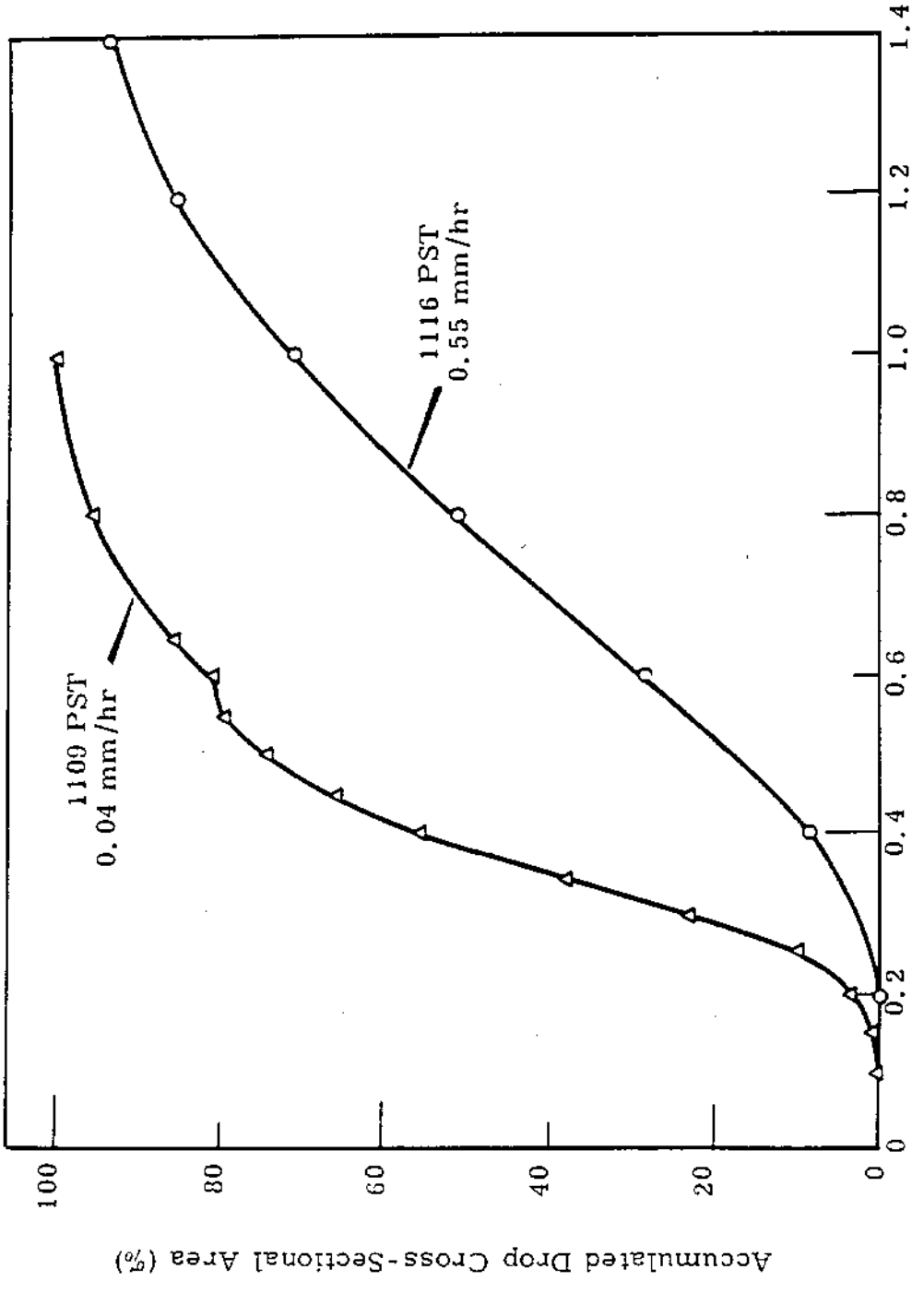

FIGURE 1.8
Scavenging Area of Drops in Hanford Rain of January 6, 1962

flow patterns for Reynold's numbers up to 40 (0.39 mm diameter raindrop). These patterns reveal a wake to the rear and side of the drop wherein fluid moves toward the axis of translation. This means that a drop (or particle) may move horizontally to enter the wake of another, then accelerate downwards with respect to that wake, and finally overtake the lead drop. This permits efficiencies in excess of 1.0. As the Reynold's number increases, the wake narrows, and Pearcey and Hill predicted that the efficiency must reach a maximum. From their computations for smaller Reynold's numbers, they felt that the peak might occur at Re = 100, or a drop diameter of 0.6 mm, in the absence of turbulence. Small scale turbulence would tend to part approaching drops and lower the sizes at which a peak efficiency occurs.

Hocking [1.18] objected to the use of the Oseen approximation when the raindrops were close together, and he also objected to Pearcey and Hill's assumption that a droplet's inertia is sufficient to carry it through the thin boundary layer on the leading side of a drop. Several pieces of evidence in the literature indicate that the boundary layer and wake might be very important to scavenging. Writers, in addition to Pearcey and Hill, have made statements concerning collection to the rear of the drop. Those with experimental evidence were often noncommittal, however. Some investigators detected signs of drops moving laterally into the wake of larger drops.[1.19, 1.20, 1.21] Gregory [1.22] found downwind deposit of 32-μ spores on the back of narrow cylinders at very low wind speeds. Rosinski and Nagamoto [1.23] found zinc sulfide particles on the downwind side of a 1 cm cylinder at low wind speeds, and attributed this to electrostatic effects.*

---

* Predictions by Cochet [1.24] and Kraemer and Johnstone [1.25] indicate that electrical effects are of account in rainfall scavenging only in the case of very small (slowly falling) drops and relatively high charges. These conditions can occur in rains, but are more apt to occur in the case of scavenging by snow. A pilot test conducted at Hanford showed that snowflakes were effective scavengers, and that the same technique may be used to measure scavenging by snow as is used for rain.

Walton and Woolcock,[1.26] in laboratory tests with freely falling drops, found that 0.5 mm drops seemed more efficient than 2.6 mm drops, but felt that this could be attributed to the fact that the large drops were falling at much less than terminal velocity. They were not satisfied with the experimental errors in this stationary cloud-falling drop arrangement and changed the experiment design. Raindrops were suspended from capillaries and the particulate cloud moved upward past the drops. The 0.5 mm drop was no longer more efficient. However, it is obvious that normal wakes cannot be expected in this situation. Magarvey and Geldart[1.21] reported from a laboratory experiment that at least five of ten collisions observed between 2.0 and 0.5 mm drops occurred in the wake of a 2 mm drop. Wake collisions were observed between larger drops also, but the percentage was less. Smaller drops were apparently not investigated.

Microphotographs of the flow past cylinders at various Reynold's numbers have been provided by Fage and reproduced by Goldstein.[1.27] Sketches made from these photographs are shown in Figure 1.9 for Reynold's numbers of 17.7, 21, 47, and 104, which correspond to raindrop diameters of 0.27, 0.29, 0.42, and 0.62 mm. Notice that the wake is symmetrical and remains attached to the cylinder at low Reynold's numbers. The strength of the vortices appears to increase until, at a critical Reynold's number, they are shed from the cylinder, with new vortices forming to break away in their turn. Particles caught in the wake of a raindrop would have a degree of opportunity for impaction on the trailing (upper) side of the raindrop, which would depend on the strength of the vortex, and the time before the vortex breaks off from the drop. It is believed that this wake phenomenon explains the peak efficiency observed with a drop about 0.45 or 0.5 mm diameter.

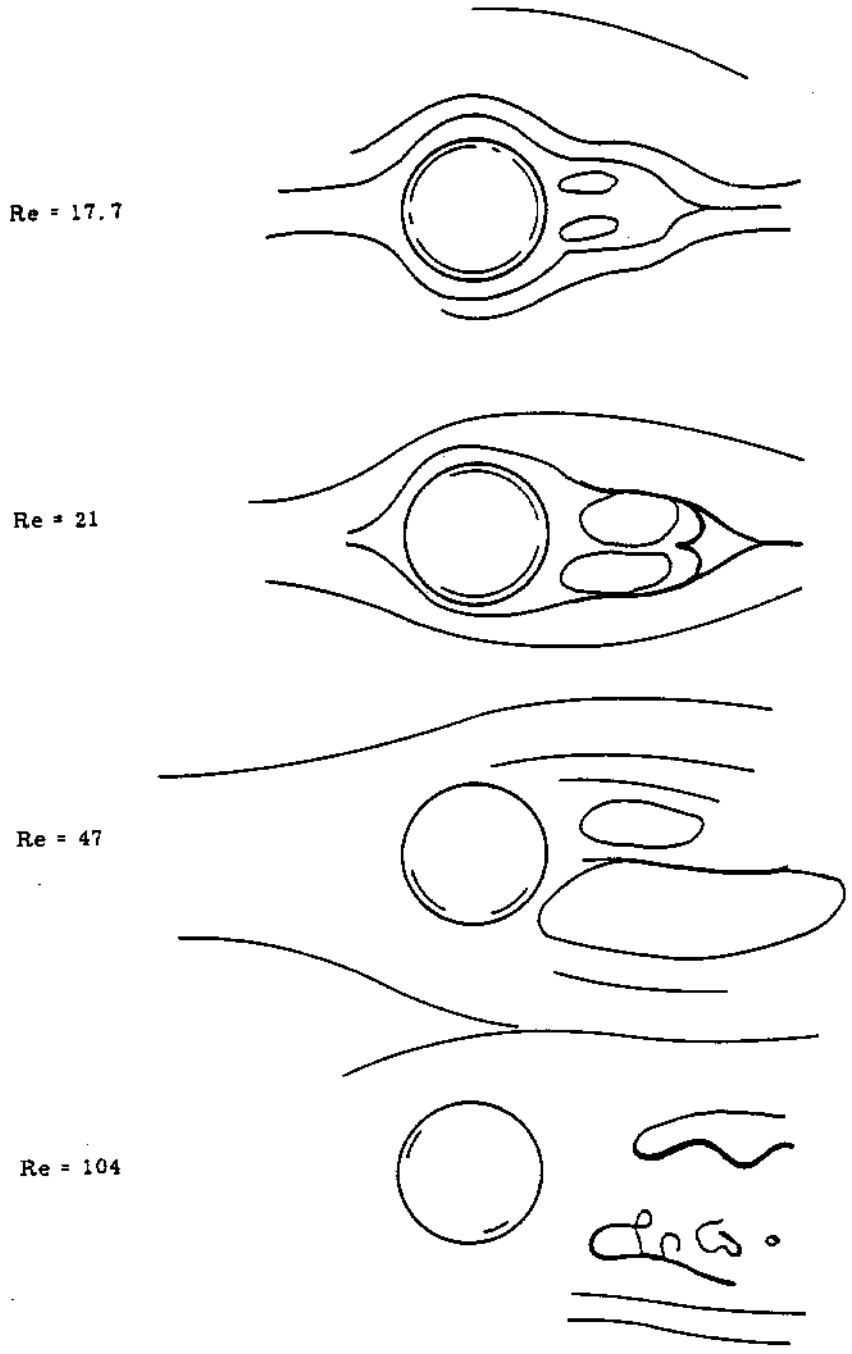

FIGURE 1.9

Flow About a Small Cylinder at Various Reynold's Numbers (as sketched from plates in Modern Developments in Fluid Dynamics, S. Goldstein, editor).
Flow is from left to right. The vortices intensify as the Reynold's number increases, and finally break away.

Advances in Atmospheric Tracer Technology - P. W. Nickola and J. J. Fuquay

The Hanford fluorescent tracer technique for the study of diffusion in the lower atmosphere continued to yield excellent quality data. The continued quality results at Hanford led to the request for and use of this technique in the investigation of dispersion phenomena at Vandenberg and Cape Canaveral missile ranges.

The development of a real time sampler for use with the existing tracer technique is described.

Progress in the development of multitracer techniques is reviewed. Techniques of this nature have application in improved definition of such parameters as source height and contaminant physical properties in studies of dispersion and deposition.

The main basis for investigating dispersion in the lower atmosphere is the emission of known quantities of an identifiable tracer and the quantitative sampling of this tracer to determine its subsequent spatial distribution. The Hanford fluorescent tracer technique perfected in 1960 has continued to yield excellent results from the standpoint of quantity and quality. The ease and speed with which field filters can be analyzed by the "Rankin Counter" permits an intensive field sampling program. Additionally, the low detection limit of about 6×10^{-9} g of fluorescent pigment permits an extensive field network when desirable. The horizontal distribution of the emitted tracer has been satisfactorily determined at a distance of 16 miles from the tracer source.

Since June 1959, more than 80 Hanford field experiments have been completed in which roughly 40,000 filters were exposed and analyzed. In addition, approximately 40,000 filters were assayed in support of diffusion experiments carried out at Vandenberg Air Force Base, California, and at Cape Canaveral, Florida. The Atmospheric Physics Laboratory's tracer technique and analysis procedures were employed at the two missile sites.

The Rankin filter-assaying technique referred to above, is used to assay bulk filter samples of fluorescent tracer 2210 collected in the field. These samples are representative of the dosage at the collection point resulting from

an entire period of tracer emission. There is also an interest in the resolution with time of the tracer concentration at a given point. This type of information is valuable in investigating such relationships as the maximum short-period concentration to be expected, the peak to mean ratios of concentration, and the arrival time of a contaminant at some point remote from the source.

To date, the HAPO sampling device with a time resolution capability has been the drum sampler. This sampler consists of a drum rotating at a constant rate (say 1 rev/hr). Sampled air is directed by an orifice at the outside surface of the rotating drum, and the tracer particles are impacted on the siliconed sticky surface.

Although these drum samplers have generated a great deal of useful information, they have several disadvantages: (1) The tedious and time-consuming counting procedure under microscope and ultraviolet illuminations, (2) The impossibility of accurately counting the high density portions of the trace, (3) The time and effort required in cleaning and preparing the drum for a new field experiment, and (4) The lack of resolution of very short period peaks in concentration. Inasmuch as the jet of impacting sample air has a finite trace length along the path of drum rotation, the resolution is directly proportional to the speed of drum; and yet the desire to sample over a period of more than a few minutes requires a slow rotation rate. Under normal field conditions, the arrival of a tracer particle cannot be stated with a greater accuracy than about ± 2 min.

A real time sampler has been developed in conjunction with the Nucleonics Instrumentation Operation which improves on the performance of the drum sampler. In this device, the ZnS-laden air is drawn through a chamber where a lamp rich in ultraviolet initiates fluorescence and the subsequent phosphorescence (or afterglow). The glowing particulates are then directed to a dark chamber monitored by a multiplier phototube. The plate current of this tube is recorded on a strip-chart recorder, and gives an indication of the pigment concentration in the counting chamber.

Although the prototype of this device has been tested to the extent that it is known that it responds qualitatively to increases in fluorescent pigment concentration, it has not been accurately calibrated. Crude estimates of calibration suggest that this real time sampler is linear in response to tracer concentration and has a surprisingly low detection limit of about 2×10^{-6} g/m^3.

The real time tracer sampler should improve on the drum sampler in the four areas previously mentioned as drum disadvantages. It should be particularly adapted to more accurate indication of peak concentrations with a finer time resolution. Plans are presently being finalized on a field model of the sampler.

Efforts are also being directed toward the ability to detect more than one tracer collected simultaneously on the same filter surface. The use of a multitracer technique in the atmosphere would be very convenient. The vagaries of the atmosphere make it a difficult medium for controlled experiment. Duplication of field experimental conditions is essentially impossible. Thus, one of the first uses of a multitracer technique could be to perform two or more diffusion field experiments simultaneously. For instance, efforts to study the effect of source height on the dosage of a contaminant at a downwind position would be simplified. If two (or more) experiments were performed using a single tracer, an analyst would be faced with the task of separating the source height effect from all other variable differing between the two experiments (such as differences in the magnitude and variance of wind speed, differences in the variance of wind direction, terrain differences, and differences in the stability of the atmosphere). With a multitracer technique, these differences would be automatically removed, leaving only the source height to affect the observed dosage or concentration.

Inasmuch as the fluorescent pigment technique was available, it seemed wise to look for a second tracer which would not disturb the previous assaying technique, and which could be independently detected. J. D. Ludwick, of the Chemical Research Operation, described such a technique in the 1960

issue of this report.(1.28) This technique involves the use of a water soluble fluorescein dye as a second tracer. The fluorescein should give essentially no cross interference to the assaying of the present ZnS tracer. Conversely, after analysis for the ZnS 2210 pigment, the technique prescribes a method for reducing the cross interference of the ZnS to a negligible amount during the analysis for fluorescein.

Recently, the first field generation of both fluorescein and the standard pigment 2210 was carried out. Essentially identical amounts of pigment 2210 and fluorescein were emitted from side by side sources. Although the cross-wind profiles of mass collected are very similar in character, they differ in degree. Analysis disclosed that the mass of pigment 2210 collected was about 30% less than the mass of fluorescein retained on the same filter. The reason for the discrepancy--be it faulty tracer generation, collection, or analysis--is being investigated.

There have also been efforts made to locate a second fluorescent powder which would have fluorescent properties sufficiently different from pigment 2210 to enable discrimination between the two pigments in Rankin counters. The Rankin counter works as scintillation counter in reverse. Rather than counting scintillations to determine the strength of an unknown source, the strength of the source is fixed and the rate of scintillation determines the amount of scintillator (ZnS pigment 2210).

Among methods considered for pigment differentiation in the Rankin counter were those based on the difference in fluorescing wave length of two pigments. However, no satisfaction was obtained by the use of various optical filters with a given type multiplying phototube, or by the choosing of multiplying phototubes whose peak sensitivities were near the fluorescing wave lengths.

Differentiation of pigments in the Rankin counter based on pulse height analysis, however, shows some promise. It was found, that pigment 2210 has one of the largest pulse heights of any of the 28 fluorescent pigments obtained for testing. Accordingly, five pigments whose scintillating pulse heights were small were chosen as candidates for the second tracer.

One of the five prospective tracers (pigment 2234) has a size distribution of particulates and a specific gravity quite similar to pigment 2210. These properties are requirements if differences in mass collected during simultaneous field generation are to be attributed to differences in source location only. A field generator is presently being purged of all pigment 2210 in preparation for field testing of pigment 2234.

The other four prospective "second" pigments are of larger particle size than pigment 2210. If emitted simultaneously to pigment 2210, their potential as tracers lies chiefly in investigation of the effect of particle size distribution on deposition phenomena.

See in this report:

(1) J. D. Ludwick. "Analysis of Grass and Ground Deposited Atmospheric Zinc Sulfide Particulate," Page 3.20.

(2) J. D. Ludwick and P. W. Nickola. "A Fluorescein Analysis Technique for Use in Atmospheric Diffusion Studies," Page 3.15.

REFERENCES

1.1 M. L. Barad and J. J. Fuquay (eds.) "The Green Glow Diffusion Program," Geophysical Research Papers No. 73. Air Force Cambridge Research Laboratories, Geophysics Research Directorate, Mass. Also HW-71400 Vol. I and Vol. II. 1962.

1.2 J. J. Fuquay, C. L. Simpson and C. E. Elderkin. Tracer Techniques and Field Procedures Used in the Cape Canaveral and Vandenberg Air Force Base Diffusion Experiments, HW-SA-2723. August 29, 1962.

1.3 C. L. Simpson. Some Measurements of the Deposition of Matter and Its Relation to Diffusion from a Continuous Point Source in a Stable Atmosphere, HW-69292 REV. April 1961.

1.4 F. Pasquill. Atmospheric Diffusion, D. Van Nostrand Co., Ltd. 1962.

1.5 M. L. Barad and J. J. Fuquay. "Diffusion in Shear Flow," J. Appl. Meteor., vol. 1, no. 2. pp. 257-264. 1962.

1.6 I. Langmuir. "The Production of Rain by a Chain Reaction in Cumulus Clouds at Temperatures Above Freezing," J. Met. vol.5, pp. 175-192. 1948.

1.7 C. R. McCully, Morris Fisher, Gerhard Langer, Jan Rosinski, Harvey Glaess, and D. Werle. "Scavenging Action of Rain on Air-Borne Particulate Matter," Ind. Eng. Chem. vol. 48, pp. 1512-1516. 1956.

1.8 A. C. Best. "The Evaporation of Raindrops," Q. J. Roy. Met. Soc. vol. 78, pp. 200-225. 1952.

1.9 N. K. Adam. The Physics and Chemistry of Surfaces. Oxford. 1930.

1.10 W. B. Kunkel. "The Static Electrification of Dust Particles on Dispersion into a Cloud," J. Appl. Phys. vol. 21, pp 820-832. 1950.

REFERENCES (Contd.)

1.11 C. S. Pemberton. "Scavenging Action of Rain on Non-Wettable Particulate Matter Suspended in the Atmospheres," Aerodynamic Capture of Particles. E. G. Richardson (ed.) pp. 168-178. Pergamon Press, New York. 1960.

1.12 J. Rosinski. Unpublished Data. 1962. (Private Communication)

1.13 R. J. Engelmann. Feasibility of Precipitation and Cloud Scavenging Experiments at Hanford, and Pertinent Climatology, HW-70135. November 29, 1960.

1.14 D. C. Blanchard and A. T. Spencer. "Raindrop Measurements During Project Shower," Tellus vol. 9, pp. 541-552. 1957.

1.15 B. J. Mason and J. B. Andrews. "Drop-Size Distributions from Various Types of Rain," Q. J. Roy. Met. Soc. vol. 86, pp. 346-353. 1960.

1.16 G. D. Kinzer and W. E. Cobb. "Laboratory Measurements and Analysis of the Growth and Collection Efficiency of Cloud Droplets," J. Met. vol. 15, pp. 138-148.

1.17 T. Pearcey and G. W. Hill. "A Theoretical Estimate of the Collection Efficiencies of Small Droplets," Q. J. Roy. Met. Soc. vol. 83, pp. 77-92. Also vol. 83, pp. 555-556. 1957.

1.18 L. M. Hocking. "The Collision Efficiency of Small Drops," Q. J. Roy. Met. Soc. vol. 85, pp. 44-50. 1959.

1.19 D. Sartor. "A Laboratory Investigation of Collision Efficiencies, Coalescence and Electrical Charging of Simulated Cloud Droplets," J. Met. vol. 11, pp. 91-103. 1954.

1.20 J. W. Telford, N. S. Thorndike, and E. G. Bowen. "The Coalescence Between Small Water Drops," Q. J. Roy. Met. Soc. vol 81, pp. 241-250. 1955.

REFERENCES (Contd.)

1.21 R. H. Magarvey and J. W. Geldart. "Drop Collisions Under Conditions of Free Fall," J. of the Atmospheric Sciences, vol. 19, pp. 107-113. 1962.

1.22 P. H. Gregory. "Deposition of Air-borne Lycopodium Spores on Cylinders," Ann. Appl. Biol., vol. 38, pp. 357-375. 1951.

1.23 J. Rosinski and C. Nagamoto. "Particle Trajectories and Adherence to Cylindrical Sticky Surfaces," Koll. Z. vol. 175, pp. 29-33. 1961.

1.24 R. Cochet. "Captation de Particules Neutres Par un Obstacle Electrise," J. Rech. vol. 4, pp. 153-180. 1952.

1.25 H. F. Kraemer and H. F. Johnstone. "Collection of Aerosol Particles in Presence of Electrostatic Fields," Ind. Eng. Chem. vol. 47, pp. 2426-2434 1955. Revised edition vol. 48, page 812, 1956.

1.26 W. Walton and A. Woolcock. "The Suppression of Airborne Dust by Water Spray," Aerodynamic Capture of Particles, pp. 129-153. E. G. Richardson (ed.). Pergamon Press, New York. 1960.

1.27 S. Goldstein. Modern Developments in Fluid Dynamics. Oxford. 1938.

1.28 J. D. Ludwick. Dual Atmospheric Tracer Techniques for Diffusion Studies Using Phosphorescence - Fluorescence Analysis, HW-70050. Page 103. January 1961.

RADIOLOGICAL PHYSICS

Shadow Shield Whole Body Counter - H. E. Palmer

The shadow shield whole body counter was calibrated for Zn^{65} and Cs^{137}. It was used to measure the radioactivity in Alaskan Eskimos and the decrease in total body potassium produced in patients by an artificial kidney and to locate tumors tagged with I^{131}. A shadow shield counter is being built in a truck by the Hanford Radiation Protection Operation for use in their control activities.

The development and calibration of the shadow shield whole body counter has been reported.[2.1] This paper describes further calibration results and several applications of the counter. A sketch of one of these counters, in which the lead bricks have been encased in steel, is shown in Figure 2.1.

Calibration

In 1961 the counter was calibrated for the measurement of body burdens of potassium.[2.2] In 1962 it was calibrated for Cs^{137} and Zn^{65}. These calibrations were made by counting subjects with known body burdens of the two isotopes. The results are given in Table 2.1.

TABLE 2.1

RESULTS OF COUNTING KNOWN BODY BURDENS OF Cs^{137} AND Zn^{65}

Subject		Counts/min/nc
Cs^{137} Calibration		
1		5.57
2		5.74
	Avg.	5.65
Zn^{65} Calibration		
3		3.18
4		3.09
	Avg.	3.14

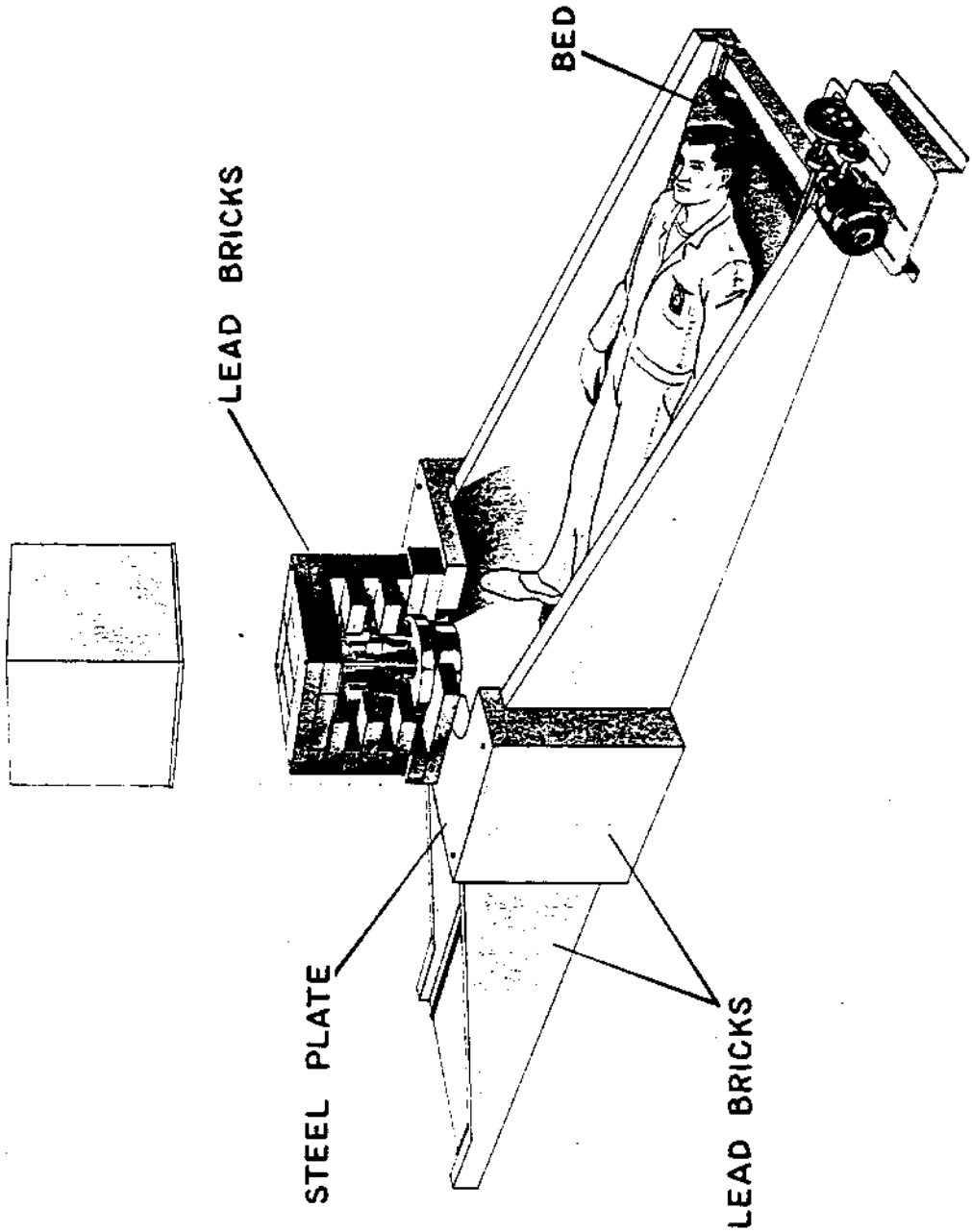

FIGURE 2.1
Shadow Shield Whole Body Counter

Radioactivity in Alaskan Eskimos

During the summer of 1962, the counter was used to count over 700 people, mostly Eskimos, in several villages above the Arctic Circle in Alaska. The principal problem was transportation of the counter, but this did not prove too difficult. Since the shielding consists of standard lead bricks, it was easy to assemble and disassemble. Some sort of facilities were always available to handle the heavy boxes of bricks. The counter and equipment were shipped to Fairbanks by a barge and truck route. From Fairbanks everything was carried by air freight. All of the equipment normally used with the counter was taken along. A motor-generator set was taken to provide power in those villages where it was not available. No equipment malfunctions occurred during the trip.

Where possible, the counter was placed on a concrete floor in existing buildings. At one location a floor to support the counter was not available so it was put together outside and on the ground. A hole was dug down through the wet spongy tundra until permafrost was reached. Sections of 8- by 12-in. timbers were placed in the hole and the counter built on them. Since most of the weight of the counter is in the center section, a hole only 4 by 4 ft was required. A temporary floor was made from sheets of plywood placed on the ground around the counter and a temporary wood framework covered with plastic was erected to protect the counter from rain and dust. The time required to assemble the counter was about 6 hr when placed on a concrete floor and 8 to 10 hr for an outside location.

The very open construction of the shadow shield proved a great help in dealing with the Eskimos. None of them showed any nervousness about being counted because they could always see what was happening and could talk to us or other Eskimos as they were going through the counter. The results of this study are described in later papers in this report.

Potassium in Artificial Kidney Patients

The counter was taken to Seattle, Washington, and set up in the Northwest Research Institute of the Swedish Hospital. Patients being treated with an artificial kidney were measured before and after their treatment to determine the change in the amount of potassium in their bodies that resulted. These patients are connected to the artificial kidney once or twice a week and their blood is circulated through it to remove acids, excess potassium, and other poisons. The typical decrease in potassium according to our measurements was about 15 g, or about 10% of the total in the body.

Use as a Differential Scanning Counter: Tumor Scans, Potassium Distribution

In the usual mode of operation of the shadow shield whole body counter the subject is placed on a bed that moves beneath the scintillator. A pulse height spectrum is collected throughout this period. This mode can be called the integral scanning mode. In differential scanning, a spectrum would be collected during increments of motion beneath the scintillator or a one-channel analyzer would be fed into a counting rate meter while the bed was moved continuously. Differential scans provide information on the distribution of isotopes within the body. The lead housing of the scintillator provides some natural collimation which narrows the field of view during a scan. For the use with I^{131} described below much sharper collimation was desired. Two sheets of lead slightly separated were placed over the face of the scintillator. Each contained a narrow slit; the slits were parallel to each other so that they defined a long, narrow field of view. Provision was included for orienting the slits at different angles to the direction of motion of the bed. Ideally, two different scans with the slits at different angles would suffice to locate the projection of the position of a source of radiation on the plane of the bed (but not, of course, vertically). In tests with point sources, the sources could be located to within about half an inch.

While the counter was set up in Seattle some patients from the Tumor Institute of the Swedish Hospital were given differential scans. These patients had known tumors and suspected metastases. They had been given 5-iododeoxyuridine tagged with I^{131}. Experiments on animals had indicated that this compound would either concentrate in or be held longer in tumors than in normal tissues. The differential scans were done with a counting rate meter recording the output of a single channel analyzer set on the I^{131} photopeak. Much of the isotope was diffused throughout the body, but often specific organs or known tumors could be identified as having high concentrations. Quite valuable results were obtained in a few cases. Figure 2.2 shows two scans taken of one woman. The first scan showed a very large peak over the bladder. It also showed two "satellite" peaks on either side of the large peak. These were later identified as due to leakage of radiation into the scintillator around the edges of the lead sheets containing the slits; in later measurements these "satellites" were removed by better shielding. After a trip to the bathroom, the peak over the bladder almost disappeared, but a small peak remained over the xiphoid area. Later examination showed metastases in this area that had been hidden on X-ray pictures by the shadow of the heart. Figure 2.3a shows scans of a normal subject who contained the tagged compound and of a woman who was found to have liver and bladder involvement in her disease.

The natural collimation of the counter was applied in a study of the distribution of potassium in the body. Counts of 20 min were taken at four positions along the bodies of two subjects, first to determine the distribution of natural potassium and then of K^{42} at 16 to 18 and at 24 hr after ingestion. Correction was made for K^{42} eliminated from the body. Results were normalized and are shown in Figure 2.3b. They show that even after 24 hr there is not complete equilibrium of the K^{42} with the natural potassium in the body.

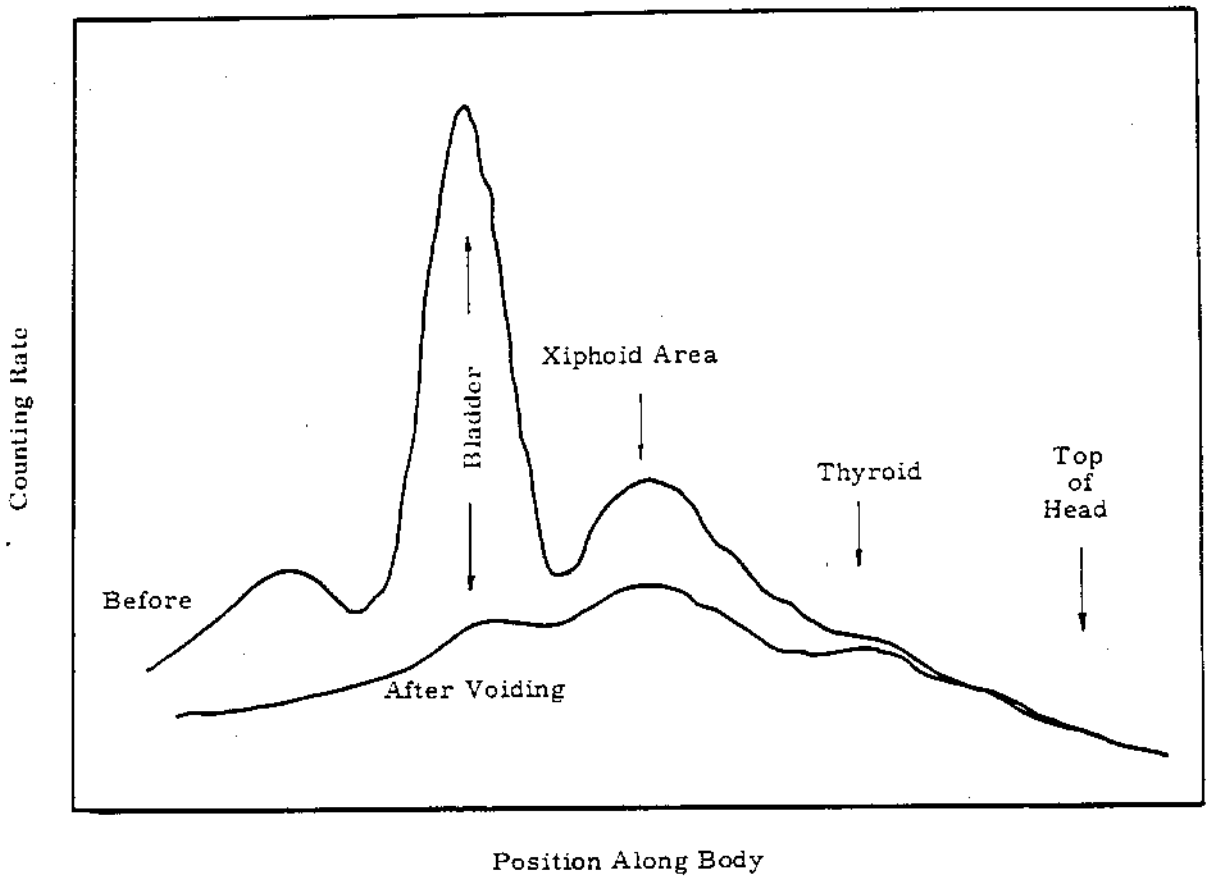

FIGURE 2.2

I^{131} Differential Scan
(Metastases in xiphoid area)

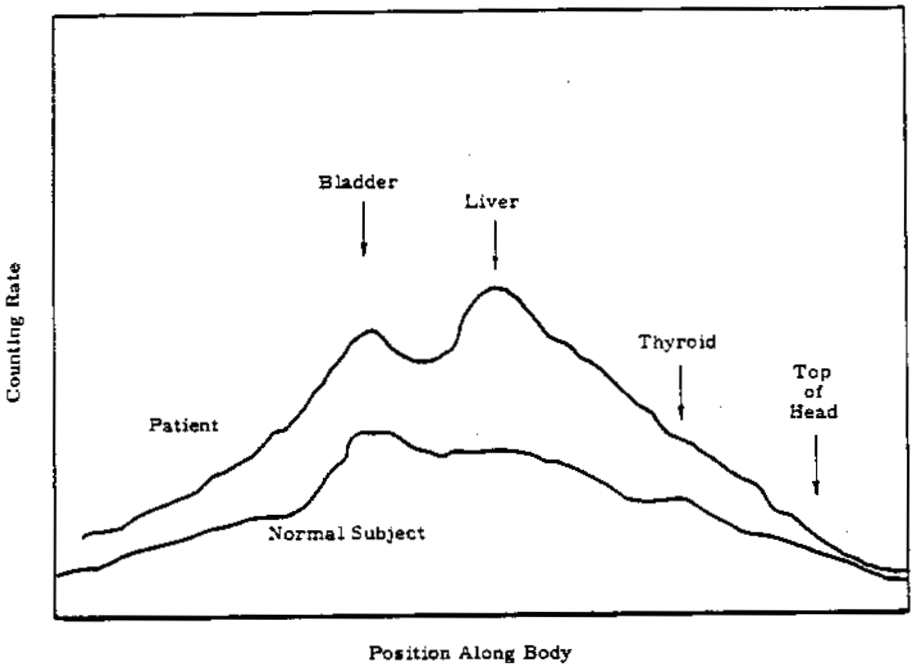

FIGURE 2.3a

Differential Scan
(Tumor patient with liver and bladder involvement)

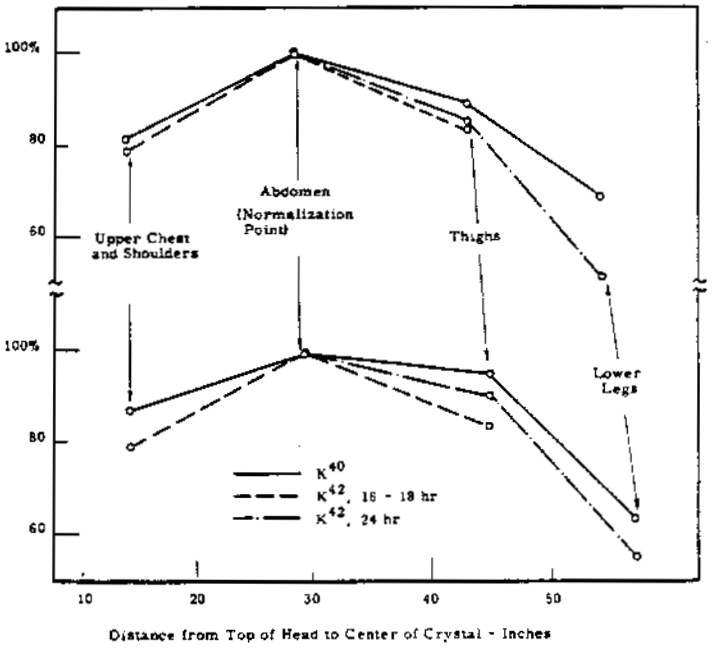

FIGURE 2.3b

K^{40} and K^{42} Differential Scans

Mobile Shadow Shield Whole Body Counter

The Hanford Radiation Protection Operation began preparation of a shadow shield counter in the body of a truck-trailer. It was necessary to strengthen the bed of the trailer slightly and to install suitable wiring. Otherwise, the changes to the trailer were to give it a pleasing appearance. The lead bricks in the shield were pinned together and encased in steel sheets. This is illustrated in Figure 2.1. The scintillator was shock-mounted. The mobile counter will be used as an adjunct to the Hanford Whole Body Counter in their radiation protection control activities.

Cs^{137} in Alaskan Eskimos - H. E. Palmer, W. C. Hanson, and B. I. Griffin

A trip was made to Alaska in the summer of 1962 to measure the radioactivity in Eskimos with the Shadow Shield whole body counter. Over 700 people were counted. Body burdens of Cs^{137} up to more than 100 times the average in the rest of the United States were found.

Members of the Hanford Laboratories have participated since 1959 in a bioenvironmental study program in the Cape Thompson area of northern Alaska as part of Project Chariot. One of the early results of these studies was the discovery of high levels of Cs^{137} in lichens and caribou. This stimulated interest in the body burdens of fallout isotopes in Eskimos in that area. Attempts to obtain autopsy samples of these Eskimos were of very limited success. In the Fall of 1960, high body burdens of Cs^{137} were discovered in Norwegians [2.3] and subsequently in Swedish and Finnish Lapps.[2.4] The latter high burdens were felt to be connected with the food chain, lichen-reindeer-man. During this period, a Shadow Shield whole body counter was developed at this laboratory for other purposes. This counter was light enough and its construction was such as to permit it being easily transported. During the summer of 1962, the counter was taken to various locations in northern Alaska and the body burdens of over 700 people were measured.

The Shadow Shield whole body counter has been described in earlier reports [2.1, 2.2, 2.5, 2.6] and elsewhere in this report. It weighs about 5 tons. It was shipped to Fairbanks by barge and truck. From Fairbanks everything was carried by air freight. A transistorized 512-channel pulse height analyzer was used to analyze pulses from the scintillator. Backgrounds were taken with a sugar sack phantom, stored in the analyzer, and automatically subtracted from the spectrum of each subject. Data were recorded by electric typewriter and on punched paper tape. Power was obtained from local power lines or from a portable motor-generator. No difficulties were encountered with the instrumentation during the trip. Where possible, the counter was placed on a concrete floor, but at some locations it was assembled outside the ground.

The counter was calibrated for K^{40} and Cs^{137}. The variations in counter sensitivity with body size are unimportant within the range of sizes encountered. Counting periods of 5 or 10 min were used.

Figure 2.4 shows a map of Alaska. The four Eskimo villages where the counter was located are marked with circles. The approximate Eskimo population is shown under the name of each village. The counter was located at Kotzebue, Barrow, Anaktuvuk Pass, Kotzebue, and Point Hope, in that order. The second stop at Kotzebue was made to count people from Little Diomede Island. They come to Kotzebue to trade every summer after the sea ice has broken up and disappeared.

The Eskimos were very cooperative in these measurements. A Point Hope Eskimo was hired to help us contact the natives and to interpret for us in the cases where the Eskimo did not speak English. At Kotzebue, subjects were obtained through a sign placed in the village post office. At Barrow and Point Hope, each person over 12 yr old was sent a written invitation describing what we were doing and suggesting a time they could be counted. At Barrow, about 50% of those invited came in to be counted. At Point Hope, almost all those invited were counted. In the smaller village of Anaktuvuk Pass, the request was passed by word of mouth and almost everyone over 12 responded.

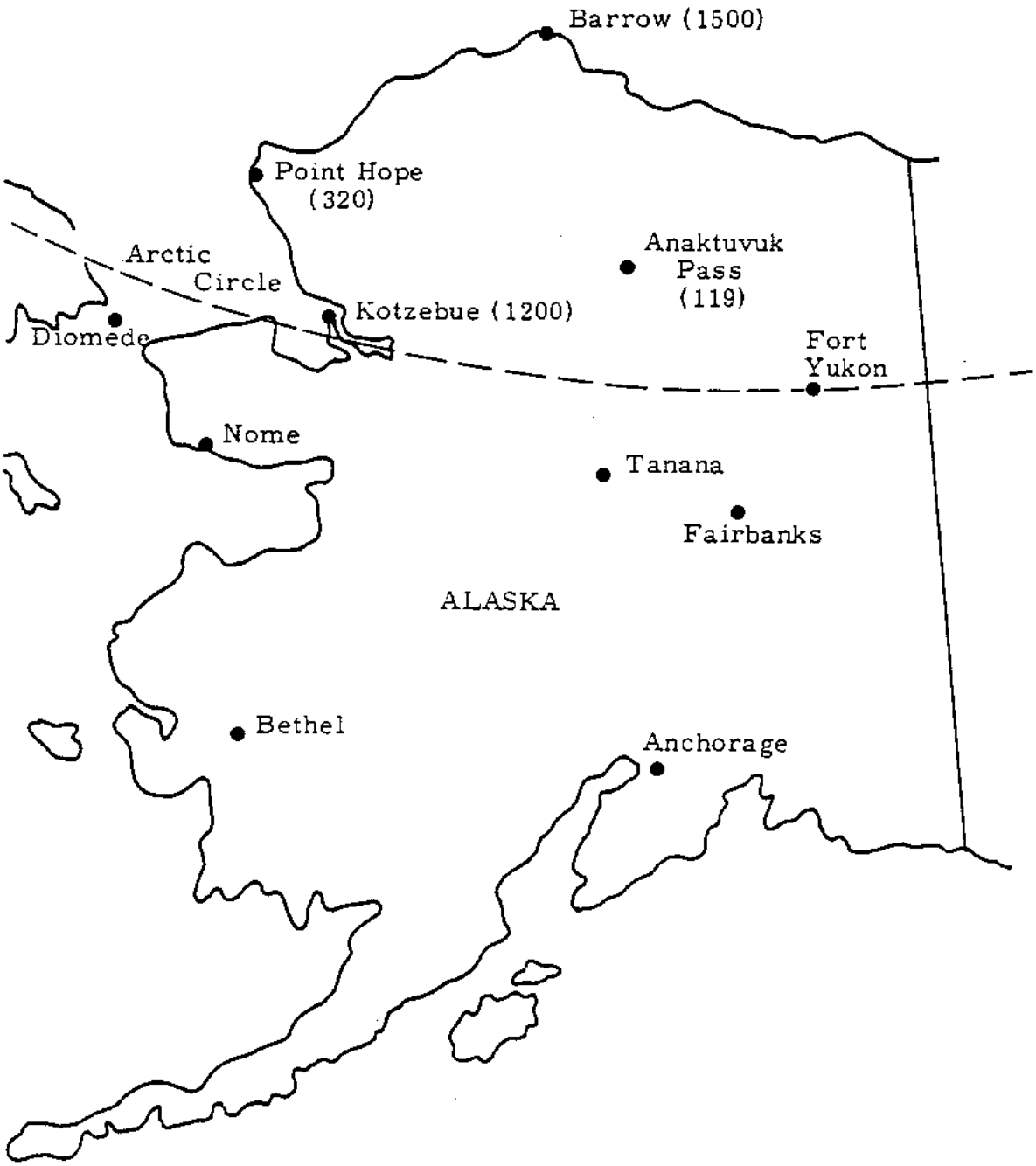

FIGURE 2.4
Map of Alaska

ARCHIVE RICHLAND, WASH

Table 2.2 gives the average, minimum and maximum body burdens of Cs^{137} of permanent Eskimos residents of the villages that were studied. Figure 2.5 gives histograms of the amounts found. For comparison, the average body burden of Cs^{137} of subjects counted at the Hanford whole body counter at Richland, Washington, during this period was about 5 to 7 nc. The first measurements on Lapps gave as high as 361 nc. Numerous measurements made in the Fall of 1961 gave 320 and 190 nc average body burdens for male and female Swedish Lapps and 243 and 123 nc for Finnish Lapps, respectively.(2.7)

TABLE 2.2

Cs^{137} (nc) BODY BURDENS IN ALASKAN ESKIMO VILLAGES

Village	Number of Subjects	Minimum	Maximum	Average	Average for Males	Average for Females
Point Hope	107	3	119	17	20	13
Diomede	12	8	35	22	--	--
Barrow	259	8	166	52	66	40
Kotzebue	132	17	518	138	147	118
Anaktuvuk	52	83	790	421	474	343

While at Kotzebue, natives from villages nearby were counted when they came in for treatment at a Public Health Service hospital there. The results of these measurements are given in Table 2.3. Because of the small number of subjects from each village, the differences in average burden are not too significant. However, they suggest that differences may exist even between neighboring villages.

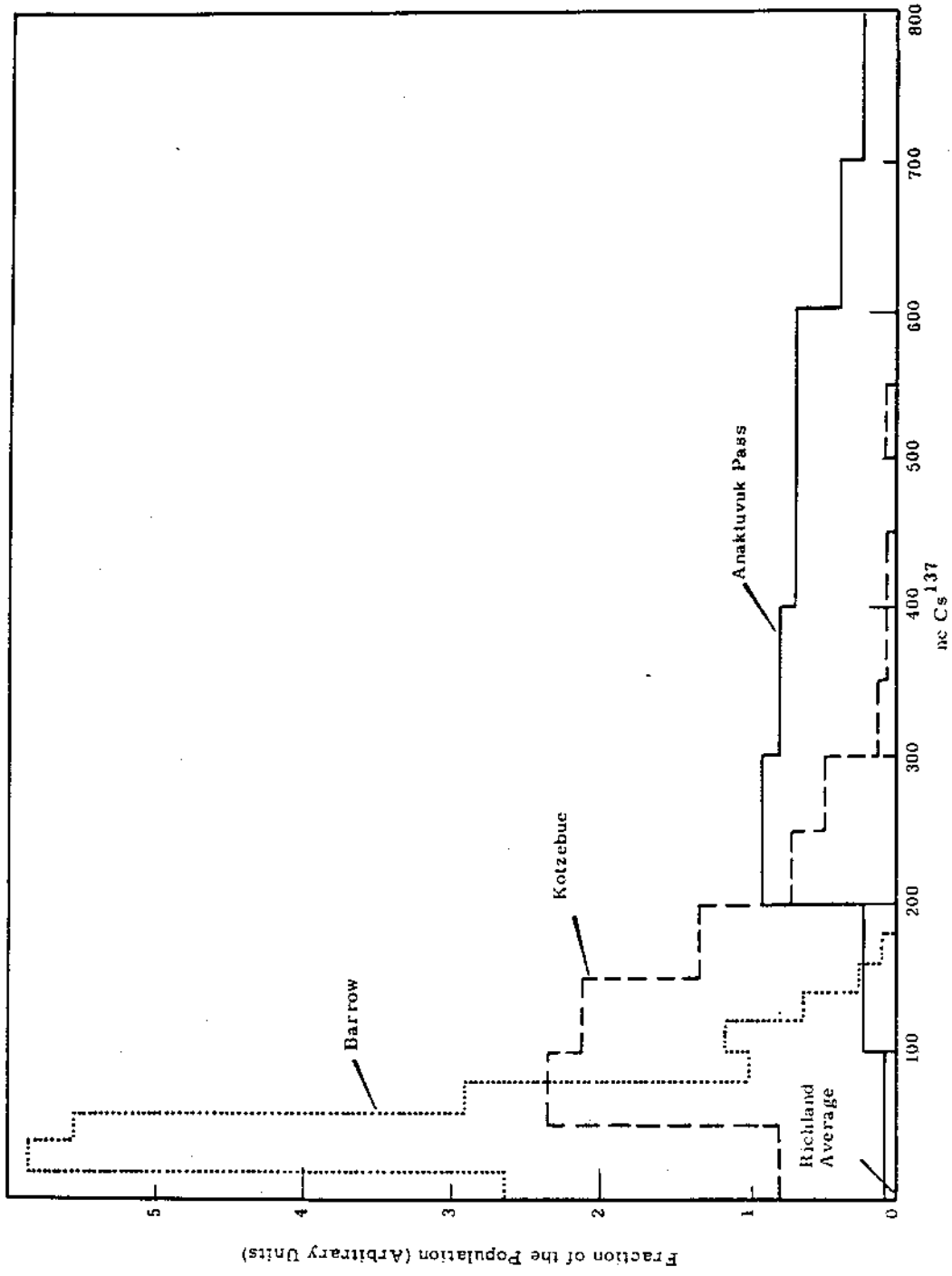

FIGURE 2.5

Distribution of Cs^{137} in Permanent Residents of Alaskan Eskimo Villages

TABLE 2.3

Cs^{137} IN ESKIMOS FROM NEAR KOTZEBUE

Village	Number of Subjects	Average nc Cs^{137}
Ambler	1	233
Deering	3	133
Elim	1	50
Kiana	2	212
Kivalina	3	91
Kobuck	2	273
Noatak	3	129
Noorvick	3	174
Point Hope	3	45
Selawick	1	131
Shungnak	1	221

The school system maintained for the Alaskan Eskimos requires that the children of high school age be away from home at boarding schools from September through May of each year. Our measurements were made during the period when the students were at home and included many of them. Table 2.4 lists the average Cs^{137} body burdens of the students. They are lower on the average than those of the permanent residents of the same villages. This is to be expected. While at school, the students are on diets consisting almost exclusively of food shipped in from outside Alaska and having a relatively low Cs^{137} content. During the school year, their body burdens would decrease (the effective half life of cesium in the body is about 100 days) and would increase again during the summer months, but on the average would be lower than if constantly on the same diet as the permanent residents.

TABLE 2.4

Cs^{137} BODY BURDENS OF ESKIMO STUDENTS

Village	Number of Students	Average nc Cs^{137}	
		Permanent Residents	Students
Point Hope	9	17	14
Barrow	44	52	11
Kotzebue	13	138	29
Anaktuvuk	4	421	227

No isotopes other than Cs^{137} and K^{40} were detected in the Eskimos except for two subjects who had a few nanocuries of Zn^{65}. These people occasionally ate canned oysters which probably led to the Zn^{65} burdens. External body contamination, mainly Zr-Nb^{95}, was frequently noticed. There were no facilities for having the Eskimo shower, but they did change from their own clothes into paper shirts and pants. The interference from this external Zr-Nb^{95} was minor and easily corrected.

At both Barrow and Kotzebue there were significant numbers of white people who did not eat any native foods. Fourteen such people were counted at Barrow and 54 at Kotzebue. The body burdens were typical of those of people in the rest of the United States: averages of 6 and 7 nc, respectively, at Barrow and Kotzebue.

It is expected that the high body burdens and the differences between the body burdens of the Eskimos from different villages can be explained by differences in dietary habits. All of the subjects were questioned at length about their diet. Environmental and food samples were collected and were either counted on special holders in the shadow shield whole body counter or were subjected to examination in the laboratory. A comprehensive ecological study of these Alaskan communities based on these data, the whole body counting results, and data obtained in previous years will be prepared. At present, however, it appears that the high body burdens can largely be correlated with high levels of Cs^{137} in reindeer and caribou and that the latter are produced by high levels accumulated in lichens.

Acknowledgements

The authors are indebted to Kasumi Kasugi of the Public Health Service for the use of the hospital facilities at Kotzebue and Barrow; to Max C. Brewer, Director of Arctic Research Laboratory, for invaluable support in transporting equipment to Barrow and Anaktuvuk Pass and the use of the laboratory facilities; and to Amos Lane for his help in contacting Eskimo subjects and for interpreting.

Cs^{134} in Alaskan Eskimos and in Fallout - H. E. Palmer and R. W. Perkins

Whole body counter measurements of Alaskan Eskimos during the summer of 1962 showed the presence of Cs^{134} as well as Cs^{137}. Cs^{134} was also found in reindeer and caribou meat, and its analysis was confirmed by coincidence counting. There was generally about 1% as much Cs^{134} as Cs^{137}. Cs^{134} was also found on air filters collected at Richland, Washington.

The first report concerning Cs^{137} in Laplanders [2.4] also mentioned a small bump in the pulse height spectrum at 800 kev. After further study, Liden and Andersson concluded that the bump was caused by Cs^{134}. [2.8] The identification was made through coincidence counting and half-life measurements. The Cs^{134} was found both in people and in reindeer meat and in the same abundance relative to Cs^{137} in both. There was about 1.6% as much Cs^{134} as Cs^{137} in measurements made in March of 1961.

The same Cs^{134} peak was found in the spectra of some Alaskan Eskimos during the work described in the preceding paper. Figure 2.6 shows the average spectrum for the ten Eskimos with the highest body burdens found in 1962. The peak is clearly visible. It is also visible in the spectra of the individual Eskimos of this group, particularly that of the highest individual (790 nc Cs^{137}), but better statistics are obtained by averaging the spectra. All of the individuals in this high group were from Anaktuvuk Pass. The average spectrum of all the people counted at Anaktuvuk Pass showed the Cs^{134}, but it was not as well resolved as in the spectrum of the high group.

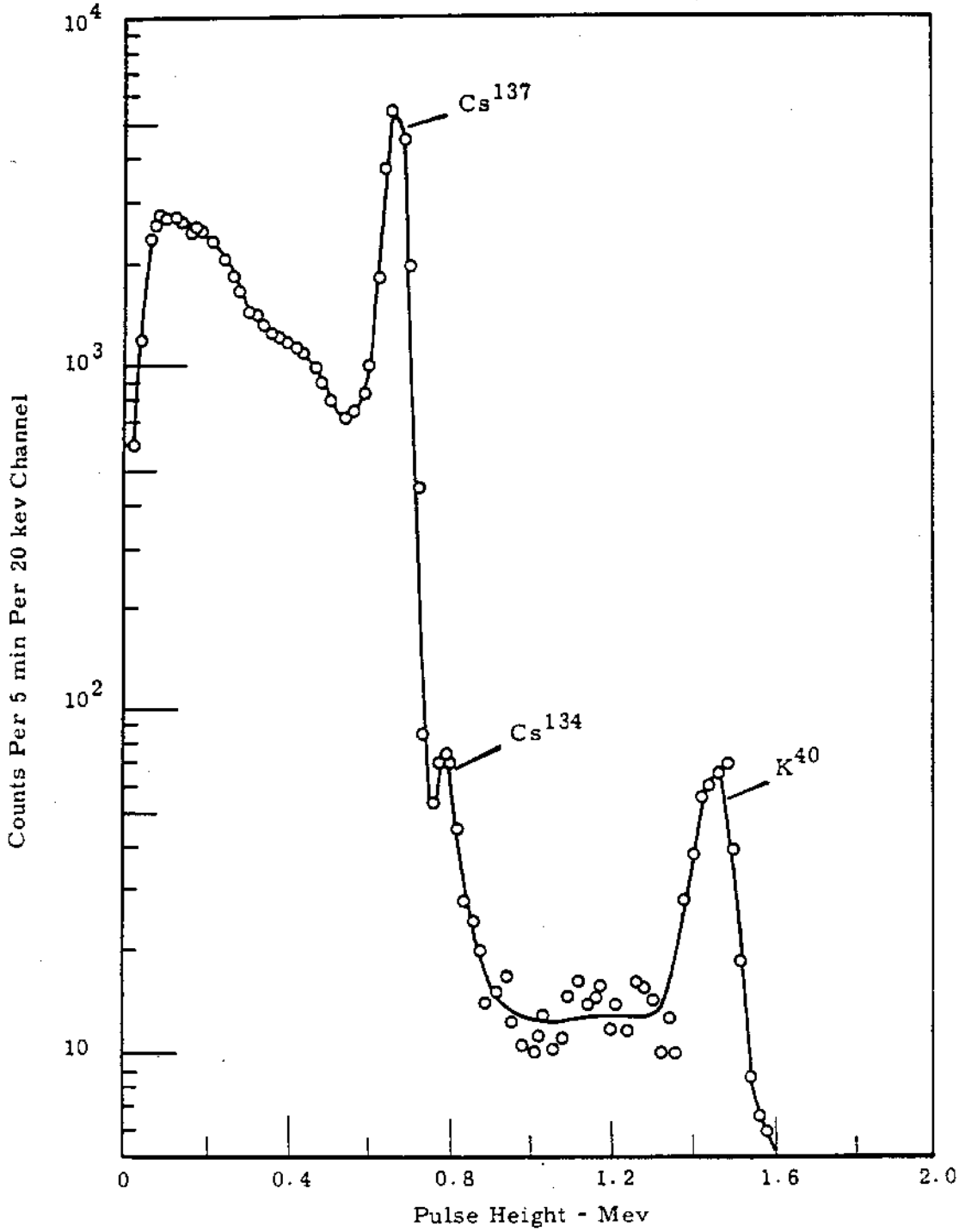

FIGURE 2.6

Average Pulse Height Spectrum for the Ten Eskimos Counted in Alaska in 1962 that had the Highest Body Burden

The peak could not be identified in the spectra of individuals or groups from elsewhere in Alaska. It was felt that this might be due to poor statistics in the groups with the lower body burdens. The average spectrum of 200 people counted (for 20 min each instead of 5 to 10 min for the Eskimos) at the Hanford Whole Body Counter at Richland, Washington, during 1961 was computed to see if any evidence for Cs^{134} could be found. The statistical uncertainity in the K^{40} and Cs^{137} contributions to the spectrum in the neighborhood of the Cs^{134} peak was still so great, however, that a peak a few percent as high as the Cs^{137} peak could not have been discerned had it been there.

Comparing photopeak heights and correcting for gamma ray abundances and counter efficiency and resolution gave a Cs^{134}/Cs^{137} activity ratio of 1.18%. Matching the sum spectrum of the Eskimos with Cs^{134} and Cs^{137} sources in water gave 1.25%. The Eskimo measurements were made in July, 1962. Correcting for decay of the two isotopes gives a ratio of 1.8% for March, 1961. This is reasonable agreement with the ratio found in Lapland.

Measurements of reindeer and caribou meat collected in Alaska in the summer of 1962 also showed the presence of Cs^{134}. The Cs^{134} content of these meat samples was verified and measured by gamma-gamma coincidence counting of the 0.605 and 0.797 Mev cascade photons in the manner reported by Liden and Andersson. A 3-lb meat sample was sandwiched between two 9-3/8 in. diameter by 4 in. thick NaI(Tl) scintillators. The output from one of these crystals was routed to the mixer amplifier of an RIDL 400 channel transistorized analyser, while the signal from the other crystal was fed to the normal signal input of the analyzer. Pulses greater than 0.51 Mev from the first crystal allowed coincidence pulses from the second crystal to be stored. The coincidence spectrum obtained in this manner was compared with that of a standard Cs^{134} source of similar geometry. These measurements showed the Cs^{134} to be present in a concentration of 0.82% of the Cs^{137}.

Cs^{134} has also been found in fallout at Richland, Washington. An air filter which collected fallout from early December 1962 through early January 1963, showed a Cs^{134}/Cs^{137} ratio of 1.6%. Although Cs^{134} is produced in reactors, there is no reason to suspect the Hanford plant as the source of the isotope on this filter. The activity on the filter is comparable with that on other filters obtained throughout the Pacific Northwest. Presumably most of the cesium on this filter was produced during the weapon testing that started late in 1961.

The presence of Cs^{134} in Alaska and in the Northwest (particularly, in the latter case, in recent fallout) has an important bearing on the discussion as to its source. The formation of Cs^{134} at concentrations of 1.6% of the Cs^{137} from U^{235} fission would require a Cs^{134} fission yield of 7×10^{-3}%. This is about 500 times higher than the reported upper limit to the fission yield.[2.9] Cs^{134} can be formed in nuclear reactors by neutron capture in the fission product Cs^{133}. Liden and Andersson refer to Prawitz who calculated that 6 mo exposure of U^{235} to a flux density of 10^{13} neutrons/cm^2/sec would result in a Cs^{134}/Cs^{137} ratio of 0.33.[2.10] Blomeke and Todd, however, would give a ratio of 0.023 for these same conditions.[2.11] An elementary calculation was made which agreed with the low value of Blomeke and Todd. Liden and Andersson considered the possibility that the Cs^{134} in Lapland had come from the accident at Windscale. The high reactor yield predicted by Pawitz made this possibility seem reasonable. This hypothesis no longer seems reasonable, however, for several reasons: (1) Prawit's calculated yield is apparently too high by a factor of about ten, (2) the presence of Cs^{134} in other regions very remote from Lapland and its constant proportion to the Cs^{137} present seems very hard to explain as the result of a particular accident, and (3) the presence of Cs^{134} in current fallout at about the same proportion as must have been present in earlier fallout indicates that it is still being formed. We feel that the source of the Cs^{134} remains to be identified.

Cs^{137} Urinary Excretion by Alaskan Eskimos - H. E. Palmer, W. C. Hanson and B. I. Griffin

Twenty-four hour urine samples were obtained from 15 Eskimos with Cs^{137} body burdens between 36 and 684 nc. The urinary excretion rate was 0.6% of the body burden per day. Better correlation was obtained by relating the Cs^{137} and potassium excretion: 0.22% of the body burden was excreted in the urine per gram of potassium in the urine.

During the study described in the preceding papers, opportunity was taken to study the relations between the body burden of Cs^{137} and the amount eliminated in the urine. These data are of basic physiological interest and are also of interest in establishing the usefulness of urinalysis as a method for studing body burdens.

Both the body burdens and the amount of Cs^{137} in the urine were determined by counting with the Shadow Shield whole body counter. The urine collected was diluted with water to 2 liters and placed in a standard position below the scintillator. Standard solutions of Cs^{137} gave a calibration of 4000 counts/20 min/nc. A person with a body burden of 50 nc would excrete 0.35 nc in one day if the biological half-life is 100 days; this would give 1400 counts over a background of 240 counts.

Fifteen Eskimos were asked to collect all the urine they passed in a 24 hr period. These Eskimos lived at Kotzebue, Barrow, and Anaktuvuk Pass; those with the highest body burdens came from Anaktuvuk Pass. The body burdens ranged from 36 to 684 nc.

Figure 2.7 shows the Cs^{137} body burden versus the Cs^{137} in the urine samples. The line drawn through the points is a least-squares fit and has a slope of 0.6% of the body burden per day. Taylor, Vennart, and Taylor recently reported (2.12) an average urinary excretion rate of 0.6% of the body burden per day for five men involved in an accident. A literature search produced twenty other studies of cesium elimination with reported effective half-lives of 63 to 157 days with an average of 119 days. A 119 day half-life is equivalent to a total excretion rate of 0.58% of the body burden per day;

about 90% of the cesium excreted is in the urine making the urinary excretion rate 0.52% of the body burden per day.

The line in Figure 2.7 was fitted by least squares but was required to pass through the origin. This resulted in several points being at considerable distances from the line. Scatter in the data were expected because of the wide variations that had been reported in effective half-life and because of statistical uncertainties in the counting. In addition, however, it was known that due to misunderstandings, full day urine samples were probably not collected by some of the Eskimos. This was apparent from the volume collected and from the amount of potassium present in it. The potassium was determined by measuring the amount of K^{40} present in the same count in which the Cs^{137} was determined.

Since cesium and potassium are somewhat similarly metabolized in the body, it seemed reasonable to compare the amounts present in the urine. Figure 2.8 shows the Cs^{137} body burdens versus the ratio of the amounts of Cs^{137} and potassium in the urine. The points fall around the least-squares line much better than they do in Figure 2.7. The line has a slope of 0.22% of the body burden per gram of potassium in the urine.

The good correlation between the Cs^{137} body burden and the cesium-potassium ratio in the urine indicates that measurements of the latter among groups of people should give a good estimate of their average body burden and indicate that full day samples are not absolutely necessary.

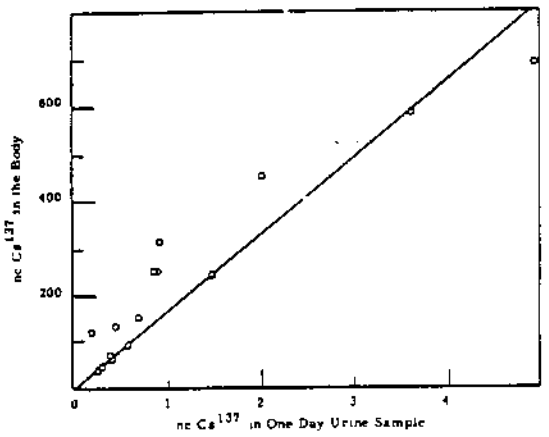

FIGURE 2.7

Cs^{137} in the Whole Body
and in One Day Urine Samples of Alaskan Eskimos

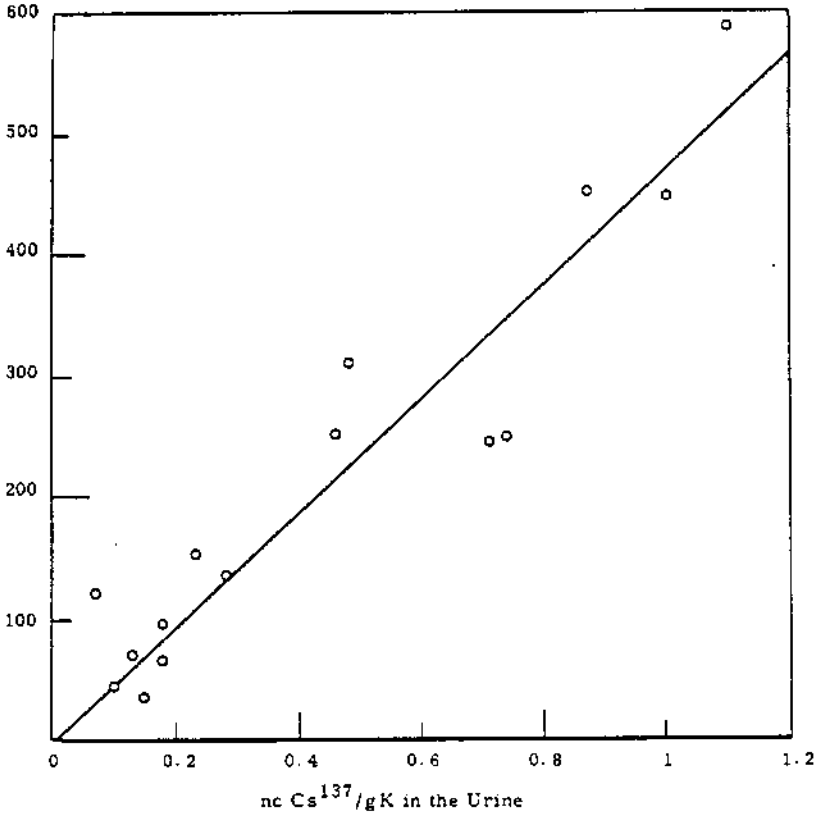

FIGURE 2.8

Cs^{137} in the Whole Body and in the Urine of Alaskan Eskimos. (That in the urine is normalized to the amount of potassium in the urine)

Determination of P^{32} in Vivo - H. E. Palmer

To combat interference from Zn^{65}, the P^{32} counter was moved to a position over the head of the subject. Some improvement in the correction for the presence of other isotopes also resulted. The background of the counter decreased by substituting air for the lucite in the light pipe.

A method for determining as little as 250 nc of P^{32} in the human body in the presence of the normal amounts of radioactivity has been described.[2.13, 2.14] Bremsstrahlung emitted during the decay of the P^{32} or produced by the beta rays is detected in a large, thin NaI(Tl) scintillator. Zn^{65} was found to be a serious interference in the use of this method for determining P^{32} in subjects who had eaten whitefish from the Columbia River. Large body burdens of Zn^{65} also result from the whitefish diet and much of the isotope is initially deposited in the liver. Since the P^{32} counter was centered over the lower end of the sternum, part of the liver was directly below the counter, and much scattered Zn^{65} radiation that could not be distinguished from the bremsstrahlung was detected.

To decrease the interference from Zn^{65}, the P^{32} counter was moved to a position alongside the head. Counts on patients receiving P^{32} therapy indicated that the counting rate for P^{32} at the head position was 73% of that over the sternum. To correct for the interference of other isotopes comparative counts were made of subjects believed to contain no P^{32} with the large, whole body counter scintillation crystal and with the P^{32} counter. With the P^{32} counter over the sternum no reasonable correlation was ever obtained between the counting rates in the two counters. The present practice is to position the two counters at symmetrical positions at the head. The apparatus is shown in use in Figure 2.9. In this position the correlation between the two counters is better; but, with the reduced sensitivity, the uncertainties permit detection only down to body burdens of about 200 nc.

FIGURE 2.9

Apparatus for P^{32} Counting

As a test of how well body burdens can be determined at low burdens of P^{32}, three subjects with known burdens of P^{32}, and for whom individual backgrounds were known, were counted for 30 min at the head position. The results are given in Table 2.5.

TABLE 2.5

TEST OF THE P^{32} COUNTER

Subject	Body Burden nc P^{32}	nc P^{32} as Determined With P^{32} Counter
1	145	165 ● 43
2	86	56 ± 43
3	57	90 ± 43

These results indicate that P^{32} body burdens of about 50 nc can be detected when there is an individual background available but that the estimate of their size may be in error by a factor of two.

A further improvement in the P^{32} counter was obtained by reducing the background inherent in the counter components. A study of this backgroun showed that about half of it was originating in the lucite light pipe--probably from Cerenkov radiation. Operation with an air light pipe was tried. The scintillator was mounted at about the same distance from the phototube but on a hollow cylinder lined with shiny aluminum foil. Background was reduced by one-third and the pulse height slightly increased.

The P^{32} counter was applied to a study to see if P^{32} could be detected in people eating whitefish from the Columbia River. In particular, one subject who ate whitefish regularly was counted at intervals throughout the year.(2.15) In the late fall when the P^{32} concentration in the whitefish was the highest, his P^{32} burden could be detected above his burden of about 120 nc of Zn^{65}. It was estimated that he contained several hundred nanocuries of P^{3}

Acknowledgement

The subjects receiving P^{32} therapy were patients of E. E. Osgood of the University of Oregon Medical School; their services were obtained through him.

Whole Body Counting Following the Recuplex Accident - H. E. Palmer

Measurements of neutron induced Na^{24} in the bodies of the people exposed in the Recuplex accident were used to estimate neutron doses. K^{42}, Au^{198}, and P^{32} were also observed.

On April 7, 1962, a criticality accident occurred in a plutonium waste chemical recovery facility at Hanford known as Recuplex. When the accident occurred, there were 22 people in the building housing the facility. After examination and treatment at the hospital, four persons, including the three most highly exposed, were sent to the Hanford Whole Body Counter [2.16] for examination. The next day all but one of those remaining were also examined at the counter; the last man was examined the following day. The measured values of Na^{24} activity, corrected for decay since the time of the accident, and the individual's weights are given in Table 2.6. No correction was made for Na^{24} that might have been eliminated before the counting took place, it is estimated that only a few percent was missed in this way for those counted immediately. The quotient of the number of microcuries by the body weight in kilograms was multiplied by 215 rad-kg/μc to obtain the first collision dose to the person.

The factor 215 rad-kg/μc was obtained by averaging the following two experimental values. Measurements [2.17] with a burro at the mockup of the Oak Ridge criticality accident gave 204 rad-kg/μc. An experiment with solutions of sodium salts in bottles at the Godiva II reactor gave 226 rad-kg/μc. [2.18]

Recently the dosimetry investigation of the Vinca critical accident was reported [2.19] for which an average factor of 81 rad-kg/μc was used (neglecting corrections for the weights of the individual persons). The difference between this figure and those above is due to the presence of a very large proportion of low energy neutrons near the Vinca reactor. If the threshold detector measurements reported for that reactor and those available from a detector situated near the present criticality accident are used to estimate the neutron first collision dose per unit Na^{24} activation, [2.20], the

TABLE 2.6

WHOLE BODY COUNTING RESULTS

$\mu c\ Na^{24}$	Weight (kg)	Neutron First Collision Dose (rads)
7.55	70.4	23
4.20	98.1	9.2
1.12	82.4	2.9
0.088	55.3	0.34
0.055	72.7	0.16
0.034	70.3	0.10
0.022	95.4	0.05
0.019	85	0.05
0.014	71.8	0.04
0.010	84.8	0.02
0.008	75.9	0.02
0.006	71.7	0.02
0.004	71.2	0.01
0.003	67.1	< 0.01
0.002	68.5	< 0.01
0.001	85.3	< 0.01
0.001	93.4	< 0.01
0.001	61.2	< 0.01
0.001	73.5	< 0.01
0.001	70.8	< 0.01
0.001	56.7	< 0.01
0.001	78.9	< 0.01

rad-kg/μc factor for the Hanford accident is about 2.3 times that for the Vinca, i.e. about 190 rad-kg/μc. This is satisfactorily close to the value used above. The threshold detector measurements for the Hanford accident probably represent a different spectrum than that to which the employees were exposed because of different attenuation and scattering. The comparison of the Vinca and Hanford spectra to estimate the above factor, however, is not much affected by the difference.

It is estimated that the Na^{24} burdens were determined to an accuracy of about 5% where counting data were not limited by statistics. Counting statistics became important for burdens of about 0.001 μc (before correction for decay). Those employees in whom less than 0.001 μc was detected were assigned a dose of less than 0.01 rad.

The whole body counter measurements of Na^{24} were in good agreement with Na^{24} measurements of the blood of the three most highly exposed persons. These two data were used to estimate the neutron doses, because the available neutron personnel dosimeters had been rendered inoperative by the accompanying high gamma ray exposure. Supplementary information was obtained from P^{32} measurements of hair and radioactivity measurements of objects on the persons of those exposed.

The presence of K^{42} was noticed in those people who had large Na^{24} burdens. The amounts present were consistent with estimates from abundance and cross-section data which indicate that there should be about one seventh as many microcuries of K^{42} as of Na^{24}. The three most highly exposed people were counted several more times at the whole body counter. The Na^{24} was observed to disappear with the expected 15 hr half-life. Each of these three men was found to have had some Au^{198} produced in fillings in his teeth. In one case the gold was in bridge-work that could be removed. This made it possible to count him with the P^{32} counter.(2.13) After publication of the original report on the counter, a counting position over the head rather than over the chest was used to reduce interference by other isotopes; the presence of radioactive gold fillings would have prevented measurements over the head.

The first count for P^{32} was made 10 days after the accident. The P^{32} was easily detected. The counting rate due to the P^{32} decreased exponentially with a 14.5 day half-life (i.e., the radioactive decay half-life) rather than the 8 to 10 day half-life observed for subjects who received P^{32} intravenously. This indicated that most of the P^{32} being observed was formed in the relatively tightly bound phosphorous, probably that in the skull, rather than that more mobile portion in which intravenously injected P^{32} appears. Thus, the calibration of the counter, which was done with intravenously injected subjects, was not applicable; if applied anyway, the calibration would have indicated two to three times as much P^{32} as predicted from the activity of the Na^{24} present.

Plutonium X-Ray Scintillation Counters - B. I. Griffin and W. C. Roesch

> Reduced dark-noise in photomultiplier tubes and reduced background from counter components and shields have made it feasible to plan sensitive X-ray counters for the detection of plutonium in vivo.

Scintillation counters for the detection of the X-rays which are emitted following the decay of plutonium have been in use for some time in the detection and measurement of plutonium in shallow wounds in the body.[2.21] Similar larger counters have been considered for detection of plutonium deeper in the body, particularly in the lungs.[2.22] The principal problem in such an application is the reduction of the background rate of the counter to a sufficiently low value that statistically significant measurements can be made of the low X-ray fluxes of interest.

A major source of the background in X-ray scintillation counters for plutonium is the counting rate associated with the dark current of the photomultiplier tubes, i.e., the dark-noise. The pulse height spectrum of the dark-noise for a typical photomultiplier exhibits two (or more) exponential distributions; see Figure 2.10. The tail of the spectrum extends into the region in which the pulses from the plutonium X-rays fall. Since they cannot be distinguished in any simple way from the pulses from the scintillator, they constitute a background of the counter. Different types of photomultiplier tubes

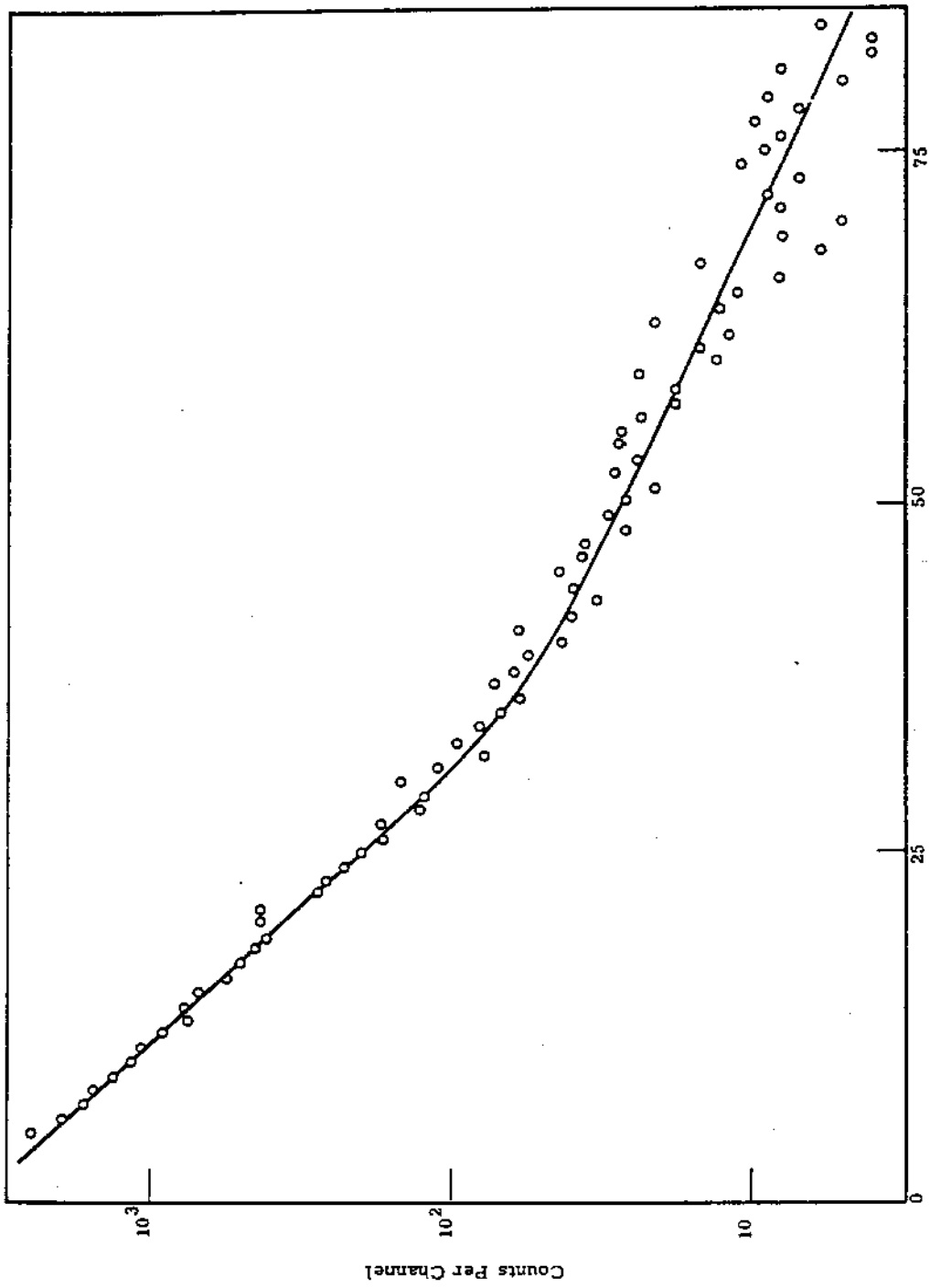

FIGURE 2.10

Pulse Height Spectrum of the Dark-Noise for a Typical (9514-S) Photomultiplier Tube

differ considerably in the background rate from dark-noise. Figure 2.11 shows the background counting rates of a particular scintillator when on two different types of tubes. The gains of the two tubes were adjusted by changing the voltage to make them as nearly identical as possible. The large increase in the background rate of the 6292 below 20 kev is due to the dark-noise of that tube; the dark-noise of the 9514 does not become important until below a pulse height equivalent to about a few kilovolts. The range of pulse heights ordinarily used for the counting of plutonium is shown on the figure. It is quite evident that the smaller dark-noise of the 9514 will be very important in applications to X-ray counting. Table 2.7 lists the rate at which counts due to dark-noise were received in the channel used for counting plutonium X-rays for several different tubes.

TABLE 2.7

DARK NOISE IN THE PLUTONIUM X-RAY CHANNEL

Tube	Counts/Minutes
DuMont 6292	99
DuMont K1428	20
RCA 6655A	10
EMI/US 9536 S or B	0.5
EMI/US 9514 S or B	0.1

The next most important source of background in X-ray scintillation counters has been the radioactivity in nearby objects. The following tests were performed with counters similar to those used for wound countings;[2.2] the NaI(Tl) scintillator was 1 mm thick by 1-3/4 in diameter, covered by a 0.001-in. thick aluminum window, and mounted on glass which was in turn mounted on a 2-in. photomultiplier tube. The mounting glass was stripped from another scintillator and placed in front of the counter. The background rate increased by more than 50%. A quartz mounting glass did not increase the background appreciably. The aluminum housing from the scintillator did

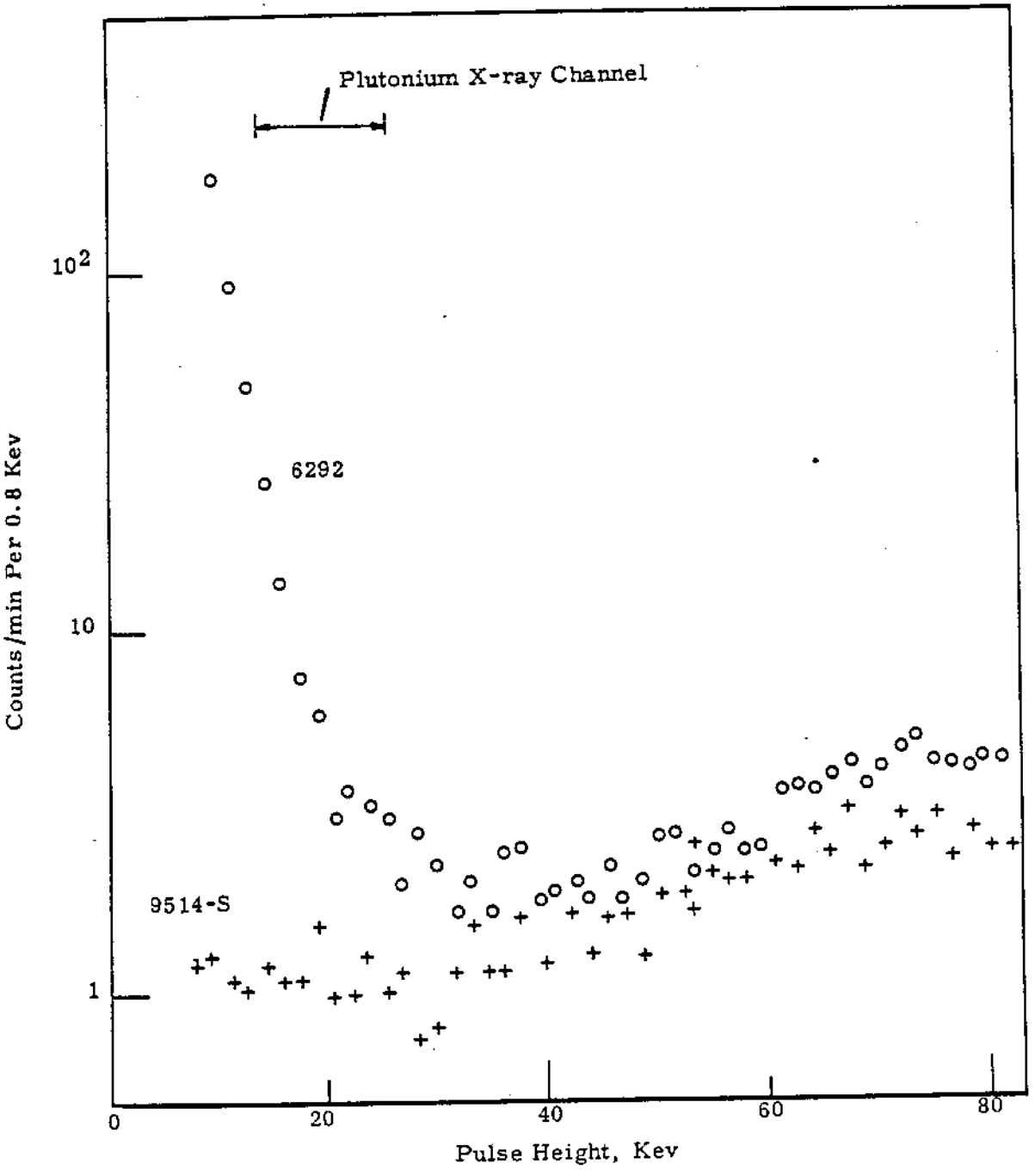

FIGURE 2.11

Comparison of the Background Pulse Height Spectra
of the Same Scintillator on Two Different Photomultiplier Tubes

not increase the background appreciably. The background counts from materials such as these, which are in direct contact with the scintillator crystal, could be produced by beta rays. The background from objects separated from the crystal by more material would be due to gamma radiation. The response to gamma radiation is minimized by using thin crystals. Making them too thin does not help in this regard, however, because very thin crystals will respond to secondary electrons formed by gamma rays in the material surrounding the crystal. A scintillator 0.5 mm thick was tested and found to have approximately the same background rate as the 1 mm crystal, so further reduction in thickness does not seem worthwhile.

A lead shield was used in these studies to eliminate external radiation. There is some radioactivity in the lead, however. Most of the gamma rays emitted in the lead are of high energy that would not count efficiently in the X-ray counter. Still, these rays scatter and lose energy in the lead and reach quite low energies before being absorbed. The low energies are detected quite efficiently by the counter. Figure 2.12 shows the background spectrum of the counter described above when inside a lead shield. There is a broad peak in the region around 80 kev. This corresponds to the relative minimum in the absorption coefficient of lead below the K absorption edge which permits more rays in this energy range to penetrate through the lead; fluorescence radiation from the lead is also in this energy range. The rise in the spectrum at low energies is presumably due to the production of lower energy radiation by degradation of the higher energy rays in the low atomic number materials of the counter. The rays contributing to the peak can be reduced in number by the use of Thoraeus filters, layers of absorbers placed on the inner walls of the lead shield with each layer of lower atomic number than the one outside it. The thickness of the layers should be chosen to absorb efficiently radiation of the above type from the shield in front of it but not so thick as to permit appreciable buildup of low energy radiation from even higher energy radiation from the lead. Fluoresence radiation emitted by the layer will be lower in energy than that of the shield ahead of it and in the final shield will l degraded to energies too low to interfere with the counting. Figure 2.12 also

shows the reduction in the background spectrum resulting from lining the lead shield with a Thoraeus filter consisting of 0.140, 0.015, and 0.028 in. of cadmium, copper, and aluminum, respectively.

When the scintillator described above, mounted on glass, was used with a good 9536-B photomultiplier tube and used in the lead shield plus Thoraeus filter described above, the background counting rate in the plutonium X-ray channels was 1.5 counts/min. With the 9514 tubes and quartz-mounted scintillators the background should be even less. This puts it in the range of counting rates expected from maximum permissible body burdens of plutonium in the lung. Of course, to obtain statistically useful results it would be necessary to use a multiple-counter array. Design and construction of such a counter is being planned.

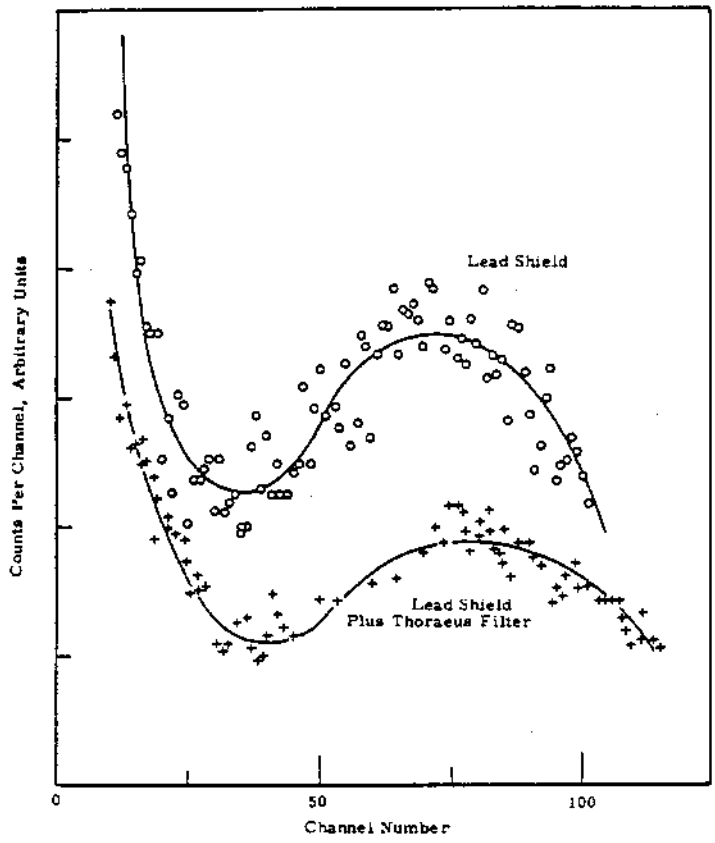

FIGURE 2.12

Effect of a Thoraeus Filter
on the Background Spectrum of an X-ray Counter in a Lead Shield

Pulse Shape Discrimination in Fast Neutron Dosimetry - L. L. Nichols and W. C. Roesch

Pulse shape discrimination circuits were built and tested; the space charge method was adopted for further study. The pulse spectra from stilbene with pulse shape discrimination were measured for known doses of monoenergetic fast neutrons.

Scintillation counters employing organic scintillators would be useful in fast neutron dosimetry if the scintillations due to recoil protons could be distinguished from those due to secondary electrons from gamma rays. Such scintillators would have high efficiency and the absorbed dose in the scintillator would be very nearly the same as that in tissue because their compositions are fairly similar to that of tissue. Simple pulse height discrimination cannot distinguish between scintillations from recoil protons and those from secondary electrons. Indeed, scintillations due to protons are smaller than those due to electrons of the same energy. Brooks (2.23) found, however, that while scintillations from the two have a similar sequence of events (each has a fast decay with a decay time of a few nanoseconds followed by a slow component with a decay time of a few hundred nanoseconds) the scintillations from the recoil protons have a relatively greater part of their energy given off in the slow component. This fact can be used to distinguish scintillations from the two types of particles and is called pulse shape discrimination.

Several pulse shape discrimination circuits described in the literature (2.23, 2.24, 2.25, 2.26) were built and tested. Circuits employing diodes were found to give trouble with pile-up, stability, and nonlinearity; therefore, circuits employing space charge effects in the photomultiplier tube were chosen for further study. In these circuits the voltage of the last dynode is kept only a few volts negative with respect to the anode. During the fast part of a scintillation the current is so great that it becomes space charge limited in this region. The result is that the voltage pulse appearing at the last dynode is negative rather than positive during this part of the scintillation. It goes positiv

only during the slow component of the scintillation. By suitably balancing the positive and negative components of the voltage pulse, the net pulse appearing at the last dynode can be made nearly zero for the recoil electrons. Then, because of the relatively greater slow scintillation component from protons, the protons will produce a net positive pulse. These positive pulses can be used as gating pulses for a multichannel analyzer while the latter analyzes pulses from an earlier dynode where voltage pulses proportional to the total amount of light released are obtained.

A 1/2-in. thick by 1-1/2-in. diameter stilbene crystal mounted on an RCA 7265 photomultiplier tube was exposed to 1 mrad of fast neutrons of various energies produced by the Van de Graaff. Monitoring was done with the precision long counter. Figure 2.13 shows representative pulse spectra obtained as described above. The signal supplying the gating pulse was passed through a pulse height discriminator that was adjusted so that 98% of the pulses from a Co^{60} source were rejected. At this level protons of 600 kev or more could be counted.

In the ideal case of perfect linearity between the energy of the recoil particles and the resulting pulse height and perfect discrimination between protons and electrons without rejection of any protons, the area under the pulse height spectrum curve would be proportional to the absorbed dose in the scintillator, i.e., the areas under all of the curves in Figure 2.13 would be equal. None of these ideal conditions hold, of course. This investigation is still in progress to determine how the pulse spectra for different energies should be combined to give a result proportional to the neutron absorbed dose.

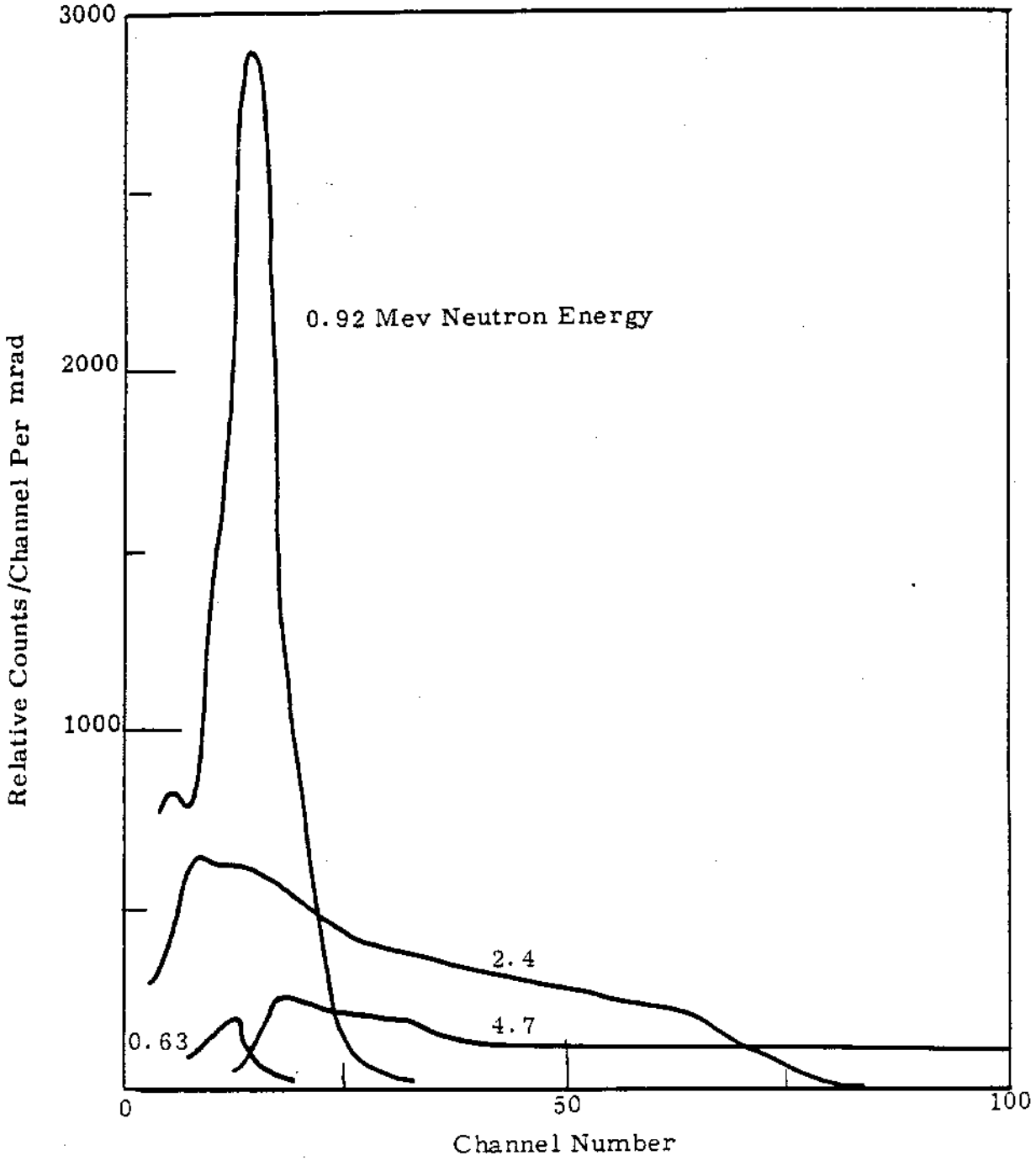

FIGURE 2.13

Pulse Spectra from Stilbene
with Pulse Shape Discrimination for Monoenergetic Neutrons

AEC-GE RICHLAND, WASH.

Lithium-Sandwich Fast Neutron Spectrometer - L. L. Nichols and J. De Pangher

A fast neutron spectrometer consisting of a thin layer of lithium fluoride sandwiched between two solid state detectors was tested for linearity and resolution. It was used to measure spectra of a Pu-Be source and of the Physical Constants Test Reactor.

A fast neutron spectrometer designed by Love and Murray (2.27) consists of a thin layer of lithium^6 fluoride sandwiched between two silicon surface barrier counters. Neutron energy is measured by observing

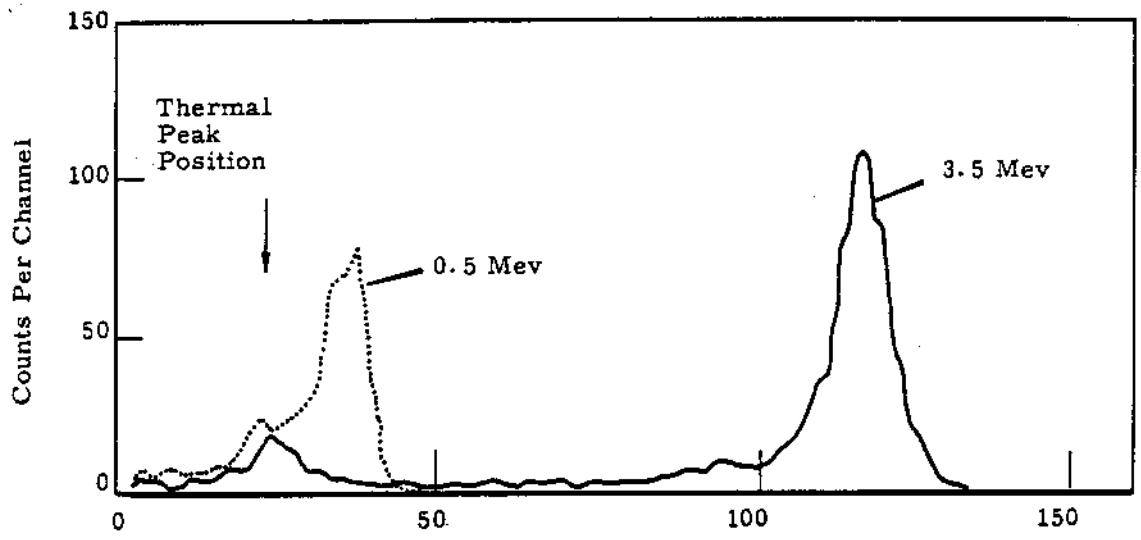

FIGURE 2.14

Response of Lithium-Sandwich Spectrometer
to Monoenergetic Neutrons

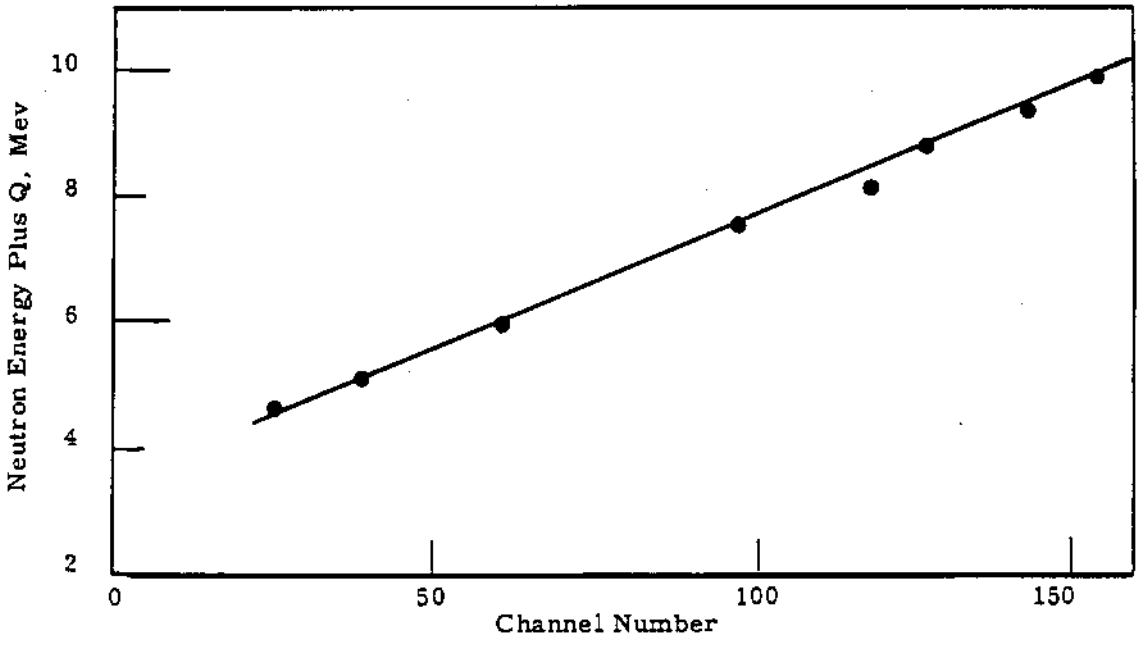

FIGURE 2.15

Relation of Peak Position
to Neutron Energy for the Lithium Sandwich Spectrometer

AEC-GE RICHLAND, WASH.

full-width-at-half-maximum of the peaks was about 300 kev. Neutrons of 16.5 Mev produced reactions leading to charged particle emission from the gold and silicon in the counter. These produced complex pulse spectra that would make spectrographic applications difficult at these high energies. Figure 2.15 illustrates the excellent linearity of the spectrometer.

Figure 2.16 shows the pulse spectrum obtained from a Pu-Be source. The source strength was 1.2×10^5 neutrons/sec. The spectrometer was placed directly in contact with the source. The spectrum was accumulated in 27.5 hr. This example illustrates the chief difficulty in using this sort of spectrometer for radiological physics work: its low sensitivity. At best, only semiquantitative information on the neutron spectrum can be obtained from Figure 2.16.

Figure 2.17 shows a spectrum obtained in the Physical Constants Test Reactor. The spectrometer was placed against a fuel element while the reactor was operated 10 min. . At power levels a few times this, the counting rate became so high and the gamma ray pile-up so bad, that the spectra were seriously distorted. An attempt was made to eliminate the thermal peak by surrounding the counter with cadmium, but so much cadmium was required that it altered the spectrum in the part of the reactor where the device was located. This method of obtaining spectra is being adopted by groups studying radiation damage in in-reactor experiments.

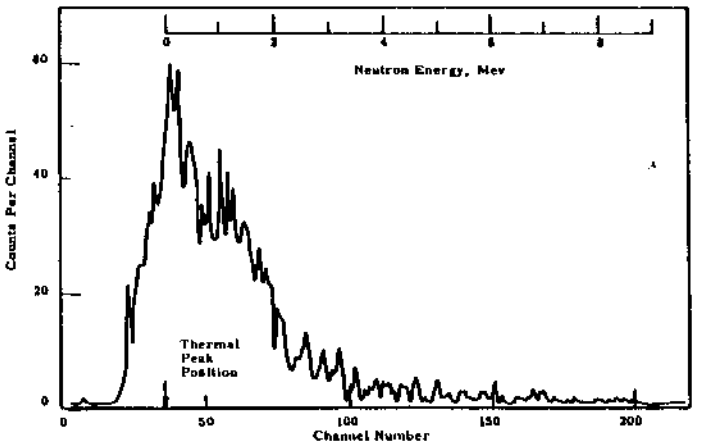

FIGURE 2.16

Pulse Height Spectrum
for Pu Be Neutrons Obtained with the Lithium Sandwich Spectrometer

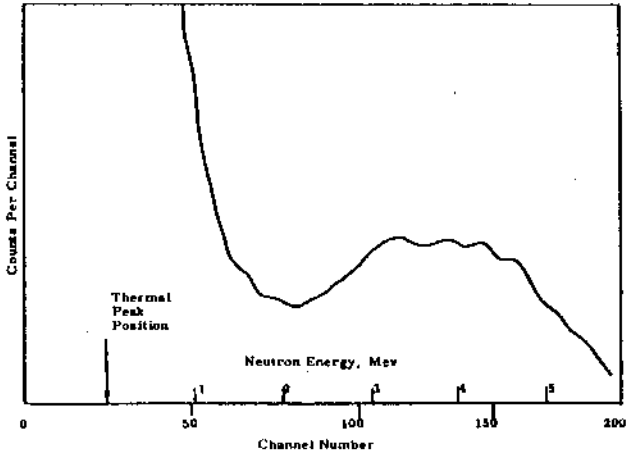

FIGURE 2.17

Pulse Height Spectrum
Obtained in the PCTR with the Lithium-Sandwich Spectrometer

Precision Long Counter: Scattering Corrections - J. De Pangher

Several attempts were made to improve the allowance for scattered neutrons in precision long counter measurements. No improvement resulted. More work is needed to improve the accuracy of precision measurements.

A general method used in studies of the precision long counter was to measure counting rates near different radioactive and accelerator neutron sources and fit them to the equation

$$\mathring{A} = a + \frac{b}{(x + c)^2} \qquad (1)$$

Here $\mathring{A}$ is the counting rate, corrected for deadtime loss, when the center of the source is a distance x from the plane of the front face of the outer polyethylene shield. Constants to be determined are a, b, and c. Two assumptions are implicit in the use of this equation: (1) that the source and the precision long counter act like a point source and point detector, respectively, with the center of the detector a distance c behind its front face. This is implied by the second term of the equation. (2) that there is a scattered flux density of neutrons, represented by a, that is approximately constant in the region where the measurements are made. The constants a, b, and c are determined by an electronic data processing program that minimizes the sums of the fractional deviations of the counting rates from the fitted values. A 1 m from a source the first term in Equation (1) is about 2.5% the size of the second for measurements in the low scattering room at the Hanford Van de Graaff; the uncertainty in the estimate of b is about 0.4 %.

Other expressions have been proposed with the idea that they might fit the data better and lead to improved estimates of b, which is related to the source strength. Anderson [2.28] has used

$$\mathring{A} = (1 - kx)\, a + \frac{b}{(x + c)^2}, \qquad (2)$$

and the equation

$$\overset{\circ}{A} = (1 - \frac{k}{x})\, a + \frac{b}{(x + c)^2} \qquad (3)$$

was suggested in an NBS study on air scattering. The same data to which Equation (1) was fitted were fitted by Equations (2) and (3) by the data processing program. In both cases, however, the uncertainty in b indicated by the program was larger than when Equation (1) was used.

An attempt was made to measure a by using a shadow shield between the source and the precision long counter. The shield is made of polyethylene loaded with 5% boron. It is a frustrum of a cone, 28 in. long with diameters of 2 and 8 in. The effectiveness of the shield in absorbing neutrons coming directly from the source was shown by placing a cylinder of polyethylene 8 in. in diameter by 10-1/2 in. long between it and the counter; this reduced the counting rate only another 3%. Measurements with a Ra-Be source and a Pu-Be source gave counting rates 30% greater than the corresponding a of Equation (1). This could mean that Equation (1) is an inadequate representat of the situation, or it could mean that because of its proximity to the source the shadow shield scatters more neutrons into other scattering masses which then return them to the counter.

The results of the shadow shield measurements were used to fix a in Equation (1) and a and k in Equations (2) and (3). Then the data processing processing program was used to select b anc c to fit the counting data. The resulting uncertainties were again much higher than the original fitting to Equation (1).

These last calculations did serve to explain the discrepancy between Hanford and Harwell efforts to locate the effective center of the counter. At Harwell, a of Equation (1) was determined by a shadow shield measurements and then b and c by curve fitting. When this is done with the Hanford data, as just described, reasonable agreement with the Harwell value of c is obtained.

Calibration of the Polyethylene Double Moderator - R. A. R. Kent

A double moderator system employing polyethylene moderators and a new type BF_3 tube was compared with the original system to obtain the calibration data necessary for its proper use.

The double moderator neutron dosemeter-fluxmeter [2.29] developed by J. De Pangher used paraffin moderators and a privately produced BF_3 tube. In later developments the moderator was changed to polyethylene and commercially produced BF_3 tubes were used. It was felt that the accumulation of changes required a new calibration of the system. Since the earlier system had been carefully calibrated, it was felt that it was only necessary to compare the counting rates of the two systems in the same radiation field to establish the calibration of the later one. The two detectors were exposed simultaneously to monoenergetic neutrons from the Van de Graaff. The $Li^7(p, n)Be^7$, $T(p, n)He^3$, $C^{12}(d, n)N^{13}$, and $D(d, n)He^3$ reactions were used to produce neutrons from 0.063 to 4.15 Mev.

Figure 2.18 shows the experimental data for

$$\frac{PO^{S}_1}{PA^{S}_1} = \frac{\text{Polyethylene dosemeter counts}}{\text{Paraffin dosemeter counts}},$$

and

$$\frac{PO^{S}_2}{PA^{S}_2} = \frac{\text{Polyethylene fluxmeter counts}}{\text{Paraffin fluxmeter counts}}.$$

These data were fitted by least squares by an IBM program. The results for the energy range studied were:

$$\frac{PO^{S}_1}{PA^{S}_1} = 0.681 + 0.168\ E - 0.0401\ E^2 + 0.00334\ E^3,$$

and

$$\frac{PO^{S}_2}{PA^{S}_2} = 0.949 + 0.00768\ E + 0.00443\ E^2 - 0.00106\ E^3.$$

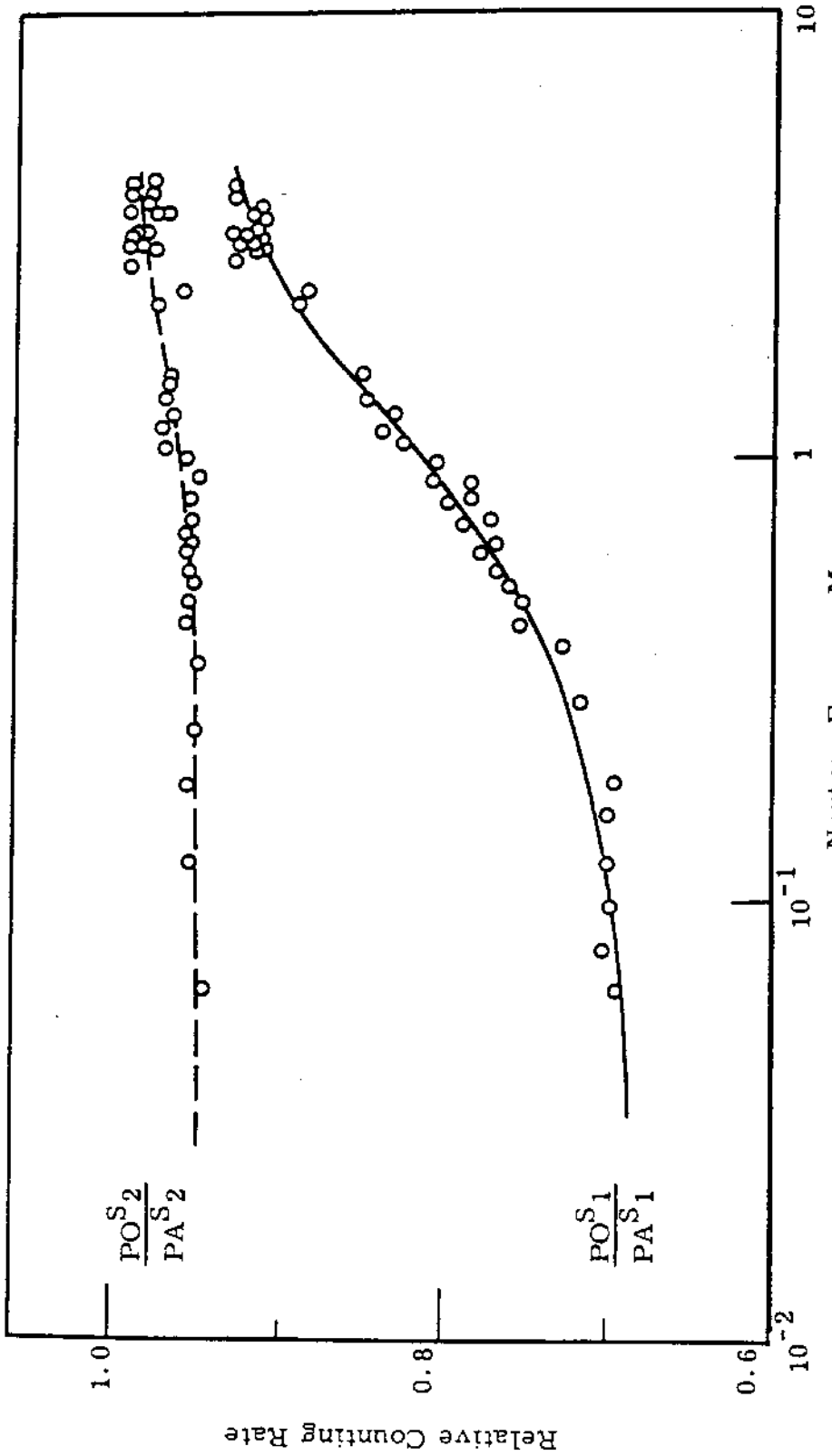

FIGURE 2.18
Comparison of Polyethylene and Paraffin Double Moderators

In using the double moderator one also uses the ratio $r = PO^{S_1(E)}/PA^{S_2(E)}$, which can be obtained from the above data and that for the paraffin system. From the least squares fit:

$$r = 0.157 + 0.258\,E + 0.206\,E^2 - 0.187\,E^3 + 0.0623\,E^4 - 0.00950\,E^5 + 0.000550\,E^6.$$

The relative response of the polyethylene system to neutrons having the same flux density but incident from different directions was also measured. Neutrons from a Pu-Be source were used. The results are shown in Figure 2.19.

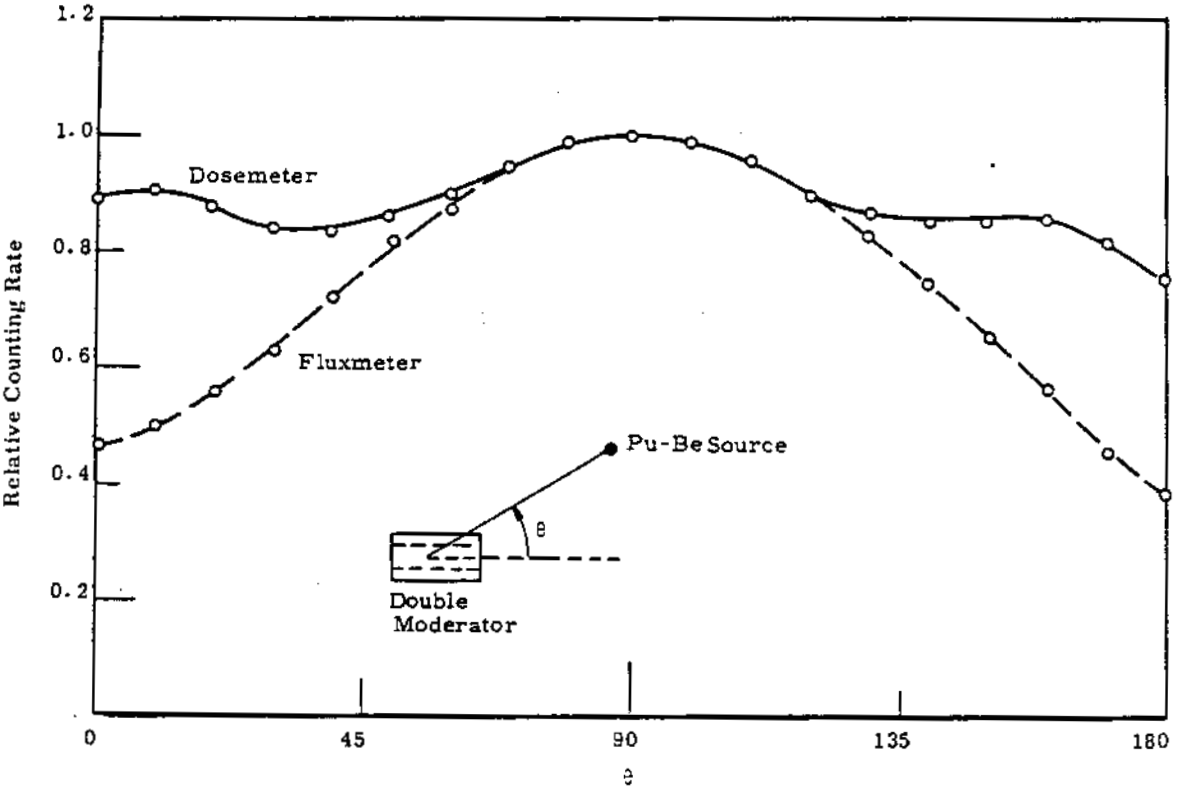

FIGURE 2.19

Dependence of Polyethylene Double Moderator on Angle of Incidence of the Neutrons

Cosmic-Ray Neutron Measurements - R. A. R. Kent

A polyethylene double moderator neutron dosemeter-fluxmeter was used to measure the flux density, dose rate, and average energy of the neutrons produced by cosmic rays near sea level.

Measurements of cosmic-ray neutron dose rate, flux density, and average energy were made with a polyethylene double moderator dosemeter-fluxmeter.[2.29, 2.30] The center of the counter was placed 3 ft above the ground with the BF_3 tube axis perpendicular to the ground. Data were taken at altitudes from 400 to 6400 ft above sea level at latitude 46°N. Data were taken at one location with a Simpson pile during these measurements to compensate for any general change that might have taken place in cosmic ray fluxes

At sea level the dosemeter has an average counting rate of 62 counts/hr. The standard deviation of this hourly value due to statistical fluctuations is 13%. Background counts due to recoil events, counter contamination, and star production in the walls and gas are estimated to be less than 2% of the total counting rate.

Several corrections to the data were necessary to make them meaningful A correction was necessary for the variation in sensitivity of the detector with the angle of incidence of the neutrons.[2.30] Correction was necessary for changes in atmospheric pressure that took place during the measurements. Cosmic-ray neutron detectors increase in counting rate as the atmospheric pressure decreases.[2.31] Near sea level the relation between the two is very nearly exponential.[2.32] It has been reported that during 1957 the average attenuation length for cosmic-ray neutrons in the atmosphere at high latitudes and near sea level was less than the usually accepted value of 145 g/cm^2 by 7 g/cm^2 and that the value of the attenuation length is affected by primary cosm ray spectral changes.[2.31] However, for a typical pressure change of 4 g/cm the attenuation length could be in error by 30 g/cm^2 before the corrected counting rate would be in error by 1%. There are also errors introduced from the limited accuracy of the pressure recording instruments.[2.33]

Measurements and corrections are still in progress. The following values, however, will probably not be changed much by this further work. At sea level the dose rate was 0.66 mrad/yr, the flux density was 0.0073 neutrons/cm^2sec, and the average energy of the neutrons was 0.96 Mev.

Characteristics of a Large Neutron Moderator for Activation Studies* - J. De Pangher, L. L. Nichols, and R. A. R. Kent

The large neutron moderator described last year (2.34) was put into use for neutron activation studies. The neutron source used for this purpose was a thick beryllium target bombarded by up to 15 μamp of 1.85 Mev deuterons. Slow neutron fluence is monitored with copper foils that were standardized by absolute measurements of Na^{24} production. Thermal neutron flux densities of 6 to 7 x 10^7 n/cm^2-sec accompanied by gamma ray exposure rates of 70 to 80 r/hr are possible.

Film Activation Studies Following the Recuplex Accident - J. De Pangher, R. A. R. Kent, and L. L. Nichols

The relative amount of developed silver in film badge dosimeters was determined by measurement of activity induced in the silver by slow neutrons; the results permitted estimates of gamma ray doses to heavily exposed film. Combined neutron and gamma ray calibrations were used to arrive at an estimate of the slow neutron fluence.

On April 7, 1962, a criticality accident occurred in a plutonium waste chemical recovery facility at Hanford known as Recuplex. Three men were close to the critical vessel. They were each wearing a film badge dosimeter containing a sensitive (508) and an insensitive (1290) film. The developed 508 films had optical densities of about 3. Densities that high are very hard to measure. The densities of the 1290 films were in the readily measurable range and were used to establish the exposure doses to the men. It was decided to use the method of comparing activities induced by

* Published as HW-73913. August 1, 1962.

neutrons in the developed silver in the personnel and calibration badges [2.35, 2.36] to see if supplementary estimates of exposure could be made.

The activation of the films was done in the large moderator used for producing slow neutron fluxes with the Van de Graaff.[2.34] The results are shown in Figure 2.20. The two points shown for each Recuplex film are for two different activation measurements. The relative activities are plotted versus the exposure dose given in the calibration for the calibration film and versus that measured from 1290 film for the Recuples film. The agreement is reasonably good, but is not as good as hoped for because the exposures proved to be in the range where film reversal occurs.[2.37] Accurate measurements are not possible near the broad flat peak that results.

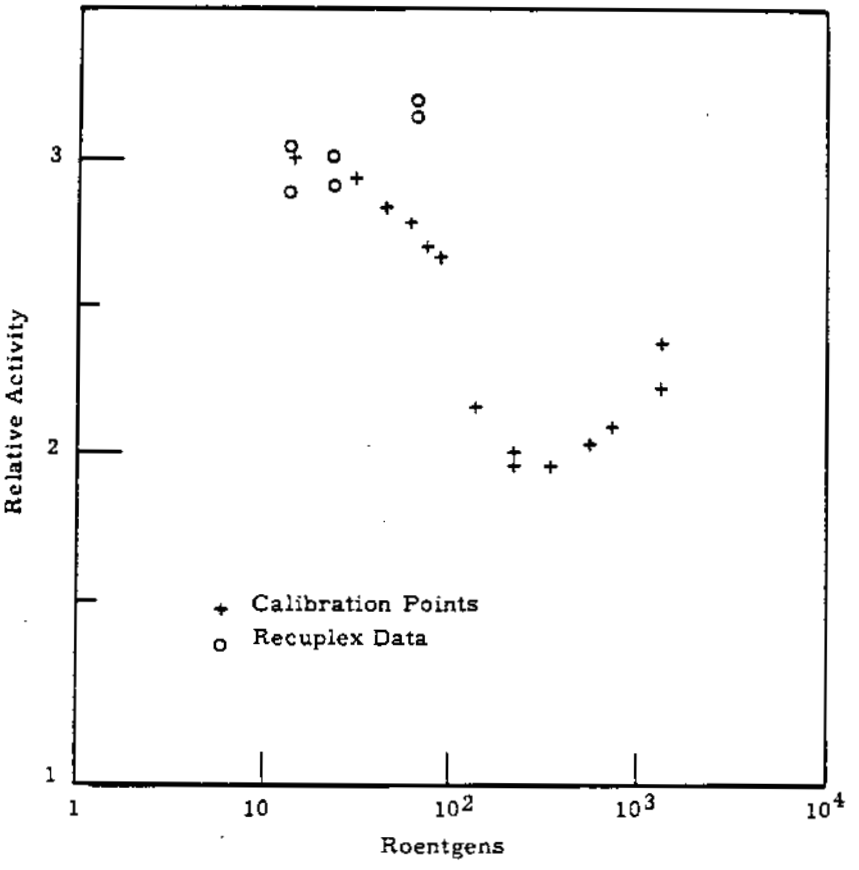

FIGURE 2.20

Relative Activity of 508 Films After Slow Neutron Exposure Versus the Exposure They Received in Calibration or Were Believed to Have Received in the Recuplex Accident

Because of neutron activation of aluminum and silver absorbers in the film badge dosimeters, there was additional darkening of the areas of the film covered by them. To aid in the interpretation of the 1290 films these density patterns were reproduced by mixed gamma ray and neutron exposures. Films were exposed to gamma ray doses in the range of those to which the people were exposed and then exposed to slow neutrons in the large moderator.

The thermal neutron fluences that were required to produce the observed density patterns were used to estimate the thermal neutron fluences during the accident. The cadmium ratio in the large moderator was 75.7 at the exposure position. This was large enough to attribute all the activation to thermal neutrons. A criticality dosimeter located at the scene of the accident gave a cadmium ratio of 1.6. This made it necessary to estimate the relative fluences of thermal and intermediate energy neutrons. It was calculated that 79% of the activation of silver in the badges was due to thermal neutrons during the accident so the thermal fluences measured in the large moderator were multiplied by 0.79. The resulting fluences were 2.3, 0.65, and 0.31 x 10^{10} neutrons/cm^2 with estimated uncertainties of 10, 50, and 200% respectively. The last two values agreed quite well with estimates made by measuring Cu^{64} activity produced in the silver of the badge during the accident; the first value, however, was about two times higher.

Calorimetric Determination of the Half-Life of Sb^{124} - D. M. Fleming

The half-life of Sb^{124} was found to be 60.20 ± 0.01 (standard deviation) days. No correction has yet been made for Sb^{125} present in the source.

Sb-Be neutron sources are important tools in neutron dosimetry. For effective use, an accurate decay correction is necessary. Since published half-lives are in disagreement, an improved value was obtained

using a gamma-ray calorimeter [2.38] to measure the total heat output of a sample of the isotope.

The antimony used in the experiment was a 99.999% pure, 31 g cylinder which had been irradiated in a Hanford reactor to an activity of about 40 curies.

The calorimeter was periodically calibrated by removing the antimony and applying a voltage to a calibrating coil. Data were collected over a period of three half-lives and included about 160 points. The data were fitted by least squares with an IBM 7090 computer. The result for the half-life was 60.20 ± 0.01 days. The uncertainty indicated is the standard deviation. A literature search revealed the best published value of 60.1 ± 0.3 days. [2.39]

The value of 60.20 days does not take into consideration effects of Sb^{125} due to neutron absorption by Sb^{124}. By early 1963 the Sb^{124} had decayed to the point where the longer-lived Sb^{125} could be detected by coincidence counting techniques using NaI scintillation counters. The ratio of Sb^{125} to Sb^{124} activity was still too small to measure accurately enough to make a correction to the half-life of Sb^{124}. Calculations based on published cross section and the approximate neutron fluence during the irradiation indicate there should be enough Sb^{125} present to lower the half life by 0.1 to 0.2% depending on the flux density.

A mass-spectrographic analysis of the Sb^{125} content is being attempted, but results so far have not been promising. It will be late 1963 before an accurate correction can be made through counting techniques.

Heat Output of Plutonium - D. M. Fleming

Calorimetric measurements of plutonium at Hanford and at Mound Laboratory are in good agreement and in fair agreement with heat output calculated from decay schemes and mass spectrometer measurements.

The availability of a 50 g sample of plutonium provided an opportunity to test the accuracy of the gamma ray calorimeter.[2.38] The heat output of the sample was measured with the calorimeter and was compared with a value calculated from a isotopic composition based on mass spectrometer measurements and from known decay schemes of the isotopes. The sample was also measured with a calorimeter at Mound Laboratory to compare with our measurement.

A series of readings was taken starting August 24, 1961, and another series starting May 12, 1962. The results were 116.6 and 117.6 mw, respectively. They are shown in Figure 2.21. The increase is due to the buildup of the daughter product, Am^{241}. The increase is 0.13% per month. On April 19, 1962, the sample was measured at Mound Laboratory. Their result was 117.3 mw. When allowance is made for the Am^{241} buildup the measurements at the two laboratories agree to within 0.2%.

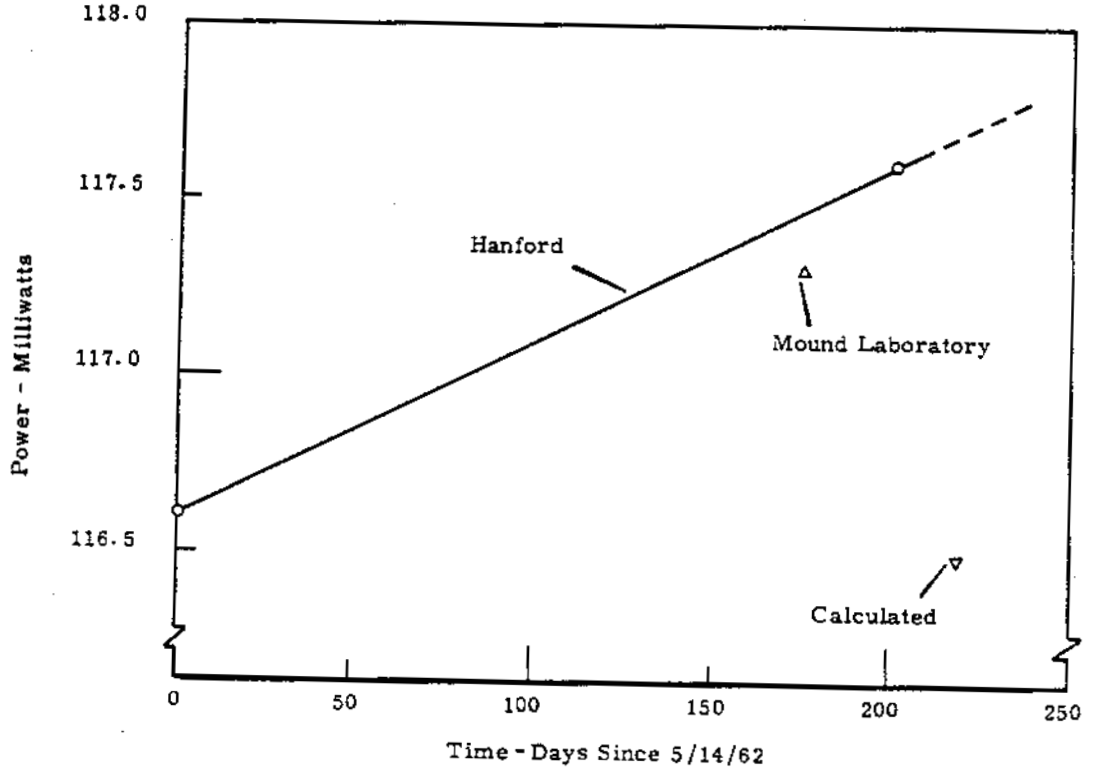

FIGURE 2.21

Heat Output Measurements and Calculations for a Plutonium Sample

An August 1, 1961, spectrographic analysis of the sample gave: Pu^{239}, 92.8%; Pu^{240}, 6.1%; Pu^{241}, 0.8%; and Pu^{242}, 0.3%. The Pu^{238} content was determined by alpha particle pulse height analysis on December 1, 1961. Before an Am^{241} separation, 2.4% of the pulses fell in the Am^{241}-Pu^{238} pulse; after the separation the value was 2.2%. Total weight of the sample was 50.13 g. Calculations based on these analyses and on published nuclear data led to the following rates of heat production as of June 1, 1962.

Pu^{238}	2.64 mw
Pu^{239}	88.53
Pu^{240}	21.56
Pu^{241}	1.87
Pu^{242}	0.01
Am^{241}	1.87
	116.48 mw

Extrapolation of the results in Figure 2.21 gives 117.7 mw for June 1, 1962 a difference of 1% from the calculated value. The major part of this difference is probably due to uncertainties in the spectrographic evaluation of the isotopic content. Some of it may be due to uncertainty in the Pu^{240} half-life.

Input and Source Impedance Corrections in High Precision Voltmeter Standardization* - I. T. Myers and D. M. Fleming

The usual way of making high precision voltage measurements (0.001 to 0.1% accuracy) is to use a potentiometer. Its null balance technique eliminates effects of the internal impedance of the voltage source and of the input impedance of the measuring equipment. Digital voltmeters, voltage to frequency converters, and similar high resolution instruments must be corrected for these effects. A method of standardizing such instruments to offset the effects is described. Accuracy to 0.001% can be achieved.

* Published as HW-74638. March 20, 1962.

REFERENCES

2.1 W. C. Roesch and H. E. Palmer. "Shadow Shields," Research and Development Activities in the Radiological Sciences--1960, HW-70050. January 1961.

2.2 H. E. Palmer. "The Shadow Shield Whole Body Counter," Research and Development Activities in the Radiological Sciences--1961, HW-73337. January, 1962.

2.3 J. Baarli, K. Madshus, K. Liden and R. C. McCall. "Radiocaesium and Potassium in Norwegians," Nature, vol. 191, pp. 436-438. 1961.

2.4 K. Liden. "Cesium-137 Burdens in Swedish Laplanders and Reindeer," Acta Radiologica, vol. 56, pp 237-240. 1961.

2.5 W. C. Roesch and H. E. Palmer. "New Techniques in Whole Body Counting," presented at Radiation Research Society Meeting, Washington, May, 1961. Abstract in Radiation Research, vol 14, page 494, 1961.

2.6 W. C. Roesch and H. E. Palmer. "A Shadow Shield for Whole Body Counting," presented at Health Physics Society Meeting, Las Vegas, June, 1961. Abstract in Health Physics, vol. 6, page 250, 1961.

2.7 K. Liden and Y. Naversten. Unpublished Data. August, 1962. (Personal Communication)

2.8 K. Liden and I. O. Andersson. "Caesium-134 in Man," Nature vol. 195, 1040-1045. 1962.

2.9 A. P. Baerg, R. M. Bartholomew and R. H. Betts. "Search for Independent Formation of Cs^{134m} in Fission," Can. J. Chem. vol. 38 2147-2151. 1960.

2.10 Prawitz, J. "Composition of Products Formed by Thermal Neutron Fission of U^{235} III. Isotopic Composition and Atomic Weight of the Fission Product Elements," Acta Chem. Scand. vol. 13, pp. 163-173. 1959.

REFERENCES (Contd.)

2.11 J. O. Blomeke and M. F. Todd. Uranium-235 Fission-Product Production as a Function of Thermal Neutron Flux, Irradiation Time, and Decay Time, ORNL-2127, VOL I. December 19, 1957.

2.12 M. P. Taylor, J. Vennart, and D. M. Taylor. "Retention and Excretion of Caesium-137 by Man," Physics in Medicine and Biology, vol. 7, 157-165. 1962

2.13 H. E. Palmer. "Detection of P^{32} in Vivo," Radiology, vol. 78, page 115. 1962.

2.14 K. Liden and N. Starfelt. "Internal and External Bremsstrahlung Accompanying the Beta Rays of P^{32}," Physical Review, vol. 97, pp. 419-427, 1955.

2.15 I. C. Nelson, Editor. Evaluation of Radiological Conditions in the Vicinity of Hanford for 1961, HW-71999. March 1962.

2.16 W. C. Roesch, R. C. McCall and H. E. Palmer. Hanford Whole Body Counter--1959 Activities, HW-67045. December 1960.

2.17 Union Carbide Nuclear Co., Y-12 Plant, Oak Ridge, Tenn. Accidental Radiation Excursion at the Y-12 Plant, June 28, 1958. Y-1234. July 28, 1958.

2.18 P. S. Harris. "Dosimetric Calculations, Section VI," J. Occup. Med., Special Supplement, March 1961. vol. 3, number 3, pp. 178-183. 1961.

2.19 G. S. Hurst, R. H. Ritchie, F. W. Sanders, P. W. Reinhardt, J. A. Auxier, E. B. Wagner, A. D. Callihan, and K. Z. Morgan. "Dosimetric Investigation of the Yugoslav Radiation Accident," Health Physics, vol. 5, pp. 179-202. 1961.

REFERENCES (Contd.)

2.20 G. S. Hurst and R. H. Ritchie (eds.). Radiation Accidents: Dosimetric Aspects of Neutron and Gamma-Ray Exposures, ORNL-2748, Part A. November 1959.

2.21 W. C. Roesch and J. W. Baum. "Detection of Plutonium in Wounds," Proceedings of the Second International Conference on the Peaceful Uses of Atomic Energy, Geneva vol. 23, pages 142-143. New York: United Nations, 1958.

2.22 W. C. Roesch and H. E. Palmer. "Detection of Plutonium in Vivo by Whole-Body Counting," Health Physics, vol. 8, pp. 773-776. 1962.

2.23 F. D. Brooks. "A Scintillation Counter with Neutron and Gamma-Ray Discriminators," Nucl. Inst. & Methods, vol. 4, pp. 151-163. 1959.

2.24 L. J. DeVries and F. Udo. "A Fast Pulse-Shape Discriminator with Applications as a Spectrometer and Sensitive Monitor for 1-30 Mev Neutrons," Nucl. Inst. & Methods, vol. 13, pp. 153-160. 1961.

2.25 J. B. Ashe, W. E. Tucker, O. M. Hudson, Jr., and J. T. Prud'homme. A Proton-Recoil Organic Scintillation Spectrometer and Investigation into a Variable Threshold Spark Counter. WADD-TR-60-293. February 18, 1959 - May 17, 1960.

2.26 R. B. Owen. "Pulse-Shape Discrimination Identifies Particle Types," Nucleonics, vol. 17, number 9, pp. 92-95. September 1959.

2.27 T. A. Love and R. B. Murray. "The Use of Surface-Barrier Diodes for Fast-Neutron Spectroscopy," IRE Trans. Nuclear Sci. vol. 8, number 1, pp. 91-97. 1961.

2.28 M. E. Anderson. Unpublished Data. January 1962. (Personal Communication)

REFERENCES (Contd.)

2.29 J. De Pangher. "Double Moderator Neutron Dosimeter," Nucl. Inst. & Methods, vol. 5 pp. 61-74. 1959.

2.30 R. A. R. Kent. Calibration of the Polyethylene Double Moderator, HW-77609, page 2.43. 1962.

2.31 K. G. McCracken and D. H. Johns. "The Attenuation Length of the High Energy Nucleonic Component of the Cosmic Radiation Near Sea Level," Nuovo Cimento, vol 13, number 10, pp. 96-107. 1959.

2.32 J. A. Simpson and W. C. Fagot. "Properties of the Low Energy Nucleonic Component at Large Atmospheric Depths," Phys. Rev., vol. 9 pp. 1068-1072. 1953.

2.33 J. A. Lockwood and A. R. Calawa. "On the Barometric Pressure Coefficient for Cosmic-Ray Neutrons," J. Atmos. Phys., vol. 11, pp. 23-30. 1957.

2.34 J. De Pangher and P. E. Bramson. A Large Neutron Moderator, HW-73337. January 15, 1962.

2.35 I. B. Berlman, H. F. Lucas and H. A. May. "The Determination of Photographic Film Exposure by Neutron Activation of Ag-107," Rev. Sci. Inst. vol. 24, pp. 396-397. 1953.

2.36 J. S. Reddie. Determination of Film Exposure by Neutron Activation of the Reduced Silver, HW-30606. January 14, 1954.

2.37 R. H. Wilson and H. V. Larson. Film Capabilities for High Level Dose Evaluation, HW-71133. September 18, 1961.

2.38 I. T. Myers, W. H. LeBlanc and D. M. Fleming. "Precision Adiabatic Gamma-Ray Calorimeter Using Thermistor Thermometry," Rev. Sci. In vol. 32, pp. 1013-1015. 1961.

2.39 J. P. Cali and L. F. Lowe. "Direct Determination of the Half-Lives of Nine Nuclides," Nucleonics, vol. 17, number 10, page 86. October 1959.

RADIOLOGICAL CHEMISTRY

Reactor Studies *

Fission Yield Studies with Pu^{239} and Pu^{241} - L. J. Kirby

Preliminary measurements have been completed for yields from the thermal neutron fission of Pu^{239} and Pu^{241}, respectively. These studies have been undertaken to measure some previously unreported yields from Pu^{239} fission, to secure more accurate measurements of the fission yields in general from Pu^{239}; and to establish the fission yield curve for Pu^{241}. A secondary goal has been the evaluation or development of radiochemical procedures for the determination of individual fission product radionuclides in the presence of plutonium and mixed fission products.

The radiochemical method was used to establish individual fission yields. Although inherently less accurate than the mass spectrometric method, the radiochemical method offered distinct advantages, especially for the measurement of fission yields for radionuclides with short half-lives. Recent advances in gamma-ray spectrometry have made these techniques especially attractive, and they were employed wherever applicable. This approach has allowed the use of carrier procedures, and the chemical yield could be determined rather than implied for each measurement.

The fission yield curve for Pu^{241} has the same general form as the familiar curves for the fission of U^{235} and Pu^{239}. The relatively steeper slopes noted for the leading edge of the low-mass peak and the trailing edge of the high-mass peak, respectively, for Pu^{241}, have necessitated very careful measurements of yields in these regions. The Pu^{241} used contained 1.3% Pu^{239}, which represented an impurity of up to 30%, in terms of the numbers of individual radionuclides produced in these mass regions. For this reason, additional evaluation is being made before the final publication of the results from this study.

A tentative summary of fission yields measured in this study is presented in Table 3.1.

---

* Not supported by the Division of Biology and Medicine

TABLE 3.1

FISSION YIELDS FROM THERMAL NEUTRON FISSION Pu^{239} AND Pu^{241}

Radionuclide Measured	Measurement	Fission Yield, %, from Pu^{239}	Fission Yield, %, from Pu^{241}
Sr^{89}	β		0.28
Sr^{90}	β		0.54
Sr^{91}	γ		1.0
Y^{93}	β		2.0
Y^{91}	β		0.96
Zr^{95}	γ		2.4
Zr^{97}	γ		3.8
Mo^{99}	γ	6.10	5.2
Ru^{103}	γ		6.1
Ru^{105}	γ	2.74	6.0
Ru^{106}	γ		
Pd^{109}	γ	1.6	3.9
Pd^{112}	γ	0.11	0.96
Ag^{111}	β, γ	0.212	1.7
Cd^{115}	β		0.040
Cd^{115}	β		0.044
Sb^{127}			~0.7
Te^{132}	γ		4.9
I^{131}	γ		4.7
I^{133}	γ		5.6
I^{135}	γ		5.6
Cs^{137}	γ	6.15	5.5
Ba^{140}	β, γ		5.1
La^{140}	β		5.1
La^{141}	β		3.9
Ce^{143}	γ		3.0
Ce^{144}	β		3.1
Pr^{145}	β		1.7
Nd^{147}	β		0.96
Pm^{149}	β		0.39

Reduction of Reactor Effluent Water Radionuclides by Addition of Sodium Silicate to Process Water* - D. E. Robertson and R. W. Perkins

Laboratory, pilot plant, and reactor studies are continuing to minimize the radionuclides reaching the Columbia River in reactor effluent water. The radionuclides As^{76} and P^{32} are of most concern because of their exposure contribution to communities using the water for drinking purposes and using its fish as food. Other radionuclides, which are important but of lesser concern, include Zn^{65}, Cr^{51}, Cu^{64}, and Np^{239}.

Most of the radionuclides present in effluent water originate when their parent elements in process water are adsorbed on the corrosion film surface of the reactor tubes and fuel element jackets, are neutron activated, and are subsequently released to the effluent stream.(3.1) Laboratory studies under simulated reactor conditions have shown that the adsorptions of $AsO_4^{\equiv}$ and $PO_4^{\equiv}$ from process water on aluminum surfaces is reduced by 1 to 3 orders of magnitude when 20-100 ppm of sodium silicate (as SiO_2) is added to the influent.(3.2) A study has been conducted to determine the effect on effluent radioactivity of adding 20 and 40 ppm of sodium silicate (as SiO_2) to the process water of a single-pass reactor tube. The effect of this addition on the effluent water radionuclides Na^{24}, Si^{31}, P^{32}, Cr^{51}, Mn^{56}, Cu^{64}, Zn^{65}, As^{76}, and Np^{239} was measured. After three weeks at 20 ppm of added silicate, the radionuclides P^{32}, Cr^{51}, Cu^{64}, As^{76}, and Np^{239} were reduced by factors of about 2, 1.4, 1.8, 2.2, and 3.0, respectively, while the Na^{24} and Si^{31} were increased as expected since they are components of the additive. The Zn^{65} showed a small increase of about a factor of 1.2. On increasing the sodium silicate feed to 40 ppm for a one week period, the As^{76} and P^{32} were further reduced to factors of about 3 and 2.5, respectively. Due to equipment and solution preparation difficulties, it was not always possible to add the sodium silicate in the intended manner and this probably resulted in a less efficient radionuclide reduction than would otherwise have been obtained.

---

* Published as HW-75782. December 10, 1962.

The Effect of Chemical Additives and Coating Materials on the Adsorption of Radionuclide Parent Elements on Aluminum Surfaces* - R. W. Perkins and D. E. Robertson

Most of the radionuclides present in reactor effluent water are produced from parent materials in process water which were adsorbed on the surface of aluminum process tubes and fuel element jackets, became neutron activated, and were subsequently released to the effluent stream. By minimizing this adsorption process, one would expect a reduction in the concentration of the effluent water radionuclides.

The effect of various surface and water treatments on the adsorption of parent elements has been studied using two experimental methods. One of these methods involved a measurement of the relative adsorption efficiency for labeled parent elements from process water onto aluminum coupons after their prior surface treatment with selected reagents, surface-active agents, and organic coatings. The second experimental setup was designed to simulate the conditions of a reactor process tube, except that no effort was made to obtain a comparably high flow rate. The arrangement used condenser jacketed, heated columns containing aluminum turnings over which process water containing the additive being tested was allowed to flow.

The coupon tests served as a rapid elimination process of less promising reagents. Of about 100 reagents tested, the surface-active agent Antaron FC-34, sodium silicate, and an organic ink were most effective, reducing arsenic tracer adsorption by factors of 5, 6, and 16, respectively.

---

* Published as HW-75976. December. 26, 1962

The silicates, Antaron FC-34, and a number of salts which are normally present in process water were added to process water at concentrations of 20-100 ppm and used in the column studies. Of these reagents tested in the columns, only the silicates produced a significant reduction in adsorption. Actually, the results with silicates were rather spectacular, reducing the adsorption of arsenic and phosphorus tracers by two or three orders of magnitude at 100 ppm (as SiO_2). The aluminum surfaces exposed to silicates remained bright and new in appearance during the one month period of the test, while those exposed to process water appeared dark and corroded. The efficiency of silicates dropped somewhat with concentration down through 20 ppm (SiO_2) and dropped considerably below 20 ppm.

Determination of Thorium in Urine by Activation Analysis - T. M. Beasley and R. W. Perkins.

A bioassay procedure employing activation analysis was developed to determine submicrogram quantities of Th^{232} in urine. Thorium is isolated from the matrix by coprecipitation with lanthanum fluoride followed by an extraction into a thenoyltrifluoroacetone-benzene solution. Thorium is stripped from the organic layer with HNO_3, the aqueous layer evaporated to dryness with $HClO_4$ and subsequently redissolved in a known volume of H_2SO_4. A suitable aliquot is taken for irradiation, along with a standard thorium spike and a reagent blank. Pa^{233} is separated from the irradiated solution by extraction into a diisobutylcarbinol-benzene solution and back-extracted into a H_2SO_4-HF solution. This back extractant is then counted in a 5-in. diameter by 5-in. thick NaI(Tl) well crystal and the Th^{232} determined by comparing the counting rate of the 0.313 Mev Pa^{233} photopeak with that obtained from an irradiated Th^{232} standard.

Th^{232} is the parent isotope in a decay series commonly called the Thorium Series. It is of interest in the nuclear field mainly because it undergoes fission with fast neutrons and can be used in a "breeder blanket" for the production of fertile U^{233} as shown:

$$Th^{232} \xrightarrow{n,\gamma} Th^{233} \xrightarrow[22.1\ min]{\beta^-} Pa^{233} \xrightarrow[27.4\ d]{\beta^-} U^{233}$$

The product, U^{233}, is a long lived fissionable material having a fission cross section of approximately 530 barns.

Chemical or metallurgical processing of thorium-containing materials presents an opportunity for internal deposition in personnel of Th^{232} and its daughter products, and a method of estimating their deposition is required. The present method deals with the determination of Th^{232} in human urine.

The capture cross section of Th^{232} for thermal neutrons is approximately 7 barns. Assuming a thermal neutron flux of 10^{14} neutrons/cm^2/sec, an irradiation time of one day, and cross sections for thermal neutron capture for Pa^{233} and Th^{233} of 40 and 1400 barns, the calculated activity of Pa^{233} per μg of irradiated Th^{232} is 2.68×10^6 dis/min. The decay scheme of Pa^{233} shows 80% of the disintegrations going by way of the 0.313 Mev gamma photon with a total internal conversion coefficient ($\alpha_k + \alpha_l$) equal to 0.925.[3.3] The number of gamma photons/min/dis is therefore 0.32, giving 8.6×10^5 gammas/min/μg of irradiated Th^{232} at 0.313 Mev. Clearly, the high Pa^{233} activity thus obtained makes the determination of Th^{232} by activation analysis an attractive method.

The procedure used for separating the Th^{232} and subsequently the Pa^{233} is an adaptation of two previously published procedures.[3.4, 3.5] The procedure consists of boiling the urine specimen down to a small volume with concentrated HNO_3 followed by two lanthanum fluoride carrier precipitations of the thorium in a manner previously described.[3.4] The second lanthanum fluoride precipitation is then taken to dryness in a Vycor evaporation dish with $HClO_4$. The residue is dissolved in a known small volume of 9 N H_2SO_4; a known aliquot of this solution is pipetted into a clean quartz ampoule and sealed; and the ampoule is irradiated in a high thermal flux for approximate 24 hr. A reagent blank and a standard thorium solution are irradiated with the sample to obtain a calibration factor (counts/min/μg Th^{232}).

Following irradiation, the sample is diluted with 10 ml of 6 N HCl, and the Pa^{233} is extracted into 10 ml of a 1:1 diisobutylcarbinol-benzene solution by mixing in a separatory funnel on a mechanical shaker for 10 min.

The organic phase is washed with three, 10 ml portions of a 6 M HCl-4% oxalic acid solution, 5 min each. It is then back-extracted with an equal volume of 6 M H_2SO - 6 M HF solution for 2 min. The aqueous is then washed for 2 min with 10 ml of fresh diisobutylcarbinol-benzene solution, transferred to a vial, and counted in a 5 in. diameter by 5 in. thick NaI(Tl) well crystal with a multichannel gamma-ray spectrometer. The Th^{232} content is determined from the ratio of the Pa^{233} in the sample compared with that in the irradiated thorium standard. The yield through the various chemical separation steps is >95%.

The procedure was tested by two analysts on "spiked," 500 ml, urine specimens containing 0.20 and 0.02 μg of Th^{232}, and the results of the measurements are summarized in Table 3.2.

The reagent blanks obtained by the above two analysts differed in thorium content by a factor >10, whereas the differences between the averaged urine blanks and the averaged reagent blanks were reasonably consistent at 0.02 μg. The agreement here is undoubtedly fortuitous as is evidenced by the spread in the data; however, it does serve to indicate the level of thorium one might expect in blank urine (urinary excreta from individuals not engaged in the processing of large quantities of thorium-containing materials).

No investigation to determine the source of the thorium in the reagent blanks was carried out, but it is assumed that the thorium comes from leaching of the vessels in which the separations are made and/or the HF used in the lanthanum fluoride precipitation step. All other reagents used were doubly distilled, the lanthanum carrier solution being contacted with TTA-benzene solution to remove any thorium present.

In summary, the determination of Th^{232} can be accomplished by the method outlined. The detection level of the Th^{232} is dependent upon the thorium content of the reagents used; but, with careful reagent purification, the detection level approaches 0.02 μg. Since a detection of 0.02 μg of Th^{232} in urinary excreta should be sufficient to detect any significant thorium content in an individual [3.4] the procedure would appear to be suitable for routine bioassay use.

TABLE 3.2

RESULTS OBTAINED IN THE ANALYSIS OF SEVERAL 500 ml URINE SPECIMENS CONTAINING KNOWN QUANTITIES OF Th^{232}

Analyst 1				Analyst 2			
Sample Number	Thorium Found, µg	Thorium Spike - Urine Blank, µg	Thorium Added, µg	Sample Number	Thorium Found, µg	Thorium Spike - Urine Blank, µg	Thorium Added, µg
1	0.29	0.13	0.20	5	0.22	0.19	0.20
2	0.35	0.19	0.20	6	0.26	0.23	0.20
3	0.18	0.02	0.02	7	0.05	0.02	0.02
4	0.17	0.01	0.02	8	0.05	0.02	0.02
* UB	0.16			UB	0.02		
UB	0.16			UB	0.03		
** RB	0.14			RB	0.01		
RB	0.14			RB	0.01		

Average urine blank minus average Reagent blank = 0.02 µg

Average urine blank minus average Reagent blank = 0.015 µg

* Urine Blank

** Reagent Blank

A Bioassay Procedure for Pm^{147} - R. W. Perkins

The radionuclide Pm^{147} (2.6 yr) is formed with a yield of about 2.7% [3.6] from U^{235} fission and is one of the major long lived fission radionuclides. It constitutes approximately 6% of the total U^{235} fission product activity 1 yr after fission, and in 5-yr-old material it is the most abundant fission product, accounting for 22% of the total activity. Pm^{147} decays by emission of low energy beta-rays and does not emit gamma photons, and for this reason it is of interest as a compact power or heat source. The permissible body burden for Pm^{147} [3.7] is orders of magnitude higher than for more hazardous radionuclides such as Pu^{239} and Sr^{90}; however, the critical organ is bone, and extreme care must be exercised in handling Pm^{147}. Adequate bioassay methods of determining exposure to individuals must be available. Promethium is a member of the rare earth group and a specific chemical separation for this element would require a "fractionation separation" (such as ion exchange column elution or multistage solvent extraction) to ensure its complete separation from other rare earth and transuranium elements.

At 300 to 1000 days after a 100-day irradiation of a uranium fuel element, all of the fission product rare earths except Ce^{144}-Pr^{144} have decayed to insignificant amounts relative to Pm^{147} (less than 3% of the Pm^{147}). The relative concentrations of Pm^{147}, Ce^{144}-Pr^{144}, and the long lived radionuclide Sm^{151} at these decay times are recorded in Table 3.3. In separating and handling Pm^{147}, the possibility of an exposure to other rare earths and Y^{91} which might be carried with the product also exists. In view of this consideration, a Pm^{147} bioassay separations procedure was developed which would also carry the other rare earths. The procedure is designed to permit a "total rare earth" measurement from a beta-ray count, and, if positive, a second count is made through an absorber to determine if the material is, in fact, Pm^{147}. From Table 3.4 it is evident that with the exception of Pm^{147} and Sm^{151} all of these rare earths have rather energetic maximum beta radiation (greater than 0.58 Mev).

Because of the very weak maximum beta energy of Pm^{147}, it is simple to determine if a rare earth sample contains significant amounts of the other rare earth radionuclides.

The Pm^{147} procedure involves the following steps. The rare earth group is separated, using a modification of a previously reported [3.9] rare earth separation which involves a fluoride precipitation followed by a thenoyltrifluoroacetone (TTA) extraction. After "plating" the residue on a 1.5-in. diameter counting dish, the sample is counted in a low background beta counter (about 1 count/min background) with no absorber and with a 14 mg/cm^2 aluminum absorber. If the attenuation imposed by the absorber is about a factor of 10, the same as that imposed on a Pm^{147} standard (which is also carried through the procedure), the sample is relatively pure Pm^{147}. If the attenuation factor is much lower, other rare earths are present. In the chemical separation, a relatively large amount of carrier is used which produces approximately 40% self absorption of the Pm^{147} beta particles (0.223 Mev) and would cause nearly 100% absorption of any Sm^{151} beta particles (0.075 Mev).

When the procedure is carried out with a water blank the resulting sample has a counting rate of about 0.5 counts/min. The total counting efficiency of Pm^{147} $(\frac{\text{counts/min}}{\text{dis/min}})$ on a low background beta proportional counter in the carrier precipitate is about 20%.

The rare earth praseodymium was selected as a carrier for the separation on the basis of tests which compared the radioactivities of the various "reasonably priced" rare earths. The sensitivity of this procedure is a function of the reagent purity, counter background, radiochemical yield, counter geometry, and counting time. For a 30-min count on a low background counter with no rare earths present, it is possible to detect about 7 dis/min of Pm^{147} at the 99% confidence level. The radiochemical yield is about 85%.

TABLE 3.3

RELATIVE CONCENTRATIONS OF THE RARE EARTHS AT 300 and 1000 DAYS AFTER A 100 DAY IRRADIATION OF NATURAL URANIUM*(3.8)

Time After Irradiation	Relative Concentration		
	Pm^{147}	$Ce\text{-}Pr^{144}$	Sm^{151}
300 Days	1	4.8	0.042
1000 Days	1	1.2	0.55

With shorter cooling times, the abundances of the short lived rare earth fission products relative to Pm^{147} are much higher. (See Table 3.4)

TABLE 3.4

RELATIVE ABUNDANCE OF THE RARE EARTH FISSION PRODUCTS AND Y^{91} AFTER A 100 DAY IRRADIATION AND A 100 DAY COOLING PERIOD *(3.8)

Radionuclide	Half-Life	Maximum Beta Energy, Mev	Relative Abundance
Pm^{147}	2.6 yr	0.223	1
Y^{91}	59 d	1.55	9.2
$Ce\text{-}Pr^{144}$	285 d-17 m	2.98**	7.3
Ce^{141}	33 d	0.581	3.7
Pr^{143}	13.7 d	0.932	0.32
La^{140}	40 hr	2.15	0.26
Nd^{147}	11 d	0.81	0.039
Sm^{151}	93 yr	0.076	0.038

* Values for the half-lives used in these computations were somewhat different than the presently accepted values.

** Pr^{144} Maximum Beta

Measurement of Cl^{38} In Reactor Effluent Water - R. W. Perkins

The radionuclide Cl^{38} is a major short lived constituent of reactor effluent water. Its concentration, as the effluent water is discharged from the single pass Hanford reactors, is comparable to that of Na^{24} and Cu^{64}. Although it is of little consequence in the Columbia River because of its very short half-life (37.3 min), it has proven troublesome in the development of automatic monitoring equipment for other radionuclides.

The decay of Cl^{38} involves the emission of three photons in cascade with a total energy of 3.5 Mev. The procedure developed simply involves the distillation of the sample containing Cl^- carrier from a dilute HNO_3 solution into a beaker containing sufficient $AgNO_3$ to precipitate all the Cl^- as AgCl. The precipitate is then immediately filtered (through an Am-3 membrane filter) and the counting rate of the 3.5 Mev Cl^{38} addition peak measured in a 5-in. diameter by 5-in. thick well crystal. The procedure is quantitative for Cl^{38} and is nearly quantitative for the radioiodine fission products. These iodine radioisotopes all have lower total energies than Cl^{38} and do not interfere with its measurement. The iodine radioisotopes can be estimated from their respective photopeaks after decay of the Cl^{38}.

Radiochemical Analysis of W^{187} in Reactor Effluent Water* - W. B. Silker

A modification of the procedure of Leliaert, et.al, (3.10) was successfully applied to the radiochemical determination of W^{187} in Hanford reactor effluent water. The final product was free from contamination, and radioassay was made by standard gamma scintillation spectrometry. A 200 ml water sample, containing an aliquot of standardized tungsten carrier was heated to boiling, and 50 ml of concentrated HCl was added. The resultan tungstic acid, which was separated by centrifuging, was transferred to a beak with 50 ml of water; 5 ml of 30% H_2O_2 was added; and the mixture was heated.

---

* Not supported by the Division of Biology and Medicine

Three ml of a 1% Na_3YO_4 solution and 20 ml of HCl were added, and the solution digested for 10 min. The WO_3 precipitate was removed by centrifuging, washed twice with 2 N HNO_3, transferred to a weighed plate, and counted on a 3 x 3 in. NaI(Tl) crystal.

Evaluation of Selected Procedures for the Separation of Radioarsenic from Reactor Effluent Water* - D. E. Robertson

The reactor effluent water radionuclide, As^{76}, is not easily measured by gamma or beta spectroscopy until a radiochemical separation is performed. Since there has been some question concerning several separations, the performances of six separation procedures were evaluated for yield, radiochemical purity, and simplicity. Those procedures evaluated were a standard HBr distillation, a benzene extraction from 3 N HCl containing HI, a chloroform extraction from 3 N HCl containing HI, a benzene extraction from 8-10 N HCl, a carrier-free butanol-chloroform-ethyl acetate extraction, and a beta-ray absorption technique. The HBr distillation procedure gave the highest As^{76} spike yield, the highest As^{76} yield from effluent water, and contained less than 3% radioactive contamination. Of the solvent extractions, the benzene-HCl-HI extraction gave the highest spike yield, equally high As^{76} yield from effluent water, contained less than 1% radioactive contamination, and is the most rapid and convenient. The beta-ray absorption technique, because of rather severe interference from other radionuclides, gave spurious, high As^{76} values from effluent water.

Determination of P^{32} in Sediments - L. L. Humphreys

As a part of the Columbia River sediment studies** it was desirable to know the concentration of P^{32} in river sediments. Dissolution of the sediments was effected with HF, HNO_3, and $HClO_4$. This was accomplished by heating a 2 g sample in a platinum crucible in an oven at 600 C for 1 hr, cooling, and evaporating to dryness under a heat lamp with

* Not supported by the Division of Biology and Medicine

** See "Columbia River Sediment Studies," page 3.61

20 ml of 48% HF. The residue was evaporated to dryness with a second 20 ml addition of HF, and 20 ml of concentrated HNO_3 were added. Evaporation was repeated on a hotplate until the volume was reduced to 5 ml. At this point, 15 ml of concentrated $HClO_4$ were added, and the solution was evaporated to dryness. The residue (now completely soluble) was transferred to a beaker with 120 ml of 1.2 N HCl, and the solution was boiled and cooled; 35 ml of 10% ammonium molybdate solution were added. The resulting phosphomolybdic acid was extracted with 30 ml of 10% butanol-1 in diethyl ether.(3.11) The organic phase was washed with 1.2 N HCl, evaporated onto a standard 1-in. stainless steel counting dish, and the beta activity was measured with a proportional counter. The chemical yield is 85 ± 8%.

Elements which could possibly interfere in this procedure include those which will form heteropolymolybdic acids.(3.12) Arsenic and zirconium fall in this group, and are present in the river water in the radioactive forms As^{76} and Zr^{95}. Arsenic does extract to the extent of about 5%, but the samples are held for about 2 wk before analysis to allow the As^{76} (26.5 hr half-life) to decay completely. Zirconium did not carry through the procedure with the phosphorus.

The specific activity of P^{32} in the top 2 in. of the sediments in McNary Dam was found to be 23 dis/min/g. Total activity resulting from P^{32} is about 125 times less than Cr^{51}, or 0.15% of the total sediment activity.

A Fluorescein Analysis Technique for Use in Atmospheric Diffusion Studies - J. D. Ludwick and P. W. Nickola

A revised analysis technique for determining sodium fluorescein dye collected from the atmosphere is described. A field experiment was carried out involving the simultaneous emission of fluorescein and ZnS to assay their compatibility as atmospheric tracers. Significant deviations in tracer behavior were observed. Work is continuing in an effort to reduce the differences in behavior and to permit their use in a dual atmospheric tracer system.

The development of valid models for specifying atmospheric diffusion is hindered by the inability to control the atmosphere. One can scarcely hope to duplicate ambient conditions of, say, temperature, humidity, wind speed, and wind direction, to say nothing of vertical gradients or variances of these parameters, from one experiment to another.

One method of investigating diffusion is to release a tracer into the atmosphere and to monitor this tracer at downwind sampling positions. It would be very convenient to be able to release two or more tracers simultaneously from the same source location. This procedure would permit the carrying out of more than one experiment at the same time under identical atmospheric conditions. Also, the simultaneous emission of two or more tracers at different elevations would greatly facilitate the investigation of source height effects.

Dual tracer analysis methods were previously developed in support of the atmospheric field testing program.[3.13] These methods prescribe the analysis of the same field filters for both fluorescein and the normally used ZnS. Some changes in the procedure of analysis were made for the first field test of the dual tracer technique. The revised analysis technique and a qualitative appraisal of results from the first field test are described.

The techniques employed for analysis of fluorescein and ZnS permitted as little as 8×10^{-10} g of fluorescein to be detected and a resultant sensitivity for ZnS of about 1×10^{-9} g. The experimental methods used allowed

the individual tracer analysis to be carried out without regard to the concentration of the second tracer and in no way affected the sensitivity for that tracer.

Experimental

A concentrated water solution of fluorescein dye was emitted through the standard generators alongside of a ZnS pigment generating source. Essentially equal amounts of the two tracers were emitted during the same time period. The resulting particulates were collected downwind on both Millipore and Gelman membrane filters.

Previous work on analysis of these tracers had involved dissolution of the filter in ethyl acetate-ethyl alcohol, with both tracers present, and subsequent fluorescence measurement for fluorescein quantity. It was found, in backround measurements, however, that the Gelman filters contributed significantly to the fluorescence and drastically reduced fluorescein sensitivity. A modified technique which resolved the tracers and eliminated even the slightest cross-interference was developed.

The filters were removed from the plastic field holders, and the crepe paper backing was removed. They were then replaced in their holders and clamped securely to the plastic with the ring cover. In normal low fluorescein concentration filters ($< 10^{-6}$ g), 2 ml of distilled water were measured from a burette and allowed to cover the top surface of the filter. The filter holder was placed on the top of a 25 ml suction flask, and after sufficient time for the water to dissolve the fluorescein dye (sdoium salt) suction was applied and the solution was collected in the flask. This procedure was repeated three times to extract all of the fluorescein. Six samples were simultaneously processed, with 6 ml of solution collected. When the fluorescein concentration was large enough to produce visible yellow-green color on the filter when wetted, up to 20 ml of water in several additional extractions were used in leaching the filters. This insured complete leaching and reduced the fluorescein concentration to levels acceptable to the spectrofluorometer.

A 3 ml portion (or 50% of the extractant) was pipetted into the quartz sample cuvettes for fluorescence analysis. The sample was pH stabilized and its fluorescence excited by addition of one drop of a 20 g/l Na_3PO_4 solution from a 5 λ pipette. This concentration was found just sufficient to stabilize the pH at 9, excite the fluorescein fluorescence to near maximum, and minimize filter background contributions. The excitation light was 490 mμ with a very narrow slit width, while the emission spectrum was observed at 522 mμ with a moderate slit width on the spectrofluorometer. Selected samples with high fluorescein activity were rerun to insure that the process removed > 95% of the initial fluorescein content. Field samples near the periphery of the tracer were used as backgrounds. The level of fluorescence observed from these background field samples corresponded to not more than 6 to 7 x 10^{-10} g of fluorescein. Calibration of the instrument was accomplished using the same techniques with standard solutions of fluorescein. The calibration results are illustrated in Figure 3.1.

The leached filters were removed from the filter holders, placed in 8 ml vials and dissolved in ethyl acetate-ethyl alcohol solution. Their retained ZnS concentration was determined using phosphorescence analysis.[3.14]

Results

Analysis of the field samples on four collection arcs downwind showed qualitative agreement between the masses of tracers; however, the fluorescein quantity was generally higher than the ZnS tracer. As a result of wind direction and arc location, only the two farthest arcs intercepted and reasonably defined crosswind distributions of the tracers. The results of these sampling arcs are illustrated in Figures 3.2 and 3.3.

Since essentially identical amounts of the tracers were generated, it would be expected that the same quantity should appear at the downwind collecting stations if they behaved similarly in the atmosphere. Nearly

identical behavior is necessary for the technique to be useful in investigating other variables such as source height effects.

This discrepancy in collected mass may be attributed to several factors, such as significant differences between the sizes of ZnS and fluorescein particles, different deposition or impaction efficiencies, and collection and analysis techniques or generation differences. The cause of this discrepancy is now under investigation.

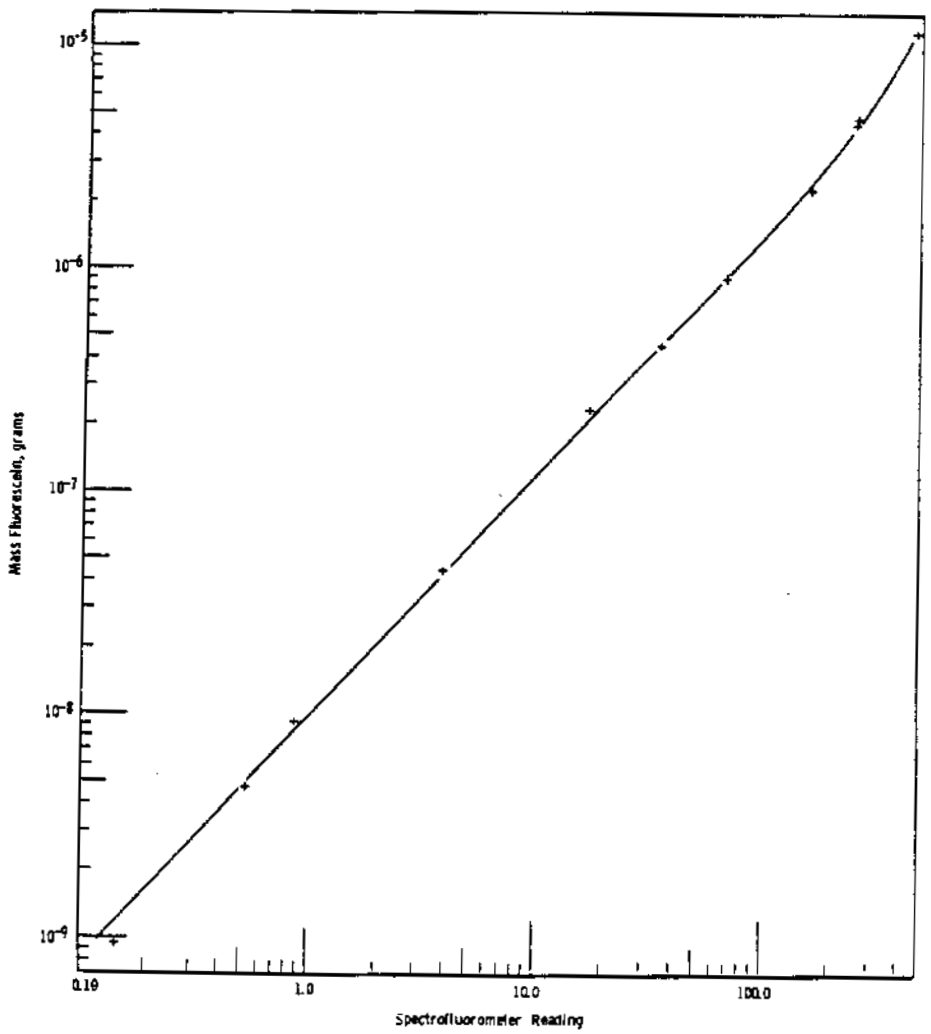

FIGURE 3.1

Spectrofluorometer Response to Aqueous Sodium Fluorescein

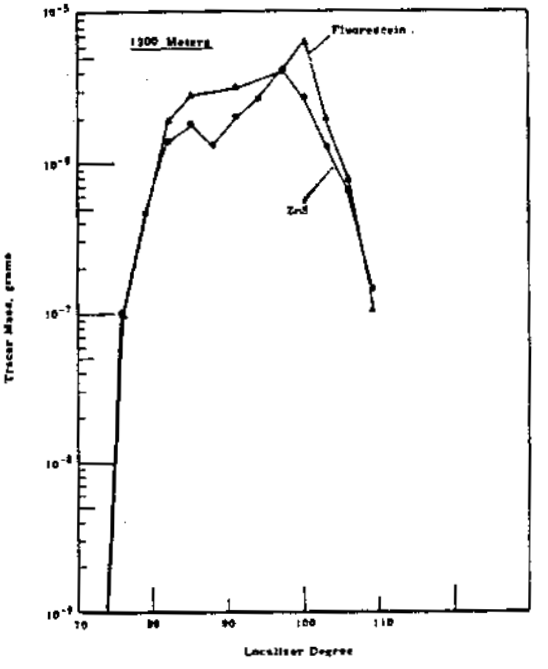

FIGURE 3.2

Crosswind Distribution of Tracers
at Approximately 1200 Meters from the Source

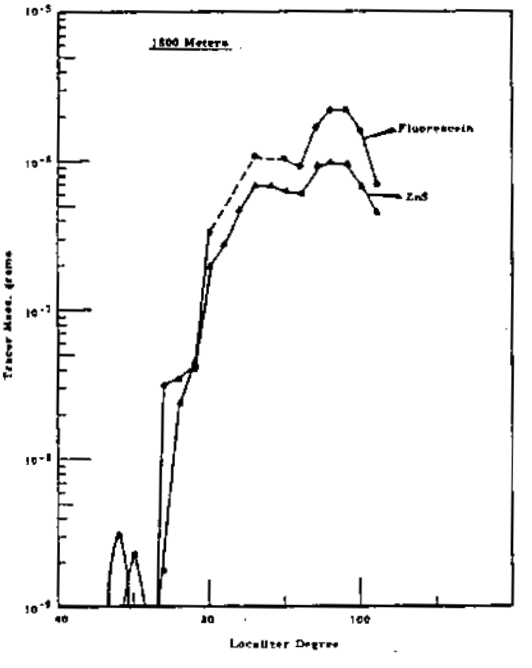

FIGURE 3.3

Crosswind Distribution of Tracers
at Approximately 1600 Meters Downwind of Source

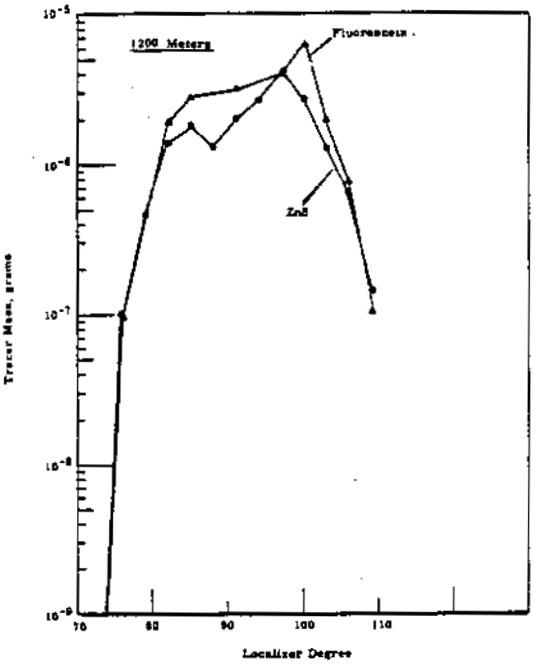

FIGURE 3.2

Crosswind Distribution of Tracers
at Approximately 1200 Meters from the Source

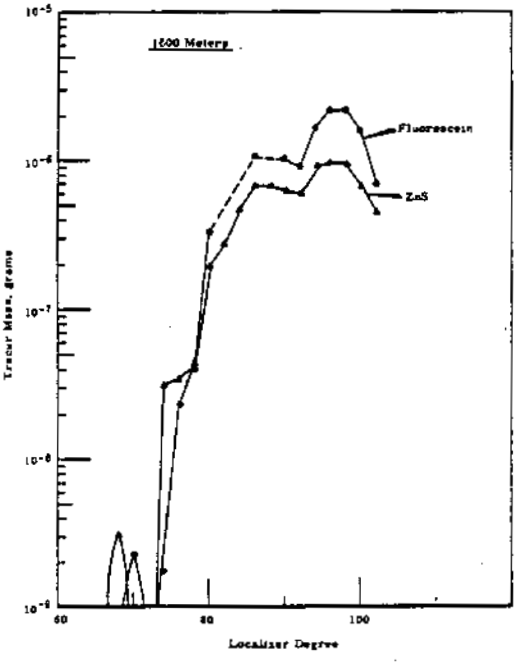

FIGURE 3.3

Crosswind Distribution of Tracers
at Approximately 1600 Meters Downwind of Source

Analysis of Grass and Ground Deposited Atmospheric Zinc Sulfide Particulate - J. D. Ludwick

Two atmospheric diffusion field experiments were conducted over cheat grass fields. Sampling and analysis were carried out to determine ground and vegetation effects upon particulate tracers.

An indication of the amount of ground and vegetation deposition from particulate atmospheric tracer materials was derived from the first cheat grass field run.[3.15] Results of this experiment indicated that 22% of the ZnS particulate could be found on the standing and ground grass within the first 100 m from dispersal point.

Two additional field tests were performed over cheat grass fields. Atmospheric conditions were more favorable than in the initial test in containing the downwind particulate within the sampling grid. Separate samples of standing and ground grass were taken downwind in arc of 10, 25, 50, and 100 m during one run and an additional 200 m arc added during the other field test.

Aliquots of cheat grass from the sampled field areas were weighed into standard 2 dram glass counting vials. The samples were baked in an oven at 400 C for about 3 days to remove the vegetable matter. The ZnS tracer was then uniformly slurried in the vial with a solution of ethyl acetate-ethyl alcohol. Then the sample was exposed to a high flux of light and automatically moved inside an iron shield for phosphorescence counting. This automatic process delay along with the counting interval consumed approximately 24 sec. Although the mineral residue from the grass does not interfere with analysis, the significant quantity of dirt found on some samples, particularly on ground grass samples, presents a problem to analysis. During the delay and counting time, high dirt content samples carried the ZnS particulate down too fast and buried them near the bottom of the vial. It was deemed necessary to stir the samples continuously while delay and counting were in progress.

Figure 3.4 illustrates the method of agitation for the samples while they were deep within the automatic iron shield. A magnet was attached to the lower elevator platform and stirring commenced as soon as the platform and sample were lowered into the counting position. Air would then strike the vanes, producing magnet rotation and subsequent stirring rod movement. A dirt laden sample vial was utilized to check the proper operation of the mechanism. The pump, which fed air into the shield, was fitted with a secondary loop containing an adjustable valve. The quantity of air flowing through the shield to properly rotate the magnet was controlled by this valve which allowed more or less air release in the secondary loop.

It was then necessary to recalibrate the instrument using stirring of standard ZnS samples. Figure 3.5 illustrates the results of recalibration, where delay (1) is a 24-sec delay in addition to the normal 6-sec interval between exposure and counting. This was necessary to differentiate grass from ZnS phosphorescence.[3.15] The first curve on Figure 3.5 was that obtained for ZnS without stirring or extra delay. Although a reduction in sensitivity was observed due to the necessary added delay, stirring has significantly improved the sensitivity. Without stirring the limit was about 1×10^{-7} g ZnS, while close to 1×10^{-8} g was detected with stirring. After counting, the samples were corrected for their dirt content utilizing colorimeter readings.

Results of analysis showed a similar large (> 30%) quantity of tracer deposition within the first 200 m from dispersal. The amount of material found on the standing grass was approximately 2 to 5 times that on the ground. This was considerably lower than the estimates of at least 5 from the first field run. This difference may be due to several factors, including atmospheric variations and cheat grass field inequalities. The analysis of samples to 200 m was possible because of the improved sensitivity from stirring.

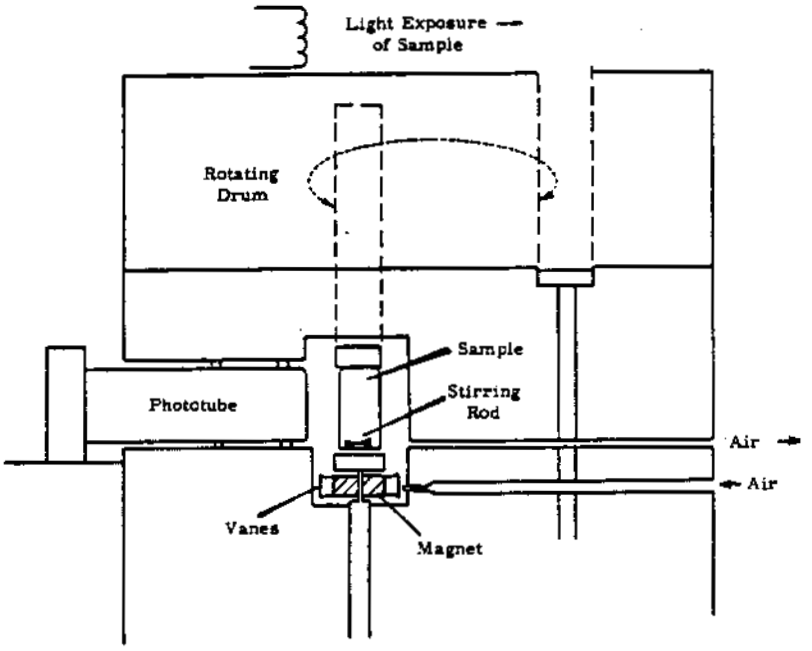

FIGURE 3.4

Automatic Sample Stirring Mechanism

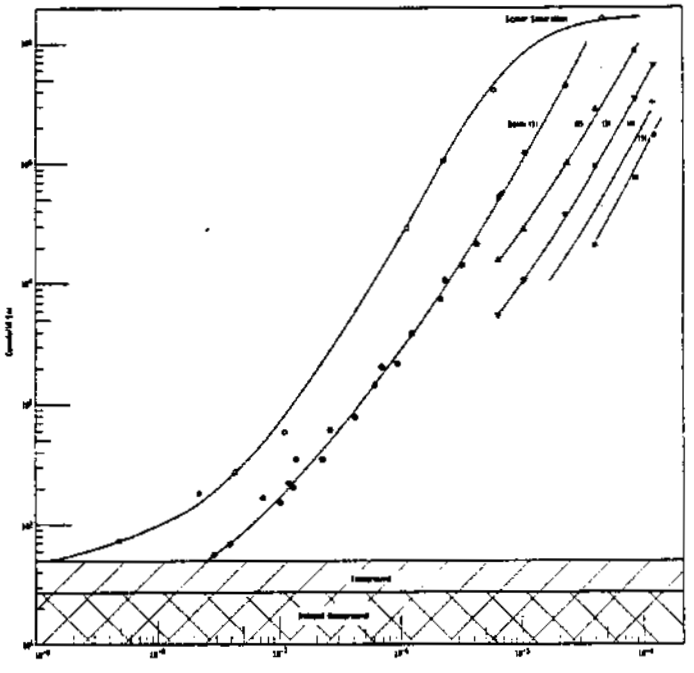

FIGURE 3.5

Instrumental Calibration of Stirring Zinc Sulfide Particulate

Liquid Scintillation Tritium Counting Improvements* - J. D. Ludwick

In a continuing study of liquid scintillation techniques and applications, improvements were made in organic phase scintillator mixtures. A considerable increase in counting efficiency was observed using the optimum mixtures. Application of liquid scintillator counting was made to the determination of tritium in reactor gas dryer condensate.

The introduction of dimethyl-POPOP as a secondary solute comparable to POPOP for use in wave length shifting was investigated. The fluorescence emission spectrum of the dimethyl derivative is slightly better matched to the common S-11 response of many multiplier phototubes such as the Dumont 6292. Since POPOP is the best secondary solute for most liquid scintillator applications, and PPO generally the most adopted primary solute, a study of comparable mixtures using POPOP and its dimethyl derivative with PPO was made. The samples were prepared by placing 10 λ of tritiated toluene in a quartz vial containing 300 λ of the scintillator mixture under question. Toluene was utilized as the primary solvent for the mixtures. The scintillator mixtures were also tested by introducing 10 λ of dibutyl phosphate containing Pu^{241}.

Figure 3.6 illustrates the results of this study for tritium. Essentially, the same results were obtained using Pu^{241}. An improvement in tritium counting efficiency was observed with dimethyl-POPOP which amounted to 17% of that normally obtained using optimum POPOP concentrations. It was noted that in low concentrations of the secondary solute such as the comparative samples, 4.0 g/liter PPO--0.3 g/liter POPOP versus 4.0 g/liter PPO--0.3 g/liter dimethyl-POPOP, essentially the same efficiency was observed for tritium. The greatest advantage shown by dimethyl--POPOP lies in its larger solubility in toluene and similar solvents, thus allowing concentrations above 0.6 g/liter for the secondary solute with a resultant increase in energy transfer effectiveness.

---

* Not supported by the Division of Biology and Medicine

The best phosphor combinations observed were 1.5 g/liter dimethyl-POPOP and 8.0 g/liter PPO. Another good mixture was 2.0 g/liter dimethyl-POPOP and 6.0 g/liter PPO. Dimethyl-POPOP solubility was about 2.0 g/liter. It was apparent that at 3.0 g/liter dimethyl-POPOP concentrations, not all of the solute was dissolved. It is also important to point out that at very high solute concentrations in the liquid scintillator, instability may result due to sample refrigeration and it is best to utilize mixtures slightly under maximum solubility conditions. Much better counting reproducibility can then be expected.

Aqueous samples from reactor dryer condensate were processed and analyzed for tritium. Samples of condensate water were passed through mixed cation-anion exchange resins of the H-OH type to remove all possible ionic contaminants. The samples were then distilled to insure purification from other solid matter. The liquid scintillation energy spectrum of the resulting samples corresponded to a 0.17 Mev beta ray energy. This may be attributed to either C^{14} or S^{35}.

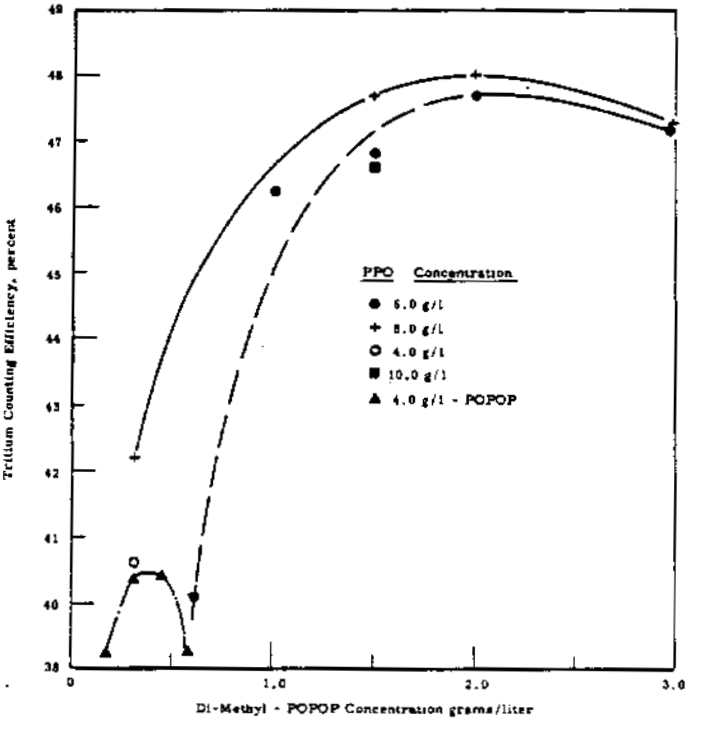

FIGURE 3.6

Tritium Counting Efficiency Using Dimethyl-POPOP in the Liquid Scintillator

Radiological Chemistry Associated with the Hanford Criticality of April 7, 1962* - R. W. Perkins and L. J. Kirby

A critical accident occurred at Hanford at 10:59 a.m. on Saturday, April 7, 1962, during which three men received radiation doses exceeding 2 rads. Implementation by the Radiation Protection Operation of their standard emergency procedures, including whole body counting and film badge dosimetry, provided a basis for the rapid evaluation of the radiation exposures. The radiochemical and bioassay measurements in connection with the accident are considered in this report. Blood Na^{24} measurements and whole body counting provided the primary and early information on the neutron exposure. Measurements of the P^{32} in hair produced by the $S^{32}(n, p) \rightarrow P^{32}$ reaction provided information for estimating the fast neutron dose at various locations on the individuals. Additional information on the neutron exposure was obtained from measurements of the induced radionuclides in the silver absorbers from the personal dosimeters and in the employees' personal effects. The time-integrated neutron flux to which these objects were exposed was determined by re-exposing these objects to a known slow neutron flux in the moderator of a Van de Graaff accelerator and remeasuring the induced radionuclides. The Na^{24} elimination in urine and feces samples was determined from measurements made for several days after the incident and is compared with the neutron doses received. The release of the short-lived fission product Cs^{138} (32.2 min) from the building ventilation exhaust system served as a monitor of the relative rate of the continuing fission process in the criticality vessel. Measurements of fission products in the criticality vessel after the incident indicated that a total of about 10^{18} fissions had occurred.

---

* Published as HW-76823. October 10, 1962.

Fast Neutron Doses from the Hanford Criticality Incident - L. J. Kirby

Fast neutron doses from the Hanford criticality incident of April 7, 1962, have been estimated from the concentrations of P^{32} in hair samples taken from the three employees nearest to the criticality vessel. Dissolution of the samples was accomplished by treatment with nitric acid, hydrogen peroxide, sulfuric acid, and perchloric acid. Phosphorous was extracted into n-butanol-diethyl ether (13% v/v) from dilute sulfuric acid solution as ammonium phosphomolybdate, the organic layer evaporated on a counting dish, and P^{32} determined with the aid of a low background proportional counter. The P^{32} measurements have made possible the estimation of incident fast neutron doses to hair from various parts of the employees' bodies, and the doses have been correlated with the locations of the employees with respect to the criticality vessel at the time of the accident. Total neutron doses calculated from the P^{32} measurements are shown to agree well with doses estimated from whole body Na^{24} and blood Na^{24} measurements. The possible use of P^{32} measurements in hair to locate a critical disturbance is discussed.

The three men nearest to the reaction vessel of the April 7, 1962, Hanford criticality accident received first collision neutron doses of about 28, 10, and 3 rads, respectively.[3.16] The doses were estimated primarily from blood-Na^{24} levels and whole body counting, with corroborative evidence being supplied by measurements of their personal dosimeters and personal effects. Measurements of P^{32} induced in hair have made possible the estimation of doses to various parts of their bodies, as in this accident the dose distributions for two of the employees were highly non-uniform. This paper describes the P^{32} measurements, and illustrates in a practical manner the utility of these measurements for determining non-uniform body doses and correlating this information with the locations of the employees with respect to the criticality vessel. Such data are shown to be potentially useful for locating the source of an accident when the possibility exists for a critical mass to accumulate in one or another of several adjacent containers.

A convincing case has been presented for the use of P^{32} measurements to determine incident neutron doses to body hair and cartilage.(3.17, 3.18) P^{32} is induced in hair by the reaction $S^{32}(n, p) \rightarrow P^{32}$, which has a threshold of about 2.5 Mev. Thermal neutrons will also induce P^{32} by the reaction $P^{31}(n,\gamma) \rightarrow P^{32}$. However, the sulfur content of hair is about 200 times the phosphorus content and the cross sections for the two reactions are nearly the same. Therefore activation of sulfur in hair by fast neutrons is the only significant source of P^{32} activity, when the neutron spectrum has not been extremely degraded.

The time-integrated neutron flux above the sulfur threshold is calculated from the expression

$$F = AW/\lambda \sigma NS; \quad (1)$$

where F is the flux above 2.5 Mev in neutrons/cm^2; A is the activity of P^{32} in dis/min/g sample at time of exposure; W is the atomic weight of sulfur in grams; λ is the decay constant of P^{32}, 3.37×10^{-5} min^{-1}; σ is the cross section for the reaction of interest, 225×10^{-27} cm^2/atom; N is Avogadro's number, 6.02×10^{23} atoms; and S is the number of grams of sulfur per gram of sample. For a sulfur concentration of 47.7 mg/g hair, Equation (1) becomes

$$F = 1.45 \times 10^{8} A. \quad (2)$$

Flux to dose conversion for those neutrons having energies greater than 2.5 Mev is given by

$$D = 3.83 \times 10^{-9} F. \quad (3)$$

Experimental

Hair samples were obtained from several locations on the bodies of employees No. 1, No. 17, and No. 23, and fingernail and toenail clippings were obtained from employee No. 1.

P^{32} was determined by Silker's method,(3.19) but additional work was needed to provide a method for complete dissolution of the samples. Initial attempts to dissolve the hair by treatment with HNO_3 and 30% H_2O_2 were highly

unsatisfactory. Although this treatment provided an apparently clear solution, evaporation with H_2SO_4 yielded a black syrupy mixture from which only about 40 ± 10% of the P^{32} could be extracted. The organic and aqueous layers under these conditions were not readily separable, and the P^{32} presumably was physically entrained in the organic-insoluble black material. When an evaporation with $HClO_4$ was performed before the extraction, it was possible to extract from a clear solution and the chemical yield through the entire procedure was 88.5 ± 3.0%. The detailed chemical procedure finally adopted is presented in Appendix 3.1.

The recovery and reproducibility of the procedure used were tested by spiking hair samples obtained from a local barber shop with P^{32} during the initial HNO_3-H_2O_2 treatment, then very carefully controlling all volumes and conditions during the separation. The chemical yield of 88.5 ± 3.0% was used to adjust all measured activities. Measurements were completed with a low background proportional counter, generally using overnight counts of the low activities encountered.

Petersen, et al.,[3.18] have remarked on the relatively constant concentration of sulfur in human hair. Because of the limited amounts of hair available for the measurements reported here, it was possible to measure sulfur[3.20] in only a few samples. These values lay within the range reported by Petersen, et al., and their value of 47.7 ±5.5 mg S/g hair was used to relate P^{32} activities to neutron flux.

Results

The results of the P^{32} measurements, together with calculated fluxes and doses for the hair samples, are summarized in Table 3.5. Because the sulfur content of the nails was not readily available, the data from these samples can be used only to indicate that one hand was closer to the criticality vessel than the other, and that the feet were farther from the vessel than the hands were.

TABLE 3.5

P^{32} IN HAIR AND NAILS

Employee	Hair Samples: Type	Cm from Top of Head	dis/min/g	Neutrons above 2.5 Mev: Neutrons/cm^2	First Collision Dose, rads
1	Head, (posterior)	0	16.6	2.41×10^9	9.2
	Chest	33-77	18.8	2.73×10^9	10.5
	Pubis	87	12.2	1.77×10^9	6.8
	Legs	135-161	9.61	1.39×10^9	5.3
17	Chest	43-73	7.92	1.15×10^9	4.4
	Pubis	94	5.63	8.16×10^8	3.1
	Back	34	5.52	8.01×10^8	3.1
23	Head	0	2.70	3.92×10^8	1.5
	Pubis	93	2.60	3.77×10^8	1.4
	Nail Samples				
1	Left hand		14		
	Right hand		23		
	Toes		11		

The positions of employees No. 1 and No. 17 with respect to distance from the criticality vessel are presented in Figure 3.7. As indicated in the figure, the doses calculated from the P^{32} measurements correlate very well with the employees' positions and orientations at the time of the accident. Employee No. 1 was immediately below and facing the criticality vessel, manipulating a valve at the hood face. His dose rate were highly nonuniform. Employee No. 17 was behind and to the left of No. 1, some 10 ft from and facing the vessel. His dose rates were also nonuniform, but less so than those to No. 17. Employee No. 26 was some 26 ft from the vessel, and received fairly uniform doses.

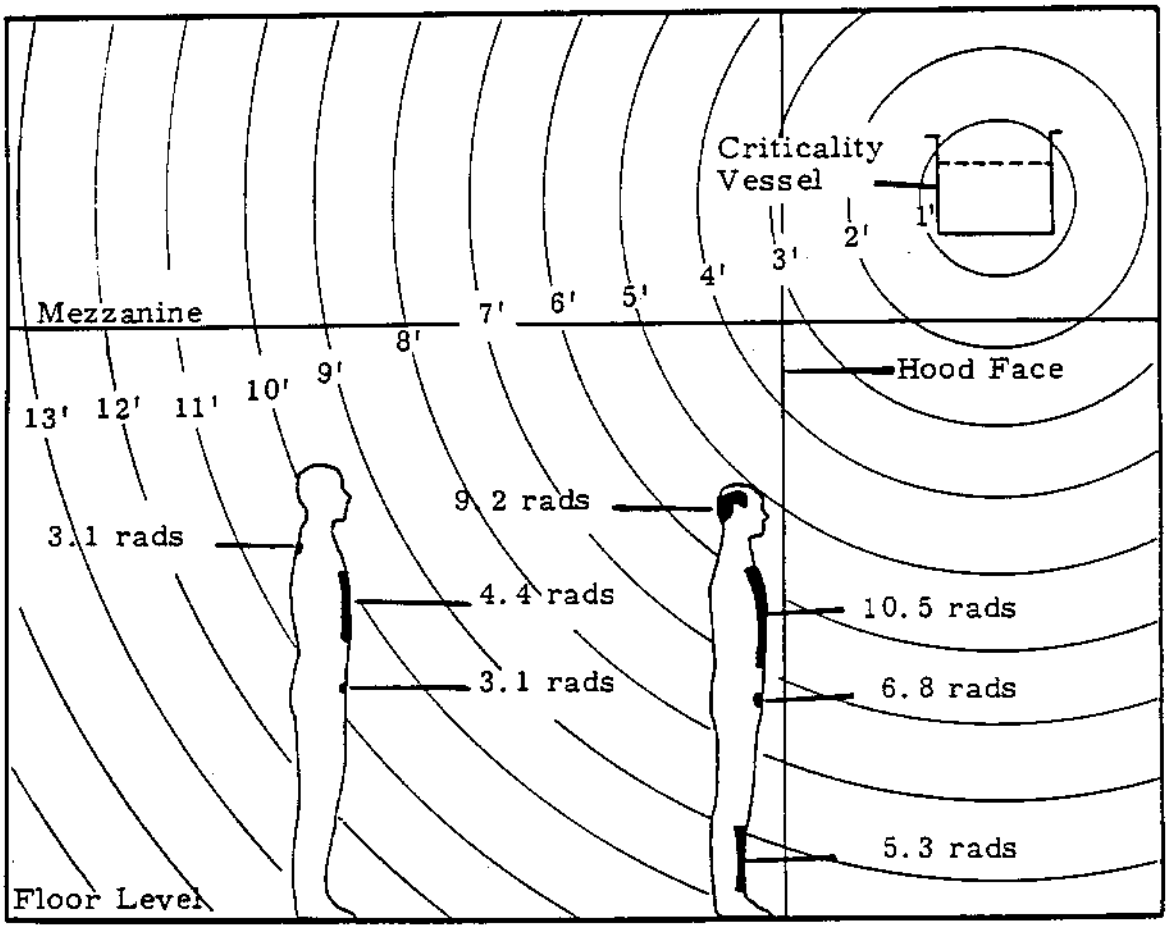

FIGURE 3.7

Neutron Doses (> 2.5 Mev) from Sulfur Activation in Hair
(Distances indicated are slant distances
from center of the critical solution)

When inverse square calculations were made to compare the doses (D) with distances (d) from the criticality vessel, all the products of D and d^2 agreed within the limits imposed by the assumed sulfur concentrations (47.7 ± 5.5 mg/g) and the accuracy of the radiochemical method used. Dd^2 for employee No. 17's back was lower than for samples taken from areas facing the criticality vessel, indicating that some degradation of the neutron spectrum had occurred during passage through his body. Similarly, Dd^2 for the posterior head sample from employee No. 1 indicated that spectral degradation had occurred during passage through his head.

Calculations of the total incident neutron doses from these data requires a detailed knowledge of the incident neutron spectrum. At the time of the criticality, a threshold detector [3.21] was located about 26 ft from the criticality vessel. At least one steel beam, the grid floor of the mezzanine, the stairway, and another hood were between the criticality vessel and the threshold detector. These certainly influenced the relative neutron spectrum reaching the detector, compared with the spectra or spectrum reaching the men. When the detector was analyzed, difficulties were encountered in the radiochemical measurement of P^{32} induced in the sulfur wafer, and there were some uncertainties in the initial calibration. These difficulties and uncertainties required that very careful consideration be given to many factors before deciding what portion of the total neutron dose was represented by the P^{32} measurements. After consultation and careful consideration of the present data, and of the neutron spectra exhibited from other accidents of this type, [3.16] it was estimated that the P^{32} measurements from the Hanford incident should represent about 25% of the total incident neutron dose.

For purposes of comparison only, one may, from Figure 3.7, assign "average" doses of about 7.5 rads to employee No. 1 and about 3.5 rads to employee No. 17. Employee No. 23 received an average dose of about 1 rad. These are the doses due to neutrons above 2.5 Mev, and a simple calculation will give the total neutron dose. Dose estimates from the P^{32} measurements are compared with dose estimates based on whole body Na^{24} and blood Na^{24} [3.16] in Table 3.6.

TABLE 3.6

SUMMARY OF FIRST COLLISION NEUTRON DOSE ESTIMATES, rads

Employee	Whole Body Na^{24}	Blood Na^{24}	P^{32} in Hair
1	23	28.5	30
17	9.2	14	14
23	2.9	3.5	4

The variations between the three neutron dose estimates reflect uncertainties in the neutron spectrum to which each employee was exposed as well as the variance in the chemical and instrumental techniques used in the measurement of induced radionuclides in the employees. Additional uncertainties resulted from the use of literature values for induced activity to neutron dose factors which were measured under somewhat different conditions than existed at the time of the Hanford accident. Agreement between the three neutron dose estimates is quite good in view of these uncertainties.

Sulfur activation in hair is strictly a surface reaction, and therefore of greatest value in estimating localized incident doses from the appropriate measurements in hair, especially in cases where considerable nonuniformity of dose distribution has occurred. Sodium activation of blood or whole body measurements, however, would be expected to provide more precise information regarding average neutron doses because of the rather uniform distribution of sodium in the body and its rapid equilibration following activation. The P^{32} measurements are not readily applicable to the determination of absorbed doses, although certain of these data, notably the concentration of P^{32} in hair from employee No. 17's chest and back, and posterior hair from employee No. 1's head, suggest this would be worthy of additional study.

It is interesting to note what fraction of the total number of fissions that occurred contributed to the doses received by these employees. Fissioning continued in the reaction vessel until about 36 hr after the incident began.

Two recording BF_3 monitors indicated an initial excursion, the exact magnitude of which cannot be determined because the flux level is recorded only every 30 sec and it may vary by orders of magnitude within such a time period. Following this initial pulse, which presumably activated the criticality alarm, there was a continuing nuclear reaction of a magnitude sufficient to keep the recorder off-scale for a period of about 30 min. After the recorder returned to on-scale readings, fissioning continued at a generally reduced rate until about 36 hr after the incident began. The threshold detector was removed about 90 min after the incident began. The recorder trace from the BF_3 monitors [3.16] indicated that most of the fissions had occurred by this time. The threshold detector was exposed to approximately 0.35×10^{10} n/cm^2 above 2.5 Mev. Employee No. 1 (average 6.5 ft from the reaction) was exposed to 2.9×10^9 n/cm^2 above 2.5 Mev, and employee No. 17 (average 9.7 ft from the reaction) was exposed to 1.4×10^9 n/cm^2 above 2.5 Mev. Inverse square calculations demonstrate that employees No. 1 and No. 17 were in the vicinity of the reaction vessel only long enough to be exposed to about 5% of the neutrons produced.

Conclusions

The measurements described here were made over a time interval of about 6 da, although such measurements are not by nature extremely time-consuming. Some of the time was devoted to the chemical separation procedure, and sampling difficulties were encountered partially because of our limited first-hand knowledge of the potential value of these measurements.

In addition to determining neutron doses, especially where these doses are highly nonuniform, measurements of P^{32} induced in human hair can be of significant value in locating the precise origin of a critical disturbance of this sort. In Figure 1, the measurements are shown to fix exactly the vertical location of the reaction vessel with respect to employee No. 1 and No. 17. A similar plot from above or below the vessel could in many instances place the employees horizontally with respect to the vessel. This is especially interesting, since in this case several vessels were originally suspect.

A stepwise chemical procedure is included in Appendix 3.1 and should prove to be a valuable addition to emergency procedures at any site where a criticality might accidentally be achieved. Detailed sampling information should include a request that hair samples be taken from head, back, upper chest, pubis and lower legs. A useful temporary substitute for these samples would be the inclusion of a sulfur button in the film badge holder, to be analyzed immediately in the event of a criticality.

APPENDIX 3.1

STEPWISE PROCEDURE FOR THE DETERMINATION OF P^{32} INDUCED IN HUMAN HAIR

1. Wash the hair by swirling in a beaker with mild detergent solution. Filter on a Buchner funnel, rinse with large quantities of water, and finally with alcohol. Draw air through the funnel until the hair is thoroughly dry. Weigh a 1-g sample.
2. Place the hair sample in a new 250 ml beaker and digest with 5-10 ml HNO^3, 5 ml H_2SO_4, and 5-10 ml 30% H_2O_2. When dissolution appears complete, evaporate the solution barely to fumes of SO_3.
3. Carefully add 10 ml HNO_3 and 3 ml $HClO_4$. Evaporate the solution to fumes of SO_3. (Note 1)
4. Cool the solution and allow the beaker to drain thoroughly into a new 100 ml graduated cylinder containing exactly 55 ml of water. Add H_2SO_4 until the volume is exactly 60 ml, then dilute the solution to 100 ml. Transfer the solution to a new 250 ml separatory funnel.
5. Rinse the beaker and the graduated cylinder with exactly 20 ml of water and add the rinses to the separatory funnel.
6. Add to the separatory funnel 30 ml of 10% ammonium molybdate solution and 35 ml of 13% (v/v) n-butanol in diethyl ether solution. Shake the funnel 60 sec after the initial pressure releases. Discard the aqueous layer.

APPENDIX 3.1 (Contd.)

7. Carefully add to the separatory funnel 20 ml of 1.2 N H_2SO_4. (Note 2) Shake 10 sec after the initial pressure release. Discard the aqueous layer.

8. Transfer the organic solution to a new 50 ml beaker and very carefully evaporate the solution to about 0.5 ml. (Note 3) Transfer the solution to a counting dish with ethanol and evaporate the dish to dryness.

9. Measure the P^{32} activity with a low background proportional counter. (Note 4)

Note 1 H_2SO_4 fumes are readily distinguishable following the evaporation of $HClO_4$. In addition, upon the removal of the last traces of $HClO_4$ the solution changes from dark to nearly colorless and H_2SO_4 begins to condense on the sides of the beaker.

Note 2 Sufficient heat is generated to require a very gentle initial agitation of the solution.

Note 3 The evaporation must be done slowly to prevent the ether from catching fire.

Note 4 The chemical yield of the procedure is 88.5 ± 3.0%.

Environmental Studies

Studies of Radioiodine and Other Fallout Radionuclides in Air - R. W. Perkins

Methods for sampling fallout from air at ground level and from aircraft have been developed and evaluated. The concentrations of the radionuclides I^{131}, Ba-La^{140}, Zr-Nb^{95}, Ru^{103}, Ru^{106}, Ce^{141}, Cs^{137}, and Pu^{239} were measured during 1962, and their levels are compared with the nuclear detonations during 1962. The chemical and physical form of I^{131} from fallout and radiochemical separations plants was measured.

The operation of nuclear reactors and of chemical processing plants for exposed reactor fuels requires very careful monitoring of the immediate environs. The presence of fallout radionuclides from nuclear weapons testing complicates this monitoring and requires that the compositions of the radionuclide mixture be known so that its source (fallout or plant origin) can be determined. The radionuclide I^{131} is of principal concern both in fallout and in release from separation plants, and it is important to know its physical and chemical form in both fallout and plant emission. The distribution of fallout radionuclides in air, both at the ground level and in vertical profiles, are also of interest. Equipment and techniques for sampling and studying the fallout radionuclides in air have been investigated, and both the physical and chemical form of I^{131} have been determined on a few samples.

Air Sampling

Several types of air filter systems have been evaluated for collecting radionuclides from air. For ground base sampling a 100 cfm vacuum pump has been used. A portable, high-velocity, light-weight, air sampler has also been used for ground base sampling and is used for air sampling from aircraft.

Filter Efficiencies

The efficiencies of several commercially available air filters have been tested for their ability to collect fallout radionuclides from the atmosphere.

In preliminary studies it was found that if two AM-3 membrane filters** were positioned in series in an air stream, the second filter contained < 1% of any of the fallout radionuclides which were collected on the first filter.

An AM-3 filter was, therefore, used as a backup filter in determining the efficiencies of the other filters which were tested. The filter efficiencies of HV-70 asbestos filters, type M fiber glass filters, AM-1 membrane filters, and IPC paper filters were tested and the results are recorded in Table 3.7.

TABLE 3.7

EFFICIENCIES OF VARIOUS TYPES OF FILTERS FOR THE FALLOUT RADIONUCLIDES

Filter Type*	Linear Velocity, ft/min	Percent of Particulate Radioactivity Held by Filter					
		$Ba\text{-}La^{140}$	Ru^{106}	$Zr\text{-}Nb^{95}$	Ru^{103}	I^{131}	Ce^{141}
HV-70, Asbestos	1000	> 94	> 93	> 99	> 99	> 90	> 93
AM-1, Membrane	200	> 99	> 99	> 99	> 99	> 99	> 99
Fiber Glass, Type-M	200	63	65	80	57	25	66
IPC, Paper	1100	74	83	90	70	--	77
IPC, Paper	4400	97	99	99	97	81	96

* AM-1 membrane filter and type-M fiber glass filters were obtained from Gelman Instrument Co., Chelsea, Michigan
IPC paper is discussed in Reference 3.22

** AM-3 membrane filters, pore size 2.0 microns, Gelman Instrument Company, Chelsea, Michigan

It is evident that an AM-1 filter is also an absolute filter for the fallout radionuclides. The HV-70 asbestos filter is also a very efficient filter. Its exact efficiency was not determined for all the radionuclides, but it was greater than 99% for $Zr\text{-}Nb^{95}$. The type M fiber glass filter, which is really designed as a prefilter, was not very efficient. The IPC filter paper is designed as a high velocity-high flow rate filter,[3.22] and its efficiency was tested at two flow rates. At the lower flow rates the efficiency of IPC filters is rather poor, but at a high flow rate (4000 linear ft/min) the efficiency is between 95 and 99% for all the radionuclides except I^{131}.

Ground Base Sampling of Fallout Radionuclides in Air

A high velocity heavy duty vacuum pump* was chosen for ground base sampling. Membrane filters (AM-1) were selected for air filtering since (1) they were essentially absolute for particulate fallout material, (2) the pressure drop across these 8 in. x 10 in. membrane filters at 100 cfm was relatively low, and (3) they can easily be dissolved for subsequent radiochemical analysis. These filters were backed with 4 in. diameter by 1-in. thick beds of activated charcoal to collect gaseous I^{131}.

Aircraft Sampling of Fallout Radionuclides in Air

The Hanford AEC twin engine Beechcraft was used for air sampling. Air filtering was normally performed at 3000, 6000, 9000, and 12,000 ft by simultaneously collecting a sample with an 8 in. x 10 in. AM-1 membrane filter backed with a 4 in. diameter by 1-in. thick charcoal bed and also collecting a "ram sample" on an 8 in x 10 in. IPC filter. The air for the AM-1 filter was drawn into the plane at a right angle to the direction of flight through a 2 in. diameter opening in the plane's door. The ram samples were collected by inserting the IPC filter on its rigid screen backing into its ram sleeve (a rectangular tube 17 in. long mounted on the door of the plane) outside the plane.

---

* Roots-Connersville Blower, S-RAI-581, Medium Pressure, 3 in. inlet pump, Number 44.

Samples were collected for 20 min at each elevation in a direction upwind from the Hanford reservation. The IPC filters collect 10-20 times as much radioactivity as the AM-1 filters; however, the flow rate is still only about 1500 linear ft/min at a plane speed of 9500 ft/min (110 mph), and collection efficiency at this linear flow rate is low and variable. The AM-1 filter system samples air at about 50 cfm, the exact flow rate being measured with a calibrated pressure plate gage. The AM-1 filter quantitatively collects the particulate material, and its charcoal trap collects the vapor I^{131}. Neither of the filter systems is completely satisfactory since they do not provide isokinetic air sampling. The AM-1 filter system which draws in air at a right angle to the direction of flight would miss some large particles, while the ram sampling technique collects more large particles than are actually associated with the volume of air sampled. The errors thus introduced are not known; however, they are considerable since radionuclide ratios on simultaneously collected AM-1 and IPC filters sometimes vary by as much as factors of 2 to 3. A modified "ram-pump" system which will permit isokinetic sampling in flight is presently being designed.

Counting Equipment

All of the filters were measured for their radionuclide content by counting them in a low background high selectivity gamma-ray spectrometric system. This spectrometer consists of a 5 in. diameter by 5 in. thick well crystal which is surrounded with a 30 in. diameter by 30 in. thick plastic phosphor anticoincidence guard.[3.23] The anticoincidence feature lowers the background by a factor of 3 to 5 and provides a reduction of 2 to 20 in Compton regions, thus permitting a very high degree of sensitivity and selectivity in measurements. This equipment makes possible the direct measurement of $Ba\text{-}La^{140}$, $Zr\text{-}Nb^{95}$, Ru^{103}, I^{131}, $Ce^{141\text{-}144}$ and a fair measurement of Ru^{106} (from its 1.14 Mev sum peak).

Observed Fallout Levels for 1962

All of the measurements reported in this section were for samples collected with sampling equipment located in a Hanford laboratory area.

In Figure 3.8, a graph of the observed concentrations of Ba^{140}, $Zr\text{-}Nb^{95}$, Ru^{103}, Ru^{106}, and $Ce^{141\text{-}144*}$ is presented. Also shown are the known USSR and U.S. atomic detonations. Fallout measurements were not started until the end of the first series of USSR tests and measurements immediately following these tests do not show any significant peaks in activity. It is interesting that the radionuclide concentration in air does decrease approximately at the rate of radioactive decay of most of the radionuclides. The first indication of fallout from the U. S.. tests, which started on April 25, 1962, was the presence of I^{131} in mid-June. Several "peaks" of activity were observed through the remainder of the year; however, because of the continuing detonations by both the U.S. and USSR it is difficult to ascribe a particular activity peak to a specific detonation.

The radionuclides Zr^{95} (65 day) and Ba^{140} (12.8 day) are easily measured with a high degree of precision and their half-lives differ sufficiently that a measure of their ratio as a function of time would be expected to be a good indicator of arrival of new fallout. Figure 3.9 presents the Zr^{95} to Ba^{140} ratio and the Ba^{140} activity as a function of time and nuclear detonations.

The Ba^{140}:Zr^{95} ratio is, of course, a measure of the relative age of the fallout. The higher the ratio, the younger the material. It is interesting that the ratio curve very nearly resembles the total Ba^{140} curves (and other radionuclide concentration curves--see Figure 3.8) indicating that the activity peaks are actually due to the arrival of fresh fallout rather than just an increased rate of deposition of fallout.

In Figure 3.10 the relative age of the fallout (as indicated by the Ba^{140} to Zr^{95} ratio) is compared with total I^{131} and the fraction of I^{131} associated

---

* $Ce^{141\text{-}144}$ measurements assume a Ce^{141}:Ce^{144} ratio of 3:1 at the end of November 1961, USSR tests and a ratio of 1:1 during all of the following tests.

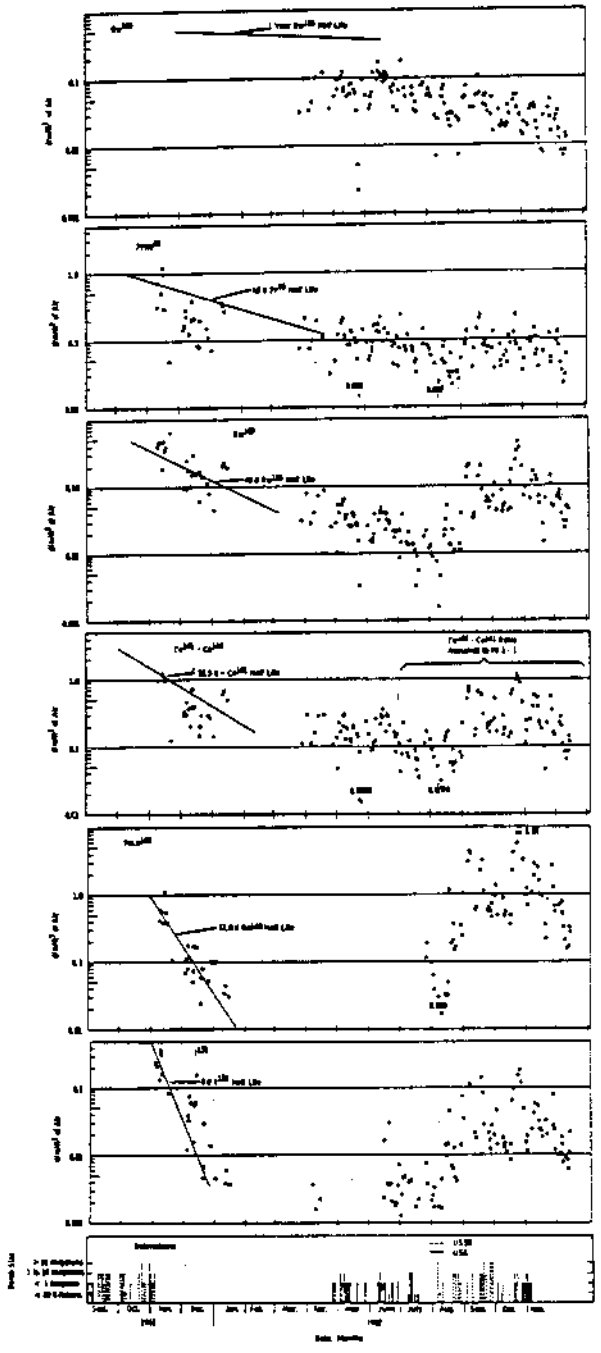

FIGURE 3.8

Observed Fallout Radionuclide Concentrations
at Hanford During 1961-1962

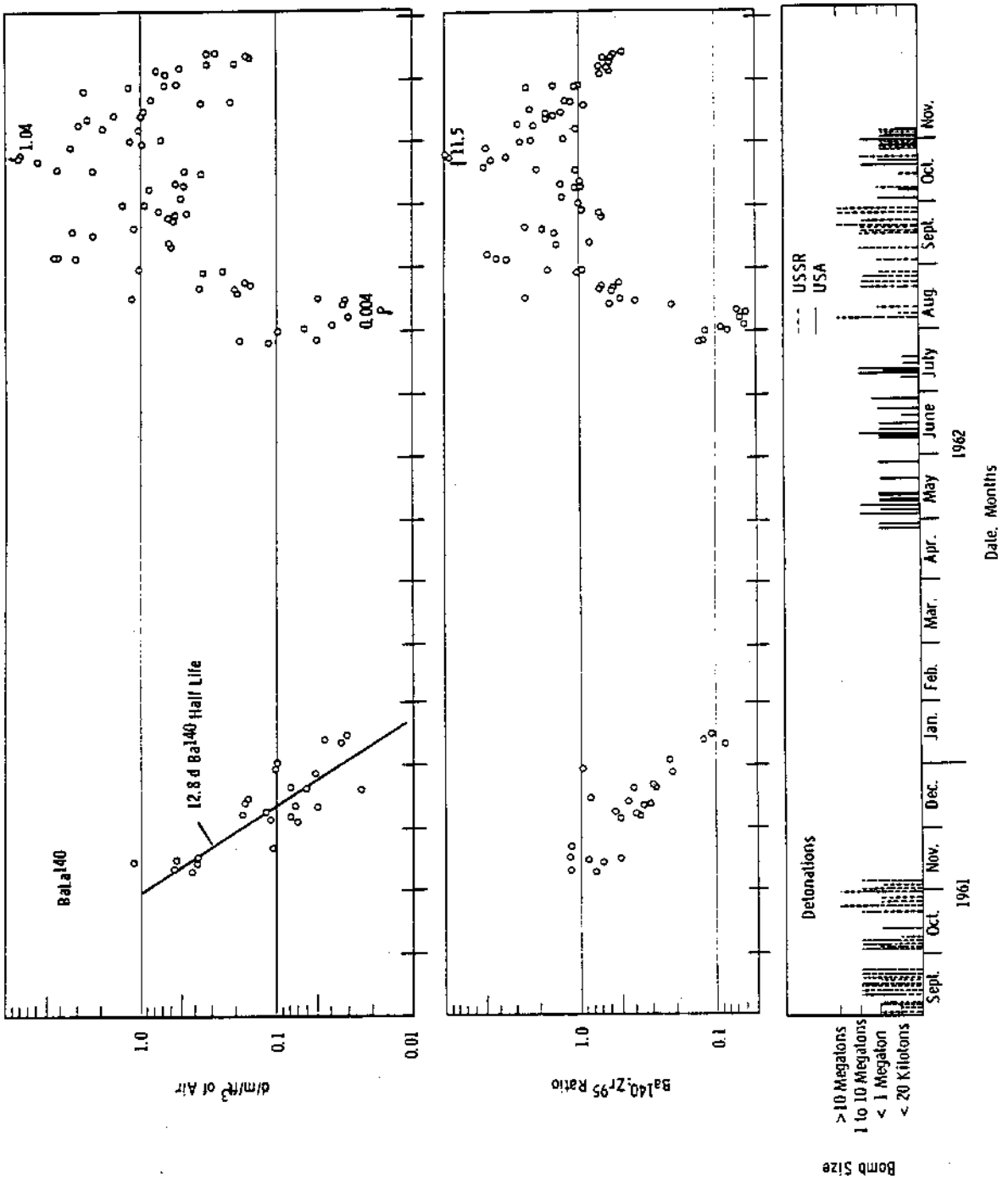

FIGURE 3.9

Ba^{140}:Zr^{95} Ratio and Total $BaLa^{140}$ Activity in Fallout Debris as a Function of Time

AEC-GE RICHLAND, WASH.

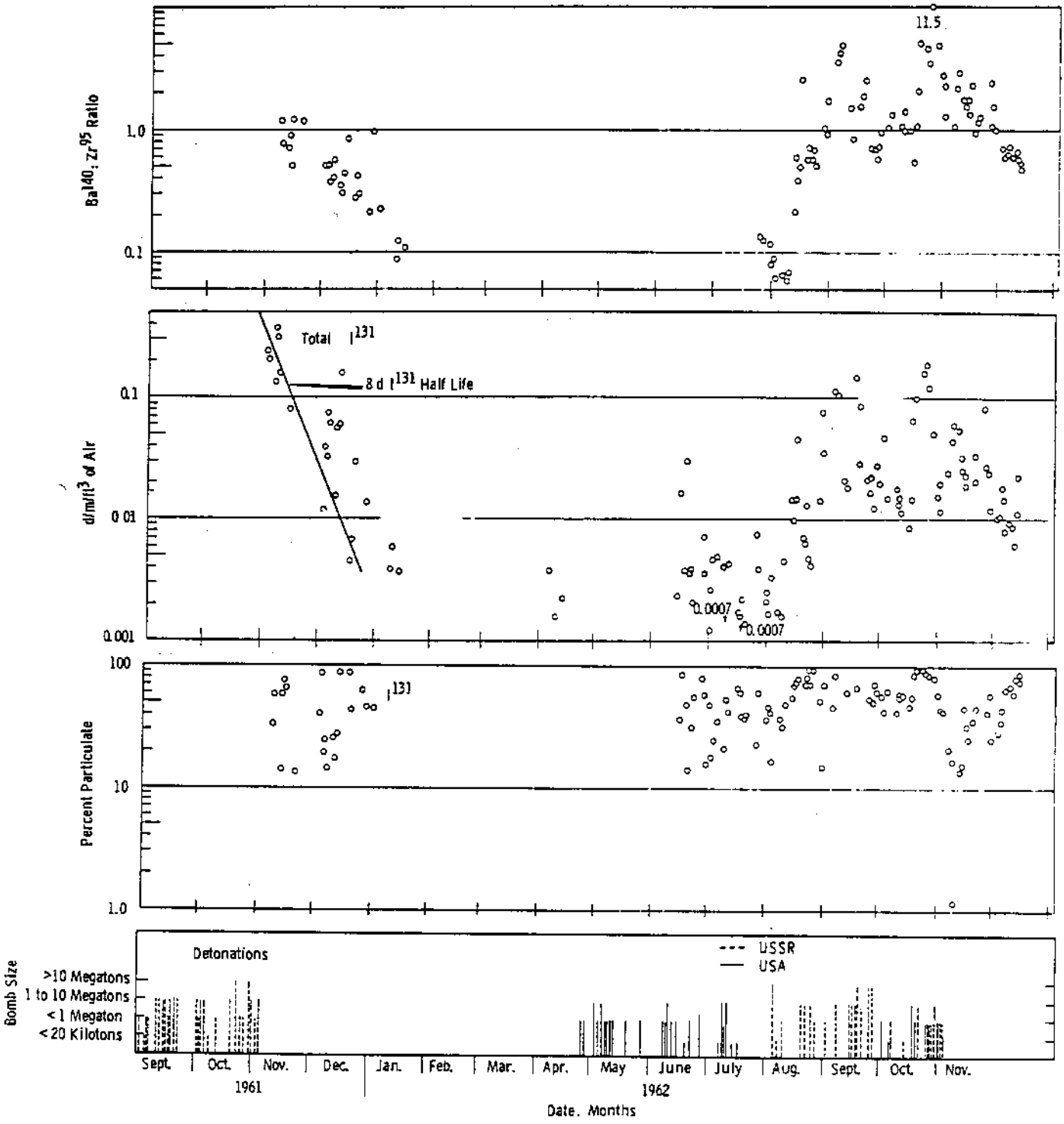

FIGURE 3.10

Physical Forms of I^{131} Compared with Relative Age of Fallout at Hanford During 1961-1962

AEC-GE RICHLAND, WASH.

with particulate material in fallout. Not all of the activity peaks, as indicated by the total I^{131} level and the Ba^{140}:Zr^{95} ratio, are accompanied by a change in physical form of I^{131}; however, two of the major peaks are accompanied by very definite changes in I^{131} form. The order of magnitude increase in total I^{131} during the last half of October was accompanied by a very significant increase in the fraction of I^{131} associated with particulate material. The somewhat smaller increase in total I^{131} during November was accompanied by a very definite decrease in the particulate associated I^{131}. The reason for these differences is not known but may be due to both the origin of the fallout and the history and movement of the air masses which carried it to this location.

The Pu^{239} and Cs^{137} content of air was measured on filter samples selected from each month of 1962 (except February when sampling was not performed). The Pu^{239} was separated by a modified bioassay procedure, (3.24) and the Cs^{137} was separated from the residues by a standard Cs^{137} procedure (3.25) which involved a silicowolframate precipitation followed by a perchlorate precipitation. The observed Pu^{239} and Cs^{137} concentrations and their ratios are presented in Table 3.8. The extreme variation in the ratio of Pu^{239} to Cs^{137} is probably due to the type of nuclear detonation– Pu^{239} bomb, U^{235} bomb, U^{238} clad hydrogen bomb, etc. The high Pu^{239} to Cs^{137} ratios during June and July evidently resulted from the earlier USSR tests. The high ratios in October and November were likely due to USSR tests but could have resulted from U.S. tests. It would be expected that after cessation of testing the Pu^{239} to Cs^{137} ratios would become nearly constant.

I^{131} Chemical Form Studies

The physical form of I^{131}, whether gaseous or particulate, is readily determined by filtering air through an absolute filter followed by a charcoal trap. Data from such measurements indicates that a large and varying amount

TABLE 3.8

OBSERVED Pu^{239} and Cs^{137} LEVELS IN AIR DURING 1962

Date of Sample Collection	Concentration dis/min/10^6ft^3 Pu^{239}	Cs^{137}	Pu^{239}/Cs^{137} x 1000
1/12 - 1/15	3.66	115	31.8
3/28 - 4/2	0.58	417	1.38
4/19 - 4/26	0.085	63.8	1.33
5/18 - 5/21	0.94	490	1.92
6/20 - 6/21	0.07	164	12.6
7/23 - 7/24	2.22	152	14.6
8/17 - 8/20	0.24	156	1.56
9/21 - 9/24	Lost	210	--
10/16 - 10/17	0.91	14.4	63.3
11/16 - 11/19	0.67	27.9	24.1
12/20 - 12/21	0.18	19.6	9.13

of I^{131} is in the gaseous state, presumably in the reduced form of I_2 (or possibly HI--see Figure 3.9). During 1962 about half (actually 10% to almost 90%) of the I^{131} collected from air passed through the membrane filter and was collected by the charcoal bed. Work was performed to determine the chemical form of the I^{131} associated with particulates. The procedure selected was designed to remove the I^{131} and measure the fractions of I^- (or I_2), IO_3^-, and IO_4^- present. This procedure was a modification of a method developed for determining the valence state of iodine radioisotopes formed from the decay of their radiotellurium precursors.(3.26) It involves placing the filter in a blender with 100 ml of ice water at pH 12 containing 0.05 meq of I^- carrier, 1 meq of IO_3^- carrier, and 5 meq of IO_4^- carrier. The mixture is blended for 2 min at maximum speed, filtered through a AM-3 membrane filter (pore size 2.0 μ), made 0.1 $\underline{N}$ in HNO_3, and the reduced iodine ($I^- + I_2$) immediately removed by two CCl_4 extractions. The

aqueous solution is then adjusted to a pH of 3, and the IO_3^- is precipitated as $Ba(IO_3)_2$. This is immediately followed by a KIO_4 precipitation to remove the IO_4^- fraction.[3.27]

Experiments with tagged $(I^{131})^-$ and $I^{131}O_3^-$ have shown that the exchange between each of these forms and the other two were very small. A considerable amount of the IO_4^- is reduced to IO_3^-; however, very little radioiodine has been observed in the IO_4^- fraction.

The major problem in determining the chemical form of I^{131} fallout on particulates has been removal of the radioiodine from the particulates (without changing its chemical form). The technique described removes 20 to 60% of the radioiodine but the chemical form of the remaining material is not known. The valence form of the I^{131} which could be removed from two AM-1 air filters is shown in Table 3.9.

TABLE 3.9

CHEMICAL FORM OF I^{131} COLLECTED ON MEMBRANE FILTERS

Date	Percent of I^{131} Leached From Filters	Fractionation of Leached I^{131} Percent		
		$I_2 + I^-$	IO_3^-	IO_4^-
10/24/62	44	~ 57	~ 38	< 5
10/25/62	42	~ 66	~ 29	< 5

If the I^{131} collected on the charcoal bed (which averages about 50% of the I^{131}) is assumed to be in the reduced state (I_2 or I^-) and if the material which is not washed from particulates is in the same valence form as that removed, it is evident that about 80-85% of the fallout I^{131} is in the reduced state (I_2 or I^-), 15 t0 20% is present as IO_3^- and a few percent or none is present as IO_4^-.

I^{131} From Separation Plant Stacks

Small amounts of I^{131} are released continuously from the chemical separations plant stacks. This I^{131} has been analyzed and is less than 1% particulate. During a period of unusually high I^{131} emission, aircraft sampling of air at an elevation of about 600 ft above ground was performed at distances of about 1, 3, 5, 10, and 25 miles from the source. The fraction of the I^{131} which was found to be associated with particulate material at these distances is shown in Table 3.10.

TABLE 3.10

PHYSICAL FORM OF I^{131} IN AIR
AT VARIOUS DISTANCES FROM THE SOURCE

(Sampled from Aircraft)

Distance from Source, Miles	Percent Particulate
1	12
3	8
5	20
10	34
20	38
25	34

The percent of I^{131} associated with particulate fallout, as measured at the ground base sampling station, was about 60% and this radioiodine was responsible for an increasingly larger part of the I^{131} collected with increased distance from the source. Although the presence of fallout I^{131} in the air at the time of these measurements caused some uncertainty, the data do indicate the I^{131} released to the atmsophere does not immediately adsorb on particulate material in the air and even after many hours (several miles away) it is still in a gaseous state.

Air Profile of Fallout Radionuclides

Several sampling flights have been made with the Hanford AEC Beechcraft. These flights are planned in conjunction with Atmospheric Physics personnel and are being timed to measure fallout concentrations under specific meteorological conditions. With present aircraft, these studies are limited to 12,000 ft. It is the aim of these studies to determine if the observed level and profile of radioactivity can be related to the origin of the air mass and to determine if correlations exist between the radionuclide profile, the air flow at midlevels, and the atmospheric temperature-lapse rate. Basic information is also being obtained on actual fallout radionuclide concentrations through 12,000 ft compared with those at ground level. Considerable variations in radionuclide concentrations have been observed through these altitudes. A graph showing the concentrations of Zr-Nb^{95}, Ru^{103}, Ba^{140}, Ce^{141}, and of both particulate and gaseous I^{131} as measured on November 13, 1962 is shown in Figure 3.11.

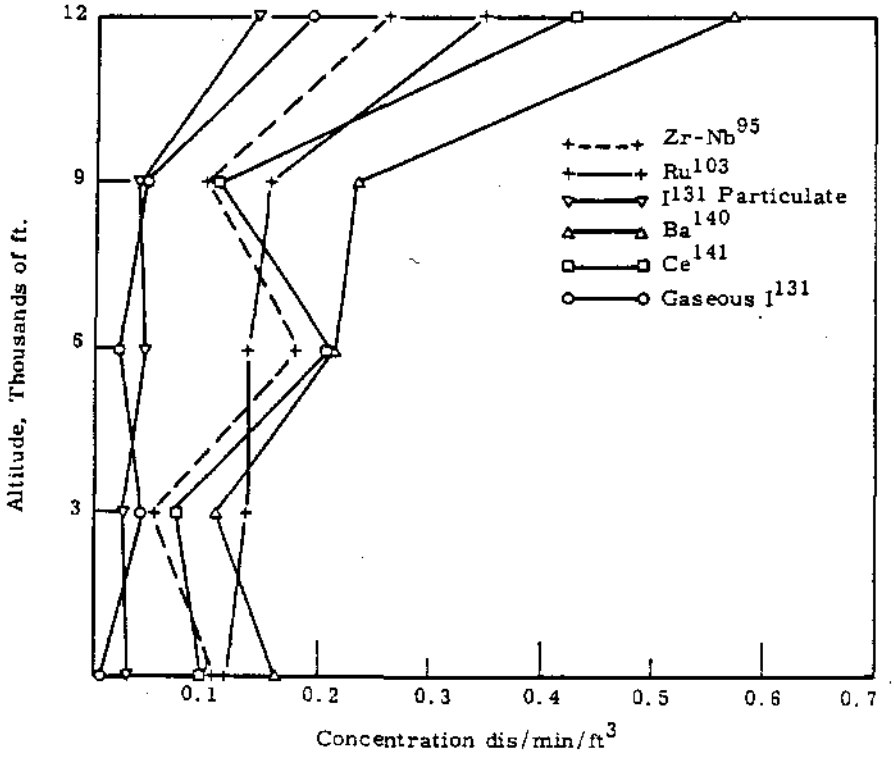

FIGURE 3.11

Radionuclide Concentration as a Function of Altitude

Cs^{134} from Fallout - R. W. Perkins and H. E. Palmer

The activity concentration of Cs^{134} relative to Cs^{137} in Alaskan Eskimos, in caribou meat from their area, and in fallout from air filters at Richland, Washington, has been found to be in reasonable agreement with that recently reported in Swedish and Finnish Lapps. This, plus the reported observations of Cs^{134} in fallout in the U.S. during 1957, indicates that Cs^{134} deposition has been essentially world-wide.

The radionuclide Cs^{134} is produced by the reaction $Cs^{133}(n,\gamma) \rightarrow Cs^{134}$ and also from thermal neutron fission, but with an independent fission yield (for U^{235}) that is probably on the order of 5×10^{-4}%.[3.28] The presence of Cs^{134} in fallout material was reported in 1958.[3.29] Particulate samples collected from air over St. Louis durign March 1957, showed Cs^{134} disintegration rates ranging from 12 to 16% of the Cs^{137} activity. More recent whole body measurements of Swedish and Finnish Lapps[3.31] during 1961 showed the Cs^{134} to be more than 1% of the Cs^{137}, while measurements of reindeer meat from their area showed the Cs^{134} to be 1.6% of the Cs^{137}. However, Cs^{134} was not detected in Swedes from Stockholm, and some efforts were made to explain this observation on the basis of geographical distribution of the fallout containing Cs^{134}. Analysis of gamma-ray spectra of Alaskan Eskimos taken during the summer of 1962[3.31] definitely showed the presence of Cs^{134} (see Figure 3.12). Measurements of the Cs radionuclides in reindeer and caribou meat which was collected in Alaska during the summer of 1962 also showed the presence of Cs^{134}. The Cs^{134} content of these meat samples was verified and measured by γ-γ coincidence counting of the 0.605 and 0.797 Mev cascade photons in the manner reported by Liden and Andersson.[3.30] For this measurement, a 3-lb meat sample was sandwiched between two 9-3/8 in. diameter by 4 in. thick NaI(Tl) crystals. The output from one of these crystals was routed to the mixer amplifier of an RIDL 400-channel transistorized analyzer, while the signal from the other crystal was fed to the normal signal input of the analyzer.

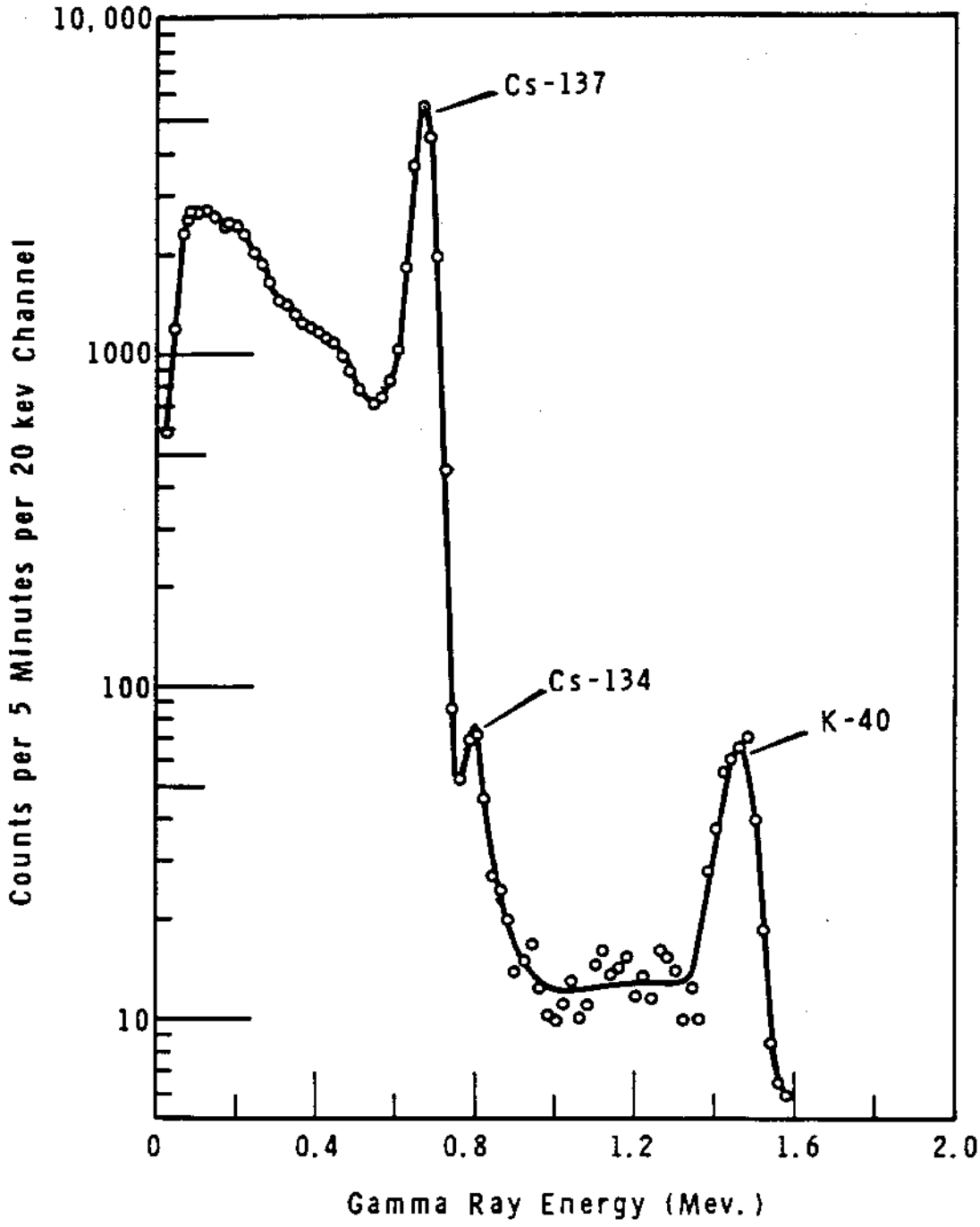

FIGURE 3.12

Net Sum Spectrum of 10 Eskimos from Anaktuvuk Pass, Alaska
Average Cs^{137} Burden 667 nc

Pulses of greater than 0.51 Mev from the first crystal allowed coincidence pulses from the second crystal to be stored. The coincidence spectrum obtained in this manner is compared with that of a standard Cs^{134} source of similar geometry, and with a spectrum of the sample that was counted without the coincidence requirement in Figure 3.13. These measurements showed the Cs^{134} to be present in an activity concentration of $0.82 \pm 0.1\%$ of the Cs^{137} at the time of sample collection.

A chemical separation of the cesium radioactivity from an air filter which was in service in Richland, Washington, during 1960 indicated Cs^{134} at an activity concentration of $< 1\%$ of the Cs^{137}; however, the total activity of this particular sample was too low to permit a precise measurement of the ratio. Very recent measurements of Cs^{134} and Cs^{137} have been made following chemical separation of cesium collected on a high volume of air filter located near Richland, Washington, which collected fallout from early December 1962 through January 1963. The Cs^{134} activity concentration on this filter was found to be $1.6 \pm 0.1\%$ of the Cs^{137}. These measurements help to establish the fact that Cs^{134} has been and is being deposited in North America as well as in northern Sweden and Finland, and that the deposition must be world-wide.

The formation of Cs^{134} at an activity of 1.6% of the Cs^{137} from U^{235} fission would require an independent fission yield for Cs^{134} of $7 \times 10^{-3}\%$. This is about an order of magnitude higher than the expected level for U^{235} fission.(3.28) The Cs^{134} yield from Pu^{239}, U^{233} and other fissionable materials has not been reported and may be high enough to account for some of the observed Cs^{134} to Cs^{137} ratios. Barring a rather high Cs^{134} yield from one of these fissionable materials, it would appear that Cs^{134} must be produced from inert Cs^{133} which is either part of the nuclear device or is added to serve as a tracer. The very high Cs^{134} to Cs^{137} ratios reported to be present in fallout from over St. Louis during March 1957, must have resulted from neutron activation of inert Cs^{133} in a

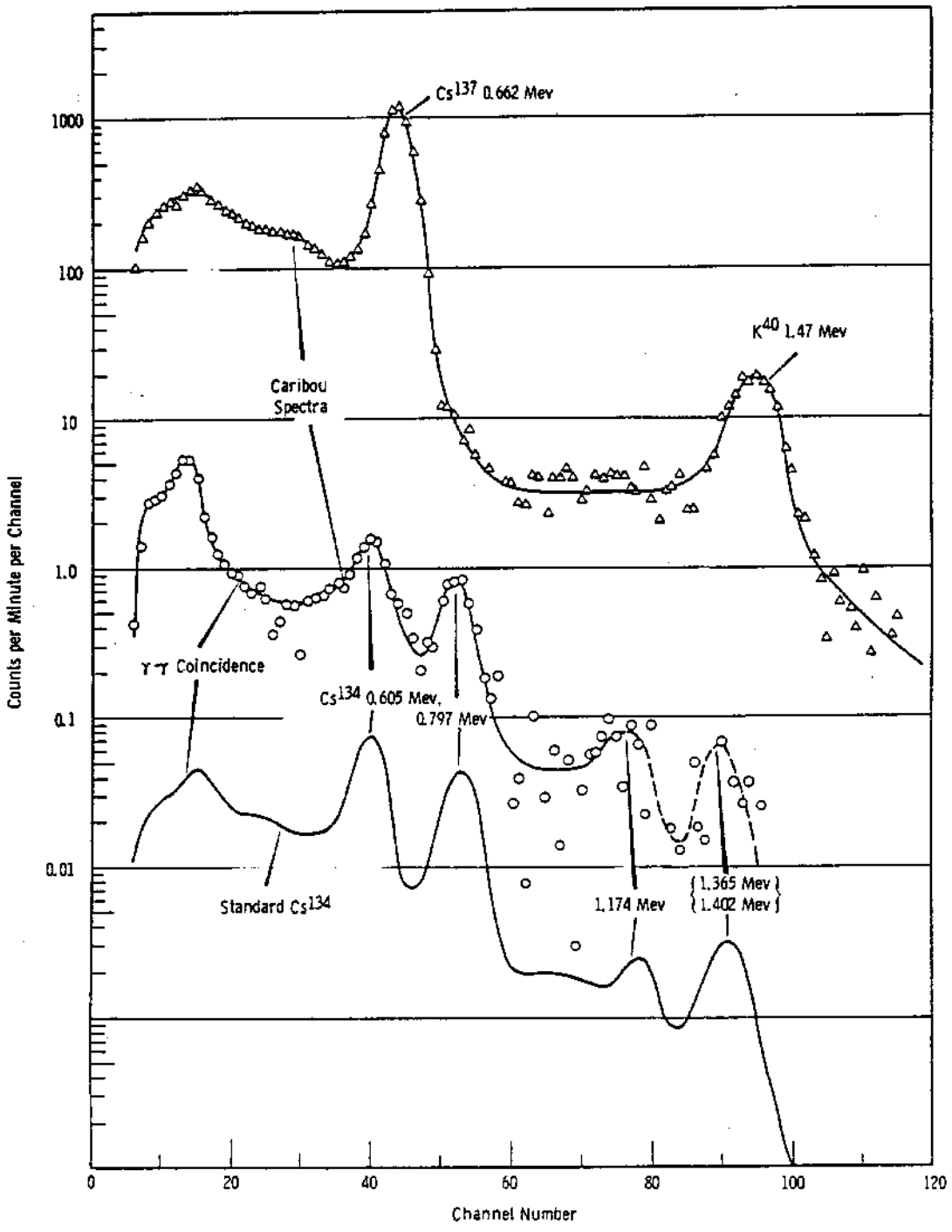

FIGURE 3.13

γ-γ Coincidence Spectrum of Caribou Meat, Normal Single Crystal Spectrum of the Sample in the Same Geometry, and γ-γ Coincidence Spectrum of a Cs^{134} Standard of Similar Size in the Same Geometry

nuclear device. Cs^{134} has been reported in a soil sample taken near ground zero following an atomic balloon shot in Nevada.(3.32) However, no Cs^{137} was observed in the sample and the Cs^{134} evidently results from neutron activation of inert Cs^{133} in the soil. It is planned to measure the Cs^{134}:Cs^{137} ratio periodically during the coming year to determine if the observed ratio (corrected for decay) remains constant. This should provide an indication of the uniformity of Cs^{134} relative to Cs^{137} in this atmsophere.

Measurement of Pu^{239} in Air - R. W. Perkins

In connection with fallout studies, (see "Studies of Radioiodine and Other Fallout Radionuclides in Air," page 3.36) it was important to measure the Pu^{239} content of air. Since fallout debris is collected from air on membrane filters (AM-1 filter, Gelman Instrument Co., Chelsea, Michigan) a procedure for removal of the Pu^{239} from the filter and from soot and dust particles which are collected simultaneously with the fallout was required.

Measurements of the Pu^{239} in air in England (3.33) during the Spring of 1962 showed a concentration of about 1.5 dis/min/10^5 ft^3 of air (our normal sample size). Since concentrations of an order of magnitude or more lower than these might be expected, a procedure was desired which would provide sensitivities of a few hundredths of a dis/min. Such a sensitivity can be obtained by nuclear track counting of chemically separated Pu^{239}. (3.34)

This procedure, involves the following steps. The air filter is placed in a beaker with 40 mg of praseodymium carrier plus 50 ml of concentrated HNO_3 and is evaporated carefully to dryness. It is muffled at 400 C overnight, and the residue is dissolved in 50 ml of 4 N HNO_3. The Pu^{239} is then carrier-precipitated twice as the fluoride with its praseodymium carrier and extracted, carrier-free, into TTA-benzene. The Pu^{239} is back extracted into HCl and finally electrodeposited on a stainless disc from a NaClO solution. The electrodeposited disc is exposed to nuclear track film in the standard method used for bioassay samples. (3.34) The radiochemical yield for the procedure is about 90%.

Plutonium in Biological Tissues - L. J. Kirby

Preliminary measurements of plutonium in lungs and lymph nodes were completed for steers which had been raised near Pasco, Kahlotus, and Selah, Washington. The steer from the Pasco area had been fed from pasture irrigated by Columbia River water withdrawn downstream from the Hanford Project. The steer from the Kahlotus area was raised on pasture which lies generally in the downwind direction from the Hanford Project. The steer from the Selah area was raised on pasture which is generally unrelated to the Hanford Project by water flow or by the prevailing winds which blow across the Project.

The tissues were decomposed by treatment with hot HNO_3-H_2O_2 solutions. Dissolution was completed by digestion in hot concentrated H_2SO_4 and finally by very carefully controlled digestion with many small volumes of hot concentrated H_2SO_4-$HClO_4$. The tissues were assumed to be completely in solution when no further evidence of oils existed. Plutonium was reduced to the trivalent state and coprecipitated on lanthanum fluoride. Following dissolution of the precipitate, Pu(IV) was adsorbed from 10 M HCl onto Dowex-1 (Cl^-). After elution with 10 M HCl -0.1 M HI, Pu(IV) was extracted into TTA-benzene solution from dilute HNO_3. The TTA solutions were evaporated on small counting dishes, and plutonium determined by alpha-counting.

The levels of plutonium in lung tissue were $\leq 1 \times 10^{-3}$ dis/min/g tissue. One sample of post mediastinal lymph nodes contained $8 \pm 6 \times 10^{-3}$ dis/min/g tissue, and two samples of bronchial nodes contained $9 \pm 7 \times 10^{-3}$ and $27 \pm 7 \times 10^{-3}$ dis/min/g tissue, respectively. These concentrations of plutonium are similar to values reported for fallout plutonium from HASP studies.[3.35] The higher concentration of plutonium in one sample of bronchial nodes tends to support the suggestion that these organs may accumulate plutonium.[3.36] The results indicate that cattle fed from pasture irrigated by Columbia River water withdrawn downstream from the Hanford Project do not accumulate plutonium in amounts significantly different from that accumulated from fallout.

Uranium Ore Dust Inhalation Studies - R. W. Perkins

High sensitivity analytical methods are being studies and developed for the quantitative measurement of the U^{238} chain radionuclides in biological samples. Preliminary studies indicate that a combination of low background alpha-energy and gamma-ray spectrometric analyses will permit direct measurements of the uranium chain from ashed samples.

A research project is being conducted in conjunction with the Biology Laboratory to determine the body distribution of uranium and its daughters in experimental animals after inhalation of uranium ore dust. Recent revisions in the recommended MPC value of air for uranium ore dust stipulate that whenever a hazard exists due to a mixture of radionuclides, the stated permissible concentration of each must be reduced to a fraction of its MPC such that the sum of these fractions equals unity. On applying this principle to uranium ore, and assuming radioequilibrium, the calculated MPC value is about 20 $\mu g/m^3$, or about one-third of the former value. It is the intent of this study to determine what departures from radioequilibrium normally exist in uranium ore dust samples and what fraction of the various uranium daughters in ore dust are solubilized in the lung with the result that they are deposited in the various organs of the body. These studies will provide basic information for justification or future reevaluation of uranium ore dust MPC values.

Normal uranium contains about 99.27% U^{238}, 0.72% U^{235} and 0.057% U^{234} by weight. U^{235} has a shorter half-life than U^{238} and contributes about 4.5% as much alpha activity as U^{238}; however, this is a minor contribution to the total dose.

The U^{338} decay chain is shown in Figure 3.14. A direct measurement of the concentration of each member of the chain is not necessary, since many sections of the chain attain equilibrium in minutes. For the initial studies, the concentrations of the U^{238}, U^{234}, Th^{230}, Ra^{226}, Po^{218}, and Po^{210} will serve as an indication of the equilibrium conditions of the U^{238} chain.

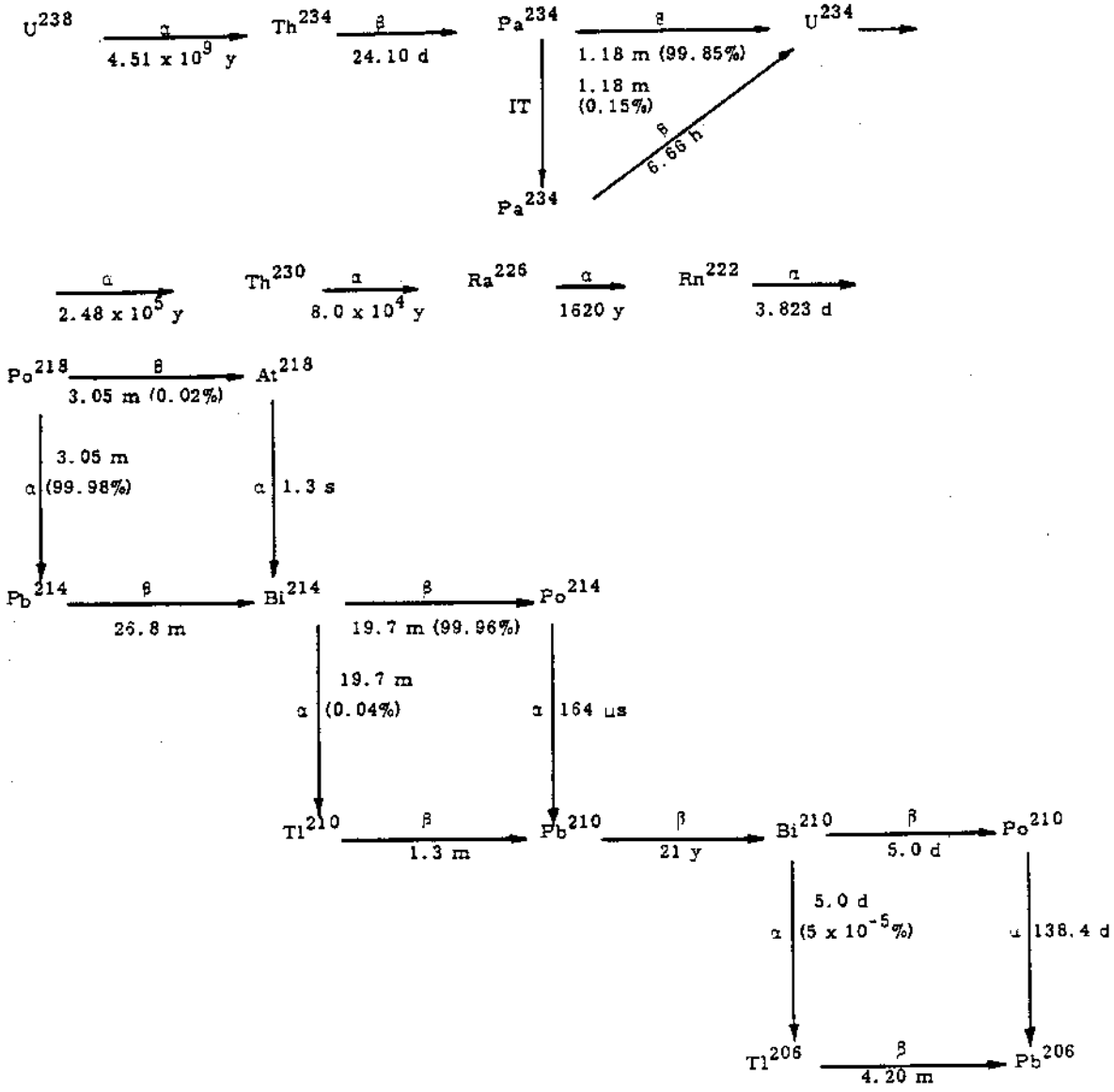

FIGURE 3.14

Decay Chain of the U^{238} Series

The measurement of the concentrations of U^{238} and its daughters is difficult due to the large number of radionuclides present, the types of radiations emitted (many α particles and weak beta and gamma-rays), and the low specific activity of natural uranium (U^{238} decays at the rate of 0.74 dis/min/μg). The problem of measuring the distribution of the U^{238} series radionuclides at the microgram or submicrogram level in the various organs of an experimental animal will certainly require the most sensitive detection equipment.

An evaluation of the most sensitive gamma-ray spectrometric equipment [3.37] indicates that several micrograms of uranium in equilibrium with its daughters must be present for their detection and measurement. A measurement of the U^{238} based on the 0.184 Mev photopeak of U^{235} would require about 50 μg of uranium. A measurement of the Ra^{226}, based on the 0.352 Mev photopeak of Pb^{214} or the 1.76 Mev photopeak of Bi^{214} would require that amounts of these radionuclides equivalent to about 20 μg of U^{238} be present. Several of the important U^{235} chain members cannot be measured directly by gamma-ray spectrometric methods.

The very recent development of an ultra large area alpha-energy spectrometer has made it possible to measure the natural alpha activity of tissue samples without chemical separation.[3.39, 3.40] This analyzer consists of a large cylindrical pulse ionization chamber which views a 15,000 cm^2 sample area. A similar detector system is being fabricated for use both in the uranium ore inhalation study and in other low-level alpha activity measurements. It is reported [3.38] that the amount of a monoenergetic alpha emitter required to double the background counting rate in the 4 to 6 Mev energy range is about 2 dis/min (or 3 μg equivalent of U^{238}).

In selecting an ore for the inhalation study, four uranium samples were considered. They varied in U^{238} concentration from about 0.2% to

20% uranium. For the initial inhalation studies, the 20% uranium ore (a pitchblende material from Lisbon Valley, Utah) was selected to provide the highest detection sensitivity. This sample of ore was ground in a ball mill to a size median diameter of 0.58 μ (mass median diameter of 1.48 μ), and 300 μg were aspirated onto a 2 in. diameter platinum disc for alpha-energy spectrometric analysis by Frisch grid chamber counting. The alpha-energy spectrum of the ore (see Figure 3.15) indicated that it was roughly in secular equilibrium. From the absence of the 8.777 Mev alpha energy of Po^{212} it was possible to determine that the Th^{232} content was less than 0.1% of the uranium in the ore and that its daughter radionuclides would not interfere significantly in alpha-energy or gamma-ray analyses. A gamma spectrum of a 0.5 g sample of the ore, which was measured with an ultra sensitive gamma-ray spectrometer,[3.37] is shown in Figure 3.16. The major photopeaks are due to U^{235}, Pb^{214}, and Bi^{214}. It is planned to use gamma-ray spectrometric methods for measuring the U^{238} series in the whole body and lungs of the animals, and a combination of gamma and alpha spectrometric techniques for the tissue measurements.

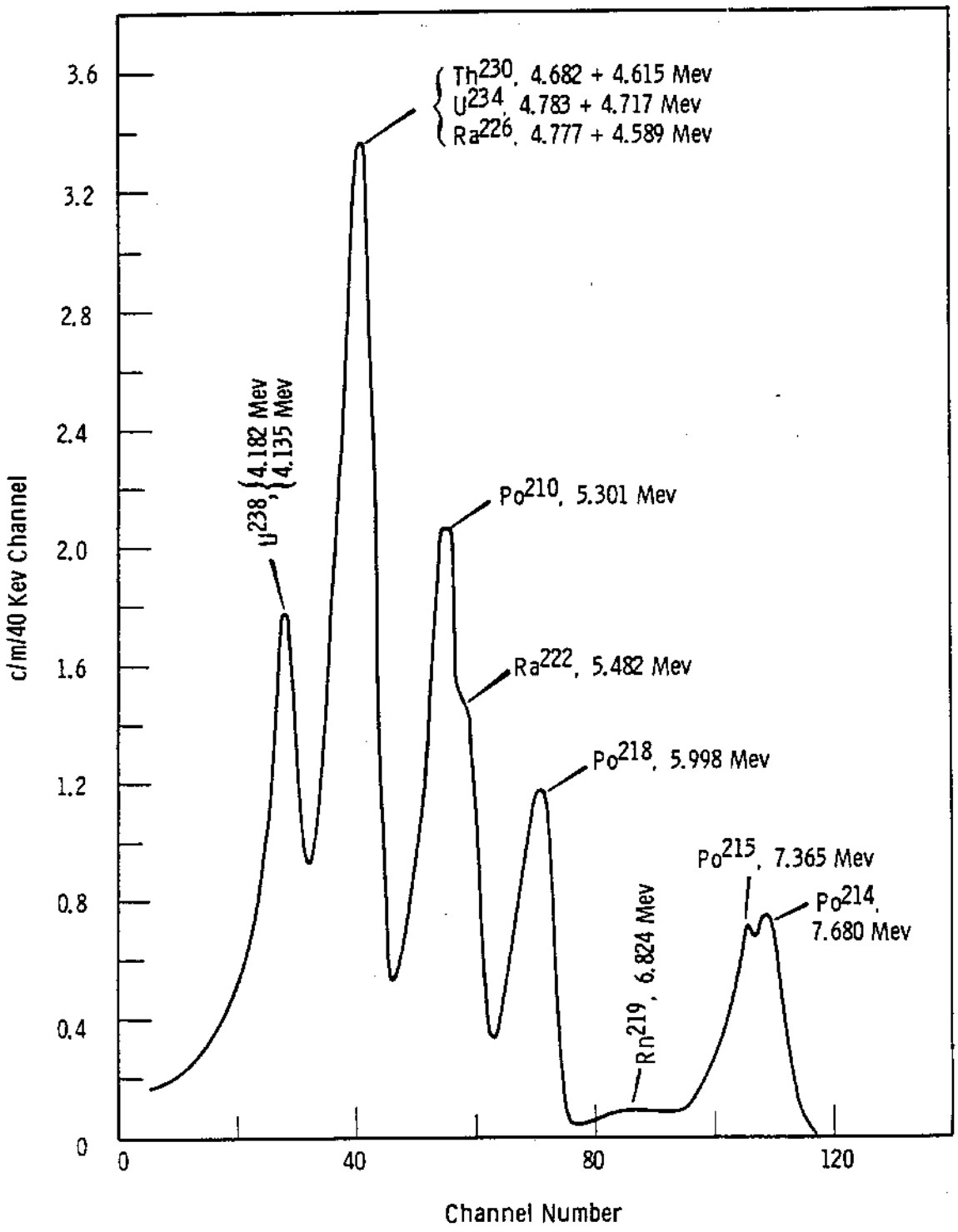

FIGURE 3.15

Alpha Energy Spectrum of 300 Microgram of Finely Ground Uranium Ore as Measured in a Frisch Grid Chamber

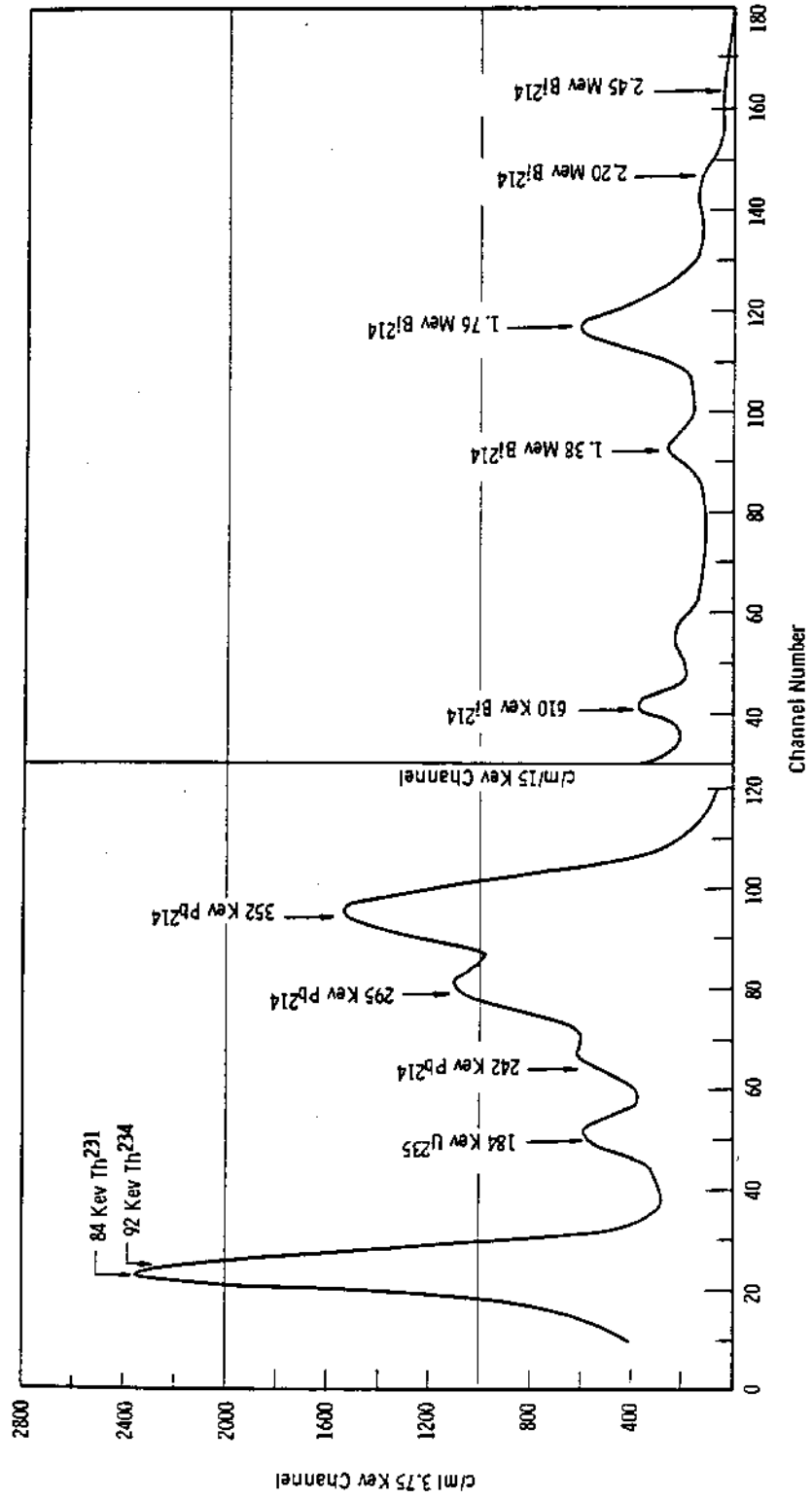

FIGURE 3.16
Gamma-Ray Spectrum of a 0.5 Gram Sample of Uranium Ore as Measured in a 5- by 5-Inch Crystal with Anticoincidence Shielding

The Columbia River Sediment Studies - L. L. Humphreys

Partially completed studies of the uptake of radioisotopes by Columbia River sediments include the separation of sediments into particle size ranges, the determination of particle size distribution, the removal of organic material, and gamma-ray spectrometric analysis of each fraction.

Evaluation of the effects of introducing radioisotopes into the Columbia River through reactor operation must include a study of the modes of exchange of these isotopes between the river water and its sediments. Essential to this study is an explanation of the variation of specific activity with the river sediment particles size. Problems encountered in this study include finding a satisfactory method for

indicate that for a 24-in. column, with a settling time of 4 hr, and by repeating the above-mentioned stirring and draining procedure ten times, removal of 5 μ particles should be 94% complete, and removal of particles < 5 μ should be essentially complete. Of course, the calculations assume ideal conditions, and are influenced by several factors.

The fractions obtained by this method were analyzed for particle size distribution with a Coulter Counter "Model B"* which was connected to a multichannel analyzer through a pulse shaper, so that printed scans of the distribution were obtained. The instrument was calibrated by the use of three different pollens of known size distributions, determined by microscopy, and checked with commercially available glass beads (for which a particle size distribution is given). Each time a determination is made, the calibration is checked with one of the standard pollens. Figure 3.17 represents the spectrum obtained from the instrument for a typical sediment sample, where number of particles are plotted versus channel number and particle size. The pulse height varies as the third power of the particle diameter, with the proportionality constant depending upon the current and gain settings on the Coulter Counter. This method of obtaining particle size distributions has proven to be effective and time-saving.

Distributions for each of two fractions obtained from the same sample are given in Figure 3.18. These curves show definite separation at the peaks of the distribution, but also indicate considerable overlap, and a study of radionuclide content as a function of particles size requires that this overlap be reduced. To effect a better separation in these subseive ranges, multistage separations and longer settling columns are being studied.

---

* Coulter Electronics Inc., 590 West 20th Street, Hialeah, Florida

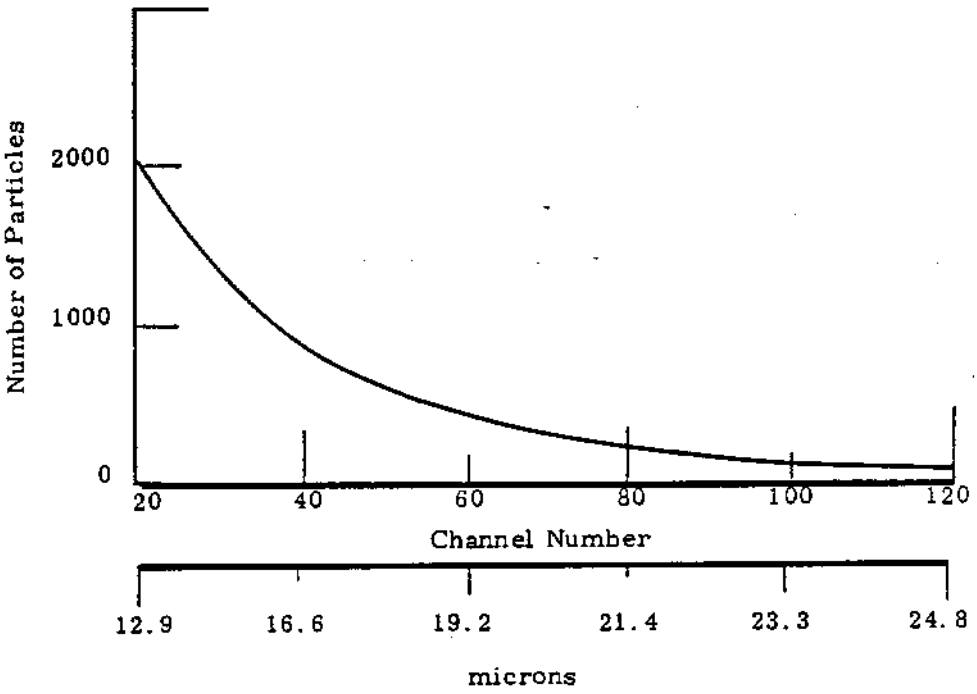

FIGURE 3.17

Particle Size Distribution
Obtained from Multichannel Analyzer and Coulter Counter

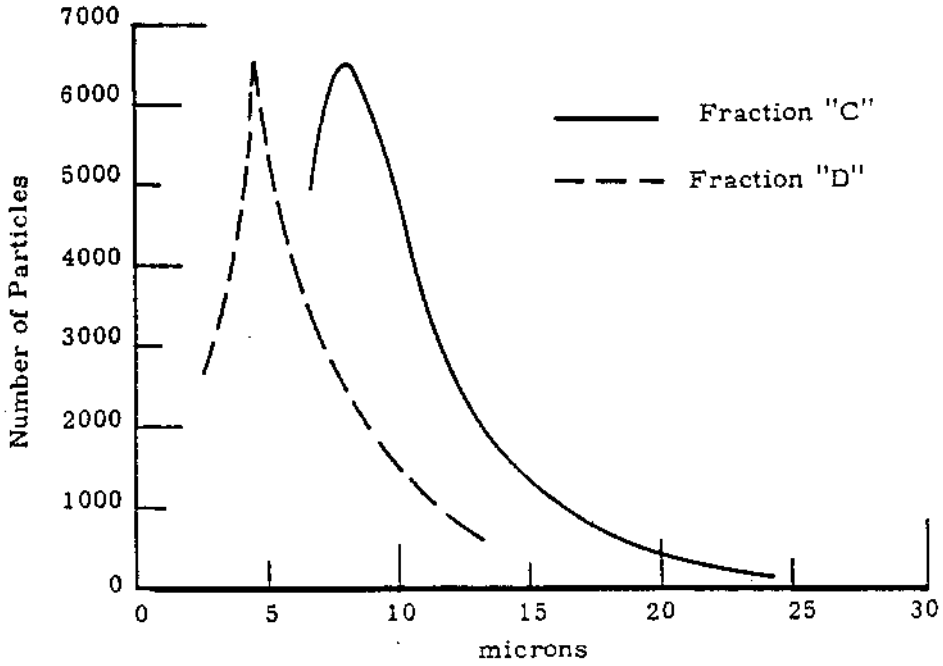

FIGURE 3.18

Particle Size Distribution of Separated Fractions

Specific activities (in dis/min/g) of the more prominent radioisotopes found in the sediments are given in Table 3.11 for total sample and for each of the fractions obtained by the single stage method of separation. Included in the table are particle size ranges and weight fractions for each of the samples.

TABLE 3.11

SPECIFIC ACTIVITIES OF COLUMBIA RIVER BED SAMPLES

Fraction	Total	A	B	C	D	E
Size Range		62	38-62	18-38	5-18	5
Weight Fraction		3.8%	8.2%	52.5%	21.3%	14.2%
Co^{60}(dis/min/g)	80	126	51	71	183	181
Sc^{46} (dis/min/g)	241	424	288	266	412	861
Zn^{65}(dis/min/g)	2730	5066	2113	2278	2587	4690

The trend expected from surface area considerations would be increasing specific activity with decreasing particle size. However, it is noted that the large particles (Fraction A) have a higher specific activity than Fractions B or C. This is attributed to the presence of organic material that stayed on a 62-μ seive. The organic material was removed from this fraction by CCl_4 floatation. The resulting relative specific activities are given in Figure 3.19, along with radioisotope distribution and weight fraction versus particle size.

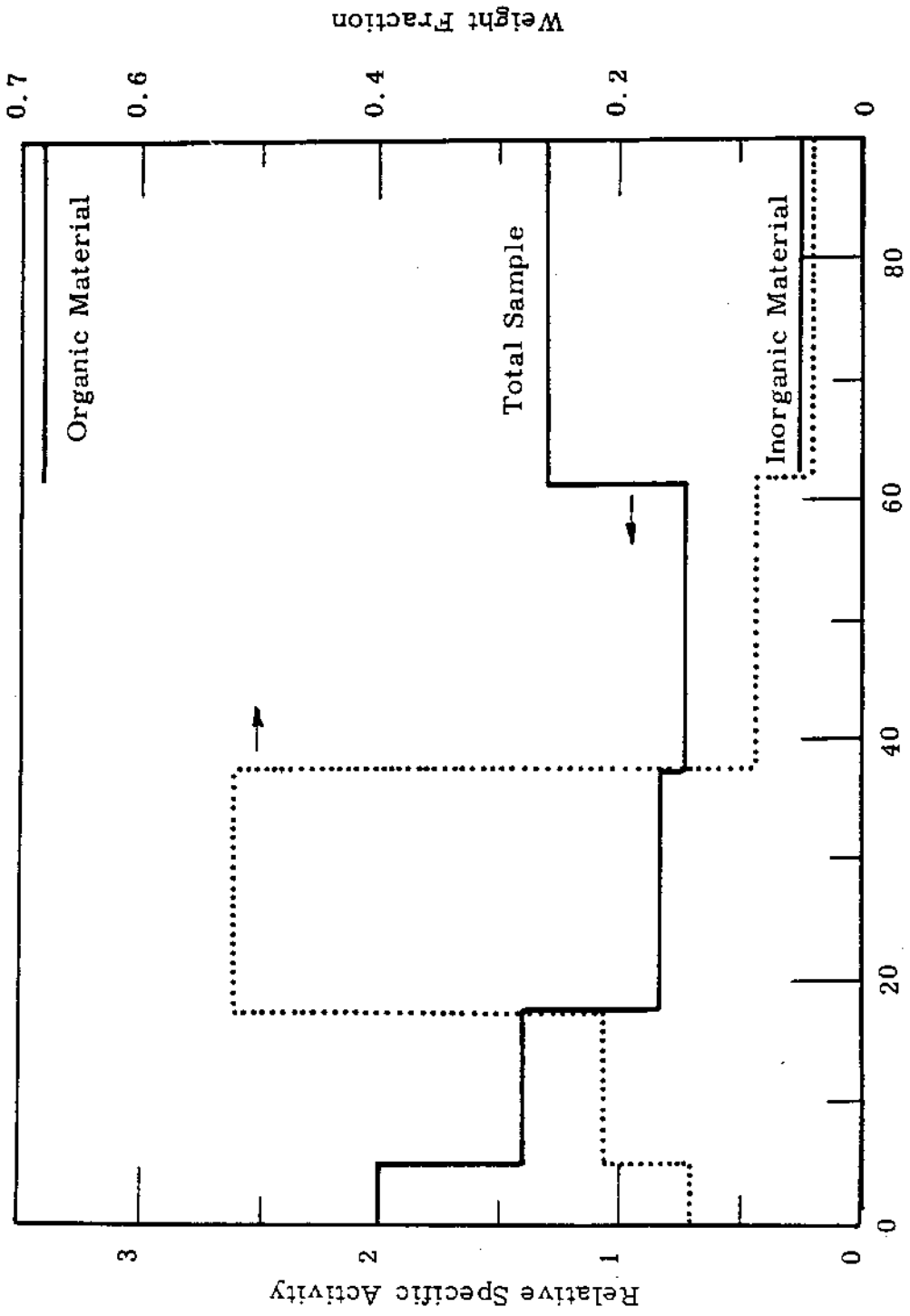

FIGURE 3.19

Relative Specific Activity Versus Particle Size of McNary Sediments

The Removal of Radioisotopes from the Columbia River by Natural Processes* - J. M. Nielsen and R. W. Perkins

Some radioisotopes are introduced into the Columbia River by return of the water used to cool the Hanford reactors. Trace amounts of both fission product and activation product radioisotopes are present and measurable by sensitive radiochemical methods to allow determination of the self-purification processes occurring as the water moves downstream. By comparing the radioisotope input at given times with the amounts present in the river after traveling downstream, a measure of the self-purification rate was obtained. Removal in the first 40 miles downstream from the reactors was about 35% for 15 of the most prominent radioisotopes. The removal rate seemed to decrease with subsequent distance traveled downstream for three radioisotopes for which measurements were made. Radiochemical analyses of water, filterable solids, and sediment samples taken at downstream locations indicate that incorporation in sediments accounts for most of the removal. Because of the intense scouring action of the Columbia River, sediments are deposited in significant amounts only in slack water sections. The first extensive slack water section downstream from Hanford is the McNary Dam reservoir, Lake Wallula. Radiochemical analyses of some of the long-lived radioisotopes, including Mn^{54}, Co^{60}, Zn^{65}, and Cs^{137} on sectioned sediment core samples indicate a widely varying rate of deposition of radioisotopes. Dating of the various sections of the cores was accomplished using isotope ratio measurements.

---

* Published as HW-SA-2411. J. M. Nielsen and R. W. Perkins. The Removal of Radioisotopes from the Columbia River by Natural Processes. April, 1962. For presentation at American Geophysical Union Meeting, Washington, D.C., April 24-27, 1962.

Variations in Elemental Concentrations in the Columbia River - W. B. Silker

The use of Columbia River water to cool the Hanford reactors results in the formation of radioactive materials due to neutron irradiation of dissolved salts in the water. An increase in the concentration of several of these radioisotopes occurs in the Spring, before the peak in the flow of the Columbia River. An extensive program was conducted, therefore, during 1961 and 1962, in which the seasonal changes in concentration of several elements in the river just above Hanford were evaluated. Measurement of the effects of various tributaries on the salt concentration of the Columbia was also made from several sets of samples collected along the U.S. portion of the river.

Manganese, copper, sodium, lanthanum, and arsenic exhibited a concentration increase during April, which coincided with the increase in activation products in the reactor coolant. During this time period in 1962, the flow of the Columbia River increased due to high runoff from the Spokane and Pend Oreille Rivers. During previous years, the activity increase was preceded by a period of high flow in the Spokane River. It was concluded that the origin of the Spring increase is the Spokane River and lowland runoff, and the delay between its introduction to the Columbia and its arrival at Hanford is due to regulation of river flow by the various upstream dams. This conclusion is also supported by a limited number of measurements of Spokane River water which showed an order of magnitude increase in the concentrations of copper and manganese during its high flow condition. A subsequent study is in progress to ascertain the effect of the Spokane River, and to investigate possible methods of controlling the release of this water to the main stream.

The concentration of any given element remained amazingly constant along the length of the Columbia River. Some exceptions were observed, for instance, fivefold increase in the sodium concentration below the mouth of the

Snake River, during periods of low river flow. Analysis of Snake River water showed that this tributary could not be the only source of the additional sodium. It was concluded that the effluent from one or more of the manufacturing plants in the vicinity of Kennewick or Pasco, Washington was contributing significant quantities of sodium to the River.

Effect of a Reactor Fuel Element Failure on the Columbia River Radionuclide Concentrations at Pasco, Washington - R. W. Perkins

Measurements of the radionuclide concentrations in Columbia River water at Pasco, Washington following a fuel element rupture in one of Hanford plutonium production reactors indicate that I^{131} in solution provides a sensitive indicator of the arrival of fission products. The Ru^{106} also showed a definite rise. The particulate fraction of the radionuclides Zr^{95}-Nb^{95}, Ru^{103}, and Np^{239} showed large but more erratic increases on arrival of the rupture debris. The travel time between the reactors and Pasco was about 15% longer than that calculated by float test equation; however, float test equations gave a good value for the arrival of the leading edge of the activity.

Radiation Chemistry

The Radiation Chemistry of Erioglaucine - D. R. Kalkwarf

Evidence is presented that erioglaucine in aerated, aqueous solutions is bleached during irradiation only as a result of reaction with hydroxyl radicals.

The usefulness of erioglaucine in comparing the reactivities of solutes with radicals formed in irradiated aqueous solutions has been described;[3.40] however, no conclusion was drawn as to whether only one type of radical was responsible for bleaching this dye in the presence of oxygen. At least three types of radicals are produced in irradiated, aerated water: $H\cdot$, $HO\cdot$ and $HO_2\cdot$. Hydrogen atoms are considered[3.41] to react rapidly with molecular oxygen to from perhydroxyl radicals, $HO_2\cdot$. This leaves

both the hydroxyl and perhydroxyl radicals as possible reactants with the dye. Two kinds of experimental evidence are described below in favor of hydroxyl radical being the only active reagent.

One line of evidence involves calculating the radical yield from the bleaching data and comparing this value with the yields of hydroxyl and perhydroxyl radicals from the radiolysis of water. This calculation is dependent on the mechanism assumed for dye bleaching; however, two experimental results restrain the form of this mechanism quite rigidly. First, the optical absorbance of erioglaucine in air-saturated water decreases exponentially with absorbed dose of Co^{60} gamma radiation at all initial concentrations. Because of this fact, the radiation sensitivities of these solutions can be expressed in terms of D_{37} is the dose in rads required to decrease the absorbance of the dye to 0.37 of its initial value. Second, the D_{37} values for these solutions increase linearly with initial dye concentration, as shown in Figure 3.20.

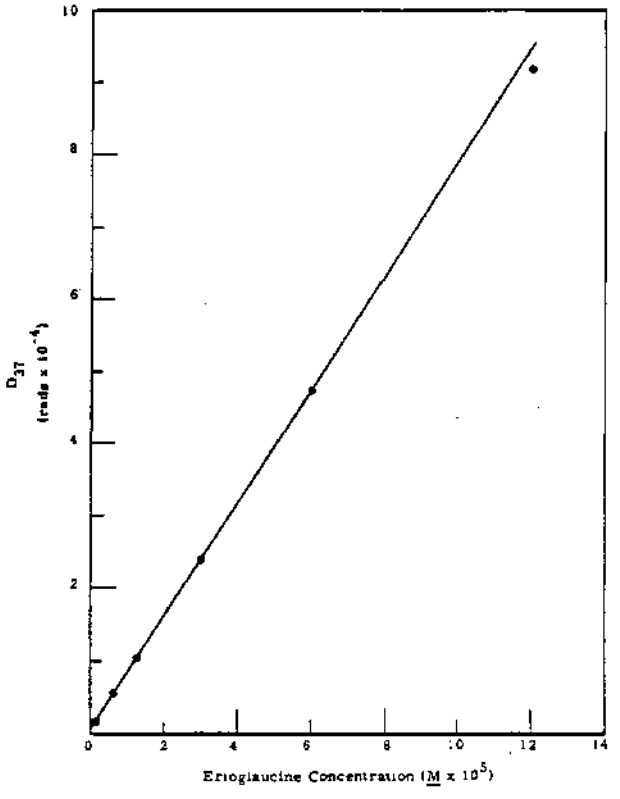

FIGURE 3.20

D_{37} for Absorbance of Erioglaucine Solutions at 631 mu

The following kinetic mechanism is consistent with the experimental observations described above and satisfies chemical intuition. Letting S_0 represent the solute, erioglaucine, and letting R represent the radicals, the possible reactions between them can be divided into two general types: Type I--those which do not involve bleaching, and Type II--those which do. These types can be represented by:

$$S_0 + R \xrightarrow{k_0} S_{01} + \cdots, \qquad \text{(Type I)}$$

and

$$S_0 + R \xrightarrow{k'_0} S'_{01} + \cdots, \qquad \text{(Type II)}$$

where the K values are specific rate constants with distinctive primes and subscripts. Consecutive reactions will follow and eventually some unprimed product molecule will be bleached, e.g.,

$$S_{01} + R \xrightarrow{k_{01}} S_{02} + \cdots,$$

$$S_{02} + R \xrightarrow{k_{02}} S_{03} + \cdots,$$

$$\vdots \qquad\qquad \vdots$$

$$S_{0M} + R \xrightarrow{k_{0M}} S'_{0(M+1)} + \cdots,$$

where $S_{0(M+1)}$ no longer absorbs at the wavelength of maximum absorption by erioglaucine.

Other reactions will also be in progress, e.g.,

$$S'_{01} + R \xrightarrow{k'_{01}} S'_{02} + \cdots$$

$$S'_{02} + R \xrightarrow{k'_{02}} S'_{03} + \cdots$$

$$\vdots \qquad\qquad \vdots$$

and,

$$S'_{0(M+1)} + R \xrightarrow{k'_{0(M+1)}} S'_{0(M+2)} + \cdots$$

$$S'_{0(M+2)} + R \xrightarrow{k'_{0(M+2)}} S'_{0(M+3)} + \cdots .$$

If an impurity solute, S, is also present, its reactions with the radicals can be represented by:

$$S_1 + R \xrightarrow{k_1} S_{11} + \cdots$$

$$S_{11} + R \xrightarrow{k_{11}} S_{12} + \cdots$$

$$\vdots \qquad\qquad \vdots$$

Letting brackets signify concentrations in moles per liter, the absorbance of a solution at the wavelength for maximum absorption is:

$$A = a[S_0] + a[S_{01}] + \cdots + a[S_{0M}],$$

where the molar absorptivity, a, for each compound is assumed equal since their structures are probably very similar. Letting D represent the radiation dose absorbed by the solution,

$$\frac{dA}{dD} = a\left(\frac{d[S_0]}{dD} + \frac{d[S_{01}]}{dD} + \cdots + \frac{d[S_{0M}]}{dD}\right).$$

Assuming that each of the bimolecular reactions listed above follow second order kinetics,

$$\frac{d[S_0]}{dD} = -k_0[S_0][R] - k'_0[S_0][R],$$

$$\frac{d[S_{01}]}{dD} = k_0[S_0][R] - k_{01}[S_{01}][R]$$

$$\vdots \qquad\qquad \vdots$$

$$\frac{d[S_{0N}]}{dD} = k_{0(N-1)}[S_{0(N-1)}][R] - k_{0N}[S_{0N}][R],$$

so that,

$$\frac{dA}{dD} = - a[R]\left(k'_0[S_0] - k_{0N}[S_{0N}]\right).$$

Since radicals are continually being formed in the solution at a rate of Y moles · liter^{-1} · rad^{-1}, one can make the assumption that the concentration of radicals rapidly attains a stationary value where:

$$\frac{d[R]}{dD} = \{Y - (k_0[S_0]+k_{01}[S_{01}]+\cdots+k'_0[S_0]+k'_{01}[S'_{01}]+\cdots+k_1[S_1] + k_{11}[S_{11}]+\cdots)[R]\} = 0,$$

or

$$[R] = \frac{Y}{k_0[S_0]+k_{01}[S_{01}]+\cdots+k'_0[S_0]+k'_{01}[S'_{01}]+\cdots+k_1[S_1]+k_{11}[S_{11}]+\cdots}.$$

Substituting this expression into the previous equation for dA/dD gives

$$\frac{dA}{dD} = \frac{-aY(k'_0[S_0]+k_{0N}[S_{0N}])}{k_0[S_0]+k_{01}[S_{01}]+\cdots+k'_0[S_0]+k'_{01}[S'_{01}]+\cdots+k_1[S_1]+k_{11}[S_{11}]+\cdots}.$$

Since k'_0 and k_{0N} are each rate constants which involve bleaching of very similar, colored species, it seems reasonable to assume they are numerically equal. Experimentally, these reactions are not allowed to progress very far so that the denominator of the above equation reduces to $2k'_0[S_0]_o + k_1[S_1]_o$, where the subscripts outside the brackets indicate initial values. Making these approximations,

$$\frac{dA}{dD} = \frac{-ak'_0 Y([S_0]+[S_{0N}])}{2k'_0[S_0]_o + k_1[S_1]_o},$$

or

$$\frac{dA}{A} = -\left\{\frac{Y}{2[S_0]_o + k_1[S_1]_o/k'_0}\right\} dD,$$

i.e.,

$$= \frac{2[S_0]o}{Y} + \frac{k_1[S_1]o}{k'_0 Y}.$$

The above mechanism is in accord with actual behavior in that it predicts that the optical absorbance of the dye should decrease exponentially with dose and that the D_{37} values should increase linearly with increasing initial dye concentration. As shown by the equations, the slope of this straight line should be two divided by the radical yield. Using the data shown in Figure 3.20, this yield was found to be 2.5 molecules per 100 ev. The yields of radicals in air-saturated water at pH 4 to 6 are G_{HO} = 2.4, G_{HO_2} (from H + O_2) = 2.9.[3.42] The close agreement between Y and G_{HO} indicates that hydroxyl radicals are the reagents predominantly responsible for bleaching the dye.

A second line of evidence that the hydroxyl radical is the active reagent in the bleaching of erioglaucine is obtained by comparing the relative rate constants for the reactions of hydroxyl radicals with various solutes. These have been evaluated[3.43, 3.44] by allowing organic compounds to compete with ferrous ion for hydroxyl radicals formed by the Fenton reaction, i.e.,

$$Fe^{2+} + H_2O_2 \xrightarrow{k_a} Fe^{3+} + OH^- + HO\cdot,$$

$$HO\cdot + Fe^{2+} \xrightarrow{k_b} Fe^{3+} + OH^-,$$

$$HO\cdot + RH \xrightarrow{k_c} H_2O + \dot{R}\,.$$

The rate-constant ratios, k_c/k_b, have been computed for several reaction pairs and are listed in Table 3.12. Also listed there are values of the rate constant ratio k_1/k_0 for comparable reactions in irradiated, aerated solutions:[3.40]

$$H_2O \xrightarrow{\gamma} \dot{R},$$

$$R + S_0 \xrightarrow{k_0} S_{01} + \cdots,$$

$$R + RH \xrightarrow{k_1} S_{11} + \cdots,$$

where S_0 = Erioglaucine, RH = competing solute, and S_{01} and S_{11} are products of these reactions.

TABLE 3.12

RELATIVE RATE CONSTANTS FOR REACTIONS WITH THE RADIOLYSIS OF ERIOGLAUCINE AND WITH THE FENTON REACTION

RH	k_c/kb	k_1/k_0	$f = (k_c/k_b)/10(k_1/k_0)$
Methanol	2.3	0.068	3
Ethanol	3.8	0.127	3
Propanol-1	2.6	0.189	1
Propanol-2	3.0	0.105	3
2-Methylpropanol-2	0.65	0.041	2
Benzoic acid	7.0	0.36	2
Glycollic acid	2.0	0.06	3
Glycine	0.035	0.00083	4
Alanine	0.12	0.0048	3
Benzene	3.2	0.11	3

As seen from the above table, the relative rate constants of compounds with the radicals fromed in aerated, irradiated solutions are proportional to their relative rate constants with hydroxyl radicals, with a few exceptions. It thus appears likely that only hydroxyl radicals are reacting with these compounds and erioglaucine in the irradiated solutions.

The Effect of Temperature on Radical-Capturing Reactions in Irradiated Aqueous Solutions - D. R. Kalkwarf

Small molecular solutes were found to compete more effectively with erioglaucine for the hydroxyl radicals formed in irradiated aqueous solutions as the temperature was decreased. To explain these observations, a theory is proposed for the free-radical oxidation of solutes in terms of the "flickering-cluster" picture of water and the transport of electrons through a hydrogen-bonded lattice.

It has often been found that the temperature dependence of a reaction-rate constant furnishes important clues concerning the detailed mechanism of the reaction. Although the radical yields derived from the radiolysis of water appear to be independent of temperature,[3.45] subsequent radical-capturing reactions of solutes, being thermal reactions, would be expected to proceed faster with a rise in temperature. With this in mind, relative rate constants for several radical-solute reactions in irradiated aqueous solutions were examined at a variety of temperatures.

The data obtained are shown in Figure 3.21. The relative rate constants were measured in solutions of competing reactants using erioglaucine as the reference solute.[3.46] As shown in the preceding article on page 3.68, the only effective radicals in these air-saturated solutions appear to be hydroxyl radicals. The data are presented in the way shown because it is generally found in chemical reactions that:

$$k = (\text{constant})e^{-E/RT},$$

where k is the rate constant at absolute temperature T, and E is the activation energy. The activation energy is the amount of energy which particular molecules must have above the average for the system in order to react. The temperature dependence of relative rate constants is similar except that the energy term is the difference in activation energies for the two reactions compared. This can be seen by letting k_1 and k_2 be the rate

constants for the two reactions. Then assuming $k_1 = A_1 e^{-E_1/RT}$ and $k_2 = A_2 e^{-E_2/RT}$,

$$\frac{k_2}{k_1} = (\text{constant}) e^{-(E_2 - E_1)/RT}.$$

Of particular interest in Figure 3.21 is that each of the solutes appear to compete more effectively with the reference solute, erioglaucine, for the radicals as the temperature decreases. Since the slopes of these plots are proportional to a difference in activation energies, a simple explanation might be that the activation energy for the erioglaucine-radical reaction is larger than that for the other solute-radical reactions. This explanation is unlikely to be true, however, since there is good evidence that the reaction between hydroxyl radicals and erioglaucine is encounter-controlled, i.e., the reaction occurs at every collision.

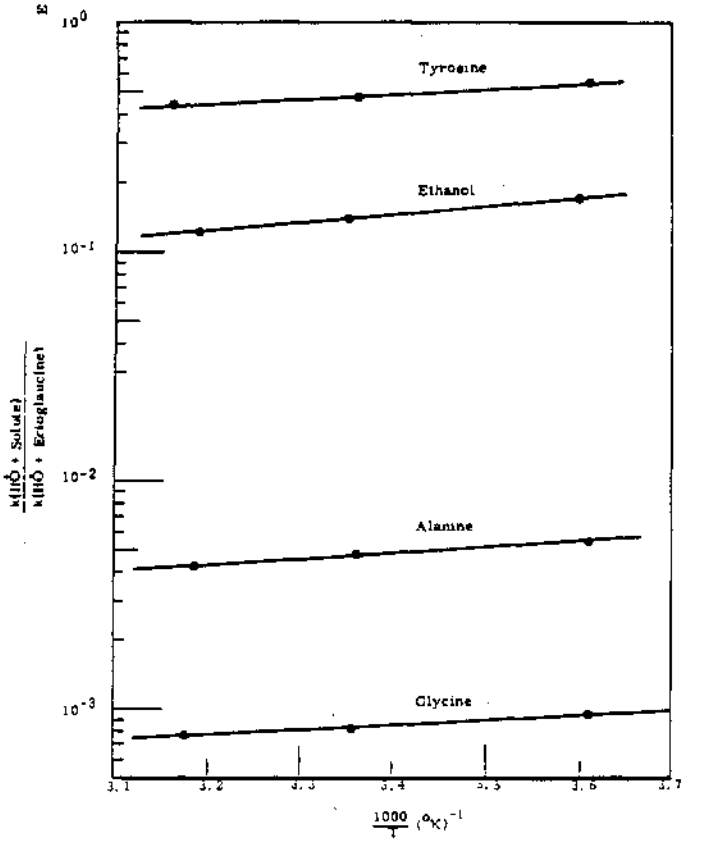

FIGURE 3.21

Relative-Rate Constants of Solutes as a Function of Temperature

The rate constant for an encounter-controlled reaction can be estimated by the equation:[3.47]

$$k = \frac{4\pi \delta_{AB} DN}{1000}$$

For the reaction between erioglaucine and hydroxyl radicals, one can assume a value of 5×10^{-8} cm for the bimolecular collision diameter, δ_{AB}, a value of 10^{-5} cm^2 sec^{-1} for the sum of the solute's diffusion constants, D, and the usual value for Avogadro's Number, N. The resultant rate constant is 4×10^9 liters $mole^{-1} sec^{-1}$. A recent determination of the rate of reaction between hydroxyl radicals and nitrite ions[3.48] gives the value 2.5×10^9 $mole^{-1} sec^{-1}$. By allowing nitrite ion to compete with erioglaucine for hydroxyl radicals in the same irradiated solution, the relative rate-constant for nitrite ion was found to be 0.55. From these data the absolute-rate constant for reaction between hydroxyl radicals and erioglaucine can be calculated to be $(2.5/0.55) \times 10^9 = 4.5 \times 10^9$ liters $mole^{-1} sec^{-1}$, or exactly the value for an encounter-controlled reaction.

A more interesting explanation for the effect of temperature on these relative rate constants can be obtained by combining a recent theory for the structures of aqueous solutions with an intuitive picture for the transport of electrons through them. One view of an aqueous solution is that it is a particular assortment of organized structures involving water molecules.[3.49] At a large distance from any solute, there are clusters of water molecules resembling miniature icebergs which are rapidly disintegrating and reforming. While the lifetimes of these clusters must be short to account for the measured dielectric relaxation time of 10^{-10} sec in water, this value is still 1000 times the period of a molecular vibration. In contrast to these hydrogen-bonded clusters, water molecules near the charged site on an ion must be held quite rigidly due to ion-dipole attraction. Between this hydration sphere and the zones of reforming clusters there is considered to be a region in which water does not attain the long-range structure of the latter zones. This disorganization can be imagined to result from the competitive attractive force

exerted by the central ion on the water molecules while they are attempting to form arrays of "ice". Near uncharged portions of a solute molecule, however, there is an insulation from competing forces so that the ice-like clusters may be even more extensive or long-lived than in pure water at the same temperature.

The resulting picture of an irradiated aqueous solution is thus one in which solutes, surrounded by hydrogen-bonded clusters of water, compete for the hydroxyl radicals continuously being formed. Considering size and chemical structure, erioglaucine must be the center of a much more extensively organized water structure at room temperature than any of the small solutes listed in Figure 3.21. As the temperature is decreased, water clusters about both large and small solutes will increase in size, however, the latter would probably be affected to a greater extent. A new layer of organized water around a small cluster would increase the cluster-volume proportionately more than would a new layer around a large cluster.

All that now remains to explain the temperature dependence of the relative rate constants shown in Figure 3.21 is to assume that a hydroxyl radical need only reach the surface of one of the clusters to oxidize the solute. Because of the hydrogen-bonded nature of the clusters, transport of an electron out to the surface only involves a realignment of these bonds without any large molecular displacements. This process is illustrated in Figure 3.22, and becomes of increasing importance in the oxidation of small solutes as the temperature decreases. As a result, these compounds are able to compete more effectively for the radicals at lower temperatures.

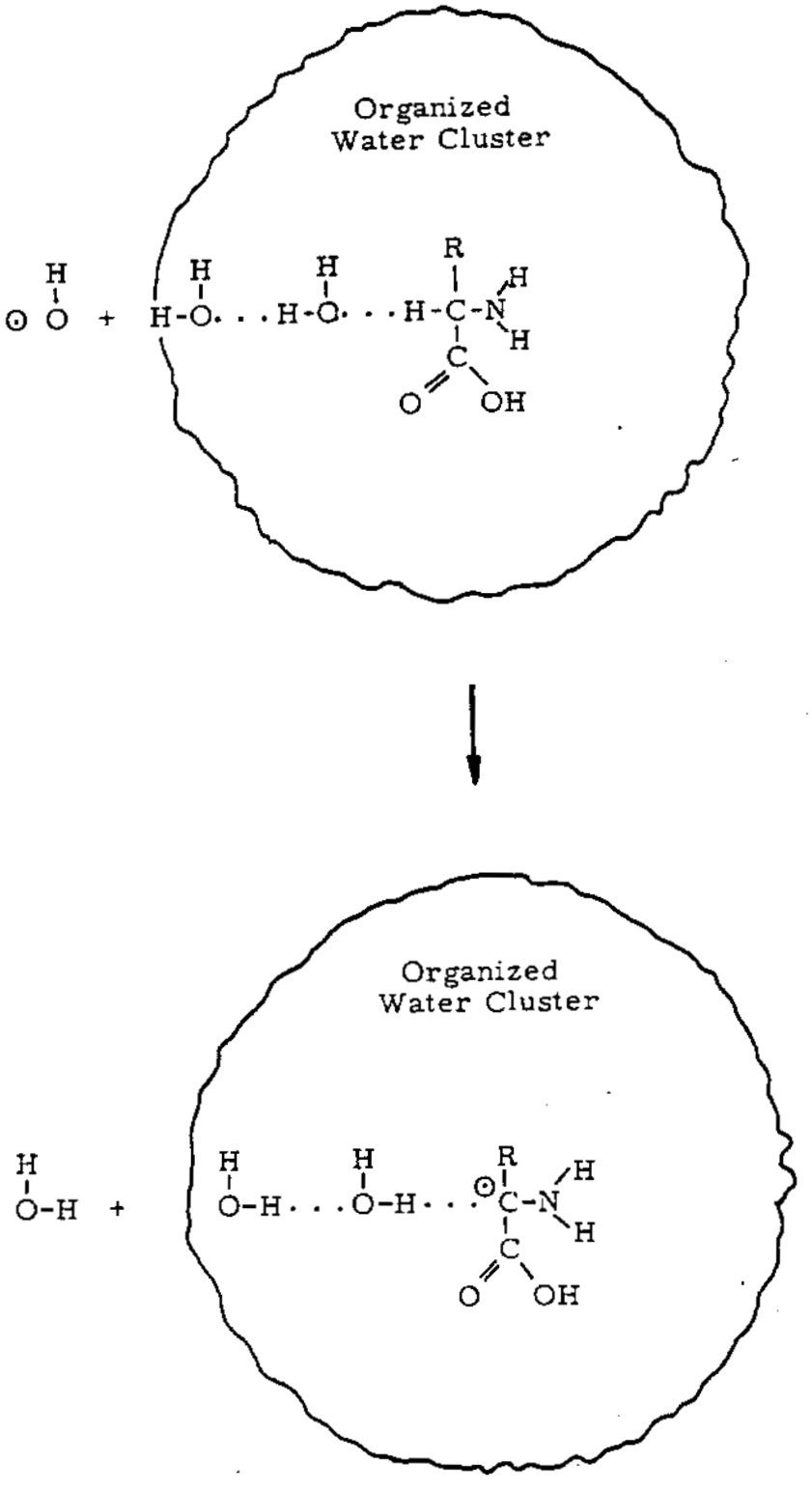

FIGURE 3.22

Proposed Mechanism for Oxidation by Hydroxyl Radicals in Irradiated Aqueous Solutions

Radical-Capturing Reactions of Galactose and Agarose in Irradiated Solutions - D. R. Kalkwarf

The relative reaction rates of radiation-produced, hydroxyl radicals with the galactose structures in monomeric, polymeric, and gel solutions were evaluated. Comparison showed that substantial numbers of galactose residues in ploymeric liquid and gel solutions appear to be inaccessible to the radicals.

The reaction rates of hydroxyl radicals with molecular solutes in irradiated aqueous systems have been found to be functions of the solutes' spatial arrangement in polymeric strands and gels.[3.50] The behavior of agarose provides further illustrations of this dependence. As shown in Figure 3.23, this compound is a linear polymer of alternate galactose and 3,6-anhydrogalactoce units. One of its unique abilities is to form firm gels in water at room temperature in concentrations as low as 0.1%.

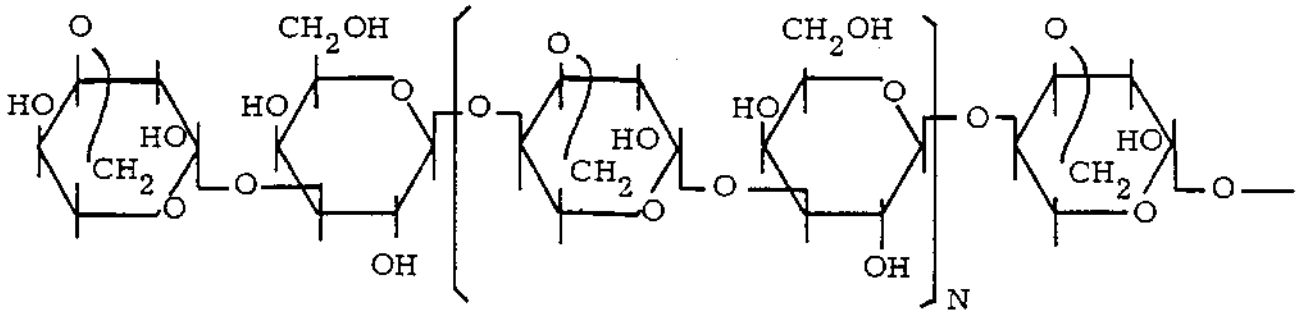

FIGURE 3.23
Structural Formula for Agarose

The relative rate constants for reaction of hydroxyl radicals with either agarose or galactose were evaluated over a wide range of concentrations by the dye-competition technique described previously.[3.46] Agarose was prepared by separation from commercial agar[3.51] and purified further by alternate freezing and thawing of concentrated gels.[3.52] Air-saturated solutions of the dye, erioglaucine, and either agarose or galactose were irradiated in borosilicate-glass containers with Co^{60} gamma radiation at a dose rate of 4.1×10^3 rad min^{-1}. Solutions with more than 0.1% agarose were saturated with air at temperatures just above the gel point and then allowed to cool so that approximately the same amount of dissolved oxygen would be present in all the systems compared.

The results of these measurements are shown in Figure 3.24 and suggest that considerable portions of the agarose chain are inaccessible to the free radicals. In the liquid state, the rate of reaction between hydroxyl radicals and agarose per unit galactose residue is only 16% of the value for monomeric galactose. This comparison requires the reasonable assumption that the radical-capturing abilities of galactose and 3,6-anhydrogalactose are equal. Rather than a random coil in aqueous solution, agarose appears to be a tightly packed structure whose interior is impervious to hydroxyl radicals.

In gel-forming concentrations, agarose appears to exclude hydroxyl radicals from still larger regions of the system. Usually the macroscopic diffusion constants of solutes in dilute gel solutions do not change[3.53] so that this exclusion volume must be divided among a large number of small sites. This behavior indicates again the care which should be taken in transposing kinetic data obtained in liquid solutions over to biological systems characterized by viscous or gel-like physical states.

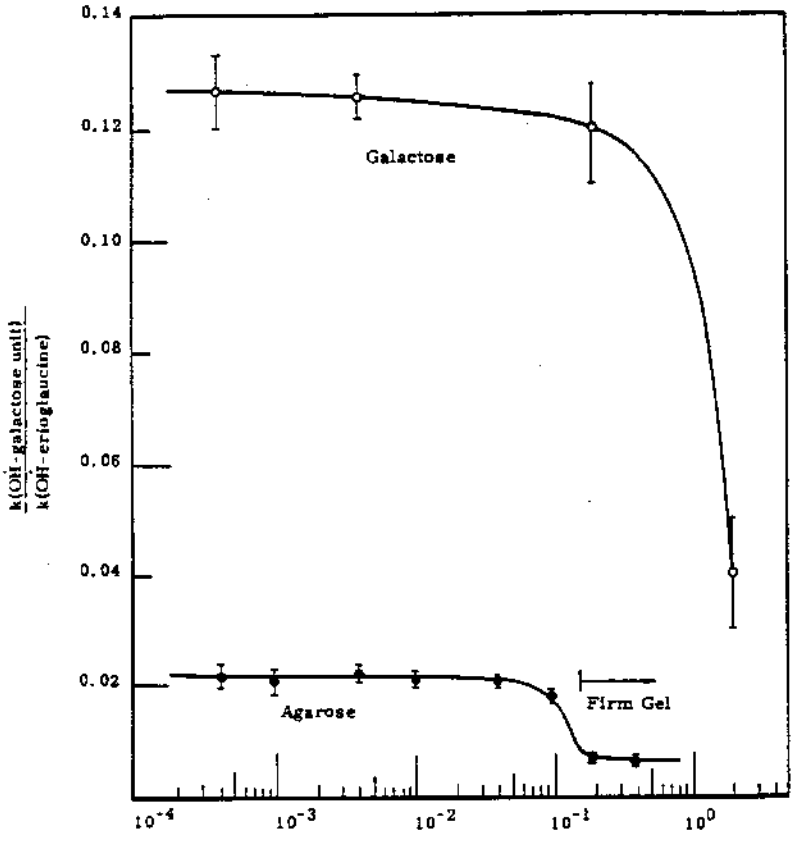

FIGURE 3.24

Relative Rate Constants
for Reaction of Galactose and Agarose with Hydroxyl Radicals

Kinetics of Radiation-Induced Hemolysis of Human Red Blood Cells - D. R. Kalkwarf and R. W. Henkens

In irradiated, aqueous suspensions, red blood cells appear to hemolyze as a result of successive attacks on their outer surfaces by free radicals formed in the surrounding solution. Additional support for this view was obtained by numerical comparison of theoretical and experimental values for the fraction of cells remaining intact as a function of time after irradiation.

One of the effects of ionizing radiation on red blood cells in aqueous suspension is the induction of premature hemolysis. Addition of certain chemicals to the suspensions before irradiation protects the cells from this damage, and the protective abilities of these additives are directly proportional

to their rates of reaction with the radicals formed in irradiated water.[3.54] This suggested that radiation damage leading to hemolysis was initiated by successive radical-attacks on the outer surfaces of the cells. A formulation of this mechanism has been made,[3.54] and supporting evidence is described below based on a numerical comparison of theoretical and experimental values for the fraction of cells remaining intact as a function of time after irradiation.

As described previously,[3.54] the mechanism of successive radical-attacks on the cell surface during irradiation generates Equation 1 where F is the fraction of nonhemolyzed cells in the suspension, D is the absorbed dose of radiation, and Q is a constant for any given suspension.

$$F = \sum_{j=o}^{N-1} (QD)^j \; e^{-QD}/j! \qquad (1)$$

The summation in Equation 1 is taken over all j terms up to N-1 where N is the number of radical-attacks which a cell has sustained if it hemolyzes in time t. Nomographs are available for evaluating this summation numerically.[3.55] The constant Q is a composite of other constants as shown in Equation 2,

$$Q = \frac{Y}{[C]_o + \sum (k_i/k_c)\,[S_i]_o} \qquad (2)$$

where Y is the yield of free radicals per rad, $[C]_o$ is the initial concentration of cells in suspension, $[S_i]_o$ is the initial concentration of any solute in the solution surrounding the cells, and k_c and k_i are specific rate constants for bimolecular reactions between the radicals and either the cells or the solutes, respectively.

The value of QD defines a hemolysis curve expressing the variation of nonhemolyzed cells with time after irradiation. It has been shown previously[3.54] that the quantity N in Equation 1 can be expressed as

$$N = \frac{Q}{b} \ln \frac{K}{t} + \frac{1}{3} \qquad (3)$$

where b and K are empirical constants obtained from hemolysis data following various absorbed doses. Substituting Equation 3 into Equation 1 gives F as an explicit function of t. Figure 3.25 shows the shape of hemolysis curves synthesized in this way. Also shown are experimental data for cells after absorbing 10 rads. Since k_c, the rate constant for reaction between radicals and cells, was unknown, its value was arbitrarily adjusted to allow the experimental and theoretical hemolysis curves to coincide at one point. The excellent agreement between the remaining points and the curve for QD = 15 indicates how well the experimental data support the radical-attack mechanism.

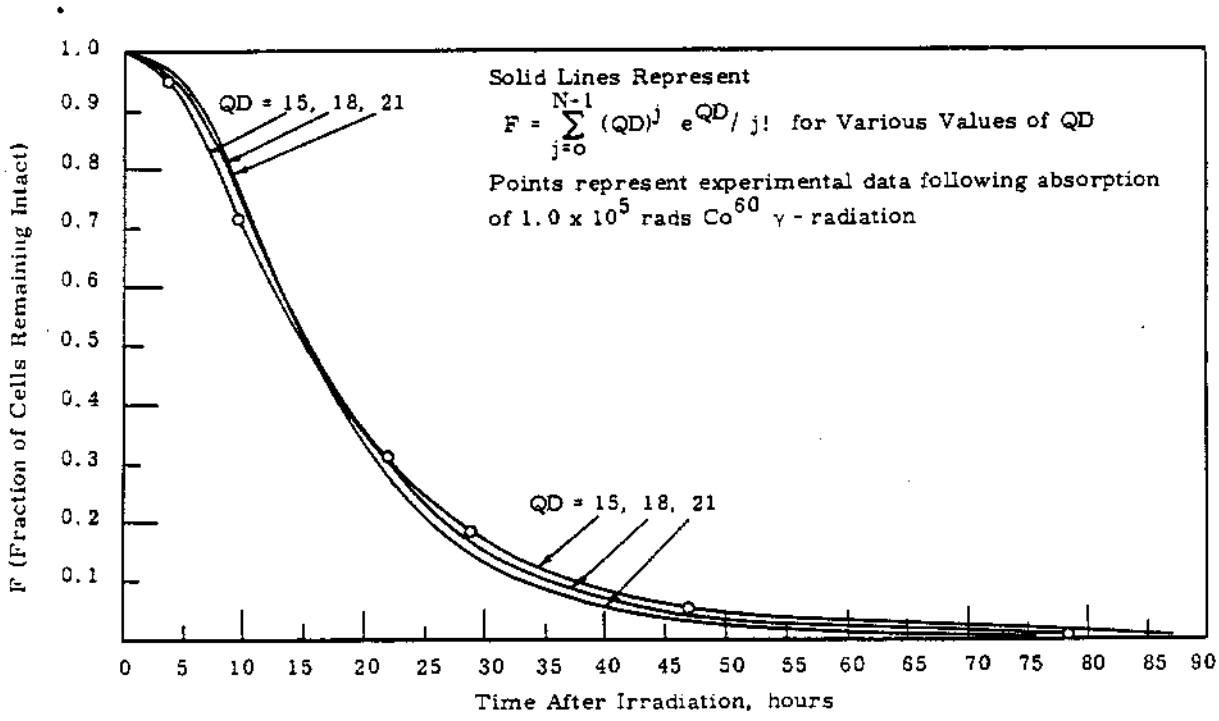

FIGURE 3.25
Hemolysis as a Function of Time After Irradiation

G Value for Tropeoline O - W. D. Felix

The G value of tropeoline O in aqueous solution, pH 11.8, was found to be 3.20. Ethanol, when added to a tropeoline O solution of nearly equivalent concentration, gave no protection against decoloration of the dye.

Relatively few investigations have been made in aqueous solutions with pH greater than 9.[3.56, 3.57] It is of interest to examine the protective properties of various chemical solutes in higher pH ranges. To facilitate such investigation, the dye, tropeoline O, was chosen as a reference compound. Tropeoline O, or Food Yellow 8, is stable at pH13 for a period of weeks before fading is detectable. Aqueous, aerated solutions of the dye are decolorized when exposed to ionizing radiation.

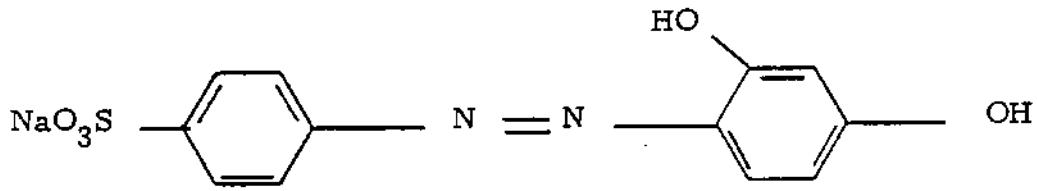

Tropeoline O

Solutions of tropeoline O were made up with concentrations varying from 1×10^{-5} M to 6×10^{-5} M in a solution buffered to pH 11.78 with $NaOH\text{-}Na_2HPO_4$. Beer's law was found to hold at the absorbance maximum, 431 mμ, for the concentration range used. The absorption spectrum shows a broad peak under this maximum such that slit width is not a particularly critical parameter. The D_{37} dose, that dose which will reduce the dye concentration to 37% of its initial value, was determined for each concentration level and plotted against the concentration as shown in Figure 3.26. From the reciprocal of the slope of this curve, the G value, the number of molecules

of dye decomposing per 100 ev absorbed by the solution, was found to be 3.20 ± 0.03. Since values for the yields of radicals from water decomposition have not yet been determined for aqueous solutions at pH greater than 7, [3.56] one cannot reasonably propose a mechanism for the dye decoloration from the limited information available. It is interesting to note, however, that the intercept of the D_{37} curve goes through the origin (0.065×10^3 by least squares fit). Most dyes, when exposed to ionizing radiation, are sensitive to impurities in the water as evidenced by a positive intercept on the ordinate.

When ethanol (1×10^{-5} M) was added to tropeoline O solutions (2.5×10^{-5}M in tropeoline O) as a protective agent, no protection of the dye against decoloration was noted. Thus, since ethanol is a scavenger of hydroxide radicals, the reaction of tropeoline O with hydroxide radicals to irreversibly form products is probably not a major reaction.

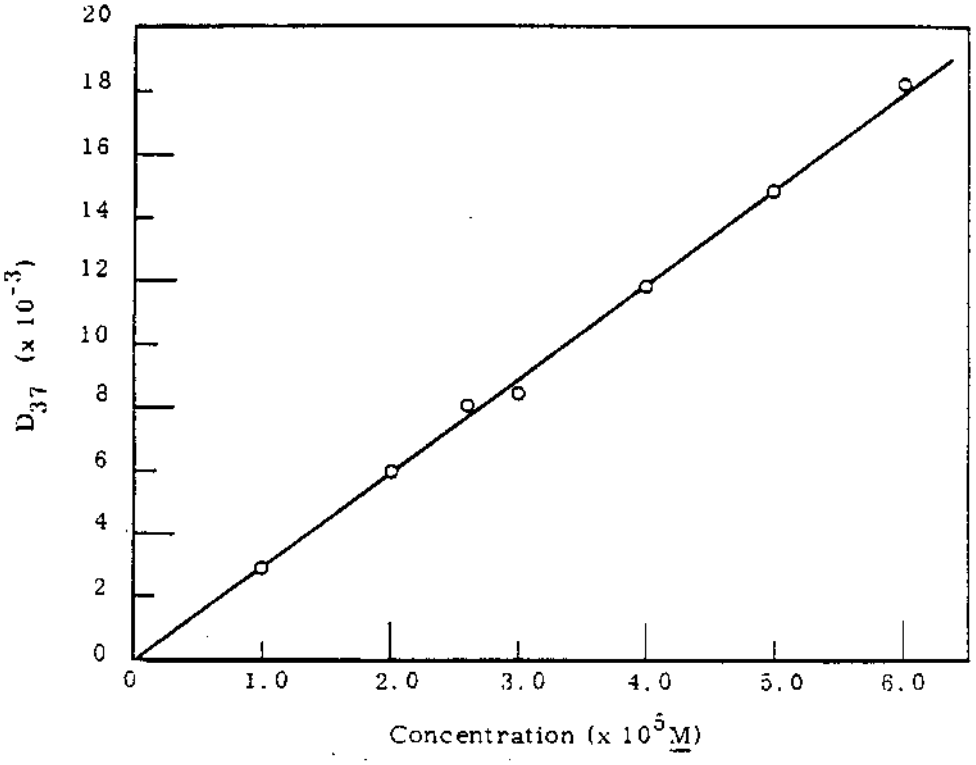

FIGURE 3.26

Variation of D_{37} Dose for Tropeoline O Solutions with Concentration (pH 11.78, Temperature 22 C)

Disc Electrophoresis of Human Serum Irradiated in Vivo -
W. D. Felix and R. W. Henkens

Disc electrophoresis patterns of sera from irradiated individuals were compared with those of normal sera. Poor resolution of the electrophoretic patterns did not allow definitive conclusions to be made.

Disc electrophoresis, a recent innovation in electrophoresis methods,[3.58, 3.59] shows a much greater resolution of serum proteins than does paper chromatography or paper electrophoresis. Disc electrophoresis, therefore, offers an interesting device to detect possible changes in the protein patterns of physiological systems exposed to radiation. The method takes advantage of the frictional properties of gels by sieving at the molecule level through pores of a synthetic polyacrylamide gel. Generally the zones are narrower than in paper electrophoresis or chromatography.

Sera collected by venipuncture from three individuals, designated 1, 2, and 3, who had received whole body irradiation of approximately 29, 14, and 4 rads respectively as determined by blood sodium analysis,[3.60] were examined by the disc electrophoresis method. Five microliter samples of serum were resolved with 5-6 ma current at 160 v for 30 min. Controls used were heparinized samples of blood collected from lanced fingers of three individuals and one serum sample collected by venipuncture from a fourth.

Photographs of the gels for the three irradiated sera and for three of the controls are presented in Figure 3.27. The resolution unfortunately was not good enough for more than a gross qualitative comparison of the samples. Apparently the electrophoresis runs were too long and were overloaded. A normal standard serum should show at least 24 distinct bands.[3.58]

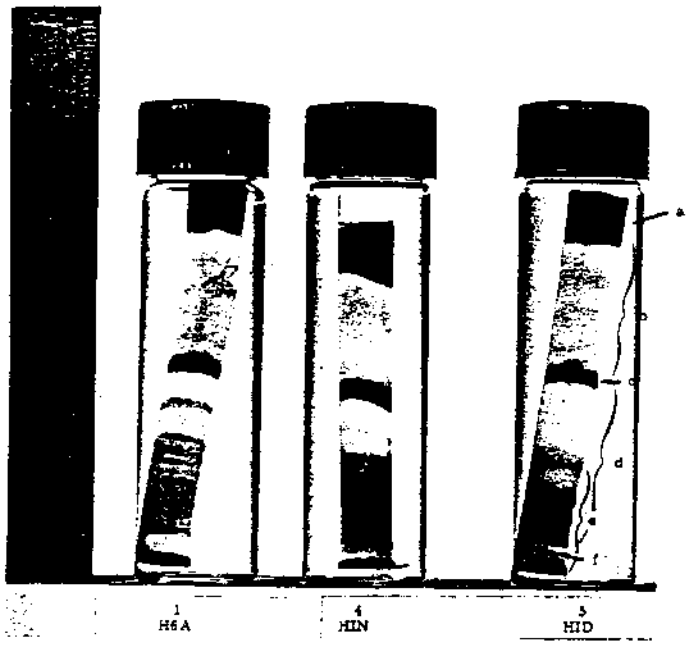

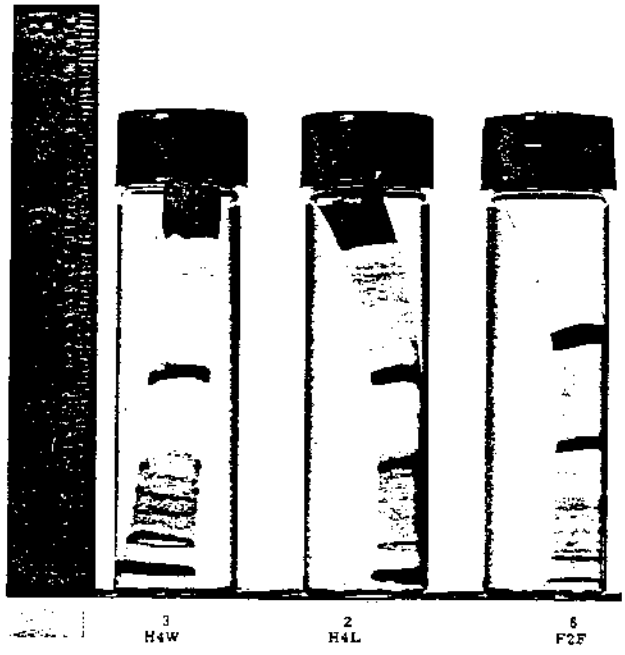

FIGURE 3.27

Disc Electrophoresis Gels: (1-3) serum; 29, 14, and 4 rad dose; (4 and 5) controls, plasma from finger; (6) control, serum. Gel 5 Pattern: (3.59)
(a) albumin (b) post albumins (c) transferrin (d) haptoglobins
(e) region of "7S" gamma globulins (f) slow lipoprotein and macroglobulin

AEC-GE RICHLAND, WASH.

One should find differences in concentration of certain of the blood protein fractions and perhaps some fractions not found in normal blood serum as a result of the corrective body processes which would take place immediately following radiation exposure. One should also find decomposition products of serum components as a direct result of radiation damage.

Observations made thus far indicate that with proper experimental conditions and technique, the method may be effectively applied to the investigation of systemic damage following radiation exposure.

Thin Layer Chromatography of Triphenylmethane Dyes - W. D. Felix

Thin layer chromatography has been used to determine purity of dyestuffs. The method was capable of separating commercial samples of FD&C Blue No. 1 into five of six possible isomers which can arise from all possible combinations of the sulfonic acid group on the two N-benzyl rings.

The preparation and color properties of the food color, FD&C Blue No. 1, have been extensively studied. The commercial product has been chromatographed both on paper (3.61) and on a column of Celite 545. (3.62) The latter work indicated the presence of five fractions which were attributed to isomers of the major component of the color.

Thin layer chromatography (TLC) employs a layer of an absorbing material which has been evenly spread on a glass plate. The dried plate is spotted with the material to be chromatographed and exposed to a suitable solvent. Separations are usually distinct; and in fact, with respect to degree of resolution, TLC may be placed between column and gas chromatography.

Commercial samples of the dye were obtained from Allied Chemical Co. A sample of dye was also synthesized by condensing benzaldehyde-3-sulfonic acid with N-ethyl-N-phenylbenzylamine-2-sulfonic acid, the intermediates having been purified by repeated recrystallization. (3.62, 3.63)

Glass plates (20 x 20 cm) were coated with a 250 μ layer of kieselguhr (with gypsum as a binder) and dried in a vacuum oven at 100 C for 30 min. Dye samples were spotted as thin lines and developed in a solvent of water-saturated butanol-acetic acid (20:1 vol/vol). The thin layer was removed from the plate as a plastic film, and line densities were read on a Photovolt densitometer.

The commercial preparation of N-ethyl-N-phenylbenzylamine-3-sulfonic acid results in a mixture of the ortho, meta, and para sulfonic acid isoners.[3.64] Unless the meta isomer is purified by repeated recrystallization the aldehyde condensation reaction

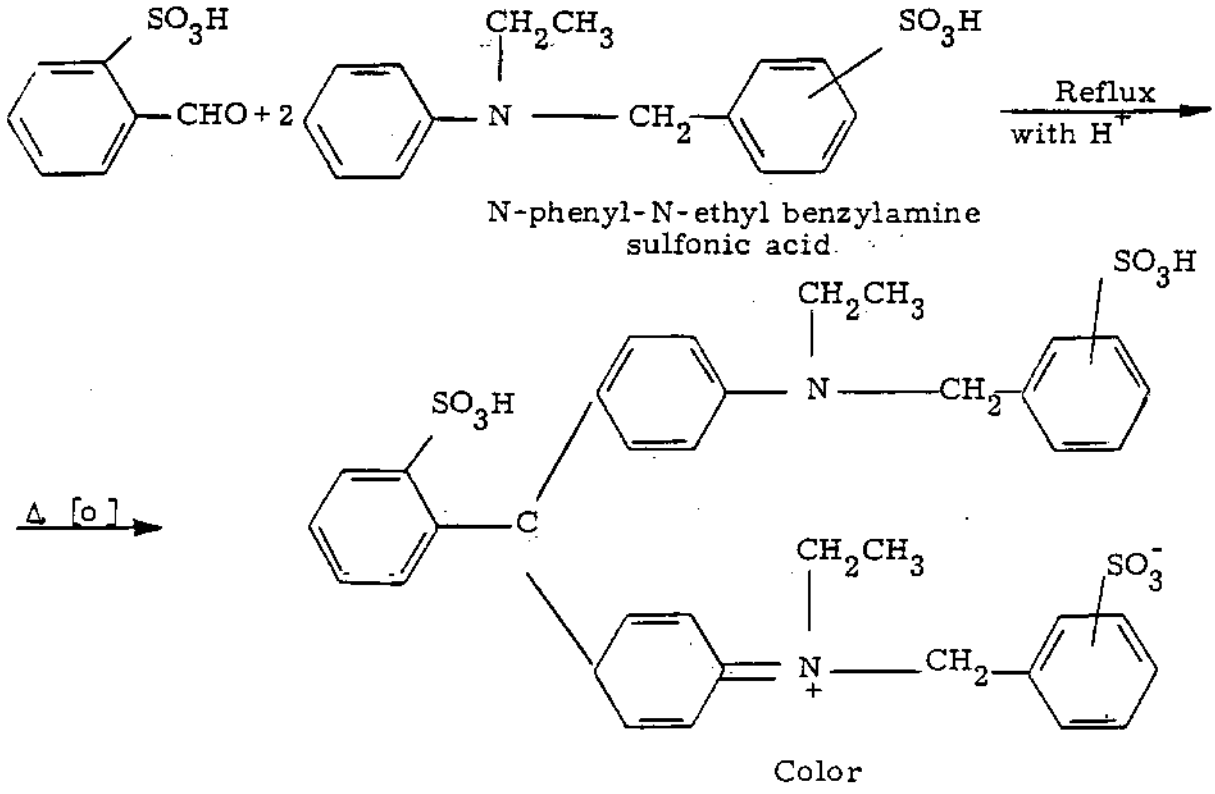

may be expected to yield six isomers formed by all possible combinations of the sulfonic group on the end rings: mm, pp, oo, mp, op, and mo.

The TLC chromatograms and the densimetric recordings for the commercial dye and for the specially synthesized sample of the mm isomer are presented in Figures 3.28 and 3.29, respectively.

Paper chromatography will not resolve any of the isomers. The method of paper electrophoresis will give three components. Column chromatography did indicate the presence of five fractions, but resolution was poor; each apparent fraction was actually contaminated with neighboring isomers. Since all six isomers have equal absorptivities and equivalent spectra,[3.63] the densimetric recordings of the dye fractions as found by TLC may be used directly to give an estimate of isomeric concentration.

TLC is thus a superior method for the detection, separation, and qualitative estimation of isomers or impurities of some dyes and colored compounds. It may be expected to be similarly effective with compounds which absorb in the ultraviolet region. This method becomes especially significant when used to detect the presence of isomers or impurities in cases where the separation would be impossible by the usual chemical and physical methods. This is of interest in the investigation of irradiated solutions where the presence of impurities becomes extremely critical.

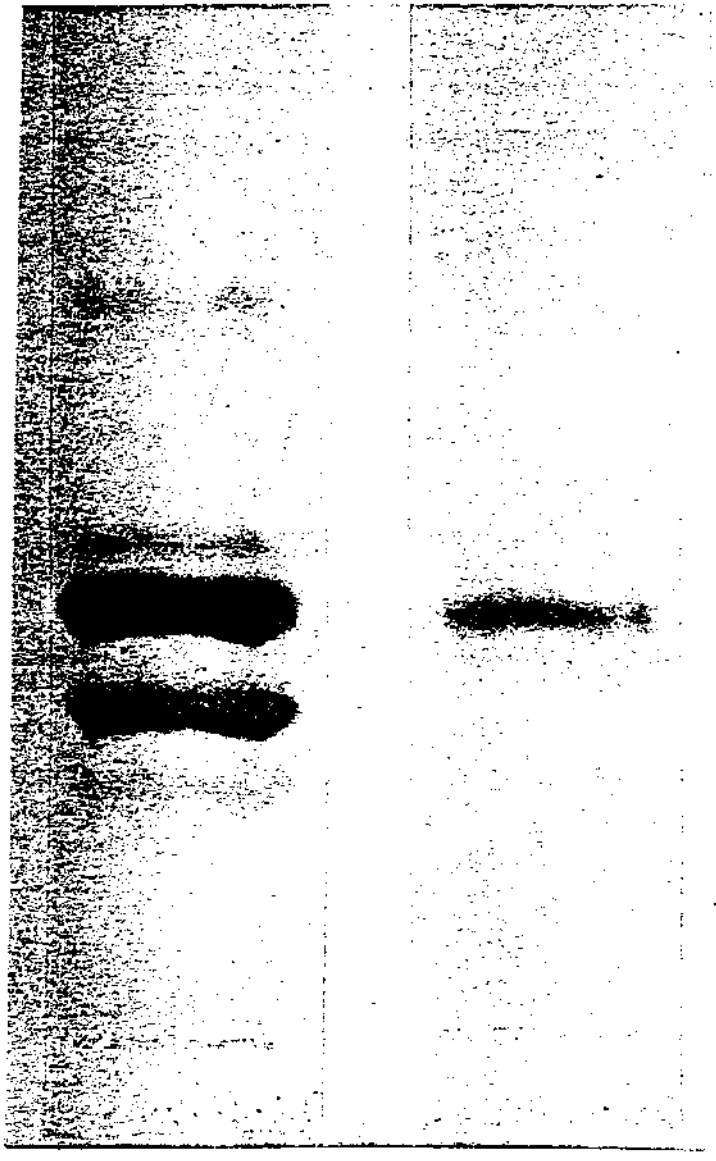

FIGURE 3.28

Thin Layer Chromatograms of FD&C Blue No. 1, 5 Samples:
(a) commercial preparation, 4.2 mg/ml
(b) meta-meta isomer, 5.2 mg/ml

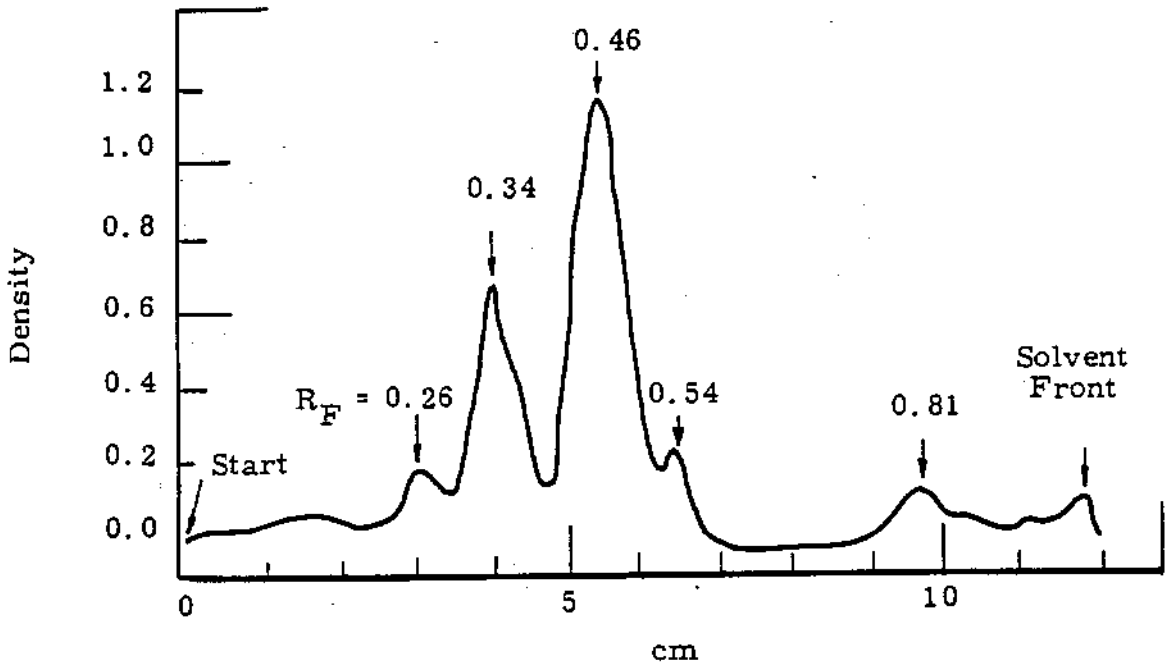

(a)

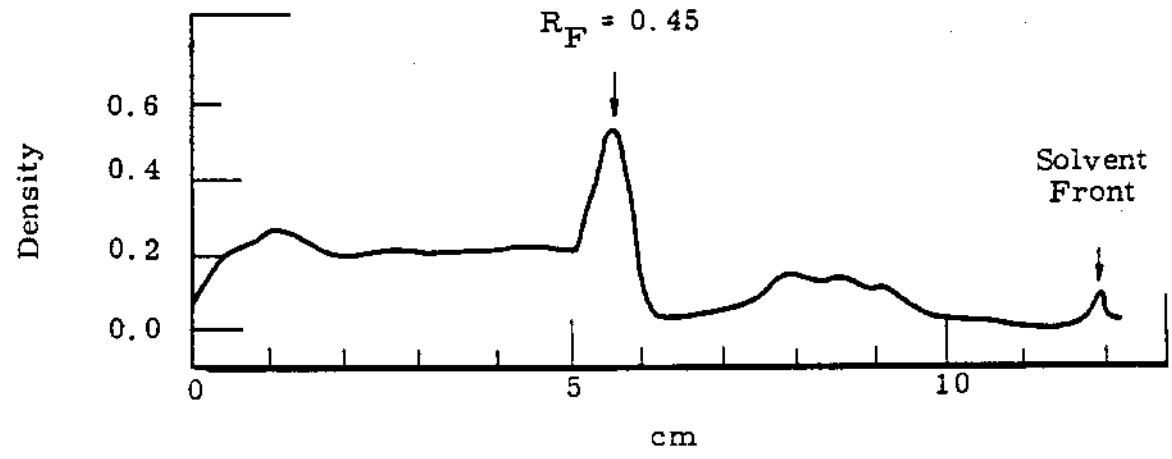

(b)

FIGURE 3.29

Densimetric Recording of Chromatographs Shown in Figure 3.28 Taken with Red Filter in Place

Low Noise Modification of an Electron Spin Resonance Spectrometer -

R. N. Diebel

Improved noise figure was obtained in an electron spin resonance (ESR) spectrometer through use of a microwave matched tee and homodyne detection system. Minor changes made in the 100 kc field modulation and control unit rendered it useful up to its maximum gain of 120 db. A long term stability of 0.5% on the signal output was achieved after modification of the 100 kc synchronous reactifier and use of a chopper stabilized follower on the output to the recorder.

To obtain the best possible signal-to-noise ratio from an ESR spectrometer system, it was converted from the V4500-40B bridge (Varian Associates), which uses a 3 db coupler, to a ferrite circulator. The use of circulators is not new, (3.65, 3.66) and the prime advantage is the small insertion loss. The gain in available microwave and signal power due to using the circulator has, however, been consumed again by use of a TE104 model dual sample cavity in place of the original TE102 single sample cavity. The power incident on the dual sample cavity is equally divided between the two sample positions; therefore, each sample sees only half of this power. Also, each sample occupies only half the total sample volume; hence, the signal from a single sample is only half what it could be in a TE102 single sample cavity. The net result is the same output signal as in the system before using the circulator. The dual sample cavity offers the great advantage of having a position for a standard which can be used to monitor changes in the quality (Q) factor of the cavity as the other sample is changed in character.

With the circulator as the bridge element, the noise level began to increase as the power reached about 40 mw instead of at 60 mw as was previously noted. (3.67) This increase in noise seemed to be associated with microphonics and could also be increased by using more than a minute fraction of the available modulation level on the automatic frequency control (AFC) of the klystron. These observations led to consideration of converting to the bimodal cavity and superheterodyne lock-in* detector system of Teany, Klein, and Portis. (3.68)

---

* Lock-in detector is synonomous with phase sensitive, synchronous, or homodyne detector.

Examination of this paper of Teany, et al, revealed that at power levels of 100 mw or less, the reactangular cavity in a bridge spectrometer using the lock-in detector would have a superior signal-to-noise ratio. In this system the lock-in detector was operated at the 30 Mc intermediate frequency (i.f.) of the superheterodyne receiver. Use of this lock-in detector considerably reduces noise due to mismatch of klystron and cavity frequency, such as would be caused by microphonics. In addition, use of balanced tee microwave detectors eliminates most of the noise from the klystron power generator.

Since the 100 kc field modulation system was available, and since no unmanageable modulation effects could be found in the cavity, and since there was no need to operate at higher power levels, it was decided to incorporate the balanced tee mixer and lock-in detection into the present system. The same objectives as the i.f. lock-in detector are achieved by operating at zero i.f. as managed in the system of Figure 3.30. A sample of power from the ESR klystron is used as the local oscillator input of a balanced tee mixer detector. The lock-in or homodyne detection now occurs directly at the microwave frequency as the diode detectors are turned on every half cycle of this reference power. The phase shifter is adjusted to observe the real part of the cavity reflection coefficient in exactly the same manner as described for the previous modification.[3.67, 3.69] Also incorporated are a second balanced tee and klystron which can be used with a variable frequency rf generator to measure the cavity Q in the manner described by Strandberg.[3.69] This second klystron can also be used as a superheterodyne local oscillator when it is necessary to observe very narrow ESR lines.

With this system shown in Figure 3.30, a power of 200 Mw in the cavity arm raises the noise level about 20% above that seen at zero power. The balanced tee and homodyne detector greatly reduce the noise level due to microphonics and carrier noise. Without the balanced tee, e.g., when one of the two detector crystal is disconnected, the AFC system is so disturbed by microphonics as to be nearly inoperative at power levels approaching 100 Mw.

This system enables the power level in the cavity arm to be varied from 200 Mw to at least 60 db below this input while maintaining adequate automatic frequency control. The circulator used* has an isolation of a little more than 40 db between the klystron and detector. The screw tuner in the cavity arm is used to balance the leakage direct power, however, the adjustment is not critical until the input power approaches 100 Mw.

It should be noted that a microwave spectrometer system such as the one described can be converted to measure the absorption directly rather than via the attenuated first derivative as must be done when magnetic field modulation is used. One must first have a cavity which can be adjusted to give a stable balance of zero reflected power in the absence of magnetic resonance. A microwave switch or modulator is then placed in the detector arm and amplitude modulation of the magnetic resonance signal is applied at 100 kc or whatever other frequency was used for the field modulation or i.f. frequency. This method of observing the absorption would be advantageous for studies of irradiated seeds where the lines are rather broad and the power levels used are low so that stability of the cavity balance is not highly critical.

Following is a description of the changes which were made in the 100 kc receiver and output circuits. Regenerative oscillation which tended to occur at gain settings above 2000 on the Varian Associates V4560 unit were eliminated when the output tube, V403, of the receiver was operated from a separate heater supply. This heater power could also be taken from T101 which supplies the transmitter section. A change also had to be made in the placement of ground connections for the amplitude controls of the transmitter and receiver to eliminate a built-in coherent signal. This stray signal could be seen as a shift in recorder output which was proportional to receiver gain at settings of about 400 and higher. The ground return points of both the amplitude controls were returned to the point nearest the origin of the signal

---

* Model SYF 3143, Sylvania Electric Products, Inc., Microwave Device Division, Mountain View, California.

instead of onto the front panel. With these two changes, operation was possible at the full 120 db gain of the receiver without problems of oscillation or baseline shift.

Since the random signal level at full gain was quite high and near the point of overloading the synchronous detector, a tuned LC load was placed in the plate of V403. At the same time the cathode bypass capacitor had to be removed to maintain the gain about the same. This filter served to decrease the noise signal on the detector level meter from about 35 to about 8.

The original cathode follower and 100 kc synchronous rectifier were occasionally unstable, and also the output baseline shifted as the phase control was adjusted. A chopper stabilized output follower was used to achieve a stable input impedance and gain. Philbrick* operational amplifiers, models K2P plus K2W, were installed in conjunction with both the 100 kc and audio frequency field modulation units.

The 100 kc synchronous rectifier circuit was revised as shown in Figure 3.31. The output is linear up to 0.4 v, however it is not known whether this linearity is impaired by large levels of random noise.

As a check on overall performance of the spectrometer, the ESR spectrum of a dilute aqueous solution of $MnCl_2$ was obtained. A five-fold improvement in signal-to-noise ratio over that seen with the original spectrometer was found.

---

* George A. Philbrick Researches, In., Boston 16, Massachusetts.

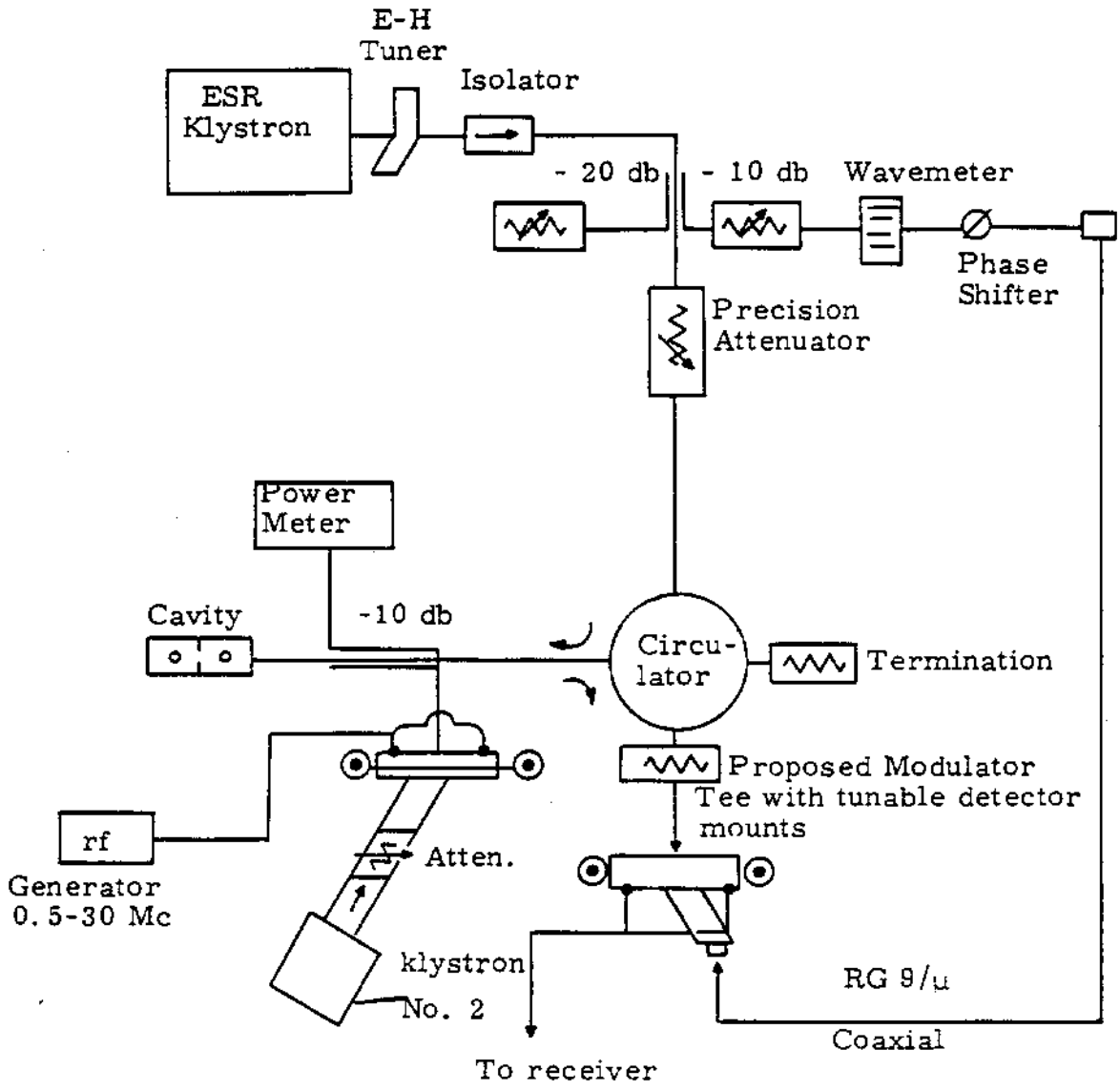

FIGURE 3.30

Balanced Tee-Homodyne Detection System
with Ferrite Circulator in ESR Spectrometer

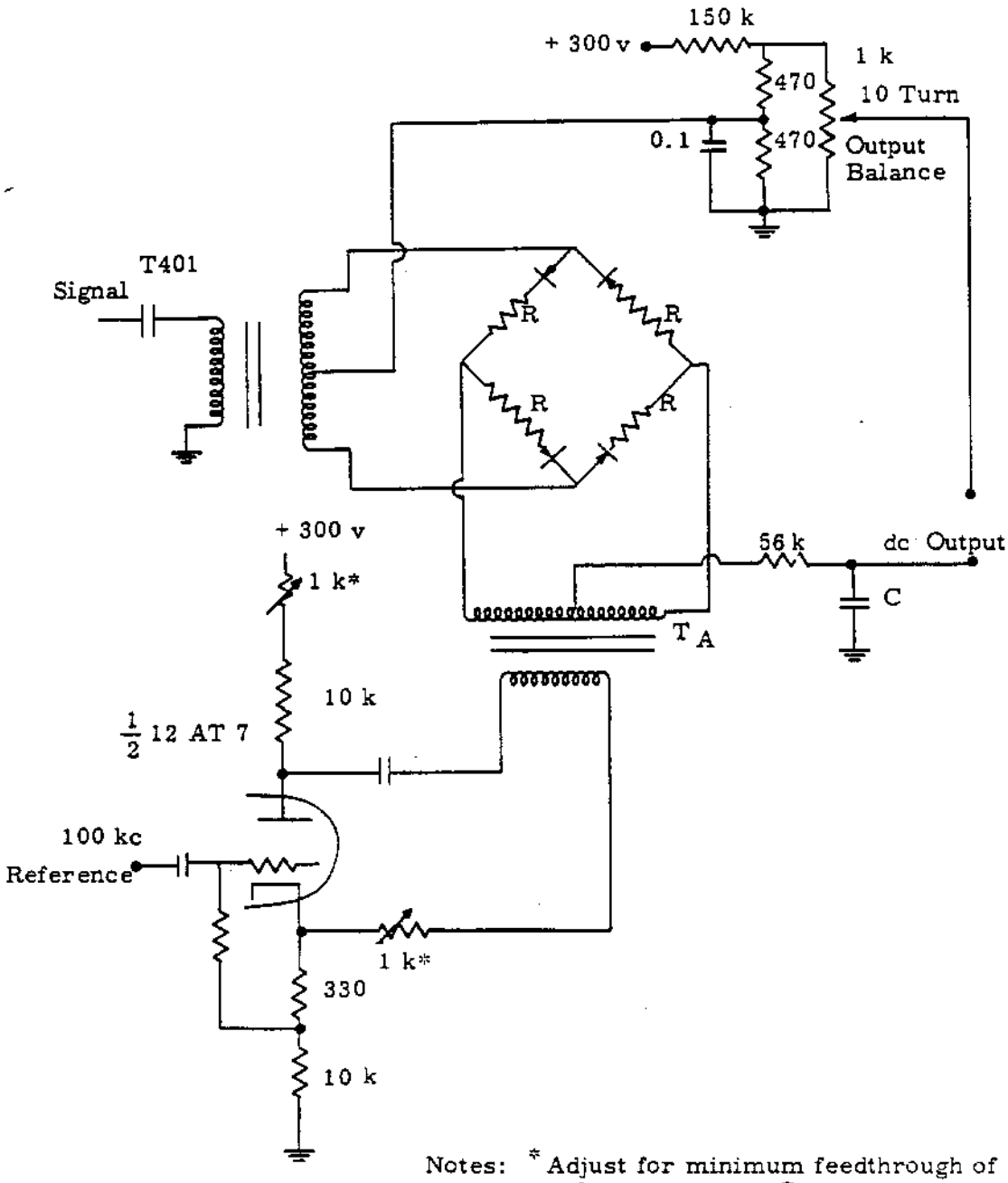

Notes: * Adjust for minimum feedthrough of 100 kc reference across C.

R = 10 k

C = 300 pf

T_A: Spectran Electronics Corp. S-005-95

FIGURE 3.31

100 kc Synchronous Detector

REFERENCES

3.1 R. W. Perkins. Source of Reactor Effluent Water Radioisotopes, HW-69969. May 1961.

3.2 D. E. Robertson and R. W. Perkins. The Effect of Chemical Additives and Coating Materials on the Adsorption of Radionuclide Parent Elements on Aluminum Surfaces, HW-75976. December 26, 1962.

3.3 D. Strominger, J. M. Hollander and G. T. Seabrog. "Table of Isotopes," Rev. Mod. Phys., vol. 30, p. 814. 1958.

3.4 R. W. Perkins and D. R. Kalkwarf. "Determination of Thorium in Urine," Anal. Chem., vol 28, pp. 1989-1993. 1956.

3.5 F. L. Moore and S. A. Reynolds. "Determination of Protactinium-233," Anal. Chem., vol.29, pp. 1596-1599. 1957.

3.6 Seymour Katcoff. "Fission-Product Yields from Neutron-Induced Fission," Nucleonics, vol. 18, no. 11, pp. 201-208. 1960.

3.7 National Bureau of Standards Handbook 69, Maximum Permissible Body Burdens and Maximum Permissible Concentrations of Radionuclides in Air and in Water for Occupational Exposure, U.S. Government Printing Office. June 5, 1959.

3.8 J. W. Healy, G. J. Pilcher and C. E. Thompson. Computed Fission Product Decay, HW-33414. December 1, 1954.

3.9 R. W. Perkins. "Radiochemical Analysis of Reactor Effluent Waste Materials at Hanford," Talanta, vol.6, pp. 117-132. 1960

3.10 G. Leliaert, J. Hoste, and Z. Eeckhaut. "Activation Analysis of Tungsten in High-Alloy Steels," Talanta, vol. 2, pp. 115-123. 1959.

3.11 W. B. Silker. "Radiochemical Determination of Phosphorus-32," Anal. Chem., vol.28, pp. 1782-1783. 1956.

REFERENCES (Contd.)

3.12 F. Ephraim, P. C. L. Thorne, and E. R. Roberts. "Inorganic Chemistry," 5th English Edition, pp. 513-516. London: Gurney and Jackson, 1948.

3.13 J. D. Ludwick. Dual Atmospheric Tracer Techniques for Diffusion Studies Using Phosphorescence - Fluorescence Analysis, HW-70892. March 1961.

3.14 J. D. Ludwick and R. W. Perkins. "Liquid Scintillation Techniques Applied to Counting Phosphorescence Emission. Measurement of Trace Quantities of Zinc Sulfide," Anal. Chem, vol. 33, pp. 1230-1235. 1961.

3.15 J. D. Ludwick. Ground and Vegetation Effects on Atmospheric Diffusion Experiments, HW-73337, p. 137. January 1962.

3.16 W. C. Roesch, C. C. Gamertsfelder, H. V. Larson, J. M. Nielsen and E. C. Watson. Unpublished Data., General Electric Co., Richland, Washington. 1963.

3.17 P. S. Harris. "Radiation Dose Estimation in the 1958 Los Alamos Criticality Accident," Health Physics, vol. 5, pp. 37-44. 1961.

3.18 D. F. Petersen, V. E. Mitchell and W. H. Langham. "Estimation of Fast Neutron Doses in Man by $S^{32}(n, p)P^{32}$ Reaction in Body Hair," Health Physics, vol. 6, pp. 1-5. 1961.

3.19 W. B. Silker. "Radiochemical Determination of Phosphorus-32," Anal. Chem., vol. 28, pp. 1782-1783. 1956.

3.20 I. Lysyj and J. E. Zarembo. "Spectrophotometric Methods for the Determination of Small Amounts of Sulfur in Organic Compounds: A Semimicro and Micro Method," Microchem J., vol. 3, pp. 173-180. 1959.

REFERENCES (Contd.)

3.21 G. S. Hurst, J. A. Harter, P. N. Hensley, W. A. Mills, M. Slater and P. W. Reinhardt. "Techniques of Measuring Neutron Spectra with Threshold Detectors - Tissue Dose Determination," Rev. Sci. Inst., vol. 27, pp 153-156. 1956.

3.22 J. P. Friend (ed.), H. W. Feely, P. R. Krey, J. Spar, and A. Walton. "The High Altitude Sampling Program. vol. 4. The Application of HASP Data. Final Report," DASA 1300, p. 141. 1961.

3.23 R. W. Perkins, J. M. Nielsen, and R. N. Diebel. "Total-Absorption Gamma-Ray Spectrometers Utilizing Anticoincidence Shielding," Rev. Sci. Instr., vol. 31, pp 1344-1349. 1960.

3.24 R. W. Perkins. Unpublished Data., General Electric Co., Richland, Washington. (HW-76888)

3.25 H. L. Finston and M. T. Kinsley. The Radiochemistry of Cesium, Procedure No. 1, NAS-NS-3035. February 1961.

3.26 W. H. Burgus and T. H. Davis. "Exchange Among Several States of Iodine and the Chemical States of Radioiodine from Tellurium Decay," Paper 19, pp. 209-219. Radiochemical Studies: The Fission Products, Book 1. New York: McGraw-Hill Book Company, Inc. 1951.

3.27 H. H. Willard and J. J. Thompson. "Qualitative Tests for Periodate and Iodate in the Presence of Each Other," J. Am. Chem. Soc., vol. 56, pp. 1827-1828. 1934.

3.28 A. P. Baerg, R. M. Bartholomew, and R. H. Betts. "Search for Independent Formation of Cs^{134m} in Fission," Can. J. Chem., vol. 38, pp 2147-2151. 1960.

3.29 G. S. Bien and De Courcey Mart, Jr. Identification of Cs^{134} in Airborne Particulate Matter, in Interim Progress Report by Hans E. Suess, AECU-4164. August 15, 1963.

REFERENCES (Contd.)

3.30 Kurt Lidén and Ingvar O. Andersson. "Caesium-134 in Man," Nature vol. 195, pp. 1040-1043. September 15, 1962.

3.31 H. E. Palmer, W. C. Hanson, B. I. Griffin and W. C. Roesch. Radioactivity in Alaskan Eskimos, HW-SA-2718. August 17, 1962. Presented at the Second Symposium on Radioactivity in Man, Northwestern University Medical School, Chicago, Illinois. September 5-7, 1962.

3.32 H. L. Krieger and D. Groche. "Occurrence of Scandium-46 and Cesium-134 in Radioactive Fallout," Science, vol. 131, pp. 40-42. 1960.

3.33 R. V. Osborne. Unpublished Data. (Personal Communication)

3.34 J. W. Healy, L. C. Schwendiman and D. L. Reid. The Application of Nuclear Track Emulsions to the Analysis of Urine for Very Low Level Plutonium, HW-22680. November 15, 1951. (Declassified 1955) Also see L. C. Schwendiman and J. W. Healy. "Nuclear-Track Techniques for Low Level Plutonium in Urine," Nucleonics, vol. 16, pp. 78-82. June 1958.

3.35 J. P. Friend (ed), H. W. Feely, P. R. Krey, J. Spar, and A. Walton. "The High Altitude Sampling Program," vol. 5. Supplementary HASP Studies. Final Report. DASA 1300. 1961.

3.36 W. J. Bair. Hanford Atomic Products Operation Report, HW-56636. 1958.

3.37 R. W. Perkins, J. M. Nielsen and R. N. Diebel. "Total Absorption Gamma-Ray Spectrometers Utilizing Anticoincidence Shielding," Rev. Sci. Instr., vol. 31, pp. 1344-1349. December, 1960.

REFERENCES (Contd.)

3.38 C. R. Hill. "A Method of Alpha Particle Spectroscopy for Materials of Very Low Specific Activity," Nuclear Instruments and Methods, vol. 12, pp. 299-306. 1961.

3.39 C. R. Hill. "Identification of α-Emitters in Normal Biological Materials," Health Physics, vol. 8, pp. 17-25. 1962.

3.40 D. R. Kalkwarf. "Radiation Sensitivity and Chemical Structure," Proceedings of the Second International Conference on Peaceful Uses of Atomic Energy, Geneva 29: pp. 379-384. New York: United Nations, 1958.

3.41 F. S. Dainton and T. J. Hardwick. "Reactivity of Hydroxyl Radicals in Aqueous Solution," Trans. Farad. Soc., vol. 53, pp. 333-343. 1957.

3.42 A. O. Allen. The Radiation Chemistry of Water and Aqueous Solution: p. 47. Princeton, N.J. D. Van Nostrand., 1961.

3.43 J. H. Mrez and W. A. Waters. "The Oxidation of Aromatic Compounds by Means of the Free Hydroxyl Radical," J. Chem. Soc., pp. 2427-2433. 1949.

3.44 J. H. Merz and W. A. Waters. "Some Oxidations Involving the Free Hydroxyl Radical," J. Chem. Soc., pp. S15-S25. 1949.

3.45 A. O. Allen. The Radiation Chemistry of Water and Aqueous Solution: p. 48. Princeton, N. J. D. Van Nostrand., 1961.

3.46 D. R. Kalkwarf. "Radiation Sensitivity and Chemical Structure," Proceedings of the Second International Conference on Peaceful Uses of Atomic Energy, Geneva: 24: pp. 379-384. New York: United Nations, 1958.

3.47 M. V. Smoluchowski. "Versuch einer Mathematischen Theorie der Koagulationskinetik kolloider Losungen," (German) Zeit. fur Physik. Chem., vol. 92, pp. 129-168. 1918.

REFERENCES (Contd.)

3.48 H. A. Schwarz. "A Determination of Some Rate Constants for the Radical Processes in the Radiation Chemistry of Water," J. Phys. Chem., vol. 66, pp. 255-262. 1962.

3.49 H. S. Frank and W. Y. Wen. "Structural Aspects of Ion-Solvent Interaction in Aqueous Solutions: A Suggested Picture of Water Structure," Discussions Faraday Society., No. 24: pp. 133-140. 1957.

3.50 D. R. Kalkwarf. Radiation Sensitivities of Metabolic Products in Dilute Aqueous Solutions, Radiological Chemistry Annual Report, HW-68533. pp. 52-56. 1960.

3.51 S. Hjerten. "Agarose as an Anticonvection Agent in Zone Electrophoresis," Biochim. et Biophys. Acta., vol. 53, pp. 514-517. 1961.

3.52 A. Bussard and D. Perrin. "Electrophoresis in Agar Plates," J. Lab. Clin. Med., vol. 4, pp 689-701. 1955.

3.53 S. Glasstone. Textbook of Physical Chemistry: p. 1262. New York: D. Van Nostrand. 1946.

3.54 D. R. Kalkwarf and R. W. Henkens. Chemical Protection of Red Blood Cells from Radiation Damage, HW-73337. January 15, 1962.

3.55 F. Thorndike. "Applications of Poisson's Probability Summation," Bell System Tech. J., vol 5, pp. 604-624. 1926.

3.56 A. O. Allen. The Radiation Chemistry of Water and Aqueous Solutions: Princeton, New Jersey: D. Van Nostrand. 1961.

3.57 A. J. Swallow. Radiation Chemistry of Organic Compounds, vol II. New York: Pergamon Press, 1960.

3.58 L. Ornstein. Unpublished Data. "Disc Electrophoresis: I. Theory".

3.59 B. J. Davis. Unpublished Data. "Disc Electrophoreis: II. Material and Methods".

REFERENCES (Contd.)

3.60 R. W. Perkins and L. J. Kirby. Unpublished Data. Radiological Chemistry Associated with the Hanford Criticality of April 7, 1962.

3.61 D. H. Tilden. "Report on Paper Chromatography of Coal-tar Colors," J. Assoc. Offic. Agric. Chem., vol. 35, pp. 423-435. 1952.

3.62 J. H. Jones, M. Dolinsky, L. S. Harrow, K. S. Heine, Jr. and M. C. Staves. "Studies on the Triphenylmethane Colors Derived from Ethylbenzylaniline Sulfonic Acid," J. Assoc. Offic. Chem., vol. 38, pp. 977-1010. 1955.

3.63 W. B. Link. "Intermediates in Food, Drug, and Cosmetic Colors," J. Assoc. Offic. Agric. Chem., vol. 44, pp. 43-53. 1961.

3.64 K. S. Heine and J. H. Jones. "The Composition of Commercial Ethylbenzylaniline Sulfonic Acid," J. Assoc. Offic. Agric. Chem., vol. 36, pp. 923-930. 1953.

3.65 J. P. Gordon. "Variable Coupling Reflection Cavity for Microwave Spectroscopy," Rev. Sci. Inst., vol. 32, pp. 658-661. 1961

3.66 E. A. Faulkner. "Improved Circuit for an Electron Spin Resonance Spectrometer," J. Sci. Inst., vol. 39, p. 135. 1962.

3.67 R. N. Diebel. Research and Development Activities in the Radiological Sciences. Physical Sciences Portion, HW-73337, p. 121-124. 1961

3.68 D. T. Teaney, M. P. Klein and A. M. Portis, "Microwave Superheterodyne Induction Spectrometer," Rev. Sci. Inst., vol 32, pp. 721-729. 1961.

3.69 M. W. P. Strandberg. "Linear, Complex-Reflection Coefficient Bridge," The Microwave J., vol 4, pp. 66-73. June 1961/

CHEMICAL EFFLUENTS TECHNOLOGY

Soil Chemistry, Geochemistry

Characterization of a Strontium-Selective Zeolite* (4.1) - L. L. Ames, Jr.

Type A zeolite, clinoptilolite, erionite, phillipsite, and alumina-silica gel were examined for their ability to selectively remove small amounts of strontium from aqueous wastes containing high concentrations of sodium salts. The methods used and the zeolite strontium selectivity and particle diffusion data from this study are reported. Type A zeolite was the most selective of the group for strontium, but more than a simple, reversible exchange reaction was responsible for this strontium selectivity.

A group of several zeolites, including Type A, clinoptilolite, erionite, phillipsite, and an alumina-silica gel were examined for the ability to selectively remove small amounts of strontium from aqueous wastes containing high concentrations of sodium salts.

Table 4.1 presents the strontium particle diffusion data for the sodium-based exchangers used in this study. These data were obtained by continuous monitoring of small columns loaded with a traced strontium solution. Activation energies for the exchange of sodium on the zeolite for strontium are considerably higher than those of cesium for sodium.

The high activation energy shown by Type A zeolite borders on that expected for the formation of a chemical compound, rather than a simple cation exchange reaction.

Figure 4.1 gives the breakthrough curves of several zeolites as a plot of C/C_o on an error function, or normal distribution scale, versus volumes of throughput on a log scale.

Note that both curves for each exchange material pass through the same 50% breakthrough point.

---

* Not Supported by the Division of Biology and Medicine

TABLE 4.1

STRONTIUM PARTICLE DIFFUSION DATA

Exchanger	Temperature, C	B, sec^{-1}	D^i, cm^2/sec	E_a, kcal/mole
Type A	56	0.00888	3.11×10^{-7}	
Type A	28	0.00075	2.62×10^{-8}	17.4
Erionite	50	0.01166	4.13×10^{-7}	
Erionite	28	0.00291	1.03×10^{-7}	12.2
Gel	36	0.00583	2.07×10^{-7}	
Gel	25	0.00300	1.06×10^{-7}	11.0
Phillipsite	35	0.00917	3.25×10^{-7}	
Phillipsite	26	0.00556	1.98×10^{-7}	10.1
Clinoptilolite	54	0.00666	2.36×10^{-7}	
Clinoptilolite	28	0.00181	6.41×10^{-8}	9.8

Influent Solution - 0.3N Sr^{+2} plus 1.0×10^{-7}N Sr^{85}

Influent pH - 6.0

Temperature - as indicated

Flow Rate - 12.8 l/hr/cm^2

Shallow Beds - 100 mg, 0.25 to 0.50 mm, sodium based exchangers

B - loading rate, sec^{-1}

D^i - apparent particle diffusion coefficient, cm^2/sec

Figure 4.2, the effect of competing sodium on the strontium capacity of columns under the same experimental conditions, confirms the above results, indicating superior strontium selectivity for Type A relative to the other zeolites tested.

The high activation energy shown by Type A probably results from formation of higher-energy chemical bonds, as well as those bonds typical of cation exchange. However, the X-ray diffraction pattern of a strontium-based Type A does not show the presence of any other chemical compound.

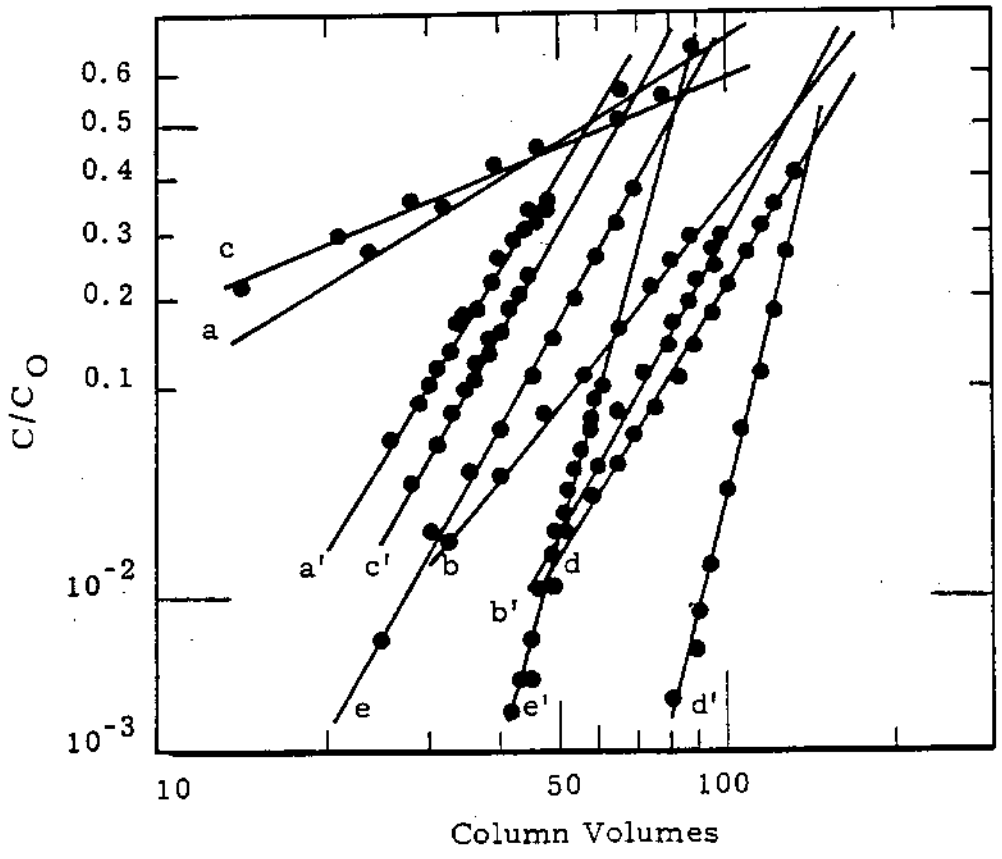

FIGURE 4.1

The Effect of Column Residence Time
on the Slope of Strontium Breakthrough Curves

Influent Solution - 0.008N Sr, 1.0×10^{-8}N Sr^{85} and 0.1N $Mg(C_2H_3O_2)_2$
Influent pH - 7.0
Temperature - 25C
Column - 1.0 to 0.25 mm, sodium-based exchangers; cross-sectional area, 2.84 cm^2; weight 50 g
Column Residence Time - as indicated

Curve Designation	Exchanger	Column Residence Time, min	Strontium Capacity, meq/100 g	Surface Area, m^2/g
a	Clinoptilolite	1.01	58.4	15-20
a'	Clinoptilolite	5.05	58.4	
b	Gel	1.05	128.0	120-150
b'	Gel	5.25	128.0	
c	Type A	1.18	72.7	10-15
c'	Type A	5.90	72.7	
d	Phillipsite	2.02	187.2	400-450
d'	Phillipsite	10.10	187.2	
e	Erionite	1.68	128.0	350-400
e'	Erionite	8.40	128.0	

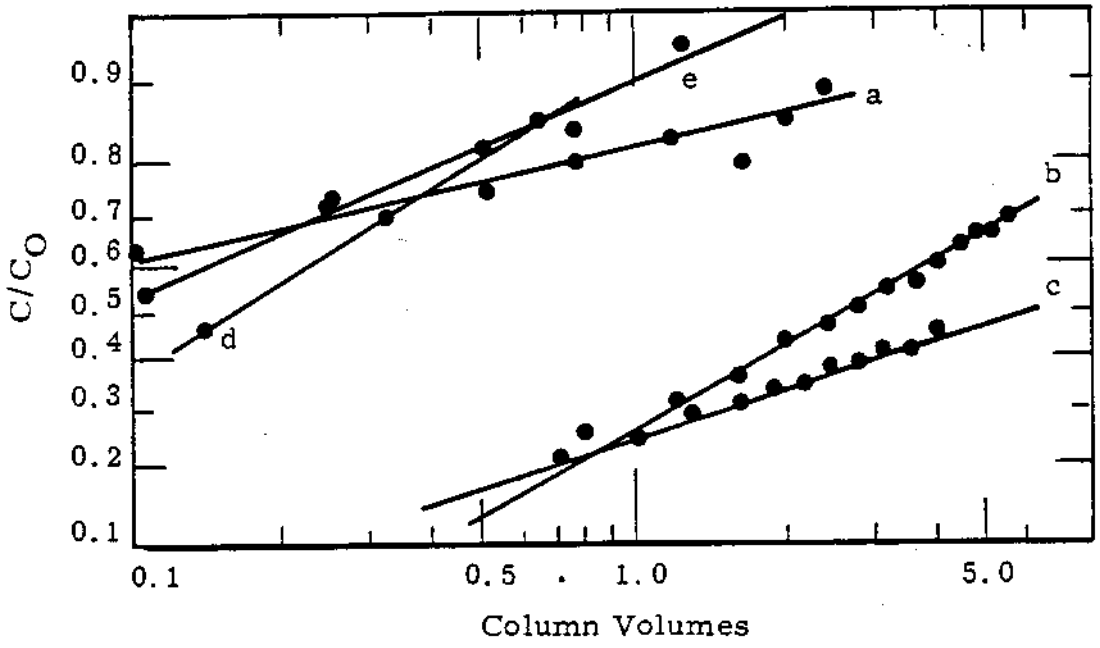

FIGURE 4.2

The Effect of Competing Sodium
on the Strontium Capacity of Several Zeolites

Influent Solution - 1.0 N Na^+, 0.008 N Sr^{+2}, 1.0×10^{-8} N Sr^{85} and 0.1 N $Mg(C_2H_3O_2)_2$

Influent pH - 7.0
Temperature - 25 C
Column - 1.0 to 0.25 mm, sodium-based exchangers; cross-sectional area, 2.84 cm^2; weight 50 g

Column
Residence Time - same as lesser values given in Figure 4.1

Curve Designation	Zeolite	Strontium Capacity, meq/100 g
a	Clinoptilolite	0.03
b	Gel	1.71
c	Type A	12.50
d	Phillipsite	0.19
e	Erionite	0.14

Mass Action Relationships of Some Zeolites in the Region of High Competing Cation Concentrations*(4.2) - L. L. Ames, Jr.

Mass action quotients for the synthetic zeolites Linde 4AXW, 13X, AW-300, AW-400, AW-500, Norton Zeolon, and the natural zeolites clinoptilolite and erionite were determined for low cesium or strontium concentrations in the binary systems cesium-sodium, cesium-potassium, cesium-rubidium, strontium-calcium, and strontium-sodium. The equilibrium systems cesium-hydrogen and strontium-hydrogen were determined for the zeolites Linde Aw-300, Norton Zeolon, and clinoptilolite. A portion of the ternary system hydrogen-sodium-cesium was determined for clinoptilolite.

Cesium mass action quotients generally declined in going from cesium-sodium to cesium-rubidium systems. Structural differences between two members of the same zeolite species often resulted in cation exchange equilibria differences as great as those between different species.

The binary curves may be used to determine column loading of the above zeolites.

Mass action quotients for the synthetic zeolites Linde 4AXW, 13-X, AW-300, AW-400, AW-500, Norton Zeolon, and the natural zeolites clinoptilolite and erionite were determined for low cesium or strontium concentrations in the binary systems cesium-sodium, cesium-potassium, cesium-rubidium, strontium-calcium, and strontium-sodium. The systems cesium-hydrogen and strontium-hydrogen were determined for the zeolites Linde AW-300, Norton Zeolon and clinoptilolite. A portion of the ternary system hydrogen-sodium-cesium was determined for clinoptilolite. Data from the ternary system are given in Figure 4.3. The same cesium content of the equilibrium solutions are connected with a solid line. Related equilibrium zeolite loadings are connected with dotted lines. Points of zeolite and solution equilibria are connected with arrows. Some of the equilibrium solution compositions were deleted from the cesium-sodium and cesium-hydrogen binary joins to avoid further cluttering of the diagram.

---

* Not Supported by the Division of Biology and Medicine

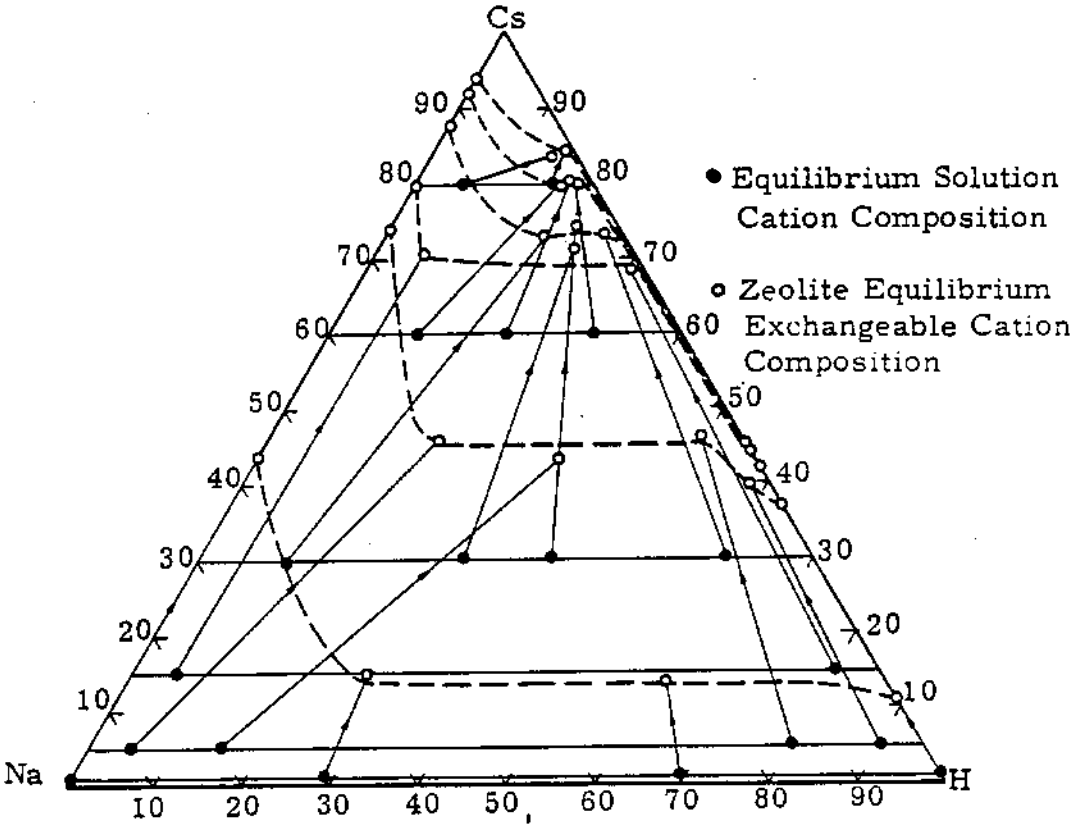

FIGURE 4.3

A Portion of the Ternary Equilibrium System
Hydrogen-Sodium-Cesium on Clinoptilolite

The complex nature of the ternary equilibria is apparent from Figure 4.3, i.e., the ternary system cannot be deduced from a consideration of the binary systems except in a very general way. It is evident also that the number of experiments required to understand thoroughly ternary equilibria can be quite large.

In general, the mass action quotient is not constant for a given cation as the zeolite approaches full loading with that cation. Rather, the quotient is a function of a given cation activity in the contacting solution and in the zeolite. Consequently, only very general conclusions may be drawn from the uncorrected mass action quotients. Table 4.2, as an example, gives the cesium mass action quotients, defined as $\frac{[Cs_z][Na_s]}{[Na_z][Cs_s]}$, for several zeolites. The z

and s refer to zeolite and equilibrium solution concentrations, respectively. The 13-X and 4AXW are cesium-selective at 1% loading, but rapidly become sodium-selective as cesium loading progresses. Note that clinoptilolite tends to maintain a relatively high cesium selectivity at 50% cesium loading.

TABLE 4.2

ZEOLITE CESIUM MASS ACTION QUOTIENTS
IN A CESIUM-SODIUM SYSTEM AT 1 and 50% OF ZEOLITE CESIUM LOADING

Zeolite	1% Cesium Loading	50% Cesium Loading
4AXW	5.04	0.134
13-X	2.52	0.176
AW-300	126.3	10.1
AW-400	288.6	50.6
AW-500	202.1	39.0
Zeolon	170.5	19.0
Clinoptilolite	149.0	68.3
Erionite	246.6	44.7

The comparison of natural and synthetic zeolite species is of interest in the cesium-sodium system. Zeolon and AW-300 are both mordenites. Structural differences between the two mordenites include the absence of "stacking faults" in the Zeolon, resulting in an effective pore diameter of about 10 Å. The AW-300, however, has an effective pore diameter of about 4 Å. The effect of the structural differences on the cesium mass action coefficient can be seen in Table 4.2. Not only are the AW-300 1 and 50% cesium loading values lower than those of Zeolon, but the relative distance between the two values is greater for AW-300. However, AW-300 with its stacking faults is the better medium for the separation of cesium from potassium and rubidium.

Erionite and AW-400 also are the same zeolite species. Except for the slightly lower cesium mass action quotients of natural erionite, AW-400 and erionite values are comparable.

Mass action quotients for cesium generally decline as the size of the competing cation approaches that of cesium. Sodium, for example, furnishes less competition for cesium than does rubidium when present in equal concentrations.

Kinetics of Cesium Reactions with Some Inorganic Cation Exchange Media*(4.3) - L. L. Ames, Jr.

The kinetics of cesium exchange for sodium were studied in the film and particle diffusion region for several cation exchange materials, including an alumina-silica gel, Type A synthetic zeolite, clinoptilolite, phillipsite, erionite, and vermiculite. The "shallow bed" technique used to investigate cation exchange kinetics of organic resins was applied to the above inorganic exchange materials. Results for the effects of temperature, flow rate, cesium concentration, and competing sodium on film diffusion loading rates are given, as well as particle diffusion data. Cesium diffusion film thickness was computed by two methods with comparable results. Loading rates of inorganic cation exchangers can be predicted through use of fundamental kinetic data.

The kinetics of cesium exchange for sodium were studied in the film and particle diffusion regions for several cation exchange materials, including an alumina-silica gel, Type A synthetic zeolite, clinoptilolite, phillipsite, erionite, and vermiculite.

Table 4.3 gives the strontium particle diffusion data. With the exception of vermiculite, activation energies are quite low. Low activation energies suggest that a large portion of the diffusion of cesium within the particle takes place in a liquid phase.

---

* Not Supported by the Division of Biology and Medicine

TABLE 4.3

CESIUM PARTICLE DIFFUSION DATA

Exchanger	Temperature, C	B, sec^{-1}	D^i, cm^2/sec	Ea, kcal/mole
Phillipsite	31	0.02222	7.88×10^{-7}	
Phillipsite	45	0.02380	8.44×10^{-7}	1.1
Erionite	35	0.04666	1.65×10^{-6}	
Erionite	55	0.06001	2.13×10^{-6}	2.6
Type A	29	0.01777	6.30×10^{-7}	
Type A	52	0.02933	1.04×10^{-6}	4.3
Clinoptilolite	29	0.01095	3.88×10^{-7}	
Clinoptilolite	30	0.01435	5.09×10^{-7}	5.0
Gel	29	0.00710	2.52×10^{-7}	
Gel	50	0.01435	5.09×10^{-7}	6.5
Vermiculite	47	1.41×10^{-5}	5.3×10^{-10}	> 15

Influent Solution - 0.3N CsCl plus 1.0×10^{-8} N Cs^{134}
Influent pH - 6.0
Flow Rate - 12.8 $l/hr/cm^2$
Temperature - as indicated
Shallow Beds - 500 mg, 0.25 to 0.50 mm, sodium-based exchangers
B_i - loading rate, sec^{-1}
D^i - apparent particle diffusion coefficient, cm^2/sec

Film diffusion cesium loading results are given in Figure 4.4. These data represent results obtained by continuous monitoring of a small zeolite bed loading with a traced cesium solution.

The average diffusion film thickness, Δr, may be computed with an approximation developed primarily to describe organic resin kinetics.[4.4] To utilize Reichenberg's technique, the quantity "$d\varphi/dt$ (initial)" must be determined in the expression,

$$d\varphi/dt \text{ (initial)} = \frac{3D^1}{(r)(\Delta r)} [\text{cation}],$$

where D^1 = the liquid diffusion coefficient for the incoming cation in cm^2/sec

r = the particle radius in cm

[cation] = the concentration of the incoming cation

$d\Phi/dt$ (initial) = the initial slope of the loading curve in meq/ml/sec.

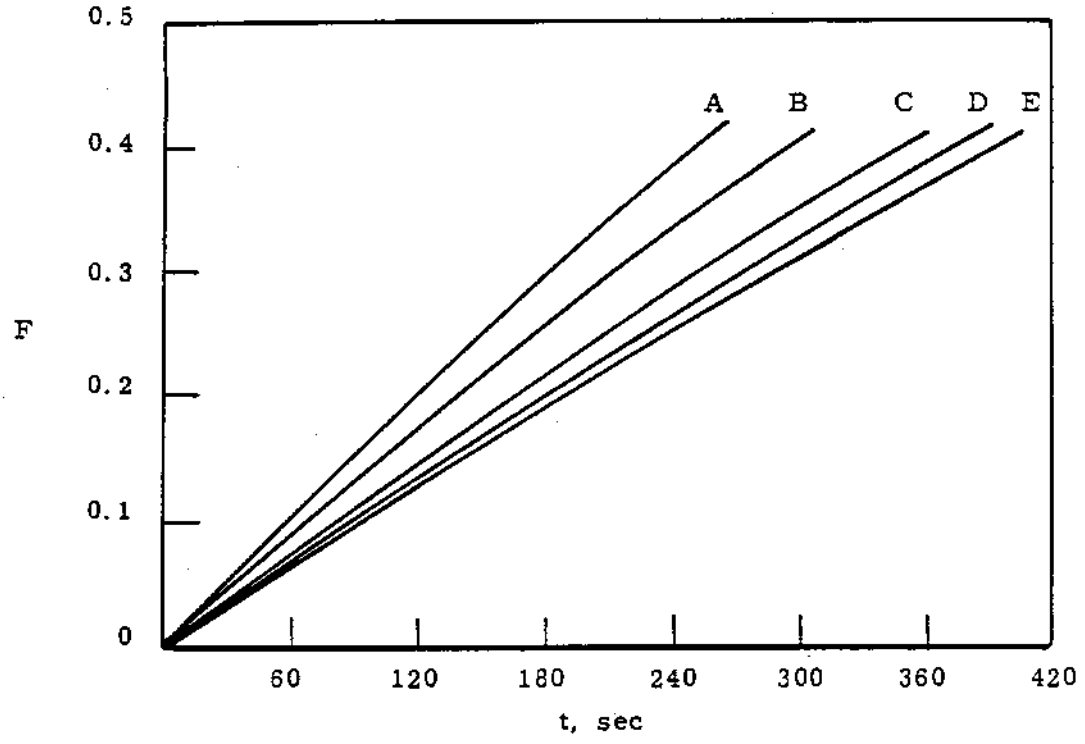

FIGURE 4.4

Curves of Cesium Loading Fraction Versus Time in the Film Diffusion Region. Experimental Conditions are Listed Below

Influent Solution	- 1×10^{-3} N CsCl + 1×10^{-8} N Cs^{134}
Influent pH	- 6.0
Temperature	- 25 C
Flow Rate	- 12.8 l/hr/cm^2
Shallow Beds	- 500 meq, 0.25 to 0.50 mm, sodium-based exchangers

Designation	Exchanger
a	Erionite
b	Phillipsite
c	Type A
d	Clinoptilolite
e	Gel

Determination of the initial curve slope is accomplished by replotting the original data to give bed exchange capacity in terms of meq/ml versus time. An example of this type of plot is given in Figure 4.5. Note that initial $d\varphi/dt$ values are the same. In this instance average film thickness for cesium diffusion was 13.3 μ. The film thickness was found tc change with both flow rate and temperature in addition to the variables in Reichenberg's expression.

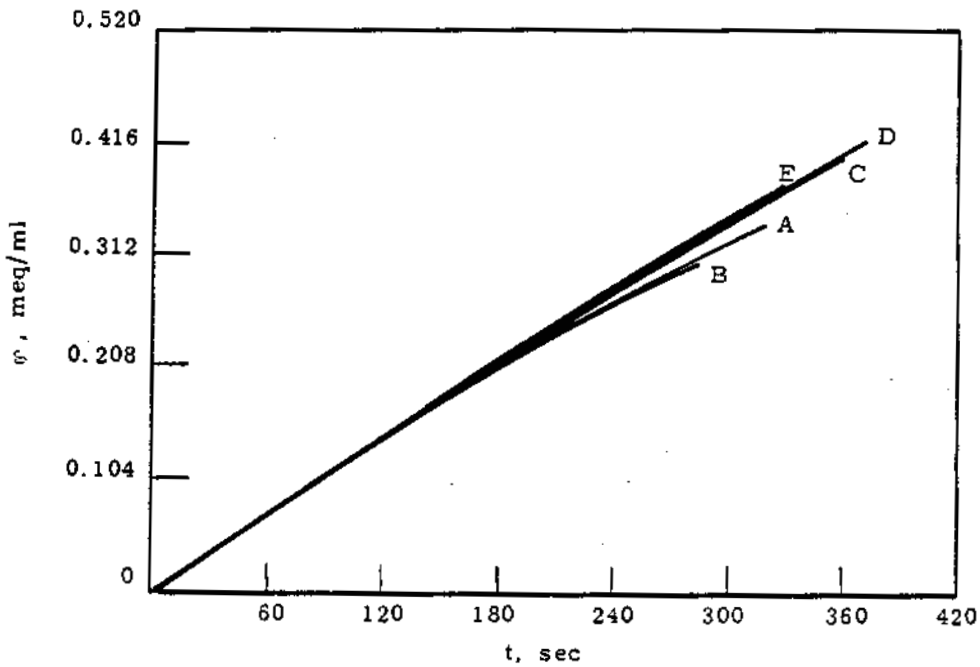

FIGURE 4.5

Curves of $\bar{\varphi}$ (cesium meq/ml of bed) Versus Time in the Film Diffusion Region. Cesium Capacities are with a 1.0×10^{-3} N CsCl Influent

Designation	Exchanger	Cesium Capacity, meq/g	Bed Density, g/ml	Cesium Capacity, meq/g
a	Erionite	1.7	0.41	0.70
b	Phillipsite	2.2	0.35	0.78
c	Type A	1.3	0.73	0.95
d	Clinoptilolite	1.4	0.75	1.04
e	Gel	1.5	0.77	1.16

Effect of Base Cation on the Cesium Kinetics of Clinoptilolite*(4.5)

L. L. Ames, Jr.

The cesium exchange kinetics of lithium-, sodium-, potassium-, hydrogen-, calcium-, and barium-based clinoptilolite samples were determined by a "shallow bed" in the film and particle diffusion regions. Results showed cesium exchange for lithium on the clinoptilolite to be the most rapid, and hydrogen exchange to be among the slowest reactions. The hydrated cation replacement series exhibited by clinoptilolite is the probable cause of the resulting cesium exchange kinetics.

The cesium exchange kinetics of lithium-, sodium-, potassium-, hydrogen-, calcium-, and barium-based clinoptilolite samples were determined by the continuous recording of cesium loading on small clinoptilolite beds. Results are shown in Figure 4.6.

As shown previously, the cation exchange kinetics of clinoptilolite do not influence its replacement series. Clinoptilolite is characterized by a strong, hydrated replacement series up to approximately 325 C, where a substantial portion of internal or zeolitic water is lost. The cesium loading rates of the alkali-metal, cation-based series and alkaline-earth metal, cation-based series shown in Figure 4.6 seemed to contradict the assumption that a hydrated replacement series prevailed. Lithium cations, as indicated by liquid diffusion coefficients, should migrate the slowest and hydrogen ions the fastest. From Figure 4.6, the apparent opposite condition of faster lithium cation migration is true.

An explanation can be found by assuming a stronger interaction between the lithium cation and internal water, resulting in a greater distance between anionic site and cation than with the relatively nonhydrated, low field strength cesium cation. Lithium, being least tightly bound to its anionic site, is the cation most easily and speedily replaced by cesium.

---

* Not Supported by the Division of Biology and Medicine

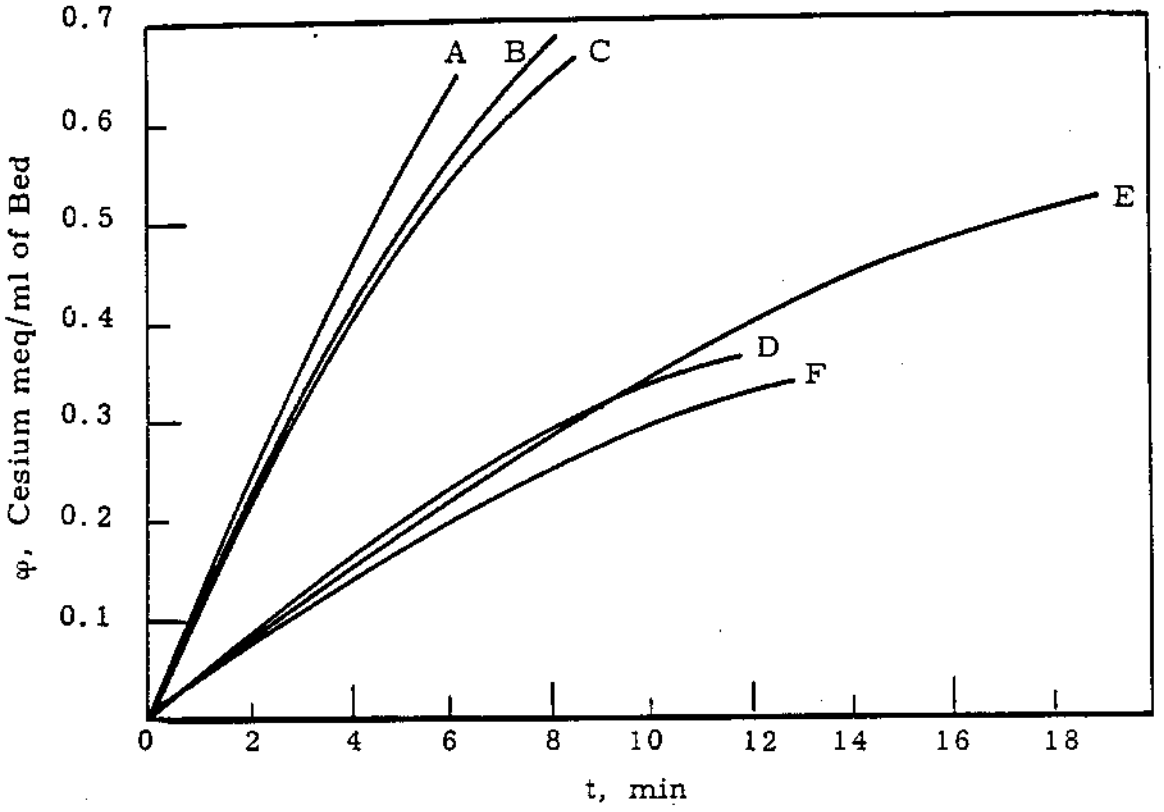

FIGURE 4.6

Curves of meq of Cesium/ml of Clinoptilolite Bed Versus Time

Influent Solution - 1.0×10^{-3} N CsCl plus 1.0×10^{-8} N Cs^{134}
Influent pH - 6.0
Temperature - 41 C
Flow Rate - 15.4 l/cm^2/hr
Shallow Beds - 50 mg, 0.25 to 0.50 mm clinoptilolite

Curve Designation	Cation on Clinoptilolite
a	Li^+
b	Na^+
c	K^+
d	H^+
e	Ca^{+2}
f	Ba^{+2}

Loading and Elution Characteristics of Some Natural and Synthetic Zeolites [4.6]* - L. L. Ames, Jr.

The cation exchange characteristics of several commercially available zeolites were evaluated. Equilibrium loading characteristics and exchange capacities were determined experimentally in the binary systems cesium-lithium, cesium-sodium, cesium-potassium, cesium-rubidium, cesium-hydrogen, cesium-ammonium, strontium-magnesium, strontium-calcium, strontium-barium, and strontium-hydrogen for the zeolites Linde AW-300, AW-400, AW-500, 4AXW, 13-X, Norton Zeolon, and clinoptilolite. Several column 50% loading capacities were determined to randomly test the validity of the above curves to predict column capacities.

Several columns loaded with known amounts of cesium and strontium radioisotopes were heated to 600 C for 24 hr to simulate a zeolite packaging dehydration cycle. Losses of cesium and strontium activity during the 24-hr period were determined. Elution of the remaining activity on the columns was accomplished with various eluting agents including dilute HNO_3, NH_4NO_3, $CaCl_2$ and $La(NO_3)_3$, and elution curves calculated for Linde AW-500, 13-X, 4A, Norton Zeolon, and Decalso.

The cation exchange characteristics of several commercially available zeolites were evaluated. Table 4.4 gives some of the pertinent properties of the zeolites studied for the sodium form at 25 C.

TABLE 4.4

ZEOLITE PROPERTIES

Zeolite	SiO_2/Al_2O_3	% Binder	Structural Type	Effective Pore Diameter, A
Linde 4AXW	2	8	(No natural counterpart)	4
Linde 4A	2	20	(No natural counterpart)	4
Linde 13X	2.8	20	Faujasite	7.4
Linde AW-300	9-10	20	Mordenite	4
Linde AW-400	6-7	20	Erionite	4
Linde AW-500	4-5	20	Chabazite	4-5
Norton Zeolon	10	Unknown	Mordenite	9-10
Clinoptilolite	8-10	5-15	Clinoptilolite	> 4

* Supported in part by the Division of Biology and Medicine

Figures 4.7 and 4.8 show typical equilibrium data for alkali metal cation systems with clinoptilolite and some synthetic zeolites.

Table 4.5 gives the capacities of the zeolites used in this study.

TABLE 4.5

ZEOLITE CATION EXCHANGE CAPACITIES

Zeolite	Capacity, meq/g
Linde 4AXW	3.9
Linde 4A	3.5
Linde 13X	3.6
Linde AW-500	2.2
Linde AW-400	2.0
Linde AW-300	1.6
Zeolon	1.9
Clinoptilolite	1.7

Table 4.6 compares predicted zeolite loading computed from the equilibrium and capacity data with actual zeolite loading values obtained in column experiments with comparable flow rates at 25 C. Note that the predicted load of Type A in 1/16-in. pellets does not agree with the actual loading capacity. Equilibrium was not attained between contacting solution and zeolite under the experimental conditions. Only under the condition of equilibrium between zeolite and solution passing through the column can the equilibrium data be used to predict column loads.

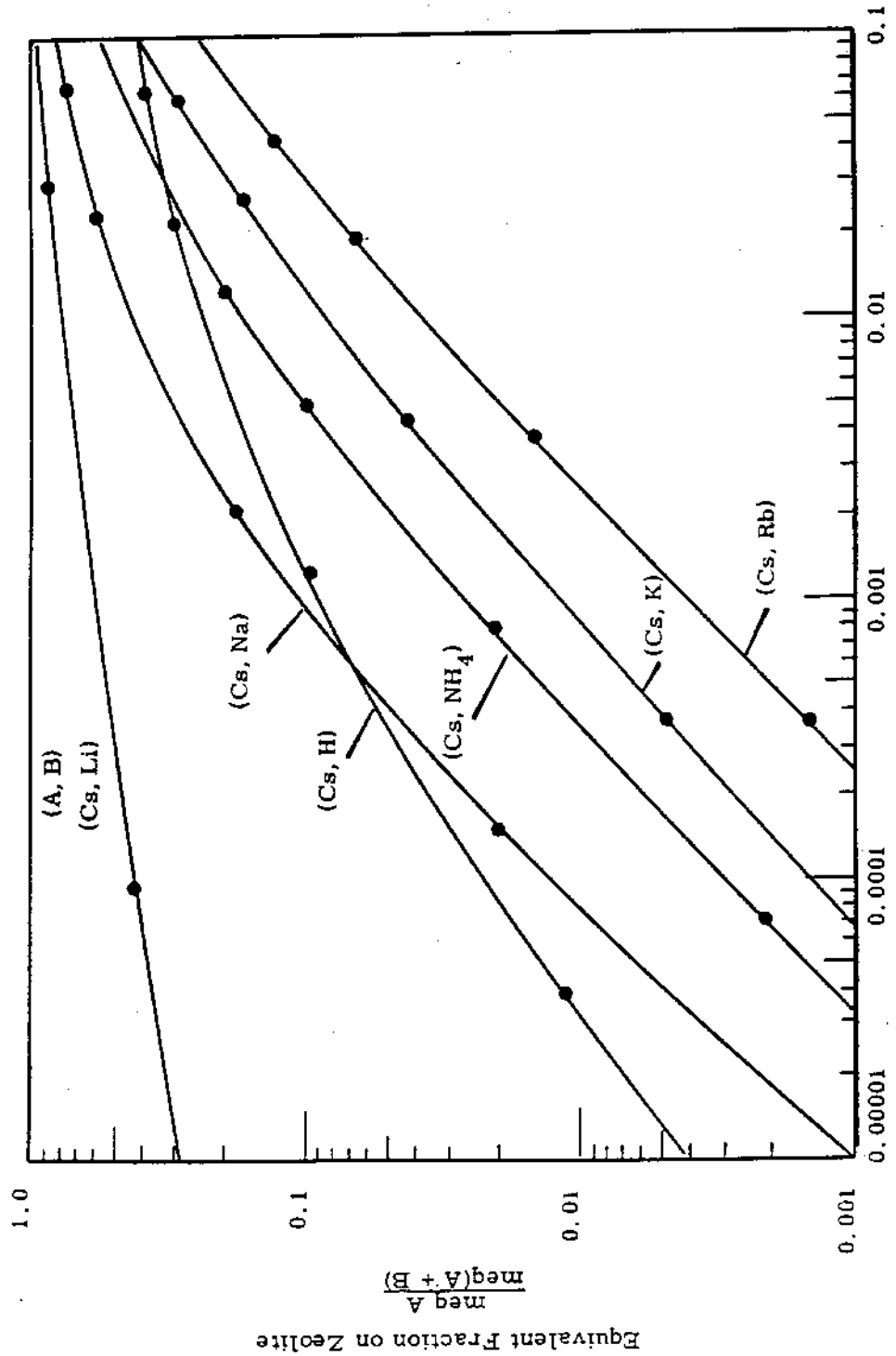

FIGURE 4.7

The Effect of Univalent Cations on the Equilibrium Cesium Loading of Clinoptilolite

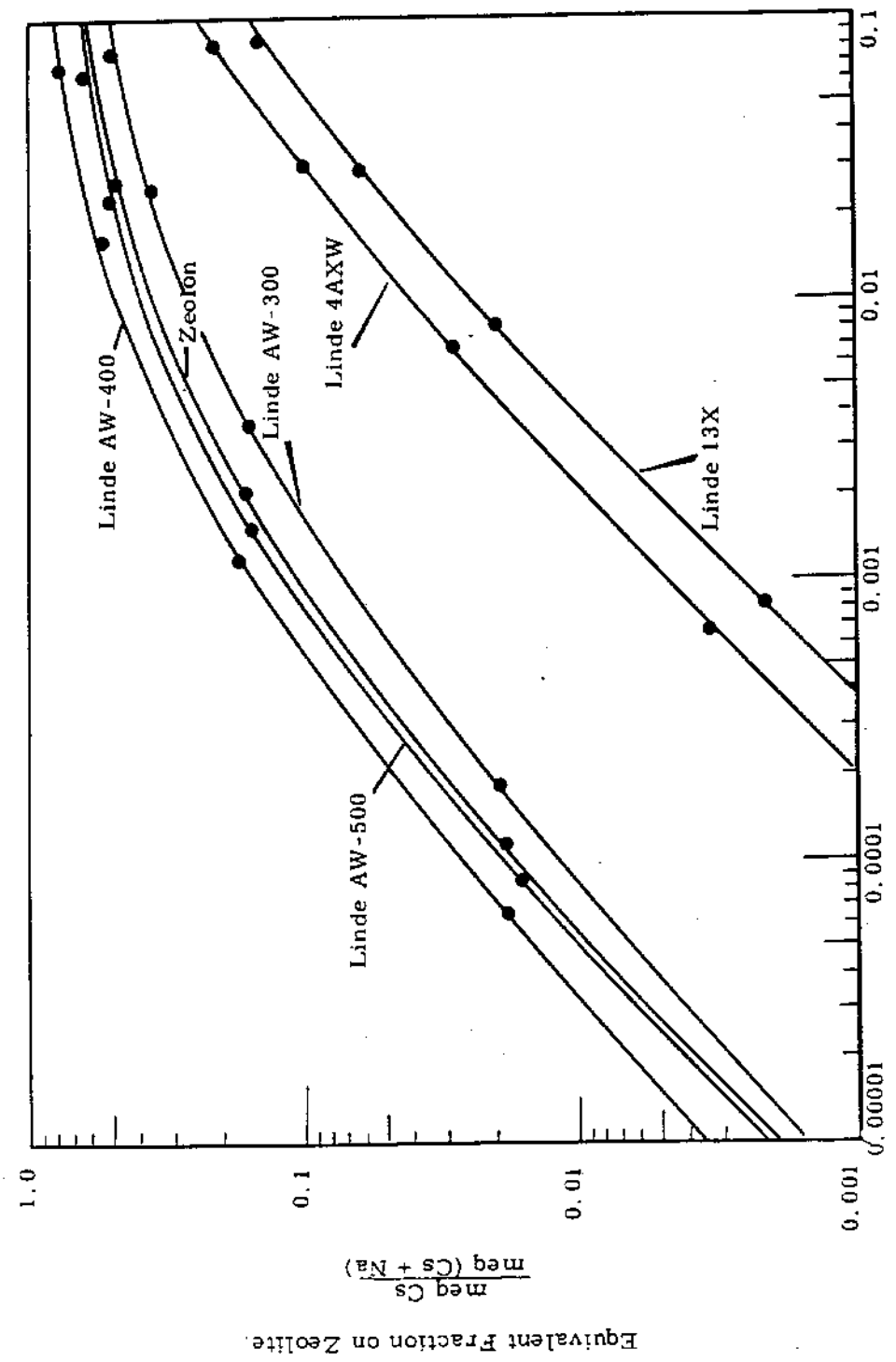

FIGURE 4.8

The Effect of Sdoium on the Equilibrium Cesium Loading of Linde 4AXW, 13X, AW-300, AW-400, AW-500 and Norton Zeolon

TABLE 4.6

PREDICTED AND ACTUAL COLUMN CAPACITIES

Zeolite	Influent Solution	Column wt/g	Grain Size Range, mm	Predicted Load, meq/g	Actual Load, meq/g
Linde 13X	0.002N Sr^{++} + Sr^{85} + 0.01N Na^{+}	5.5	0.4-0.7	3.4 (Sr)	3.2 (Sr)
Linde 4A	0.002N Sr^{++} + Sr^{85} + 0.01N Na^{+}	5.5	0.4-0-7	3.5 (Sr)	3.4 (Sr)
Linde 4A	0.07 Sr^{++} + Sr^{85} + 0.1N Na^{+}	5.5	0.4-0.7	3.5 (Sr)	3.5 (Sr)
Linde 4A	0.07N Sr^{++} + Sr^{85} + 0.1N Na^{+}	50	1/16 in. Pellets	3.5 (Sr)	1.8 (Sr, 65 C)
Clinoptilolite	0.01N Cs^{+} + Cs^{134} + 1.0N Na^{+}	50	0.25-1.00	0.75 (Cs)	0.73 (Cs)
Clinoptilolite	0.01N Cs^{+} + Cs^{134} + 0.5N Na^{+}	50	0.25-1.00	1.02 (Cs)	1.01 (Cs)
Linde AW-500	0.001N Cs^{+} + Cs^{134} + 1.0N NH_4	50	1/16 in. Pellets	0.037 (Cs)	0.039 (Cs)
Linde 4AXW	0.001N Cs^{+} Cs^{134} + 1.0N NH_4	50	1/16 in. Pellets	0.011 (Cs)	0.011 (Cs)
Linde AW-500	0.001N Cs^{+} + Cs^{134} + 1.0N K^{+}	50	1/16 in. Pellets	0.040 (Cs)	0.050 (Cs)
Clinoptilolite	0.01N Cs^{+} + Cs^{134} + 1.0N K^{+}	50	0.25-1.00	0.143 (Cs)	0.145 (Cs)
Linde AW-400	0.001N Cs^{+} + Cs^{134} + 1.1N Na^{+}	50	1/16 in. Pellets	0.240 (Cs)	0.241 (Cs)

Figure 4.9 shows that no kinetic problems with cesium loading on 13X should be encountered. Possible strontium loading problems with larger grain sizes of 13X and 4A are indicated by loading kinetics as seen in Figure 4.10. A compromise between influent flow rate, temperature, and zeolite grain size may be necessary to attain full loading as indicated by the equilibrium results. Changing only the zeolite grain size, for example, from 1.6 mm in diameter (1/16-in. pellets) to a size range of 0.4 to 0.7 mm is sufficient to attain full loading with a steep breakthrough curve.

Figure 4.11 indicates that with a reasonable flow rate, clinoptilolite can be used to remove and concentrate cesium radioisotopes from projected 1965, formaldehyde-treated, Purex waste.

A summary of cesium or strontium losses during heating to 600 C for 2 hr and the elution results are given in Table 4.7. All elutions were at room temperature. The amount of cesium or strontium lost during heating is expressed as a percent of the total load on the zeolite. A value of 0.0 indicates that the counting rates of the scrubbers and filter were at background levels with 60 min counts. It is possible that part of the radioactivity released during heating represents loading solution present due to incomplete washing of the zeolite column.

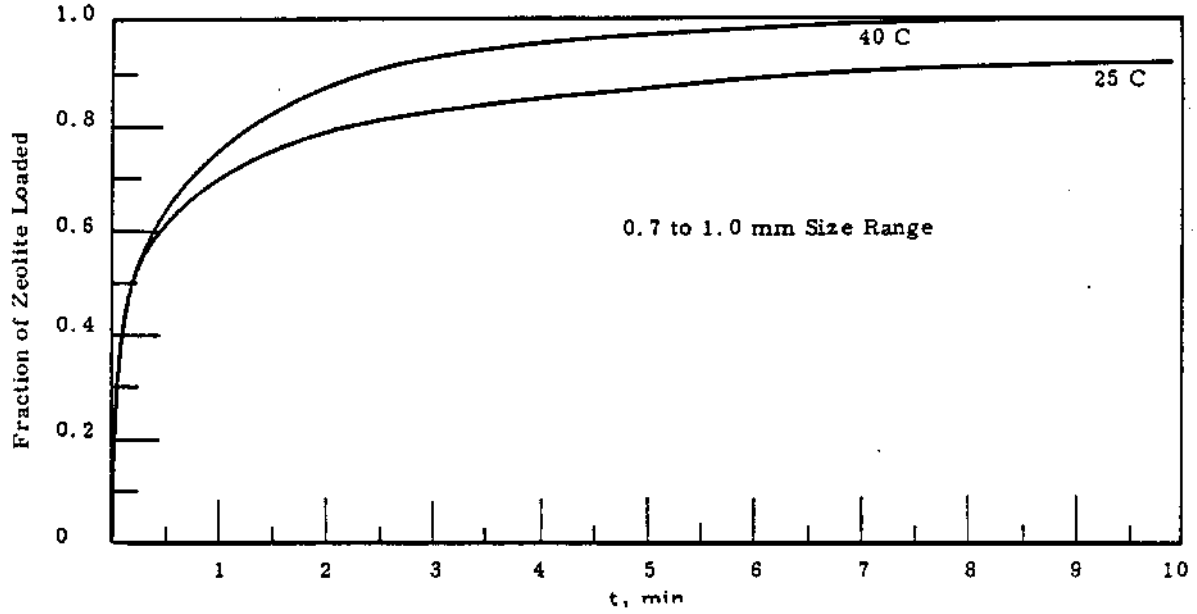

FIGURE 4.9

Cesium Loading on Linde 13X Versus Time
from a 0.1N CsCl Solution

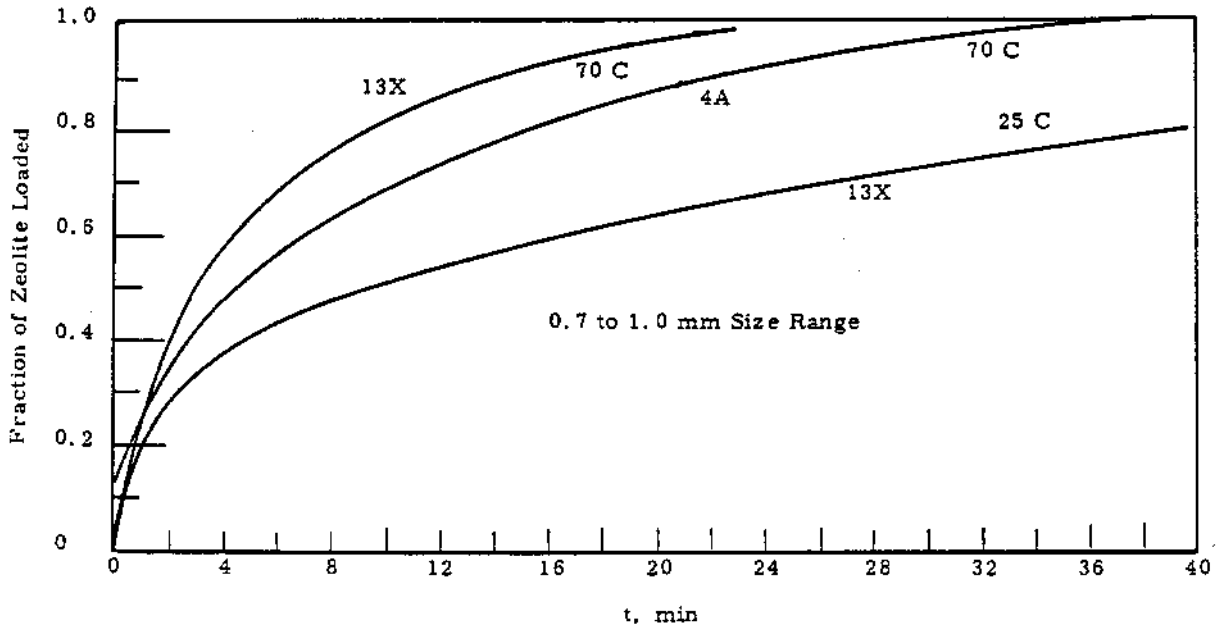

FIGURE 4.10

Strontium Loading on Linde 13X and 4A Versus Time
from a 0.1N $SrCl_2$ Solution

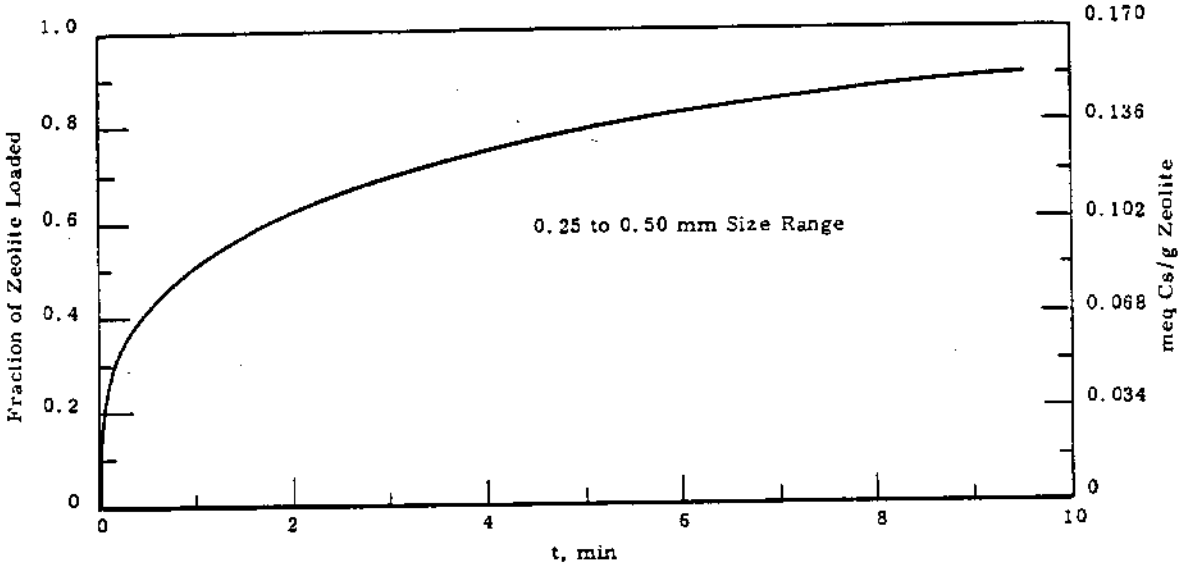

FIGURE 4.11

Cesium Loading on Clinoptilolite Versus Time
from a Simulated 1965, Formaldehyde-Treated, Purex Waste

TABLE 4.7

EFFECT OF 600 C HEAT ON LOSS AND ELUTION
OF RADIONUCLIDES FROM ZEOLITES

Zeolite	Percent Loss Static Conditions	Eluting Agent	Percent Eluted	Cation Eluted
Clinoptilolite	0.09	2N NH_4NO_3	96.6	Cs
Linde AW-500	0.0	2N NH_4NO_3	86.00	Cs
Linde AW-500	0.0	1N HNO_3	90.0	Cs
Linde 13X	0.0	2N NH_4NO_3	62.0	Cs
Linde 13X	0.0	0.5N HNO_3	97.0	Cs
Linde 13X	0.0	2N HNO_3	99.0	Cs
Norton Zeolon	--	2N NH_4NO_3	99.0	Cs
Decalso	0.016	2N NH_4NO_3	38.0	Cs
Declaso	0.0	6N $La(NO_3)_3$	22.0	Cs
Linde 4A	0.01	1N HNO_3	99.0	Sr

Soil Physics

In-Place Permeability Determination in Heterogeneous Soils - R. W. Nelson

A rather extended sequence of analysis was necessary in overcoming the computational problems associated with an in-place method of permeability determination. The sequence requires an analytical method for defining ground water potential variations in three dimensions and the derivation of more general stream functions than those currently available from classical hydrodynamics. The planned sequence is outlined and the progress to date is discussed.

The accurate duplication of ground water flow by electrical simulation requires realistic in-place measurement of the permeability distribution throughout the region. Moderate progress has been made in providing an accurate, economical method for obtaining such measurements. However, more work must be done before a finished and carefully tested set of methods is available.

After the variables of the measurement problem were defined, a basic theory was needed which used these variables in the form of existing and obtainable field data to determine the permeability distribution throughout the saturated zone. Such a theory was developed and experimentally checked to validate its application.[4.7, 4.8] The derivation of the basic theory is shown as Step 1 in Figure 4.12. This figure also shows the sequence of steps underway and leading toward the goal of defining the permeabilities (hence resistors) needed for construction of an electrical analog. In brief, the basic theory states that if ground water potentials in three dimensions are known through the region of interest and permeabilities are known along one irregular surface which intersects every stream tube comprising the flow system, than a unique solution of the permeability everywhere in the system can be obtained.

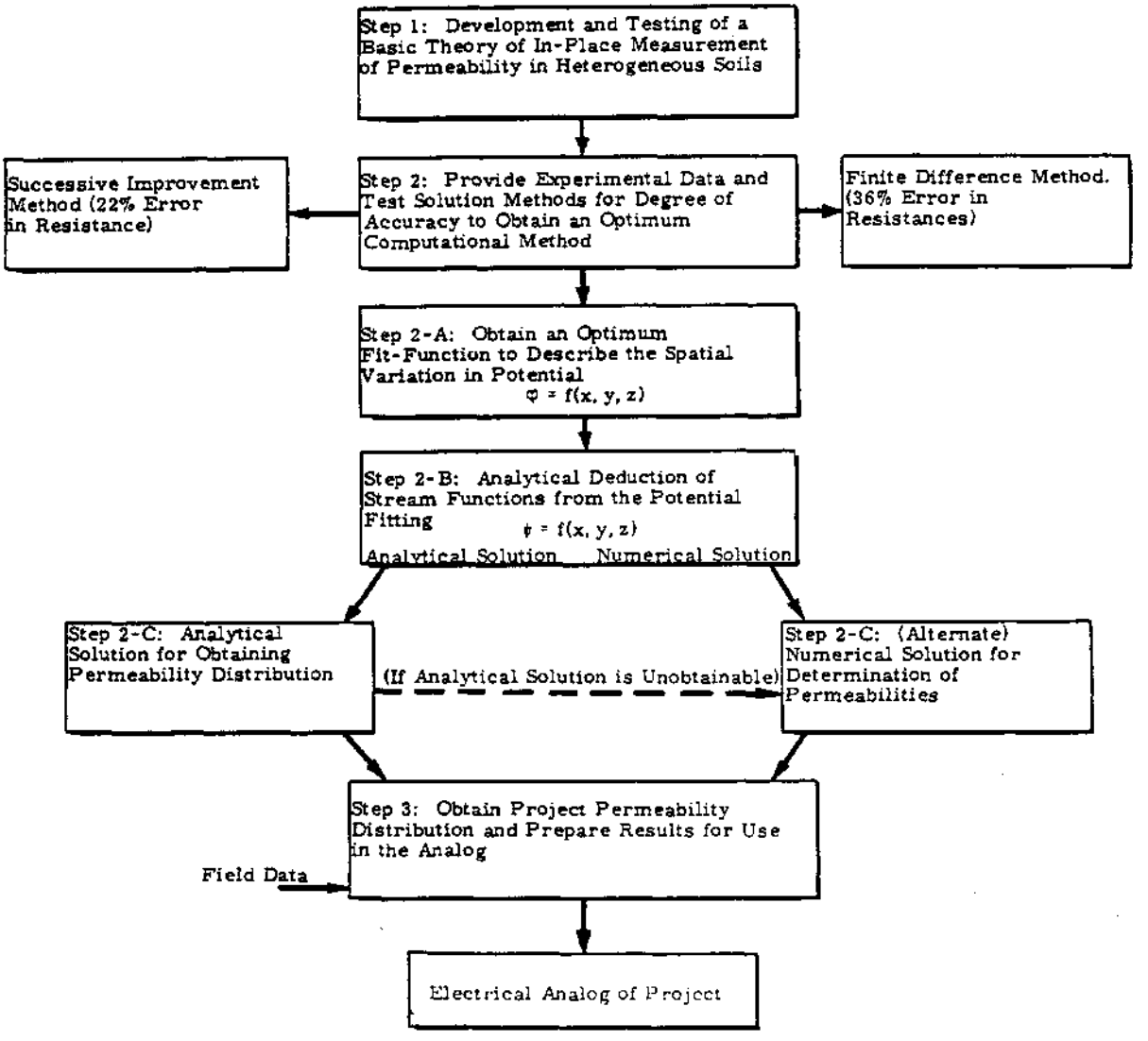

FIGURE 4.12

In-Place Permeability Determination in Heterogenous Soils

Step 2 is concerned with providing reliable experimental data to evaluate the accuracy of proposed solution methods. Experimental data obtained from sheet conductance paper measurements were found to have a potential measurement accuracy of 1% at the 99% confidence level and a resistance measurement error of 6% at the 95% confidence level. This level of experimental accuracy is desirable to permit careful examination of various solution and computational schemes.

Two computational schemes have been tested. The finite difference method was found to result in a 36% error in computed resistance. A later computational method [4.9] which utilized successive improvement of an initial permeability estimate yielded an average of 22% error in calculated resistance from the conductance paper experimental values. This error is considered excessive if results with a reasonable degree of accuracy are to be obtained from the analog.

Much of the problem is concerned with the fact that the measured potentials from wells are known as tabular data rather than as an analytical expression or mathematical function. Therefore, a method was sought for the conversion of data obtained from an irregular network (wells) to a mathematical expression. The anticipated results in this case is an equation describing the potential as a function of location, $\varphi = f(x, y, z)$, which is an intermediate point (Step 2-A) in obtaining permeabilities as a function of location.

Step 2-B concerns obtaining an analytical deduction of the stream function from the potential fitting. The stream function, ψ, defines flow paths or streamlines as functions of spatial location. The study involved careful examination of the stream function for three dimensions from inviscid hydrodynamics[4.10] to determine its validity for heterogeneous media. The existing functions were found inadequate, so appropriate generalized stream functions were obtained. The derivation of the equations describing the new stream functions constitutes a major part of Step 2-B; however, work is still

under way on methods for obtaining solutions of the stream function equations from the potential function. It is preferable to obtain an analytical solution for the stream function; however, if this is not possible, a numerical scheme will be attempted to deduce stream surfaces from the potential function.

The accomplishment of Step 2-C will result in an analytical solution method to determine the permeability distribution from the stream and potential functions. Here again an analytical solution is desirable, but if it is not obtainable, an alternate course is to get approximate permeability distribution from the stream and potential functions through numerical methods (Step 2-C alternate). Also, if it is necessary to use the numerical scheme for deducing stream surfaces (Step 2-B), then the Step 2-C alternate course will be pursued. Steps 2-A through 2-C yield expressions and methods which are essential not only to determine the permeability for analog construction but also to solve problems later using analog output data.

Step 3 uses the computational methods developed and the field data to calculate project permeabilities. These will be converted to equivalent resistance for use in the electrical analog.

Stream Functions for Steady-State Flow in Heterogeneous Porous Media - R. W. Nelson

> The analytical evaluation of flow through porous media systems requires mathematical tools to determine everywhere the flux distribution, velocity definition, and flow paths. Earlier work by others (4.10) on stream and path function provided the expressions needed to describe three-dimensional flow in homogeneous porous media. More recent work at Hanford (4.11) resulted in the development of functions for describing three-dimensional flow in heterogeneous porous media. The immediate application of these expressions is related to obtaining input data and evaluating output information from a three-dimensional groundwater analog.

Stream functions are a class of analytical tools which fit particularly well into the scheme for analyzing the flow of fluids in porous media since they provide a means for determining the flux distribution and flow paths.

Stream functions and their generalization for transient flow, path functions have been available in classical hydrodynamics for axisymmetrical and two-dimensional flow cases for many years. For the latter case, the classical theory of complex variables provides a singularly elegant stream function analysis.

After sketching the historical development of stream and path functions, Yih[4.10] more recently summarized general three-dimensional expressions for a variety of conditions found in inviscid hydrodynamics. These expressions are also valid for describing flow in homogeneous porous media, since the equations which describe this flow system are identical to those of inviscid hydrodynamics. In an attempt to extend this work further, two questions immediately arise: (1) do general stream functions exist for describing three-dimensionsal flow in heterogeneous porous media and (2) if so, do general relationships exist which include the useful properties of velocity definition, path description, and flux determination which are found in the special case of homogeneous media. If the assumption is made that the media are heterogeneous but the flow is nondiffusive, then the answer to both questions is yes, although the derived expressions are more complex than the traditional equations. The immediate application of these equations is in conjunction with a computional scheme for in situ permeability measurements in heterogeneous media.

The properties desired in the stream functions are:

(1) specification of the trajectories or paths of individual fluid elements

(2) determination of the macroscopic velocity components

(3) specification of the distribution of fluid flux in the flow system.

These are the traditional properties for stream functions in homogeneous media. Care must be taken to insure inclusion of all three properties for flow in heterogeneous media.

The steps in getting the desired functions follow, in general, the order given for the desirable properties of stream functions. The equations for a streamline are written and appropriate integrals are given to satisfy these equations. The definition of velocity components is obtained through utilizing

the streamline integrals, Darcy's Law, and the equation of continuity. Finally, the distribution of flux is found through forming appropriate integrals of the results already obtained. The derivation is presented in detail elsewhere;[4.11] only the results are summarized in this discussion.

The basic partial differential equation defining the stream function is

$$K \operatorname{grad}\varphi \cdot \operatorname{grad}\psi = 0, \tag{1}$$

where

K is the hydraulic conductivity or permeability

φ is the piezometric head, hydraulic potential, or potential function

ψ is the stream function.

The stream function, ψ, is judiciously expressed in terms of the adjunct stream function pair,

$$f(x, y, z) = a, \tag{2}$$

$$g(x, y, z) = b, \tag{3}$$

where x, y, and z are Cartesian space coordinates, and a and b are parameters. Equations 2 and 3 must satisfy the system of equations,

$$\frac{dx}{\frac{\partial \varphi}{\partial x}} = \frac{dy}{\frac{\partial \varphi}{\partial y}} = \frac{dz}{\frac{\partial \varphi}{\partial z}}. \tag{4}$$

Since Equation 4 is the expression for a streamline, a specific flow path is defined when both f and g are set equal to constants.

The ground water velocity components can be expressed in terms of the adjunct pair as

$$\underline{V} = \frac{\alpha^2 [F(T)]}{\frac{\partial f}{\partial} \frac{\partial g}{}} \left[(\operatorname{grad} f) \cdot (\operatorname{grad} g) \right], \tag{5}$$

where

$\underline{V}$ is the velocity vector

F is the flux distribution across some surface

$\Gamma(x, y, z)$ is a surface intercepting all the streamtubes of interest.

The velocity equation can be used to determine the flux distribution, Q (x, y, z), throughout the flow system:

$$Q = \int_{f_1}^{f_2} \int_{g_1}^{g_2} \frac{\partial^2 [F(\Gamma)]}{\partial f \quad \partial g} \, dg \quad df \, . \tag{6}$$

These results reduce to the classical functions for homogeneous porous media. In this case the second partial of F becomes the constant permeability, K, and can be taken outside the integral signs in Equation 6 making the result integrable directly. Further reduction to classical two-dimensional flow in homogeneous soils results by letting f equal the two-dimensional stream function, ψ, and setting g equal to a minus z.

Electrical Analog Simulation of the Hanford Ground Water Flow System - R. W. Nelson

Electrical analog simulation is a practical way to quantitatively analyze a large, complex, saturated ground water flow system such as that beneath the Hanford Project. The evaluation of output data from the Hanford analog is expected to yield accurate descriptions of the rates, directions, and quantities of flow. Also, this analytical tool will permit determination of the effects of on-plant and off-plant hydrologic environmental changes on the local ground water flow regime. The requirements for a valid analog are discussed and the steps leading toward the construction and operation of the Hanford analog are outlined.

Knowledge of the patterns and rates of ground water movement has application in a variety of practical situations, such as land drainage, utilization and replenishment of aquifers for water supply, and disposal of industrial effluents. In the disposal of low- and intermediate-level radioactive wastes, the rate of movement is particularly important.

Among the first requirements in predicting the movement of wastes is the need to obtain solutions for the expected fluid movements in the heterogeneous soils and other complex conditions of actual field situations. A practical way to deal with very complex saturated flow systems (heterogeneous soil and irregular boundaries) is through electrical analog simulation. Such methods, which use the similarity between saturated ground water and electrical current flow, are capable of mastering extreme complexities in both geometrical shape and conductance variation.

Electrical analog simulation of saturated flow of fluids in soils is not a recent innovation. Such techniques have been used, usually in two-dimensions, almost since the identities in Ohm's Law and Darcy's Law were recognized. Laws governing heat transfer and several other physical systems are also analogous. The electrical system for general use, is illustrated in Figure 4.13. The voltage at each junction corresponds to the liquid head at that point in the soil. Each network resistor represents the effective soil, reciprocal permeability of the discrete soil volume occupying that position.

The more meaningful Hanford Project analog network is shown schematically in Figure 4.14. The resistor boundaries are seen in the figure with each layer of resistors conforming analogously to the shape of the boundaries. The lower resistance boundary and part of the vertical boundaries correspond to the configuration of the impermeable basalt bedrock. The water table forms the upper boundary of resistance.

The accurate duplication of ground water flow by electrical simulation requires that the system shall yield a unique solution; that is, only one flow pattern is possible when all of the required variables are defined. The variables in this case are:

(1) the spatial permeability distribution over the project $\dot{K}$ (x, y, z)
(2) the boundary conditions in the potential
(3) the spatial potential distribution over the project φ (x. y. z).

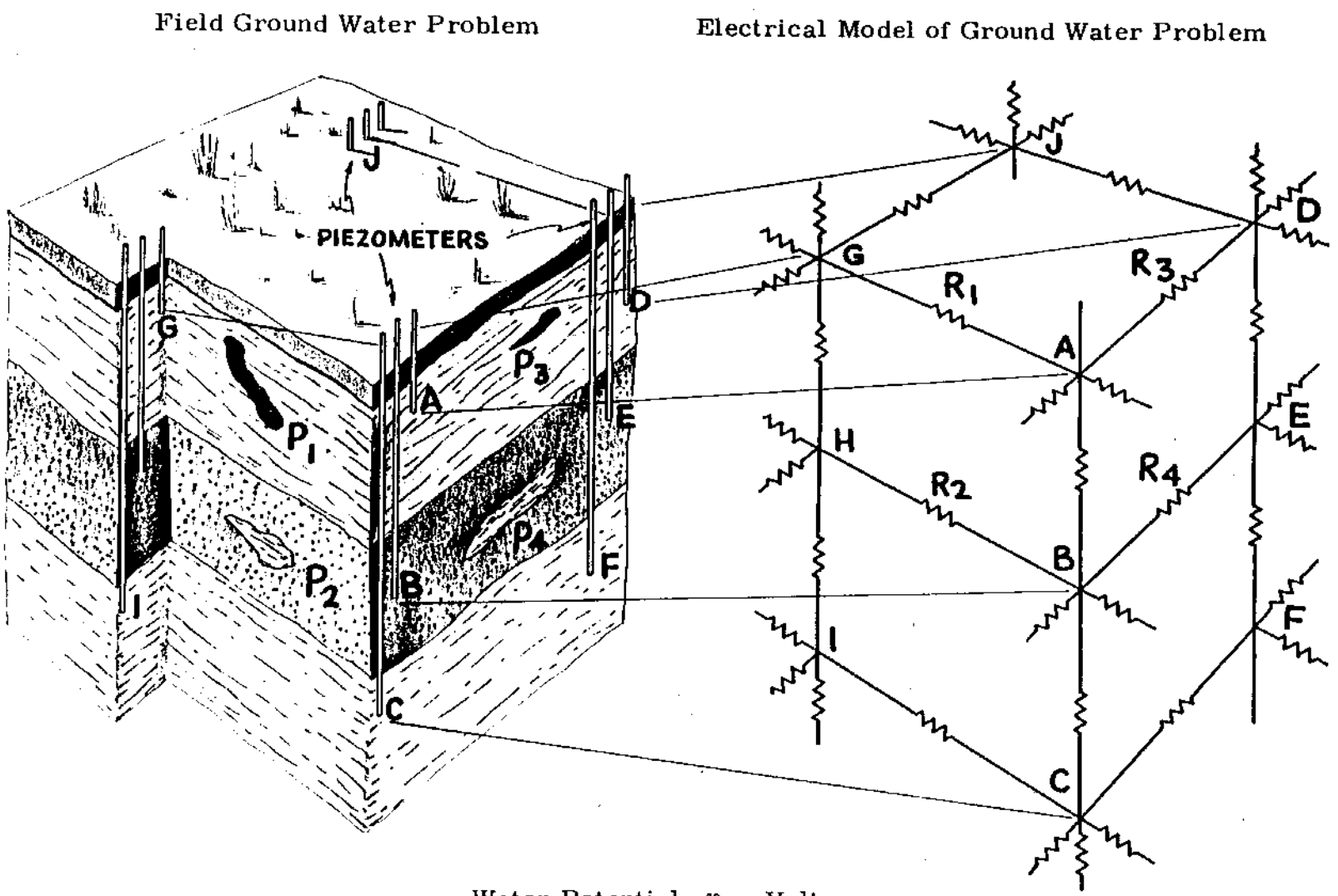

Water Potential, $\varphi \approx$ Voltage

Permeability, P, $\approx \frac{1}{\text{Resistance, R}}$

Flow Rate, Q $\approx$ Current, I

FIGURE 4.13

Schematic of Electrical Analog of Ground Water Flow

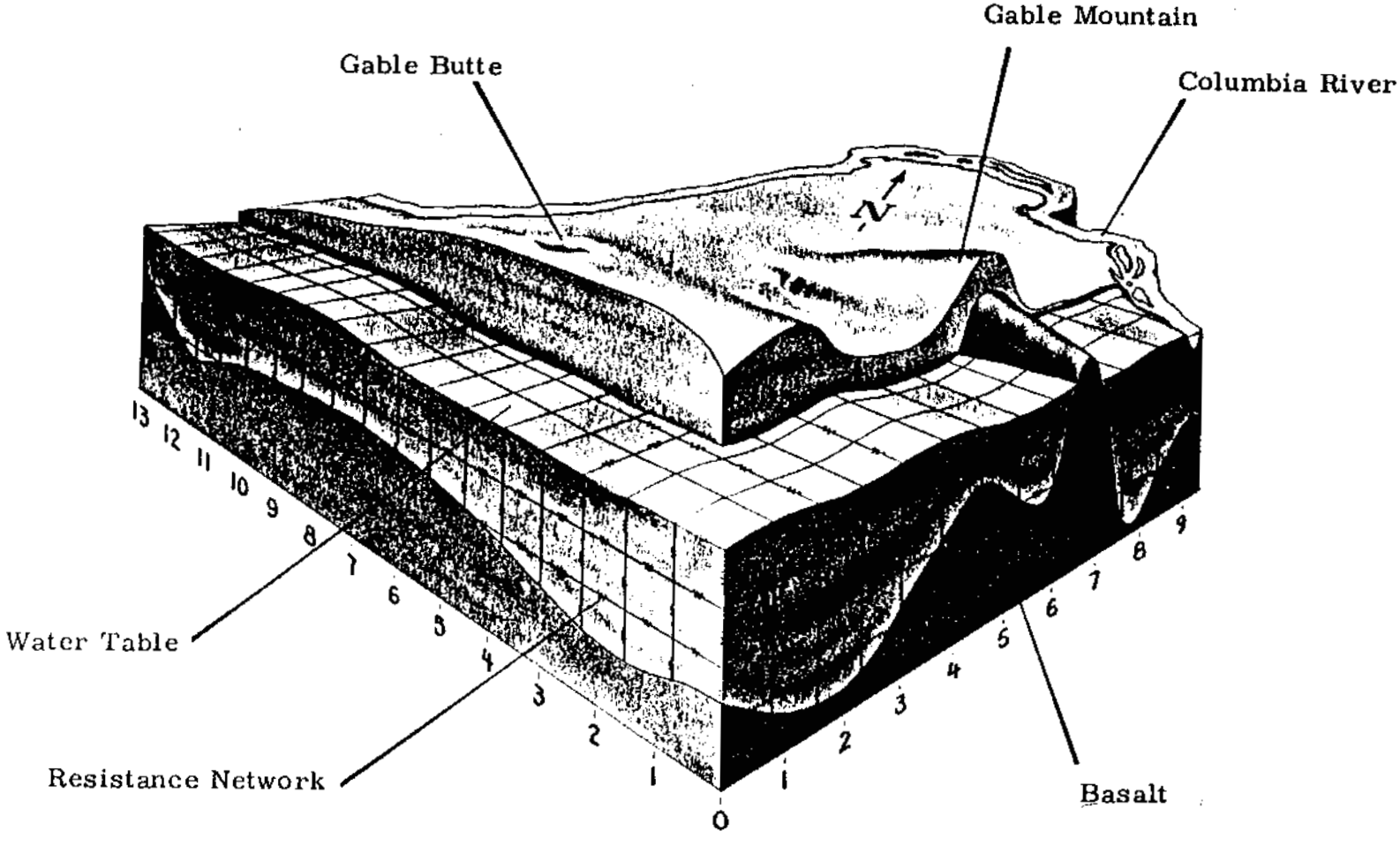

FIGURE 4.14
Electrical Analog of Ground Water Movement

A carefully formulated mathematical treatment assures that these three items are the only pertinent variables, although all are functions of the spatial location (x, y, z). If any two of the three variables are known, then the third is uniquely determined. Therefore, if the permeability distribution (Item 1) over the Hanford Project is known and the boundary conditions (Item 2) are available, then with the analog the potential distribution (Item 3) can be found through electrical measurement and conversion to the soil water potential. The purpose of the analog is to provide the potential distribution once the permeabilities and boundary conditions are known.(4.12, 4.13)

The subject of analog boundary conditions is worthy of discussion. Boundary conditions are the values of potential along some physical surface bounding the region of interest. In other words, a boundary condition includes two things: (1) the geometrical shape of some surface bounding part of the region of interest, and (2) the ground water potential condition along that geometrical surface. The geometrical configuration of the basalt beneath and in the hills west of the project is a realistic boundary condition since there is essentially no flow normal to this surface. The potential or water level of the Columbia River is also a boundary. Similarly, the water table surface is a common upper boundary which is often called a "free surface". This more difficult boundary is not known in shape a priori but is found iteratively in the process of solution. The imposed condition here is that the potential on the water table surface must equal the elevation of the surface.

Before being able to place boundary conditions representing specific plant problems on the analog, the permeability distribution (Item 1) must be known to specify the resistance values in the electrical analog. Herein lies the deterrent to the use of simulation techniques—the inability to measure in-place the permeability of heterogeneous sediments. The major effort of the past and continuing research program is to obtain realistic and economic

determinations of the spatial variations in permeability. This same problem—accurate in-place measurement of permeability—is one of the major challenges faced by scientific hydrology researchers everywhere.

Moderate progress has been made through Hanford's efforts toward providing an accurate, economical method for permeability determinations. Although there is work remaining to be done before a finished and carefully tested set of measurement methods is available, work has progressed to the extent that electrical analog equipment is being assembled for an initial 600-node model to be later expanded to 12,000 nodes.

Effects of Partially Saturated Flow Parameters on Infiltration Rate - A. E. Reisenauer

The basis for analyzing a variety of ground disposal flow problems is provided by a mathematical development describing steady-state Darcian transport of fluids in heterogeneous, partially-saturated, porous media. Solution of a group of related flow systems by computer methods permitted evaluation of the relative effects of depth to ground water, soil permeability, and heterogeneity on liquid infiltration rate and mositure distribution patterns. All three parameters were found to exert varying degrees of influence on these flow system characteristics.

Steady-state, partially-saturated flow occurs in many waste disposal systems. This is especially the case at Hanford where the water table is several hundred feet below ground surface.[4.14, 4.15] The solutions to practical flow systems of this type are now obtainable through use of the mathematical formulations and Hanford-developed computer program pertaining to steady, partially-saturated flow in heterogeneous media.[4.16, 4.17, 4.18] The computer program was applied to solve several typical and related flow system cases to demonstrate the utility of this approach.[4.19]

Flow parameters were studied for the case of a trench or canal 15 ft wide and 5 ft deep. The trench has a trapezoidal cross section and a 1.1 slope on the sides. The effects of depth to ground water on infiltration (seepage rate) from the trench was examined by solving four flow systems in which the distance from the water level to the regional ground-water table was established as 9, 19, 39, and 59 ft. Figures 4.15 and 4.16 show the calculated equipotentials, streamlines, and moisture content distribution for the 39-ft case. The relationship of depth to water table on infiltration-rate from the canal is shown in Figure 4.17. These data indicate that for this particular case a significant reduction in flow occurs as the depth to the water table is increased to about 20 ft. At depths greater than 20 ft, where unsaturated flow predominates, the effect of the distance to the water table on seepage rate is insignificant.

The influence of sediment deposited in the trench on seepage rate was evaluated by varying the permeability of the upper soil layer, which is analogous to lining an irrigation canal with a soil finer than the underlying material. The lining or sediment layer was considered to be 1 ft thick on the bottom and 0.7 ft thick on the sides. Three flow systems differing only in lining permeability were solved to obtain comparisons with the case shown in Figures 4.15 and 4.16.

Figure 4.18 shows the ratio of seepage quantities related to the ratio of lining and base soil permeabilities. Examination of the curve shows that if the saturated permeability of the lining material is 0.1 that of the base soil, the seepage rate is reduced by a factor of 0.43. These results are for a specific trench size, water table depth, base soil, and lining thickness; however, it is possible to calculate results similarly for other combinations of parameters. In general, the resulting curve for a coarser-textured soil and increased water table depth will be to the left of the curve presented in Figure 4.18. For finer soils and shallower water table depths, the curve would lie to the right of that presented, but not below a diagonal constructed between the origin and the coordinate point (1, 1). The latter is a

line representing saturated flow conditions. A saturated flow solution from Muskat,[4.20] where $K/K_o = 1$, is shown normalized with the quantity of flow calculated from the partially-saturated system.

The influence of soil heterogeneity on seepage from a canal or disposal trench is of major concern, since all practical flow systems are to a great degree heterogeneous. Figure 4.19 shows a heterogeneous pattern consisting of three soils, upon which equipotentials and streamlines were drawn. Several distortions caused by the fine, silt-loam layer are evident. The moisture content pattern for the same system, shown in Figure 4.20, differs appreciably from that of the homogeneous case shown in Figure 4.18. The seepage rate in the heterogeneous case was 14.5 ft^3/day/linear ft of canal, as compared to 26.1 ft^3/day/linear ft for the homogeneous case.

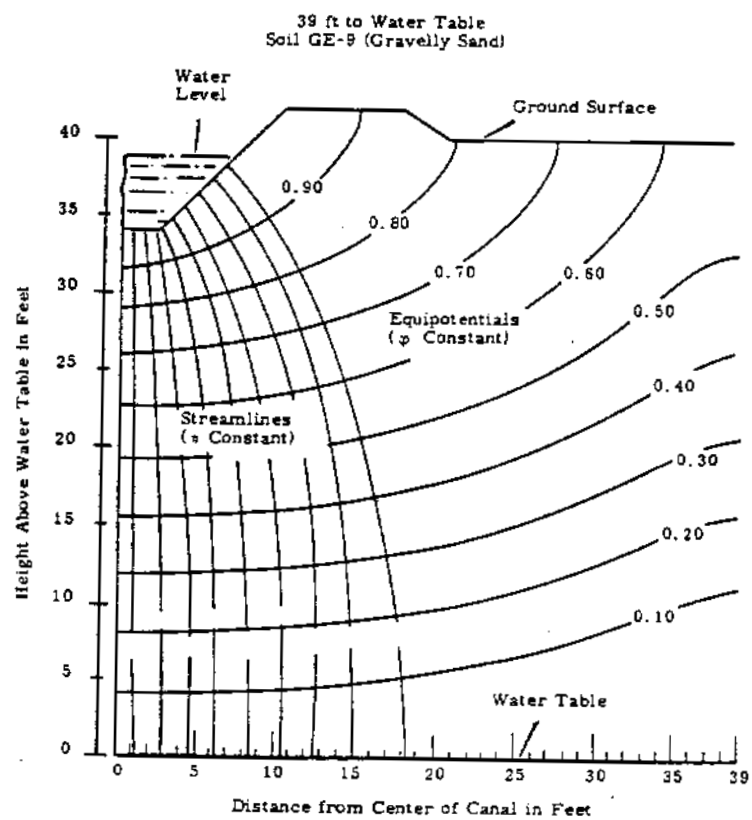

FIGURE 4.15

Two-Dimensional Flow Pattern Below a 15-ft Canal in Homogeneous Soil

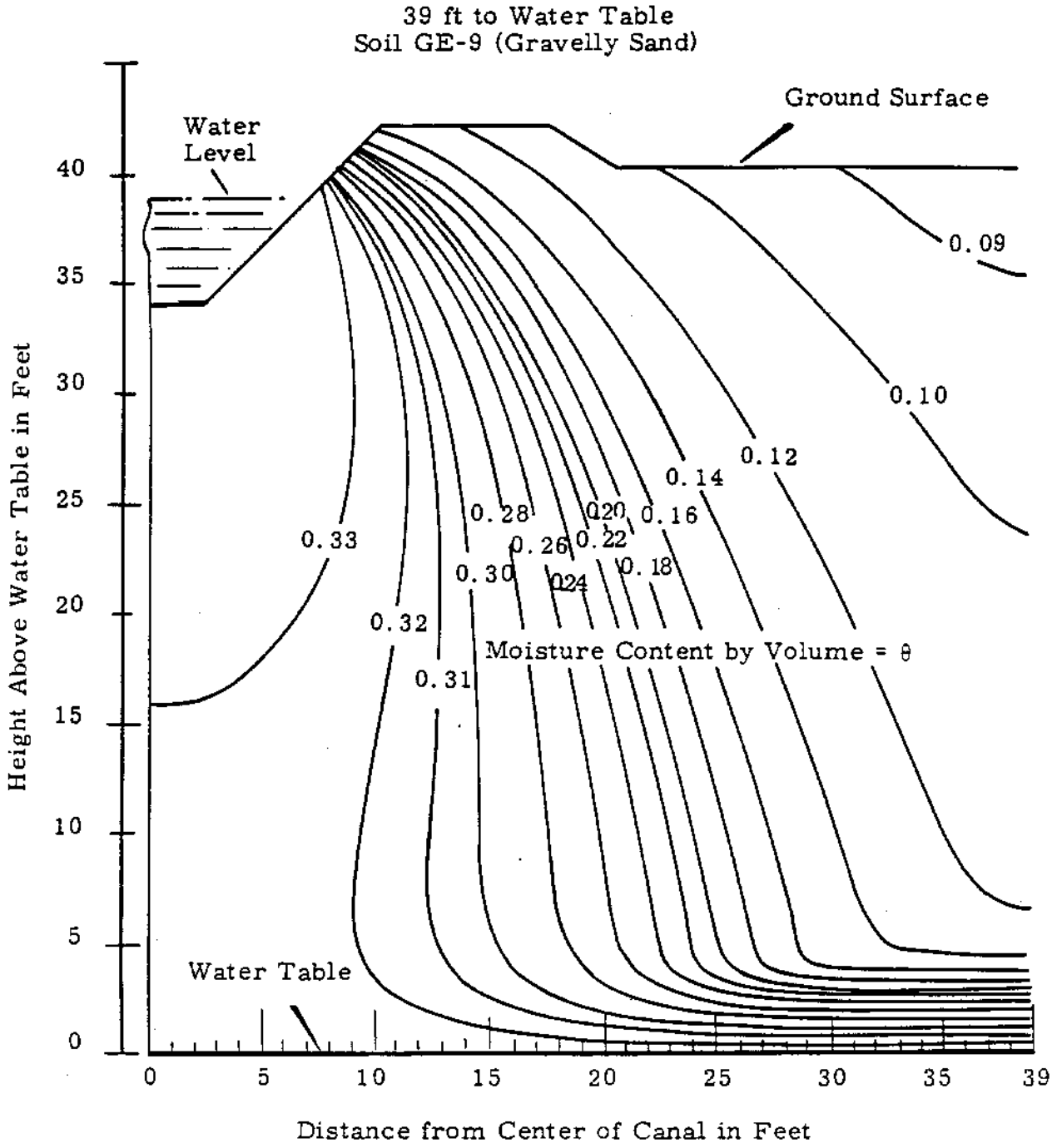

FIGURE 4.16

Two Dimensional Moisture Content
Below 15-Foot Canal in Homogeneous Soil

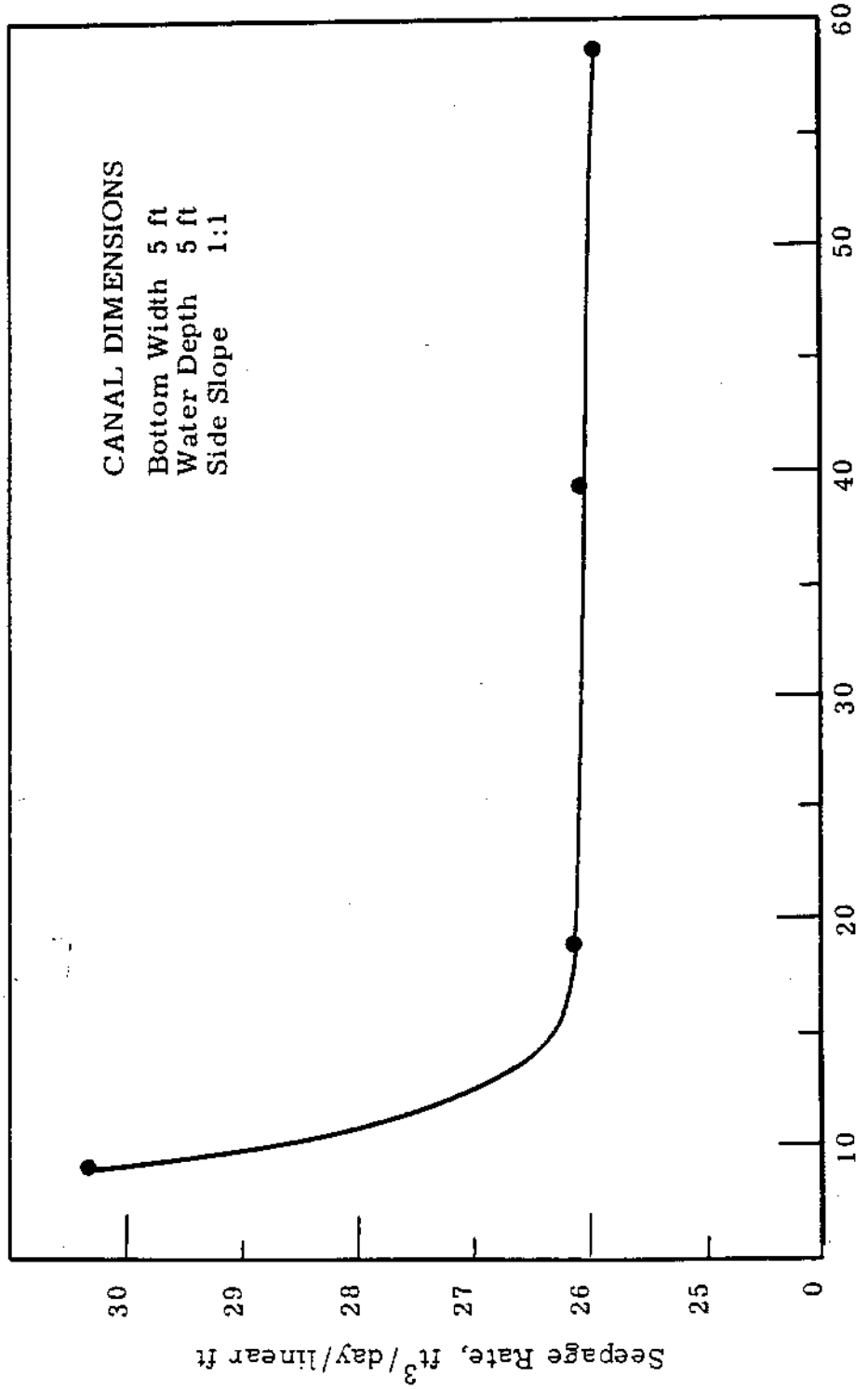

FIGURE 4.17

Relationship of Seepage Rate to Water Table Depth for Partially-Saturated Flow in Soil GE-9, K = 0.789 ft^3/ft^2 Day $\frac{ft}{ft}$

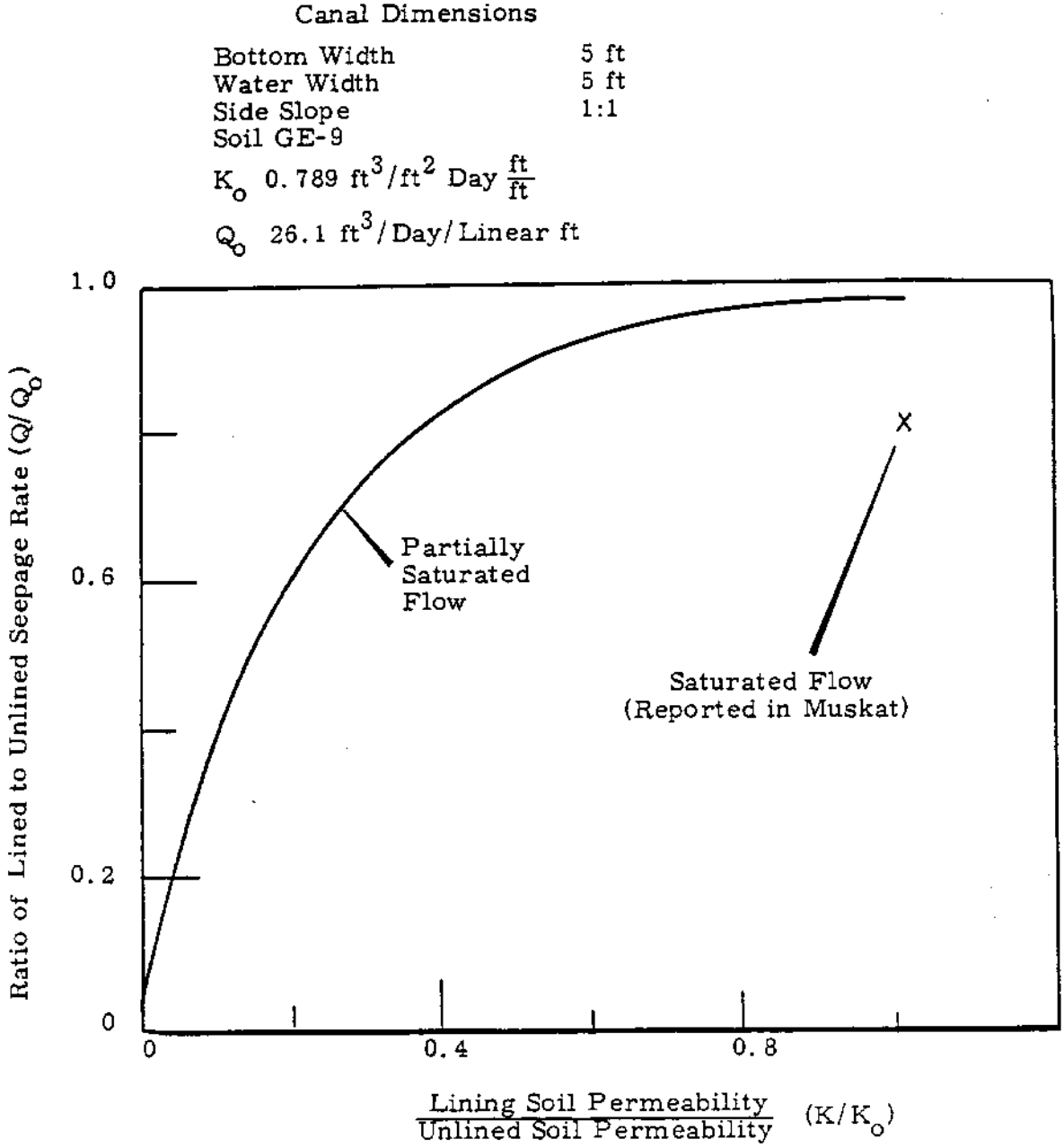

FIGURE 4.18

Effect of Earth Lining Permeability on Canal Seepage (Depth to Water 39 Feet)

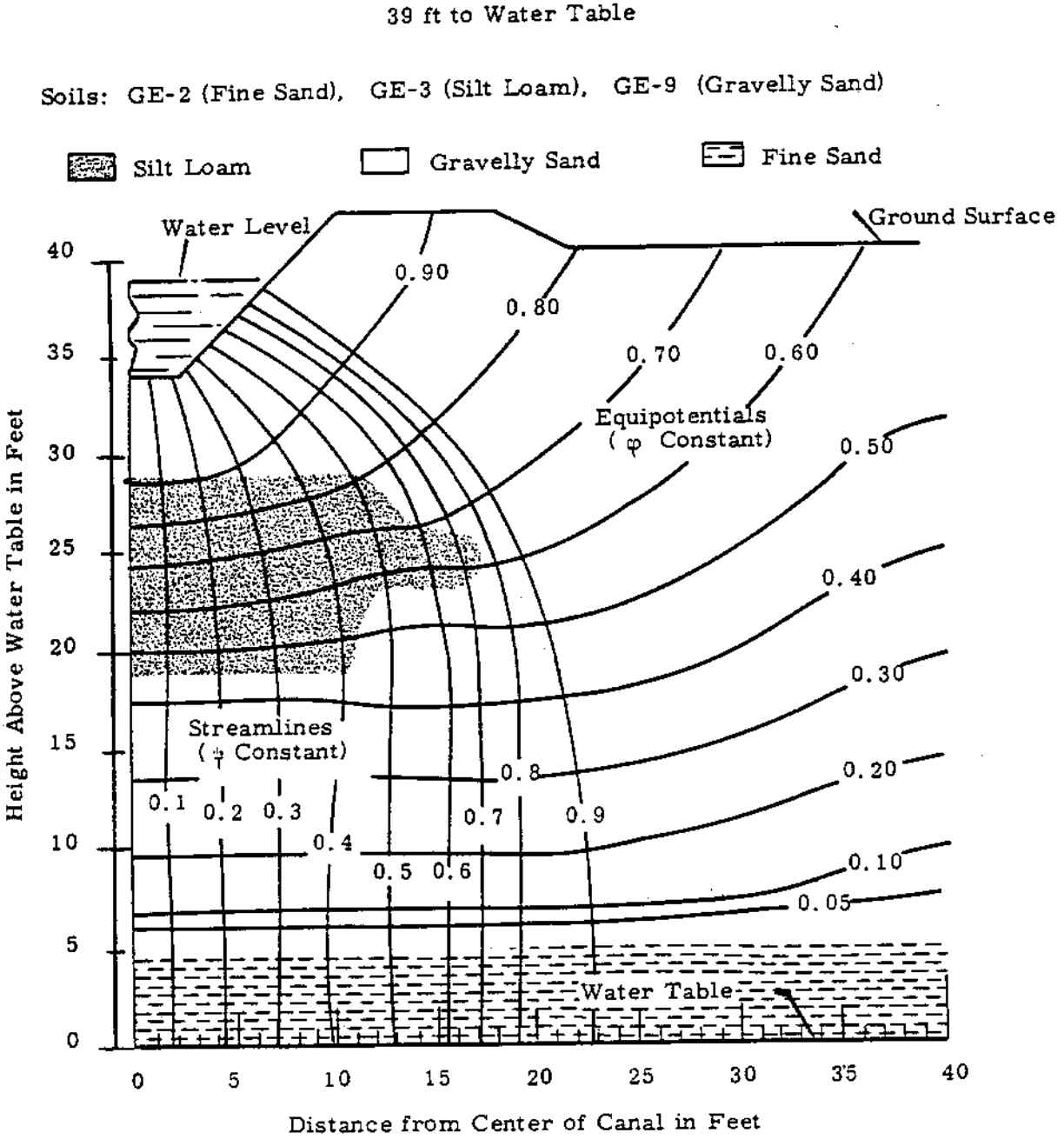

FIGURE 4.19

Two Dimensional Flow Pattern Below a 15-foot Canal in Heterogeneous Soil

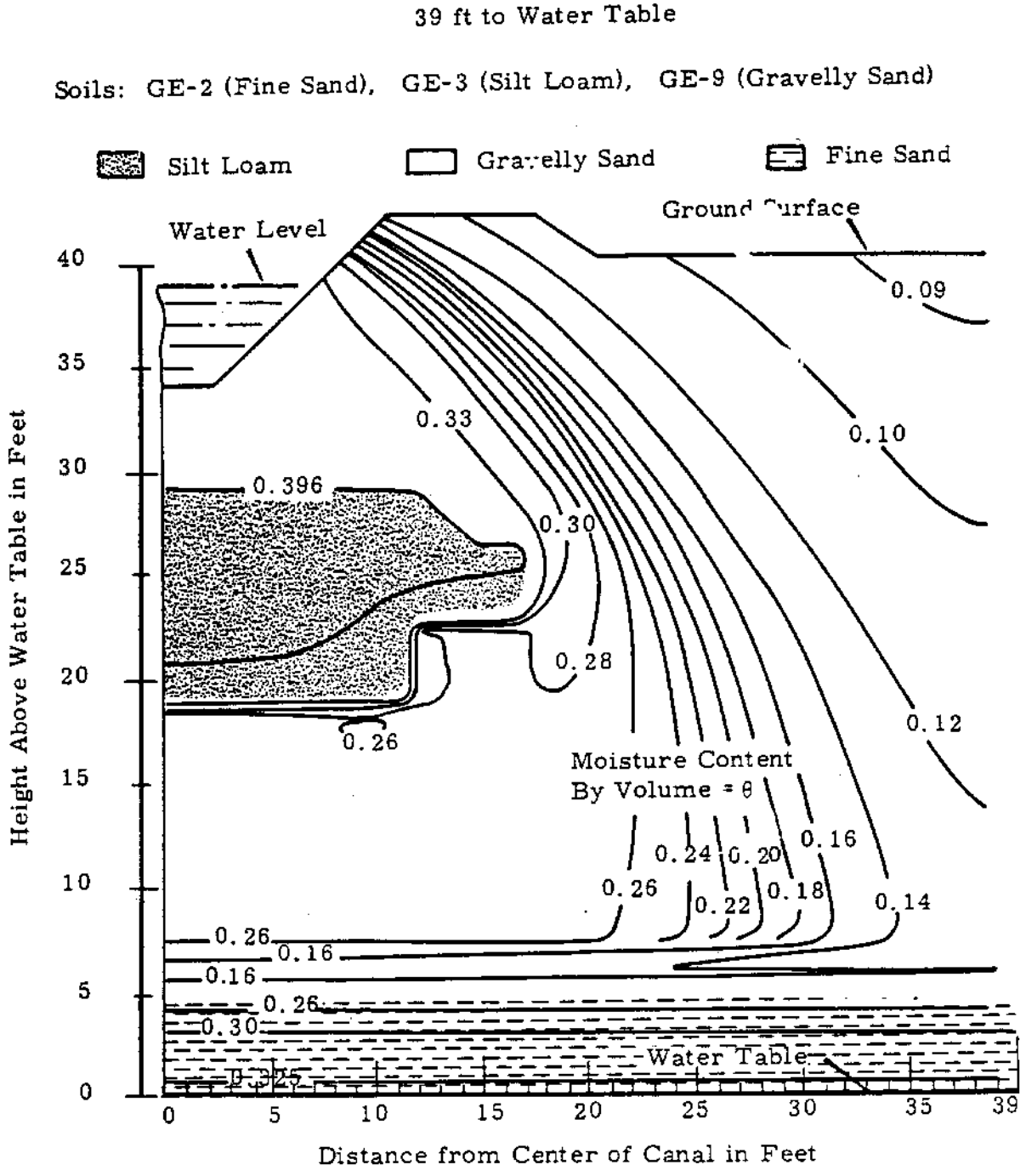

FIGURE 4.20

Two Dimensional Moisture Content Pattern Below a 15-Foot Canal in Heterogeneous Soil

Ground Water Temperature Investigations - D. J. Brown and J. R. Raymond

A Hanford-developed probe, which permits the accurate measurement of temperature profiles of the ground water, was used to obtain data for constructing isothermal maps of the Hanford Project ground water system. These maps have application in defining ground water flow patterns, and they supplement radiological monitoring data in forecasting directions and rates of ground water movement.

A special probe [4.21] was developed to permit the measurement of temperature profiles of the ground water in monitoring wells located at Hanford. An isothermal map of the water table beneath the chemical separations areas, Figure 4.21, was made from data obtained during July through December, 1962. The measurements were adjusted on the basis of the regional geothermal gradient (1 C/140 ft of depth) to correspond to readings which might be expected at an elevation of 350 ft above mean sea level.

The maximum temperature in the region shown on the map, 75 C, was noted in wells immediately adjacent to steam and process condensate waste cribs in the chemical separations areas. Ground water temperatures in wells near cooling water swamps were only several degrees above background ground-water temperatures due to appreciable atmospheric cooling of the water before infiltration into the soil. In general, the isothermal map correlates quite well with the results obtained from radiological analyses of well water samples. Clearly evident on the map are the relationships between ground water temperature patterns and the source areas of the thermally warm waste water. The higher-than-background temperatures noted in the two wells to the east (699-40-1 and 699-10-E12) are probably due to a slightly increased ground water velocity in the lowermost aquifer penetrated by the wells. (See "Geologic Features and Ground Water Flow," p. 4.43) Since sections of well 699-20-E12 were sealed-off and piezometer tubes installed, temperatures above background in that well have been evident only in the bottom aquifer.

The indicated preferential direction of warm-water movement to the southeast is probably due to waste steam condensate and cooling water discharged to Redox Plant ground disposal facilities. This movement reflects the large volume of thermally warm waste cooling water discharged to two large underground cribs at the Redox Plant during the period (1954-1957) that the Redox swamp was out of service. Essentially no ground water contamination resulted from that disposal, thus accounting for the absence of radiocontaminants in the southeast temperature extension shown on the map.

The temperature probe has also been used extensively in the reactor areas to define local ground water flow conditions and to evaluate the magnitude of waste cooling water leakage from retention basins and pipelines.

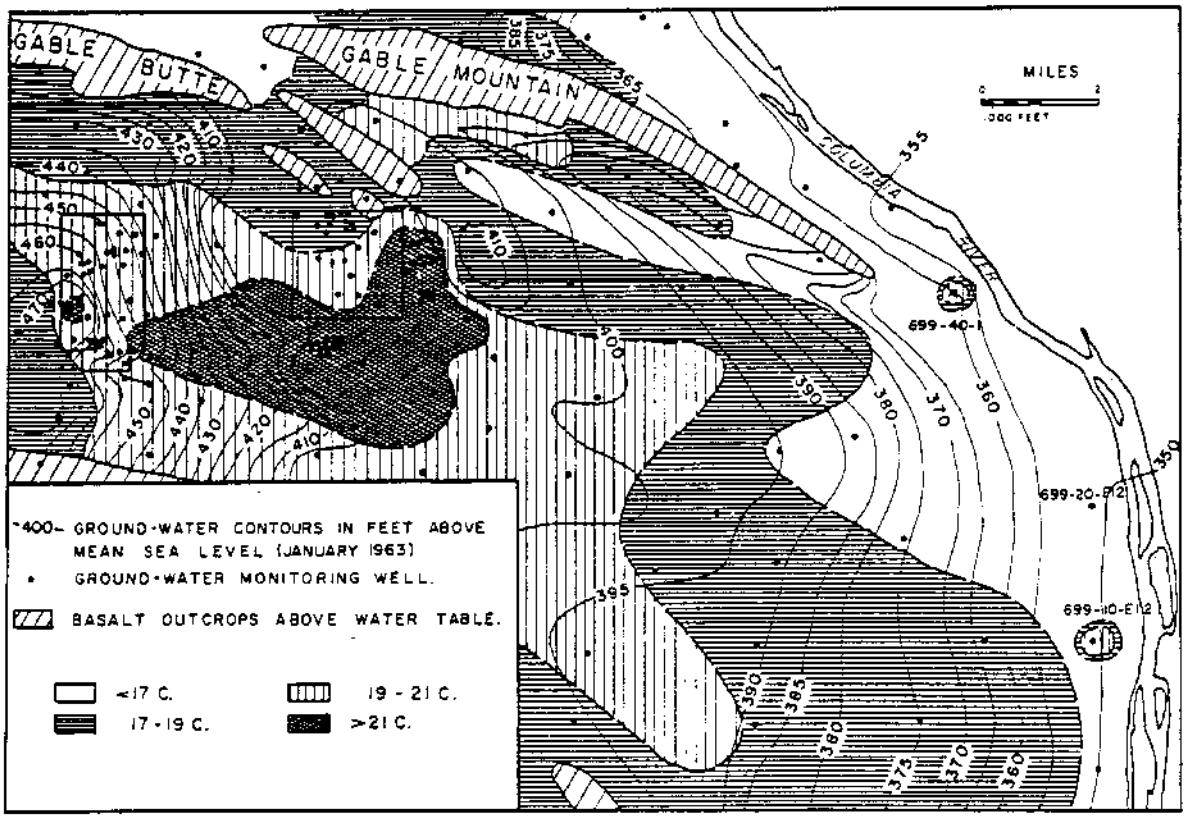

FIGURE 4.21
Ground-Water Temperatures

Geology

Geologic Features and Ground Water Flow - R. E. Brown and D. J. Brown

Geologic studies, combined with ground water potentials and temperature measurements, disclosed a confined or semiconfined aquifer overlying the upper part of the basalt series at several locations beneath the Hanford Project. Analyses of water samples from this aquifer indicate that recharge occurs in the vicinity of the separations areas, and that the rate of flow within the confined aquifer is slightly greater than the unconfined ground water flow in the same region.

Continued geological studies of the upper part of the basalt series and of the Ringold Formation disclosed several paths that low-level ground water contaminants may follow in confined or semiconfined aquifers at the Hanford Project. Temperature measurements made in well 699-20-E12, Figure 4.22, showed thermally warm water (19 C compared to an expected 16.5 C) flowing upward in the casing. Also, low concentrations of tritium were noted in water samples from the well. Several piezometers were sealed recently into various sections of the well. The liquid level in the tube sealed into the lowermost well section showed the fluid potential there to be about 25 ft greater than the pressure in overlying aquifers. Somewhat comparable situations in wells farther west suggest that the aquifer is recharged in the vicinity of the chemical separations plants, 12 miles west-northwest of well 699-20-E12.

The confined aquifer is an alluvial fan deposit laid down by an early stream that flowed from the west and here joined the Columbia River; it thus is part of the Ellensburg Formation. To the east and southeast it thins and passes beneath a later basalt flow. Beneath the Hanford Project, the overlying basalt is absent and the bed is directly overlain by the Ringold Formation clays and silts. Beneath the chemical separations plants, the basalt series and later sediments were uplifted then eroded so that the confined Ellensburg Formation aquifer is subject to recharge by unconfined

Artesian heads in the aquifer southeast of the chemical separations plant show a southwestward gradient, further indicating recharge at the plant site. Natural recharge takes place in the Rattlesnake Hills and in the Columbia Basin Irrigation Project. The extent of, path to, and site of entry of the confined ground waters in the Columbia River will be an integrated function of the geologic structure, the stratigraphy, the sites of recharge, and their respective significance.

Similar studies of the Ringold Formation disclosed that it is characteristically fluviatile in origin, contrary to early studies in the area. It is laced with numerous gravel trains representing main stream Columbia River deposits. Ground water will flow in the confined and semiconfined aquifers in that formation in response to a complex relationship between gradients or artesian head and the orientation and vectoral permeabilities of the gravel trains. Additional investigations are being made to define the possible eastward extension of the alluvial fan deposit and to determine if other such beds exist under the Hanford Project.

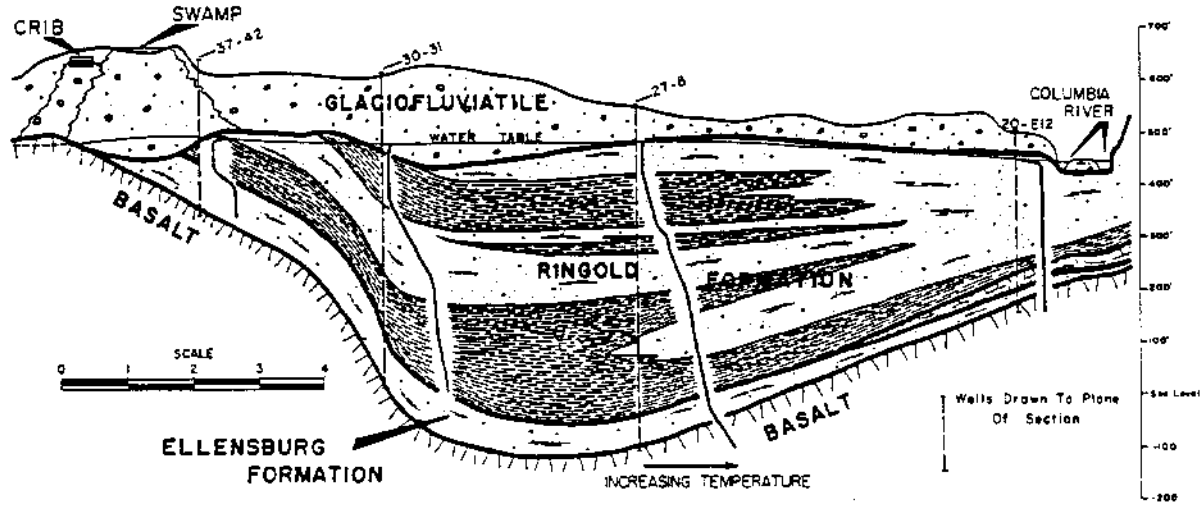

FIGURE 4.22

Geologic Profile of Location of Well 699-20-E12

Geophysical Investigation with a Scintillation Well Probe -

J. R. Raymond and D. J. Brown

A gamma scintillation well-probe system was used to investigate the feasibility of logging Hanford wells to obtain geophysical information. Comparison of scintillation logs with well drilling logs showed correlation between naturally occurring radioactive material content and type of earth material. Basalt bedrock and coarse gravels underlying the Hanford Project have the lowest natural radioactivity. The radioactivity of the geologic formations increases as the fine particel content (silt and clay size material) increases. As formation changes are often quite markedly shown on the scintillation logs, data obtained with the scintillation probe provide a valuable aid in geological evaluation.

Information on Hanford Project subsurface geology is obtained, for the most part, from well drilling logs and drilling sample examination. Reliance on logs and samples alone leads to uncertainties in data interpretation due to differences in driller's skills, accuracy of observation, report completeness, and accuracy of churn-drilled samples. It is often helpful to have other methods and techniques to assist in making geological evaluations. One such geophysical aid is the gamma scintillation probe. This instrument measures the naturally occurring radioactive material content of the earth materials penetrated by a well.

The scintillation probe designed and fabricated for this study evolved from an instrument developed several years ago for use in subsurface detection of radioactive contaminants in the vadose and groundwater zones.[4.22] The system consists of a probe, armored wire line, surface winch, and recording and control equipment. The probe consists of a 4-in. diameter by 18-in. long stainless steel shell containing a 2 in. x 2 in. NaI(Tl) crystal, photomultiplier tube and a transistorized emitter-follower. A waterproof connector couples the probe to 1000 ft of 1/8-in. diameter armored wire line. Surface equipment consists of a transistorized high-voltage power supply, pulse amplifier, count-rate meter, Electro-Technical Laboratories "Widco" well logger, and a modified 10 mv Brown recorder. The system is mounted in the back of a one-half ton

panel truck. Electrical power is supplied by a 1500 w gasoline-engine driven generator mounted on the front of the panel truck.

A number of wells were selected for scintillation logging to provide a wide variety of formation types and characteristics. Quite large variations were noted in the scintillation logs. The logs were compared with drilling reports and with well drilling samples. It was evident that radiation count-rate increased as the fine particle material content increased. Basalt bedrock exhibited a characteristically low count rate and clean sands and gravels showed an intermediate count rate. Radiological analysis of drilling samples showed gamma photopeaks typical of the natural radioactive decay chains of Th^{232} and U^{238}. The increase in radioacitve material content in the silt- and clay-size sediments is probably associated with the higher organic content of these sediments. X-ray diffraction studies indicate that the clay-size material is mostly volcanic ash and not clay mineral; therefore, the higher radioactivity cannot be explained by ion exchange or adsorption phenomena.

Stratigraphic breaks are often accompanied by changes in material size. Figure 4.23 shows a comparison of the scintillation log and the lithologic log for well 699-32-72. This well penetrates a wind-deposited sandy silt (loess) described as part of the Palouse formation. The formation is encountered at about 45 ft and extends to about 185 ft below ground surface. Glaciofluviatile sand overlies the Palouse which overlies Ringold sand and gravel. The scintillation log graphically shows these stratigraphic breaks by a 400 count/min increase at 44 ft; a gradual additional increase of about 400 counts/min to 176 ft, indicating increasing silt content; and about a 900 counts/min decrease at 178 ft where the gravel and sand occur. Some lithologic logs do not match the scintillation logs as precisely as in the above case. The driller may have allowed carry-down of material to create non-representative samples, or may have failed to recognize and identify stratigraphic changes or made errors in depth measurement. Under such conditions

the scintillation log is an excellent tool for more precisely locating stratigraphic changes. It also provides more fine detail than is available from drilling log or sample evaluation.

The gamma scintillation well probe cannot by itself provide absolute stratigraphic information. The scintillation log will not differentiate between glaciofluviatile gravel and Ringold gravel, nor between Touchet slit and Ringold silt. Also, it is sometimes difficult to distinguish a clean gravel from basalt bedrock. Therefore, it is necessary to have some geologic control or other geophysical information on an area under investigation. When this information is available, data provided by the scintillation probe are valuable in aiding geological evaluation.

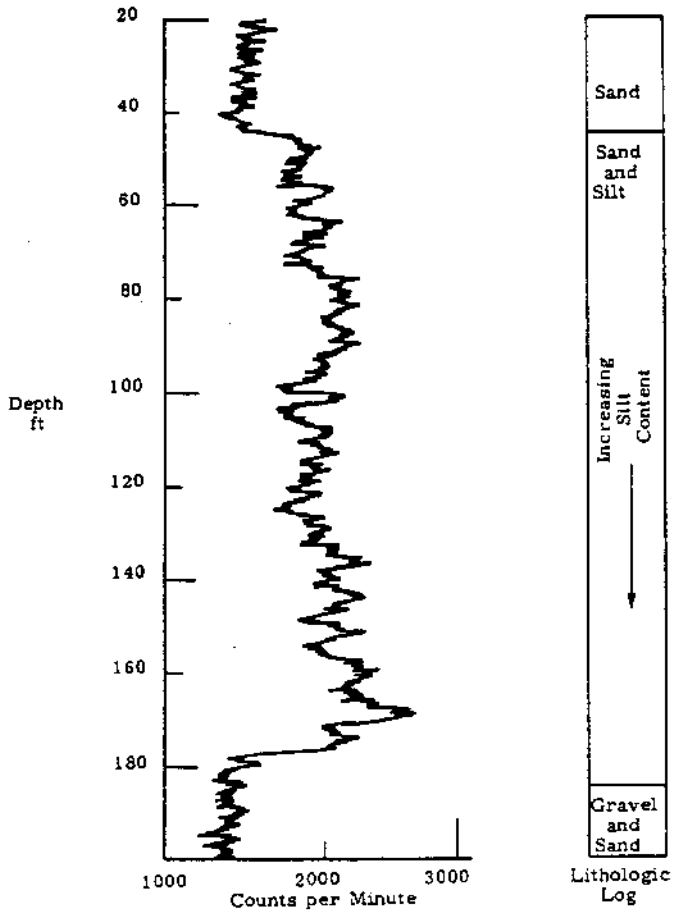

FIGURE 4.23

Comparison of Gamma Scintillation Log and Lithologic Log—Well 32-72

Radioisotopes as Particles and Volatiles

Particle Deposition and Retention in Conduits - G. A. Sehmel and L. C. Schwendiman

Particle deposition on tube walls was measured for three diameters of vertical tubing 60 ft long. For the two smaller diameters, 1.02 cm and 2.93 cm, reasonably accurate prediction of particle deposition onto the tube walls could be made using a previously developed correlation function. Disagreement between predicted and actual deposition for a 9.68 cm diameter tube was not resolved, but suggests the need for a significant tube diameter term in the correlation.

Representative samples from gaseous streams containing fine particulates of radioactive materials are commonly required in plants which process nuclear materials. Since the sample delivery lines are usually unavoidably long, information on the impaction and deposition of the particulates is required to interpret the sample results in terms of the concentration in the gaseous streams. Identifying the parameters controlling deposition on surfaces contributes also to a better understanding of deposition of airborne particles on terrain and vegetation and gives insight into the mechanisms by which particles may be retained upon entering the lung passages. The retention of particles on surfaces is also of interest in evaluating contamination spread and the degree of hazard from unusual incidents releasing appreciable quantities of radioactive aerosols.

Research continued to determine the quantitative relationships among the variables governing particle deposition in conduits and to develop deposition models which are supported by the data.

Particulate deposition during turbulent flow has been measured by Friedlander and Johnstone[4.23], and by Postma and Schwendiman.[4.24] In both studies, the deposition velocity, K, cm/sec, was determined from the average concentration of particulates in the gas stream and the number

of particulates counted on the tube wall. Deposition was measured in an incremental tube length for tube diameters of 0.54 to 2.64 cm.

In studies undertaken the past year, total deposition of ZnS particulates in tubes 58 ft long, with diameters of 1.02, 2.93, and 9.68 cm, was studied and compared with the theoretical deposition predicted from the existing deposition velocity correlations.[4.24] The comparisons show that for the particle size distribution used,* the deposition in the 1.02 cm tube[4.25] is approximately 10% greater than the predicted deposition up to a Reynolds number of approximately 8000. At a Reynolds number of 10,000, a deposition of about 90% was obtained, which agreed with the predicted deposition.

For the 2.93 cm tube, the comparison shows reasonable agreement for Reynolds numbers below about 20,000. However, the apparent maximum equilibrium deposition of about 70% reached at Reynolds numbers from 34,000 to 45,000 is 15 to 20% lower than predicted.

The deposition in the 9.68 cm tube was much greater than that predicted for flows measured to date. Ten percent deposition was found for Reynolds numbers from 2500 to 10,000 compared to that predicted, which is less than 1%. These results show that the tube diameter must be more fully accounted for in the deposition correlation.

Improved experimental techniques have reduced experimental errors and permitted more rapid acquistion and processing of data. This deposition study has yielded valuable empirical data and provided a basis for estimating with reasonable accuracy particle deposition due to turbulence in small diameter (1 to 10 cm) conduits.

---

* U.S. Radium Corp. fluorescent ZnS No. 2210., average particle size = 2 μ

Deposition of I^{131} in Conduits* - J. D. McCormack

I^{131} deposition on stack gas sample delivery lines was found to be of minor significance for routine samples taken to establish I^{131} daily emission from two fuel reprocessing plants. Laboratory experiments confirmed that deposition of molecular iodine on silver-plated tubes could be predicted using iodine diffusion coefficients and equations for laminar flow. Under similar conditions of Reynolds number and tube diameter, deposition in stainless steel tubes was significant but much less than for silver-plated (infinite sink) tubes. A glass tube, 135 times as long as the silver-plated tube, is required for 50% deposition.

Deposition and retention of I^{131} on sampling lines from exhaust stacks for fuel reprocessing plants could seriously reduce the accuracy of routine measurements of I^{131} released to the atmosphere. Recent recommendations by the Federal Radiation Council that permissible air concentrations of I^{131} be lowered to reduce potential accumulation in childrens' thyroids gave added incentive to assure that I^{131} sampling for release estimates be accurate. A brief study (4.26) was therefore undertaken to determine I^{131} deposition in installed lines, and a comparison study was initiated to more fully explore the parameters controlling I^{131} deposition in conduits.

The Redox stack sampling system comprises two lines, one entering the stack at 50 ft above the ground and one at 11 ft. A comparison of the I^{131} concentrations in exhaust air drawn from these two lines would give a reasonable estimate of iodine retention in the line, or point to other sampling errors. Identical samples were drawn simultaneously from each system; the I^{131} was collected on charcoal traps and measured using scintillation counting. The average I^{131} concentrations measured in the samples drawn from the 50 ft level were actually 12% higher in I^{131} than for samples drawn from the 11 ft level. At the Purex stack, similar sampling from the two systems, one comprising an 80-ft line, the other a 240-ft line, showed that samples taken from the 80-ft line were 10% higher in I^{131} than in samples taken from the longer line. The conclusion was that the rather large differences in sample

* Not supported by Division of Biology and Medicine

line configurations did not result in significantly different I^{131} measurements for the intended use of the data obtained.

I^{131} deposition in small diameter tubes was measured in initial studies to identify the controlling parameters. Molecular iodine was generated and passed through silver-plated tubes, and the wall deposition was measured for several Reynolds numbers. With the assumption that the wall was an "infinite sink," diffusion equations of Browning and Ackley [4.27] predicted rather accurately the observed deposition for laminar flow. In the several experiments performed using stainless steel and glass tubing, deposition was considerably less but nevertheless, appreciable. Results of these tests expressed as the length of tube to give 50% deposition are presented in Table 4.8.

TABLE 4.8

DEPOSITION OF MOLECULAR IODINE IN TUBES
Diameter = 5/16 in.

		$L_{1/2}$, cm		
		Calculated		
N_{Re}	Material	Laminar	Turbulent	Measured
5	Ag-Cu	0.43	--	0.46
100	Ag-Cu	9.5	--	8.1
300	Ag-Cu	28	--	32
1,000	Ag-Cu	95	(32)	52
3,000	Ag-Cu	284	40	193
10,000	Ag-Cu	950	48	257
100	304 SS *	--	--	16
100	304 SS **	--	--	33
100	Pyrex	--	--	1080

* Polished with steel wool

** Washed with concentrated HNO_3

In conclusion, the foregoing results show that:

(1) I^{131} deposition in two existing sampling systems is not of great concern for routine samples. Changes in stack gas composition or conditioning of the lines could conceivably change I^{131} deposition. The deposition parameters were not identified.

(2) Deposition of molecular I^{131} will be significant for stainless steel tubes and much less for glass tubes, during laminar flow.

Implications of the Use of Charcoal as a Sample Collector for I^{131} and as an I^{131} Removal Media for Process Gaseous Exhaust Streams* - J. D. McCormack

Efficiency of charcoal was shown to be significantly lower for I^{131} removal in effluent stack gas than for I^{131} generated as molecular iodine in laboratory experiments. Atmospheres giving lowered I^{131} adsorption efficiency could be produced. Hexone saturated charcoal will ignite when NO_2 at > 5% is passed through the charcoal; low concentrations do not reduce I^{131} retention. I^{131} removal efficiency decreases with the exposure of the charcoal bed to the air stream; in one case the efficiency was 58% after 2-1/2 yr of service. In another case I^{131} efficiency was not reduced after more than 1 yr of service. Testing installed charcoal efficiency periodically is needed to assure that adequate efficiency is available.

Charcoal is an effective adsorbent for radioiodine, yet air stream compositions may occur which could materially reduce the normally high removal efficiency of charcoal. Proof-of-efficiency tests are almost invariably made with iodine generated under rather ideal conditions. In actual application, however, charcoal may be used for efficient removal in process and sample streams in which iodine appears as extremely small particles, rather than molecular iodine. Again, long exposure to traces of impurities in streams may markedly affect removal efficiency. Several observations have been made relative to the use of charcoal for I^{131} removal from process streams.

---

* Not supported by the Division of Biology and Medicine

Charcoal which was consistently 99.5% efficient for removal of I^{131} generated as molecular iodine was found to be seldom more than 95% efficient for I^{131} present in chemical processing plant stacks and process streams. In some cases much lower efficiencies were recorded. Experiments were carried out in laboratory tests to deliberately provide atmospheres which might reduce charcoal efficiency, and which might conceivably be present in the stack effluents. Adsorption efficiency for molecular iodine was then measured. Hexone and NO_2 were introduced at levels corresponding to concentrations expected and had no deleterious effect on efficiency. When charcoal was saturated with hexone at 16 mm-Hg partial pressure, then exposed to > 5% NO_2 in air, however, high temperatures, and in some cases charcoal ignition, occurred. This circumstance would be extremely serious for a charcoal trap in a critical location.

Introducing an oil mist from a vacuum pump exhaust reduced charcoal efficiency by 3 to 15%. Introducing a very fine aerosol of aluminum formed by sparking likewise reduced iodine retention on charcoal by 3 to 15%.

These experiments designed to be scouting investigations did reveal some conditions under which charcoal may be indifferently efficient.

Influence of long term exposure to the air stream being passed through a charcoal bed was examined. Samples of charcoal which had been in place in the reactor ventilation exhaust air for over 1 yr were found to be 99.8% efficient for I^{131} removal.

Charcoal taken from a high level radiometallurgy cell exhaust I^{131} trap was found to be only 58% efficient for I^{131} removal. New charcoal from replacement beds was found to be 99.9% efficient under identical test conditions. This lowered I^{131} retention after 2-1/2 yr of service appears to be restricted to the surface of the charcoal grains since mild abrasion and washing with water increased the retention to 94%. Crushing from 4/8 to 14/20 mesh increased the retention to 99.7% at 100 fpm, thus indicating that only a small fraction of the ultimate charcoal capacity was utilized.

In conclusion, certain circumstances have been identified which result in lowered I^{131} retention on charcoal. Presence of extremely small solid or liquid particles reduce retention efficiency. Continued high efficiency of large scale use of charcoal traps can be assured only by periodically measuring the I^{131} retention efficiency of the charcoal used in these traps.

Uranium Oxidation and Fission Product Volatility*

Special Fission Product Release Studies—Release of Radiocesium from Clinoptilolite - D. L. Reid

To evaluate the hazards of accidently heating recovered cesium, the percent Cs^{137} released from clinoptilolite was measured as a function of temperature and time. Some solubility data were also obtained and are presented.

Knowledge of the release-temperature relationship for cesium adsorbed on the natural zeolite, clinoptilolite, is important with respect to the potential application of this mineral for waste treatment, fission product recovery, and storage and transport mediums. Experiments were performed to provide release information as a function of temperature and time, and to determine the leach rate of cesium from fused clinoptilolite glass.[4.28]

Crushed clinoptilolite, having particle sizes of 0.4 to 0.7 mm, was equilibrated with a synthetic waste traced with Cs^{137} to a total radioactive loading of 1.0 m curie/g of dried mineral. Samples were heated in air at several temperatures and times, and the fractional release of radiocesium was measured, as listed in Table 4.9.

---

* Not supported by the Division of Biology and Medicine

TABLE 4.9

TEST CONDITIONS AND PERCENT RELEASE OF CESIUM ADSORBED ON CLINOPTILOLITE

Test Number	Sample Weight (g)	Temperature (C)	Time at Temperature (hr)	Percent Cs Released
1	1.0005	590	4	2.3×10^{-4}
2	0.9692	800	4	7.2×10^{-3}
3	0.9988	1100	4	1.2×10^{-1}
4	1.0455	1350	4	1.8
5	0.5442	1350	4	2.0
6	0.9530	590	8	4.6×10^{-4}

At temperatures below the clinoptilolite softening point (~ 1150 C) the release was linear with time, at least for periods up to 8 hr. An Arrhenius plot showed the release to be exponential with temperature, and an activation energy of 28.2 kcal/mole was calculated according to the following equation:

$$R = 875\, t^{(-2.82 \times 10^4/RT)},$$

where

R = cesium release, percent
t = time, hr
R = gas constant, 1.99 cal/mole
T = temperature, K.

Above the clinoptilolite melting temperature, the cesium released followed a parabolic rate law. The diffusion constant at 1350 C was approximately 4×10^{-10} cm^2/sec.

Cursory leaching tests with tap water at room temperature were made with the fused cesium-clinoptilolite buttons from the 1350 C tests. Leaching rates approached a constant value of 9×10^{-9} $g\text{-}cm^{-2}\text{-}day^{-1}$ after 70 days submersion, lower than most glasses proposed for "ultimate" waste storage.

Fission Product Release from Uranium* - R. K. Hilliard and D. L. Reid

Refined fractional release data of radionuclides from small uranium samples heated to high temperatures are presented as a function of irradiation level. The measured higher release is explained as either the result of a concentration increase or higher oxidation rates.

The investigation of the effect of irradiation level on the release of fission products from uranium during simulated reactor accident conditions was completed.[4.29] Small, bare, uranium weighing 11.7 g were irradiated to various burnups from 2×10^{14} nvt (6.7×10^{-4} Mwd/ton) to 4×10^{20} nvt (1340 Mwd/ton) and heated out-of-reactor under carefully controlled conditions of time, temperature, and atmosphere. Table 4.10 lists the fractional releases for ten fission-product elements plus neptunium, plutonium, and uranium for low, intermediate, and high values of integrated thermal neutron flux.

The only fission products whose release rates were directly influenced by irradiation level were the volatile elements: rare gases, halogens, and alkali metals. Ruthenium and molybdenum were released at greater rates from the highest irradiated specimens, but this is now attributed to the greater extent of uranium oxidation which occurred with those specimens. These two fission products are quite volatile in their highest oxidation states, but are very nonvolatile in their elemental form. The free energies of formation are such that RuO_4 and MoO_3 are not formed until there is no competition for oxygen with uranium or UO_2. If the trace-level specimens had been heated for a longer time, so that all the uranium was oxidized, a similar increase in release of RuO_4 and MoO_3 would have resulted.[4.30]

The higher oxidation rate for uranium at the higher irradiation levels was caused by additional surface area created by the expanding fission gas bubbles.

---

* Not supported by the Division of Biology and Medicine

The observed burnup effect of xenon, iodine, and cesium results from the accumulation of these elements in bubbles and cracks in the uranium matrix during the longer irradiation period required to produce highly irradiated material. At burnups above 10^{18} nvt these bubbles contain essentially all of the rare gases and most of the iodine and cesium. Upon melting of the uranium, they expand, coalesce, and rapidly escape from the fuel.

A chief conclusion of this study is that the release mechanism, the rate of release, and the fractional release of volatile fission products is significantly different in highly irradiated uranium than in low burnup metal. Applying the results of trace-level studies to reactor accident analyses could give misleadingly low release estimates.

TABLE 4.10

EFFECT OF IRRADIATION LEVEL ON RELEASE OF FISSION PRODUCTS FROM MOLTEN URANIUM

	Fraction Released from Specimen(*)		
Element	10^{14} nvt	10^{18} nvt	4×10^{20} nvt
Xenon	0.70	0.95	1.00
Iodine	0.60	0.85	0.98
Cesium	0.30	0.60	0.80
Tellurium	0.65	0.65	0.65
Strontium	0.005	0.005	0.005
Barium	0.005	0.005	0.005
Ruthenium	0.001	0.001	0.04
Molybdenum	**	0.001	0.04
Zirconium	0.0003	0.0003	0.0003
Cerium	0.0001	0.0001	0.0001
Neptunium	**	0.0005	**
Plutonium	**	**	0.0004
Uranium	**	**	0.0003
Uranium Oxidized	0.70	0.70	0.92

* 11.7 g cylinder heated 24 min at 1200 C in air

** Not analyzed

REFERENCES

4.1 L. L. Ames, Jr. "Characterization of a Strontium-Selective Zeolite," The American Mineralogist, vol. 47, pp. 1317-1326. November-December, 1962.

4.2 L. L. Ames, Jr. Mass Action Relationships of Some Zeolites in the Region of High Competing Cation Concentrations, HW-SA-2837. November 12, 1962. (To be published in The American Mineralogist)

4.3 L. L. Ames, Jr. "Kinetics of Cesium Reactions with Some Inorganic Cation Exchange Materials," The American Mineralogist, vol. 47, pp. 1067-1078. September-October, 1962.

4.4 D. Reichenberg. "Properties of Ion-Exchange Resins in Relation to Their Structure. III. Kinetics of Exchange," J. Am. Chem. Soc., vol. 75, pp. 589-597. 1953.

4.5 L. L. Ames, Jr. "Effect of Base Cation on the Cesium Kinetics of Clinoptilolite," The American Mineralogist, vol. 47, pp. 1310-1316. November-December, 1962.

4.6 L. L. Ames, Jr. and K. C. Knoll. Loading and Elution Characteristics of Some Natural and Synthetic Zeolites, HW-74609. August 10, 1962.

4.7 R. W. Nelson. "In-Place Measurement of Permeability in Heterogeneous Media. I. Theory of a Proposed Method," J. Geophys. Research, vol. 65, no. 6, pp. 1753-1758. June 1960.

4.8 R. W. Nelson. "In-Place Measurement of Permeability in Heterogeneous Media. II. Experimental and Computational Considerations," J. Geophys. Research, vol. 66, no. 8, pp. 2469-2478. August 1961.

4.9 R. W. Nelson and A. E. Reisenauer. In-Place Measurement of Permeability in Heterogeneous Media. III. Examination of a Computational Scheme, HW-SA-2405. January 15, 1962. (For publication in J. Geophys. Research)

REFERENCES (Contd.)

4.10 Chia-Shun Yih. "Stream Functions in Three-Dimensional Flows," La Houille Blanche, vol. 12, no. 3, pp. 445-450. July-August, 1957.

4.11 R. Nelson. Stream Functions for Three-Dimensional Flow in Heterogeneous Porous Media, HW-SA-2772. March 15, 1963.

4.12 R. W. Nelson and W. A. Haney. Analog Simulation of Hanford Ground Water Flow. HW-SA-2739. August 15, 1962.

4.13 R. W. Nelson and W. A. Haney. Electrical Analog Simulation of Hanford Ground Water Flow, HW-73711. May 1962.

4.14 D. W. Pearce and J. F. Honstead. "Radioactive Waste Disposal at Hanford," Proceedings of the Thirteenth Industrial Waste Conference, Purdue University. Engineering Bulletin, Series no. 96. May 5, 6, and 7, 1958. Published by Purdue University, Lafayette, Indiana. (pp. 567-580)

4.15 R. E. Brown, H. M. Parker and J. M. Smith. "Disposal of Liquid Wastes to the Ground," Proceedings of the International Conference on the Peaceful Uses of Atomic Energy, Geneva. vol. 9, pp. 669-675. New York: United Nations, 1956.

4.16 R. W. Nelson and A. E. Reisenauer. "Partially Saturated Flow in Porous Media," Research and Development Activities in Radiological Sciences, HW-73337, pp. 204-210. January 15, 1962.

4.17 R. W. Nelson and A. E. Reisenauer. Hanford Studies on Flow in Porous Media, Second Ground Disposal of Radioactive Wastes Conference, Chalk River, Canada. TID-7928, pp. 130-144. September 26-29, 1961.

4.18 R. W. Nelson. Steady Darcian Transport of Fluids in Heterogeneous Partially Saturated Porous Media, Part 1, Mathematical and Numerical Formulation, HW-72335 PT1. June 4, 1962.

REFERENCES (Contd.)

4.19 A. E. Reisenauer and R. W. Nelson. Some Influences of Soils and Water Table Depths on Seepage from Lined and Unlined Canals, Proceedings of the Seepage Symposium, Phoenix, Arizona. HW-SA-2890. February 19-21, 1963. (Sponsored by U.S. Department of Agriculture, Agriculture Research Service, Water Conservation Laboratory)

4.20 M. Muskat. The Flow of Homogeneous Fluids Through Porous Media, pp. 331-336. McGraw-Hill Book Co., New York. 1946.

4.21 J. R. Raymond. A Well Water Temperature Logging System, HW-73994. June 5, 1962.

4.22 W. G. Spear and M. O. Rankin. A Scintillation Well Logging System, HW-39273. May 1956.

4.23 S. K. Friedlander and H. F. Johnstone. "Deposition of Suspended Particles from Turbulent Gas Streams," Ind. Eng. Chem., vol. 49, pp. 1151-1156. 1957.

4.24 A. K. Postma and L. C. Schwendiman. Studies in Micromeritics, HW-65308. 1960.

4.25 V. F. Fitzpatrick, S. M. Nielsen and L. C. Schwendiman. Particle Deposition in a One-Half Inch Conduit, HW-73404. June 8, 1962.

4.26 J. D. McCormack. I^{131} Sampling System Efficiencies at Purex and Redox Stacks, HW-73288. June 1962.

4.27 W. E. Browning, Jr. and R. D. Ackley. Particle Size Distribution of Radioactive Aersols by Diffusion Coefficient Measurements, pp. 44-50. ORNL-3319. August 24, 1962.

4.28 D. L. Reid. The Release of Radiocesium from Clinoptilolite by Elevated Temperatures and Water Leaching, HW-74927. October 4, 1962.

4.29 R. K. Hilliard and D. L. Reid. Fission Product Release from Uranium--Effect of Irradiation Level, HW-72321. June 20, 1962

4.30 R. K. Hilliard, C. E. Linderoth and A. J. Scott. "Fission Product Release from Overheated Uranium--A Laboratory Study," Health Physics, vol. 7, pp. 1-10. December 1961.

INSTRUMENTATION

Automatic Monitoring and Recording Methods

An Automatic Data System for Atmospheric Physics Studies -

C. A. Ratcliffe and E. M. Sheen

An automatic data system for atmospheric physics studies is being developed to provide detailed micrometeorological information regarding air diffusion and transport of particulates. At 5 sec intervals, data are collected from six anemometers, six wind direction vanes, and six temperature transducers located on an 80 ft portable mast or field tower. The data is digitized and presented on a printed record and on punched paper tape suitable for computer reduction.

To observe changes in atmospheric temperature, wind speed, and wind direction gradients in the first 80 to 100 ft of elevation, an automatic system for measuring and recording these parameters is being developed. These data are necessary to provide detailed micrometeorological information in support of atmospheric physics experiments.

Figure 5.1 is a block diagram of the developmental system. The transducers consist of six high performance anemometers, six high performance wind direction vanes, and six thermocouples. The sensitivity of the vanes and anemometers, combined with the rapid recording of data, will permit short-term diffusion effects to be detected and analyzed. The thermocouples are of low thermal inertia wire to avoid errors due to direct exposure to sunlight. Anemometer data are stored directly in scalers, and printed in appropriate sequence. Data from the wind vane smoothing circuits and the thermocouple amplifiers are digitized by a digital voltmeter. Timing circuits provide programming and identification and experiment time signals. A printed record is provided and a punched paper tape record is provided for reduction by the electronic data processing computer at Hanford. Approximately one-half of the planned developmental work has been completed.

The system operation is to extend from 0 to 50 mph wind speed, approximately 357-degree vane rotation for direction, and from 0 to +120 F for temperature. Accuracies to ●1% for wind speed and direction and ± 1° for the temperature are planned.

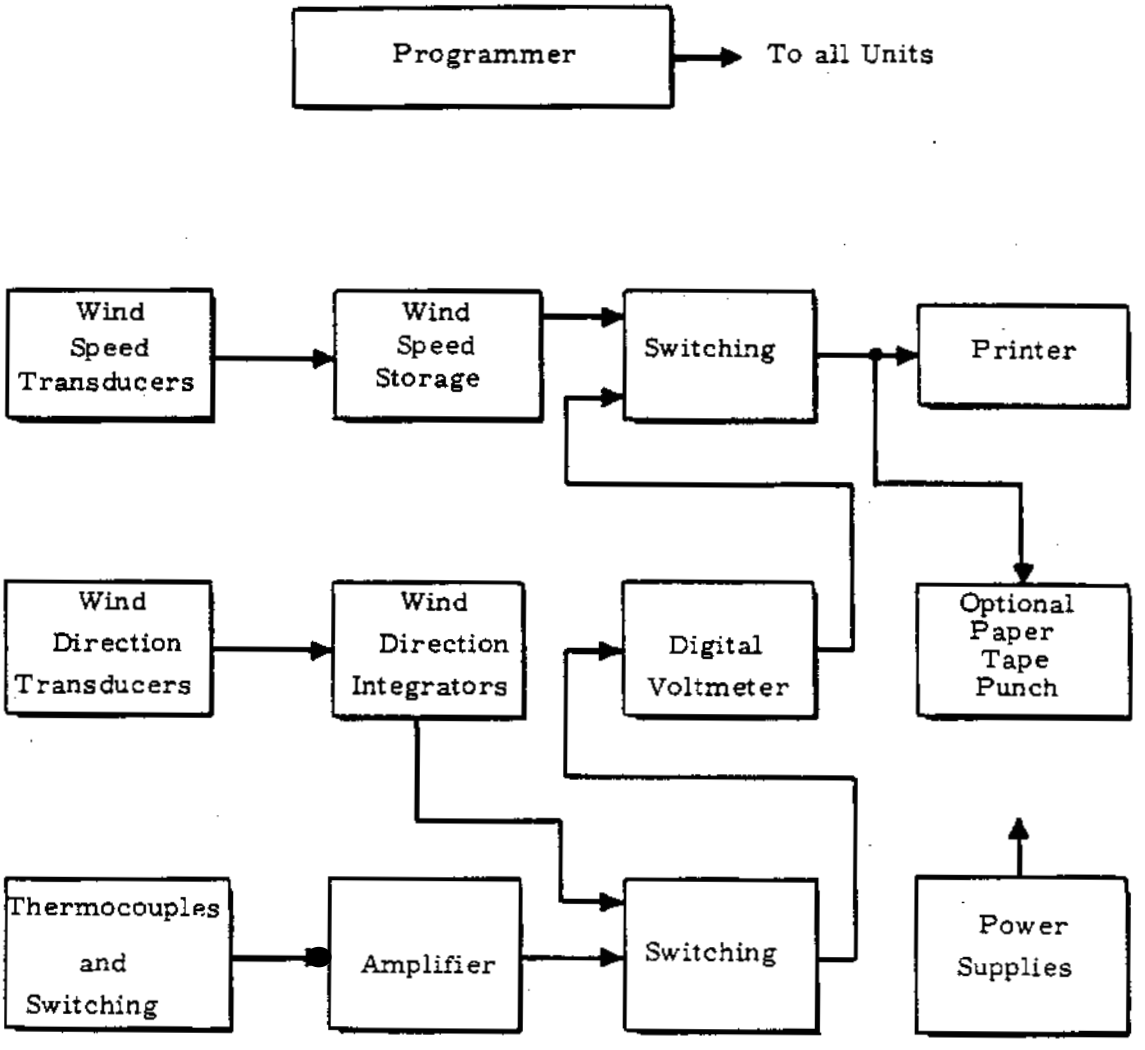

FIGURE 5.1
Automatic Data System for Atmospheric Physics Studies

Phosphorescent Particle Detection Instrument- M. O. Rankin

Many air diffusion and wind transport experiments using ZnS as tracer material have been conducted [5.1] to study the transport mechanisms of radioactive particles in the atmosphere. Presently, the method of measuring the concentration of the dispersed plume at various points is accomplished by filter-collecting the ZnS for a predetermined time and then analyzing the filter by developed laboratory procedures.[5.2, 5.3] From this information, instantaneous concentrations can only be estimated; therefore, to further these studies a method was developed to measure and record the instantaneous airborne concentrations of ZnS. Through data interpretation, the arrival time of the plume and the integrated quantity of ZnS that has passed the detector can be calculated.

The experimental phosphorescent particle detection instrument which has been extensively field tested, consists of an ultraviolet lamp, mechanical light trap, multiplier phototube, high voltage supply, amplifier, recorder, power supply, and vacuum pump. A block diagram is shown in Figure 5.2. In operation, the airborne ZnS is drawn at a 2.5 cfm rate into the chamber which contains the ultraviolet light, through the light trap, and then across the face of the multiplier phototube. The phosphorescence of the ZnS as it passes the detector produces an increase in the multiplier phototube output current which is proportional to the airborne concentration of ZnS. This signal level is amplified and recorded.

To calibrate the instrument, membrane filters were used to sample the air simultaneously with the real-time sampler in actual field tests. This work measured the total mass of ZnS which passed the detector. The area under the curve of the chart from the prototype instrument was then measured. The sensitivity was determined as approximatley 3×10^{-8} g/ft^3. In a number of field experiments, the instrument has been used successfully at distances up to 3 miles from the point of dispersal.

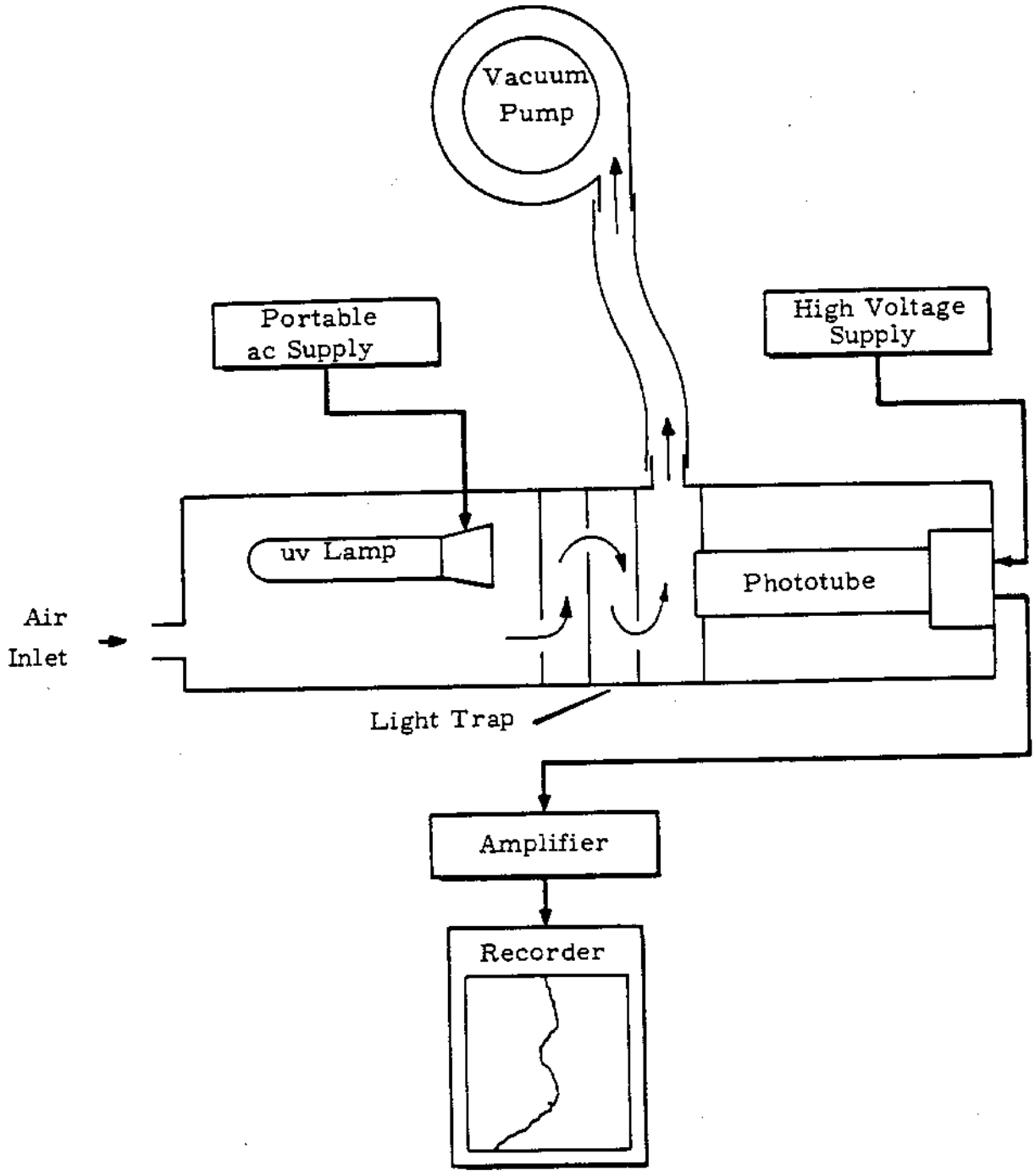

FIGURE 5.2
Phosphorescent Particle Detection Instrument

Protective Clothing Monitoring System - M. O. Rankin and W. G. Spear

Protective clothing is used at Hanford to provide a control method for spread of alpha and beta-gamma contamination. Past procedure, following garment washing, was to laboriously hand-survey all clothing with two types of radiation detection instruments. This work was done for approximately 30,000 laboratory coats and coveralls per month. To improve monitoring efficiency and control, complete automation of this operation was desired. An instrument system was developed which uses eight alpha and seven beta-gamma scintillation large-area detectors, a garment conveyor, solid state circuitry, and appropriate signal and control devices. In operation, laundered garments are placed on hangers and then conveyed past the detectors for beta-gamma and alpha contamination monitoring. Contaminated garments are rejected and dropped into a special container if spot contamination exceeds 1000 dis/min of alpha or 5000 dis/min of mixed fission products. The acceptable garments pass through the system for folding and distribution. The system, which requires only one attendant, can effectively monitor 500 garments per standard shift. System operation has been fully successful for 3 months.

An automatic conveyor-type laundry monitoring system, which monitors laboratory coats and coveralls simultaneously for both alpha and beta-gamma contamination, was developed and installed at the Hanford Laundry Facility to improve efficiency and monitoring control. The monitor, shown in Figure 5.3, consists of the 34-ft monoplane conveyor system with a speed of about 4 ft/min, two electro-mechanical reject stations, a mechanical unload station, two detector stations, an electronic console with the incorporated alarm circuitry, and a motor-driven loader.

Beta-Gamma Detection and Measurement

Mixed fission product radionuclides were considered as possible beta-gamma contaminants with average beta energies ranging from 0.07 Mev to 0.99 Mev.[5.4, 5.5] A 0.125-in. thick terphenyl-in-polyvinyltoluene organic scintillator was determined by calculation and previous experiments[5.6, 5.7, 5.8] to provide the best sensitivity for beta detection. In the monitoring system, six 5-in. diameter magnetically-shielded photomultiplier tubes are

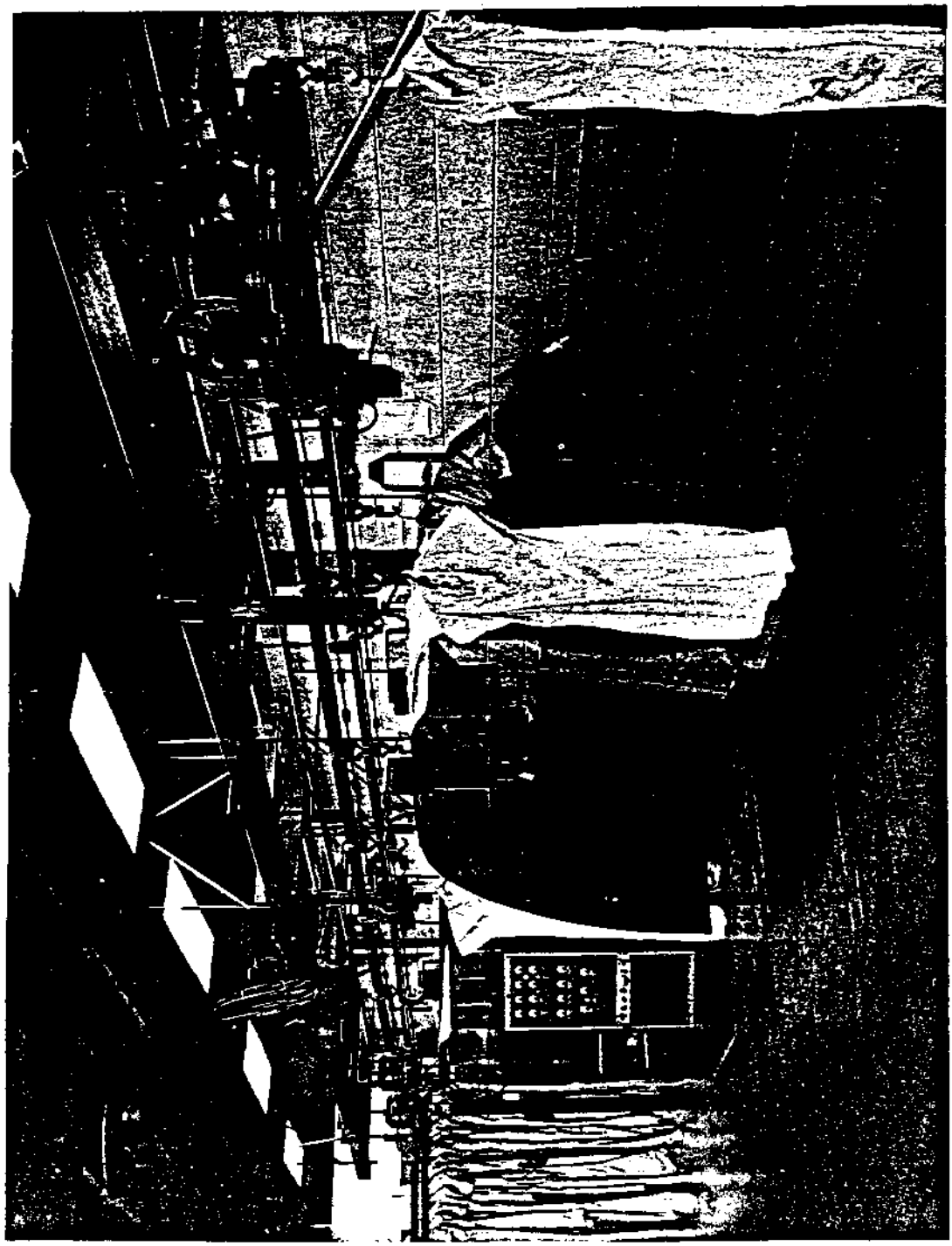

FIGURE 5.3
Protective Clothing Monitoring System

used for beta-gamma detection; the scintillators are covered with two layers of 0.9 mg/cm^2 aluminized Mylar. A seventh probe, fabricated in the same manner, is used to continuously monitor the changing gamma background in the room. The six probes effectively monitor a 5 by 30-in. area through a screened opening in a curved aluminum table.

Output pulses from each beta-gamma probe drive an emitter follower, and output pulses from each pair of emitter followers are combined to drive a six-stage amplifier. The amplifier drives a multirange count rate meter. The gross counting rate of each channel, displayed on a console meter relay, has the gross counting rate of the gamma background channel electronically subtracted, and the net difference for each channel is also console meter displayed. By using this background subtraction, low-level garment beta-gamma contamination can be easily detected in the presence of moderate and varying gamma fields. By adjusting the background subtraction circuit, the system can detect mixed fission product spot contamination of approximately 1000 counts/min or 5000 dis/min.

Alpha Detection and Measurement

The alpha channels use eight detectors, four at each of two stations, for monitoring both sides of the garment. The four detectors at each station are also mounted in a staggered pattern to assure coverage of an effective 8 by 30-in. area. Each detector assembly consists of an aluminum can, an 8 x 8 x 1/16-in. Lucite plate covered with silver-activated ZnS as a detector, an emitter follower, and a 5-in. diameter photomultiplier tube with a magnetic shield. The ZnS covered Lucite is attached to the top of the can and covered with one layer of 0.2 mg/cm^2 aluminum Dutch leaf and one layer of 0.9 mg/cm^2 double aluminized Mylar. Counting efficiency was measured to be about 25% at the detector center and about 20% at the edges for a 1000 dis/min Pu^{239} source placed on the metal-mesh protective screen.

Garments are conveyor-transported over four alpha detectors at Station 1 and then turned 180 degrees and transported over four more alpha

detectors at Station 2. Pulses from each of the detector assemblies are amplified to drive eight scaling circuits, which drive the associated meter relays. The scalers are automatically reset to zero every 15 sec by a motor-driven, cam-operated microswitch which actuates the reset circuits. During this 15 sec interval, the garment travels approximately 1 ft; and, if the alpha contamination in this monitored area produces more than seven scaler counts, the unit will alarm and the garment will be rejected. Alpha contamination producing a counting rate of greater than 400 counts/min can conceivably cause incorrect scaling; therefore, a single high-level rate alarm for each station was also incorporated. The double-alarming approach is a safety feature.

Mechanical Operation

In operation, the garments are manually placed on specially designed clothes hangers and attached to the automatic loader. Each garment is then automatically loaded singly onto the continuously moving conveyor hooks which are programmed to:

(1) Sequentially index garment 90 degrees
(2) Pull each garment over the beta-gamma and alpha detectors mounted at the first station
(3) Index garment 90 degrees
(4) Draw garment through the first reject station where contaminated garments are dropped automatically
(5) Index acceptable garments 90 degrees
(6) Pull garment over a second set of alpha detectors to survey the opposite side
(7) Index garment 270 degrees
(8) Draw garment through the second reject station where alpha contaminated garments are dropped automatically
(9) Advance the nonrejected garments to be automatically dropped onto a table for folding by the attendant
(10) Index hook 180 degrees for a new loading.

At the alpha stations, the garment is drawn between four screened alpha detectors and four large brushes which smooth out the garments and push them firmly, but gently, against the alpha detector faces to obtain good counting efficiency.

Sequentially operating microswitches and relays at the monitoring, reject, and regular drop stations provide the necessary automatic selectivity for rejecting contaminated garments, which are removed from the conveyor at the reject stations. A solenoid-operated reject device, controlled by a relay in the alarm circuit and by a cam-operated microswitch, is energized to cause rejection. Nonrejected garments are conveyed to the normal drop mechanism which consists only of a free-swinging arm which engages with the loaded hanger and lifts it off the conveyor hook to drop it onto a table for folding.

The system has been in continuous operation of two shifts per day since October, 1962. No malfunctioning has occurred and performance has been satisfactory. One operator can easily load the garments and then fold the acceptable garments after monitoring is complete. A considerable savings in manpower has been obtained, and the contaminated garment reject rate has increased to 4%; whereas, hand-monitoring methods showed a reject rate of about 2%.

General Radiological Monitoring and Circuit Development

Liquid Effluent Monitoring - E. M. Sheen

Control of radioactive wastes in liquid form requires sensitive monitoring instrumentation. Development was carried out on such a monitor for use with gamma-emitting radionuclides. The instrument, which uses an organic scintillator, transistor circuitry, and a four decade logarithmic response count rate meter, was developed to monitor the desired range from about 10^{-5} gamma μc/ml to 10^{-1} gamma μc/ml. The count-rate circuit extends from 10^2 to 10^6 counts/min, and the detector scintillator is a 3-in. diameter by 3-in. long cylinder of terphenyl-in-polyvinyltoluene. The multiplier phototube anode is capacitively coupled to the pulse amplifying and counting

instrumentation and is also directly coupled to alarm-trip circuitry. This method provides a sensitive pulse counting system capable of maintaining the alarm at very high count-rates. All circuitry is solid state for reliable, long-term, low power operation.

The experimental monitor for gamma-emitting radionuclides in liquid effluents includes a scintillation detection probe, preamplifier, pulse amplifier, and a sensitive direct current trip circuit. Amplifier output voltage pulses drive a four decade logarithmic response count rate circuit that includes a pulse threshold detector, binary, diode pump driver, and six diode pumps. The diode pump dc output is amplified, metered, and connected to two dc transistor-relay trip circuits. Trip-circuit reference adjustment is made from the front panel as shown by the main instrument photograph in Figure 5.4.

A 3-in. x 3-in. cylinder of terphenyl-in-polyvinyltoluene scintillator was used to provide adequate sensitivity, assuming a large source volume. The scintillator was optically coupled to an EMI/US 9536-B multiplier phototube. Pulses resulting from detected gammas are coupled to the input of the preamplifier circuit shown in Figure 5.5. Current through the phototube dynode high voltage resistance divider network is approximately 1 mamp, and this also provides power for the transistor preamplifier.[5.9] Signal voltage pulses from the transistor emitter are capacitor-coupled to the high voltage coaxial cable.

Multiplier phototube anode dc is cabled to the trip circuit which was used to prevent possible malfunctioning at extremely high radiation exposure levels and consequent high counting rates.

Preamplifier output pulses are coupled by the high voltage cable to the main amplifier input. The amplifier consists of two transistor feedback pairs as shown in Figure 5.6. Voltage gain of the amplifier is adjustable from 18 to 330, as required, by use of the gain potentiometer. With the described probe, the amplifier output pulses are 0 to -4 v and about 0.5 usec in width.

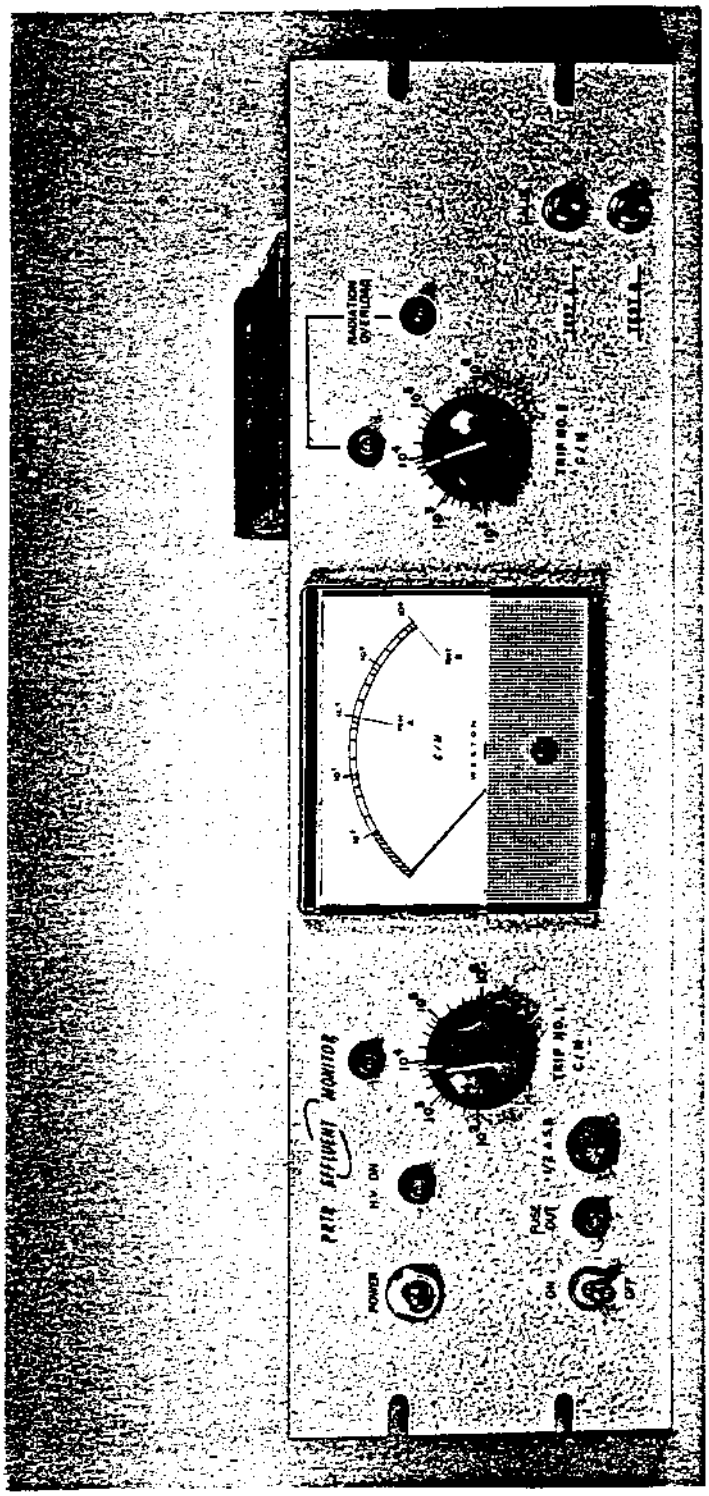

FIGURE 5.4
Liquid Effluent Monitor

Noise-caused pulses are discriminated by the threshold detector circuit also shown in Figure 5.6. Negative input pulses, larger than the threshold voltage, switch Q1 and Q2 off to provide -6 v output pulses. These pulses drive a transistor binary circuit. Transistors Q3 and Q4 form the diode pump driver. The full scale count-rate is adjusted by the calibrated input voltage from 0 to -15 vdc. The diode pump network is a slight modification of a previous circuit.[5.10] A combination of six diode pumps are used to provide four decade coverage from 10^2 to 10^5 counts/min input with 50 to 250 mv output. The prototype instrument accuracy was ±10% of the count rate reading and changed less than ±10% from 20 F to 120 F with the temperature compensation network shown. The count rate output time constant varies from approximately 15 to 1.5 sec for 10^2 to 10^6 counts/min, respectively.

Output voltage from the diode pumps is amplified by a solid state operational amplifier connected to provide 0 to 5 vdc output and sufficient current to operate a 500 μamp meter and two 0 to 5 vdc trip circuits. The trip circuit consists of a transistor voltage comparator driving two saturating transistor switches. Regenerative feedback is used to the reference input to cause positive tripping action with approximately 0.5% hystersis. A high-level trip circuit is provided which operates directly from the phototube anode dc level. This method avoids using the pulse counting circuitry to provide a reliable system for the more important trip level. A meter may be provided for this circuit as shown in Figure 5.6. The meter full scale linear indication is adjusted to be within the desired range about one decade above the limit of the ratemeter indication.

Two prototype instruments were operated for approximately 6 mo each without failure or drift. One prototype was calibrated with a 90 liter Cs^{137} source in water to simulate operational conditions. The instrument gain and threshold levels were adjusted to permit detection to 200 kev gammas. A Cs^{137} source of 10^{-5} μc/ml was detectable above background, and 10^{-4} μc/ml produced 4×10^4 counts/min above background.

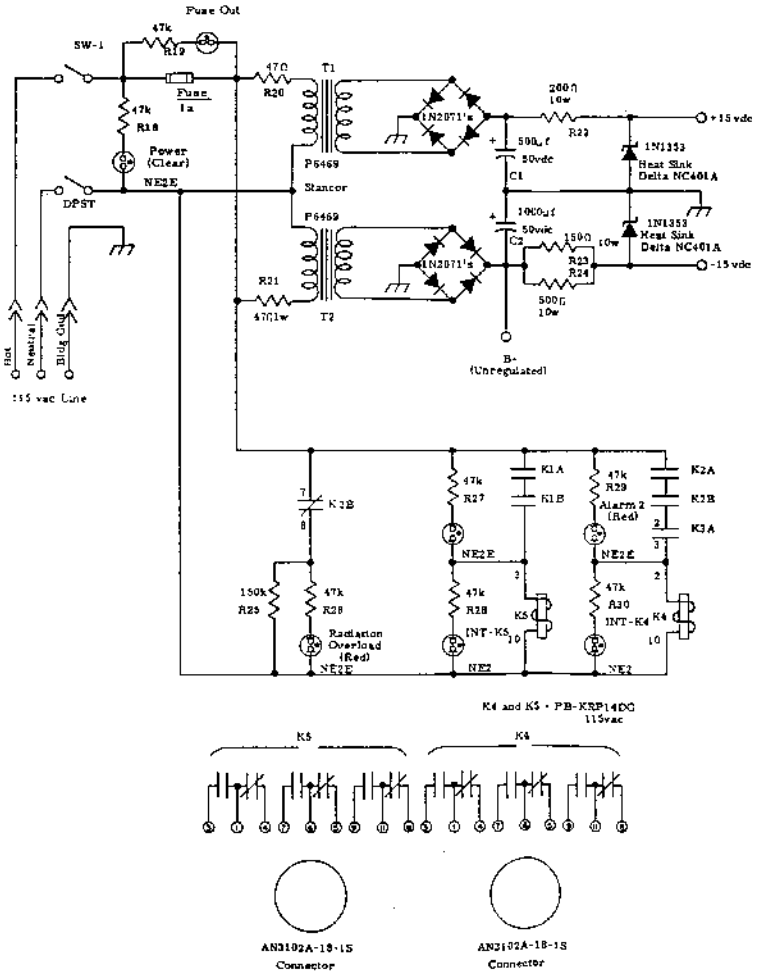

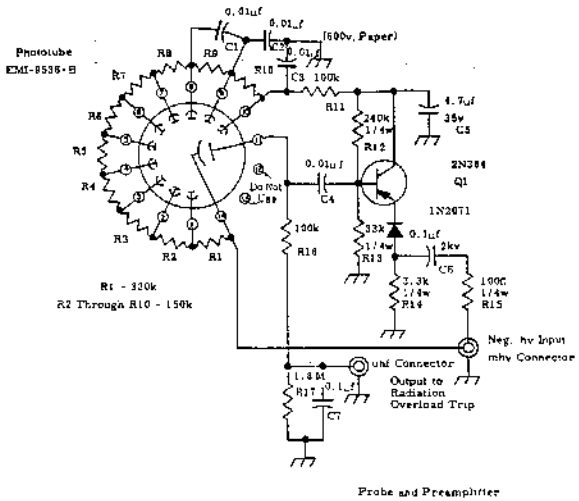

FIGURE 5.5

Power Supply and Preamplifier of Liquid Effluent Monitor

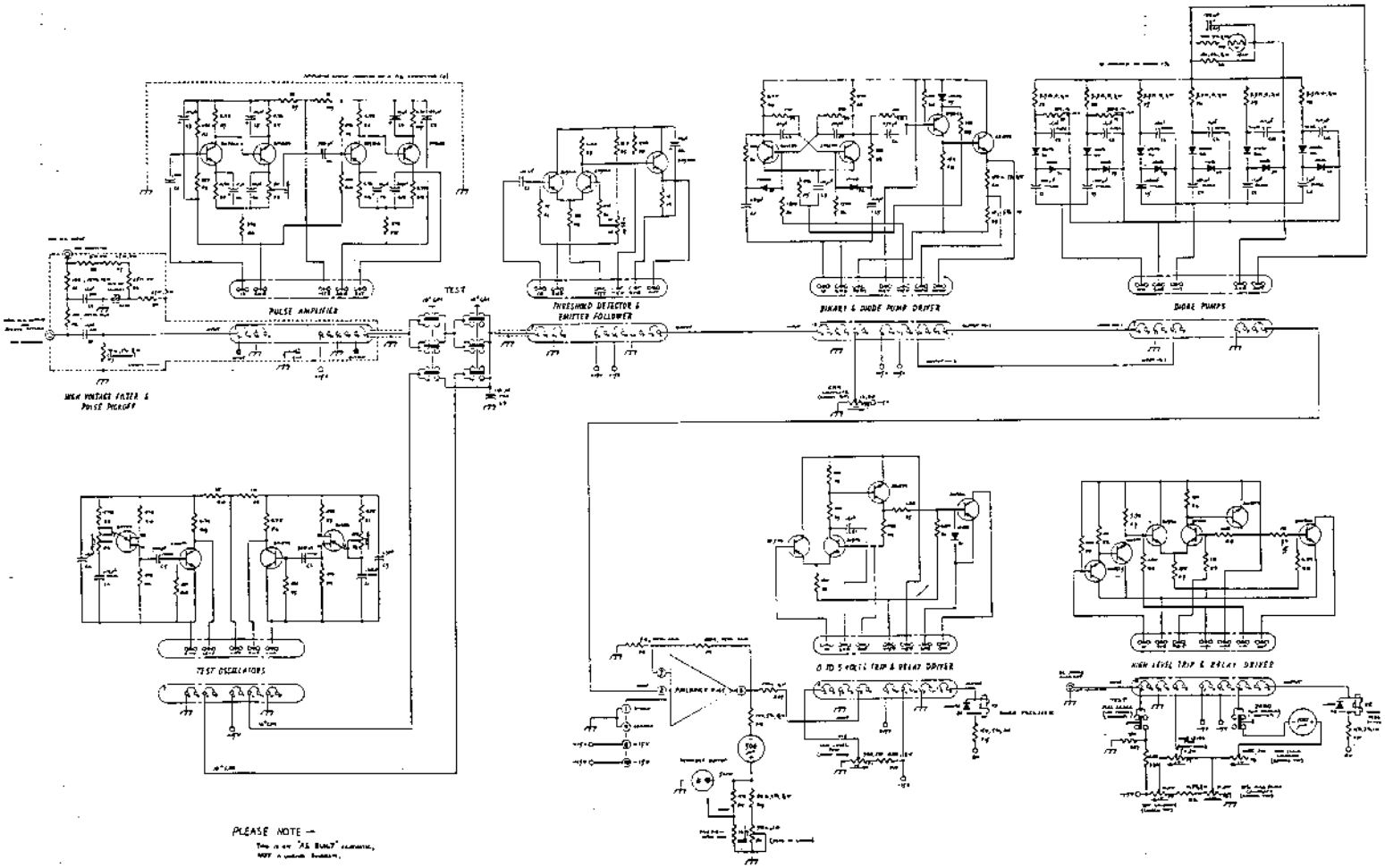

FIGURE 5.6
PRTR Logarithmic Effluent Monitor

Portable Radiation Survey Instrument - E. M. Sheen and W. G. Spear

In the usual radiation monitoring practice with portable instruments, three separate and distinct instruments are employed for alpha, beta-gamma, and neutron detection and measurement. In addition, most portable instruments require the use of headphones for low-level work and require periodic replacement of batteries. To circumvent these problems and to provide a reliable, solid-state, multipurpose instrument, development was carried out to provide both aural and meter indication, recharging ability for the battery, and the ability to employ, as required, different detection probes for alpha, beta-gamma, and neutron measurements.

The portable radiation survey instrument, shown schematically in Figure 5.7, is a considerably improved version of a previous instrument,[5.11, 5.12] which incorporated only the single transistor high voltage supply and the count-rate-meter circuit.

The pulse amplifier is a two-transistor feedback pair with the base bias resistors bootstrapped to the summing point to obtain high input resistance.[5.13, 5.14] An output potentiometer provides the necessary gain control. Output pulses from the amplifier are coupled to a two-transistor, count-rate circuit which provides three ranges of 10^2, 10^3, and 10^4 counts/min full scale on the 100 μ amp meter. The first transistor of the count-rate circuit also triggers a tone generator circuit to provide a loud aural output.[5.15] The speaker unit is of weather-proof construction. The aural output is sufficiently loud to be heard in most work locations; additionally, provision is made for headphone incorporation for survey work under extremely high ambient noise conditions.

The recharging circuit, which is not contained in the portable instrument, is a simple 110 vac to 12 vdc converter and is normally mains-connected at all times. To recharge the survey meter, it is simply inserted in the converter holder where automatic contact is made and recharging takes place.

The survey meter will operate 60 hr continuously from one full charge on the nickel-cadmium battery. Tests have shown correct performance can be obtained from -10 F to +130 F. The weight is about 4 lb and the size is 5 in. by 7 in. by 4 in.

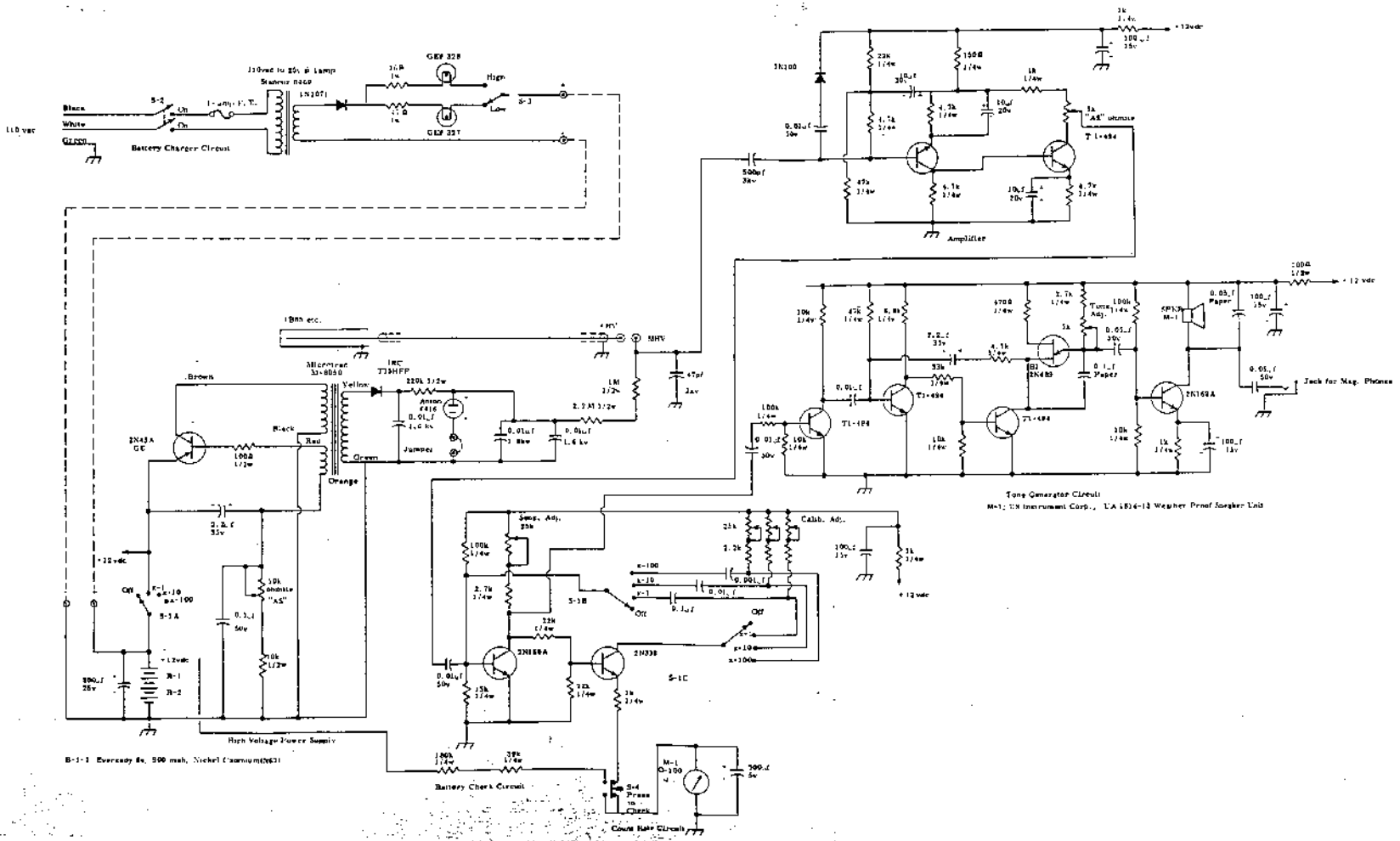

FIGURE 5.7
Portable Radiation Survey Meter

Figure 5.8 is a photograph of the instrument inserted in the automatic recharging unit. Also shown are several of the detector probes normally employed. The standard 1B85 GM probe is connected to the instrument with the coiled cord; next to it is a high level GM probe which contains a miniature halogen-quenched GM tube and a voltage divider to provide 400 vdc. The larger probe is a scintillation alpha detection probe [5.16] which has a nominal 20% counting efficiency and 2-in. x 4-in. effective area. In addition, scintillation thermal and fast neutron detection probes can be directly used with the instrument, and BF_3 proportional counters may also be used providing the counter plateau is within the limits of the instrument high voltage supply.

Tests of the instrument have been fully satisfactory and reliability is assured.

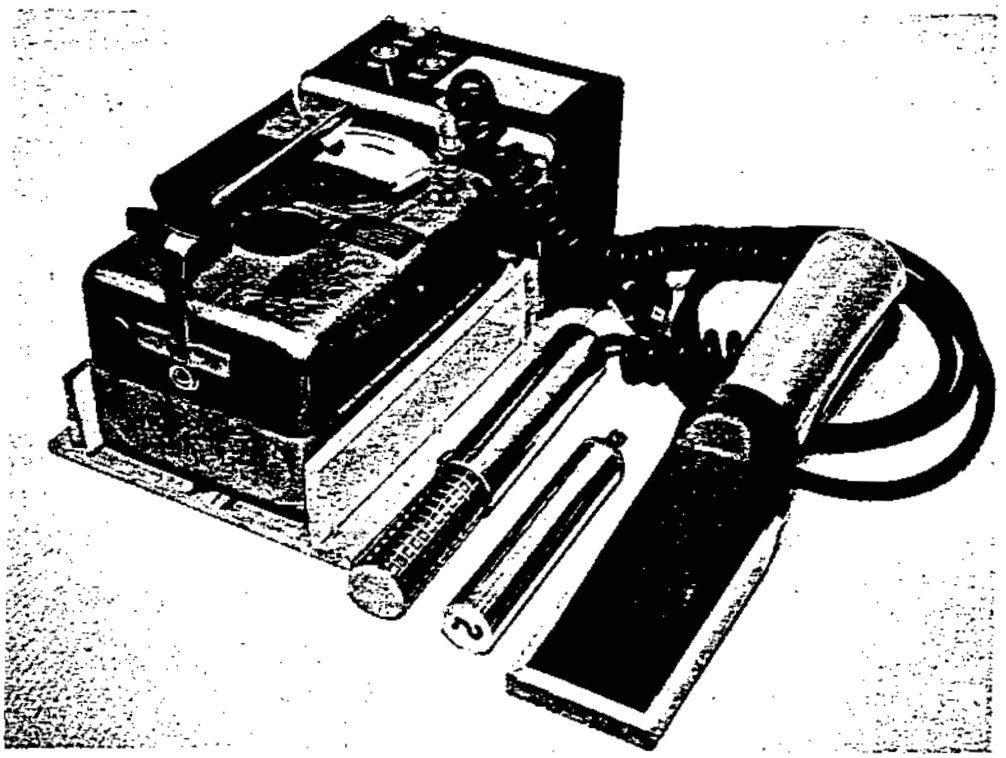

FIGURE 5.8

Portable Radiation Instrument, Recharger, and Typical Detector Probes

Area Radiation Monitor Development - W. G. Spear

Area or building radiation monitoring requirements are of two categories of the general, all-purpose type and of the specific application type. In addition, in the interests of efficiency, compatibility, and direct data conversion, it is appropriate that instrument readings of dose rate be the same whether obtained from a portable, hand-carried instrument or from a line-operated unit. Development work was carried out on two line-operated monitors and on one combination portable and line-operated type. An experimental scintillation, solid-state circuitry, logarithmic response instrument was completed and tested which provides range coverage from about 1 mr/hr to 1000 r/hr. In essence, five or 6 decade coverage in a logarithmic response fashion is attainable. A second, companion instrument was completed, quite similar to the foregoing, wherein any four consecutive decades over the range from 0.5 mr/hr to 500 r/hr may be covered in both multidecade linear and logarithmic response fashions as desired. Partial development was done regarding a small combination portable and/or line operated dose rate instrument which can cover the range from 1 mr/hr to 10 r/hr in a logarithmic response fashion and which will use a rechargeable battery.

Development work has resulted in the establishment of two prototype, line-operated, scintillation dose rate monitors suitable for stable, reliable gamma dose rate measurements from less than 1 mr/hr to 1000 r/hr as required by the particular application. In addition, the logarithmic response characteristic of particular multiplier phototubes was utilized to provide a method of using a portable type dose rate meter for direct line operation.

The two experimental direct line-operated area monitors were completed and tested for performance under conditions of line voltage fluctuations, line transients, vibration, temperature, accuracy, drift, and detector aging. Each instrument employs a stable EMI/US-9536-B phototube and a suitably-sized terphenyl-in-polyvinyltoluene scintillator in the detector probe. The phototube is operated in a direct current mode, as a high impedance current source, to directly drive, from the anode, the single interconnecting shielded cable which may be 1000 ft long. Both instruments employ

an electromechanical chopper, operated at about 100 cycles/sec, to convert the phototube output dc which is directly proportional to the gamma dose rate in which the probe is operated, to an ac signal. The ac signal is then amplified by solid state feedback amplifiers which provide a voltage gain of 20,000; the resultant signal drives a diode pump circuit to provide a proportionate high level dc signal which is used to drive the indicating meter, a chart recorder, and signaling circuits. The signaling circuits are solid state, fail-safe, with normally closed relays, which can be operator-set to provide a visual and audible signal whenever the dose rate exceeds the adjusted, desired, alarm-trip point. No meter-relays were employed since exhaustive evaluation tests showed that the developed solid state alarm-trip circuits were considerably more reliable under adverse vibration conditions than were commercially-available meter-relays. System calibration is accomplished by varying the high voltage applied to the phototube for either the required logarithmic response or the selectable linear ranges of the truments.

Figure 5.9 shows the complete circuit diagram for the experimental Mark III logarithmic response area radiation monitor. The general operation was covered in the preceding paragraphs; however, a number of features can be described. The scintillator normally used is a 2-in. by 2-in. cylinder of terphenyl-in-polyvinytoluene covered by aluminized Mylar as a light reflector and shield. The logarithmic response characteristic is obtained using a heater-power and reverse bias controlled 9004 diode. Both high and low synthetic signal inputs are available for general electronic circuitry performance checks. Two fully-adjustable signal or alarm-point trip circuits are used, and an automatic meter scale switching circuit is used to provide up to six decades of log response. On the low or sensitive scale position, a relatively high voltage is used on the phototube and the meter scale extends, for example, from 1mr/hr to 1 r/hr. If the dose rate level increases to 1 r/hr, automatic switching occurs to provide, at a considerably lower high voltage to the probe, three more decades from 1 r/hr to 1000 r/hr; thus, in total, six full decades are obtained. The appropriate meter scale is

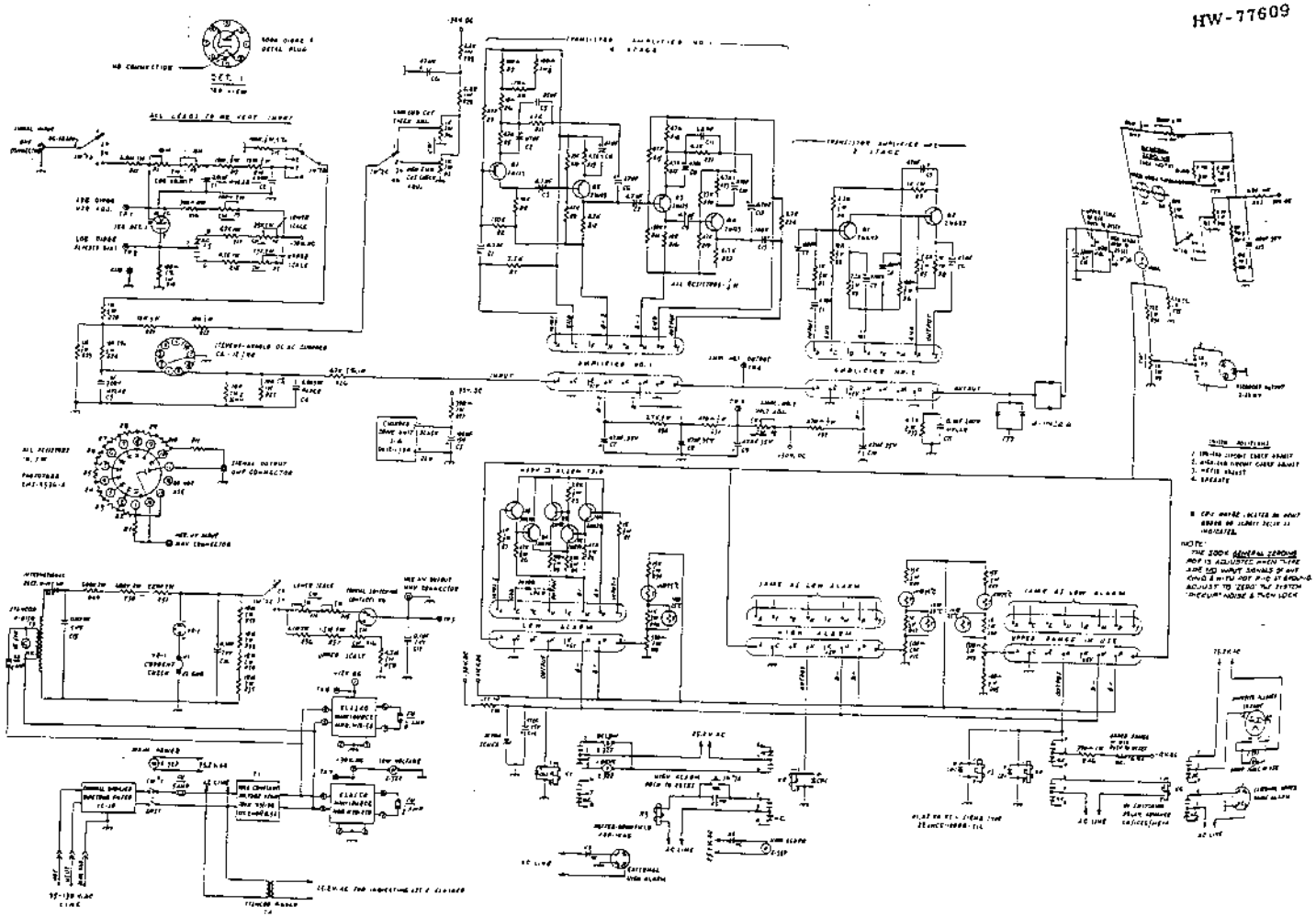

FIGURE 5.9

Mark III Scintillation Area Monitor

used in each case, and the recorder output is switched so the employed dual-pen recorder accurately follows the situation. The upper scale is latched-in, so manual reset is used to return to the sensitive scale. Actual log-scale reading errors are less than ±15% over the full six decades. If only three decades are required for a particular application, the instrument complexity can be reduced considerably.

Figure 5.10 shows the schematic for the experimental Mark II combined logarithmic and multirange linear response area radiation monitor. The general operation and performance is quite similar to that described for the Mark III logarithmic response only monitor except that, by selective switching, four separate single decade linear operational ranges may be used in addition to a single logarithmic response range covering the same four decades. This approach provides more versatility than does the logarithmic response only type. In the combination instrument, no automatic scale switching for the log coverage is needed since no more than four decades are covered. Log range performance reading accuracy remains at ±15% for any reading. The accuracy of the linear ranges is essentially limited by the accuracy of the meter employed; however, typically, the accuracy is ±2% of full scale on any linear range.

Performance tests completed on both experimental instruments indicated correct operation could be achieved for line voltages from 100 vac to 130 vac, for temperatures from 0 to + 55 C, and for considerable vibration conditions. Typical phototube anode currents vary from 10^{-9} amp at a dose rate of 1 mr/hr to 10^{-5} amp at a dose rate of 10 r/hr for the four decade combination logarithmic and linear response. For the six decade logarithmic response unit, the sensitive scale or lower three decades involves anode currents of 10^{-9} to 10^{-6} amp; and, similarly, since the high voltage is automatically switched to a lower value on the upper scale, the top three decades require the same current ranging. The anode current noise level of the EMI/US-9536-B phototubes is only 10^{-10} amp or less at the high voltages

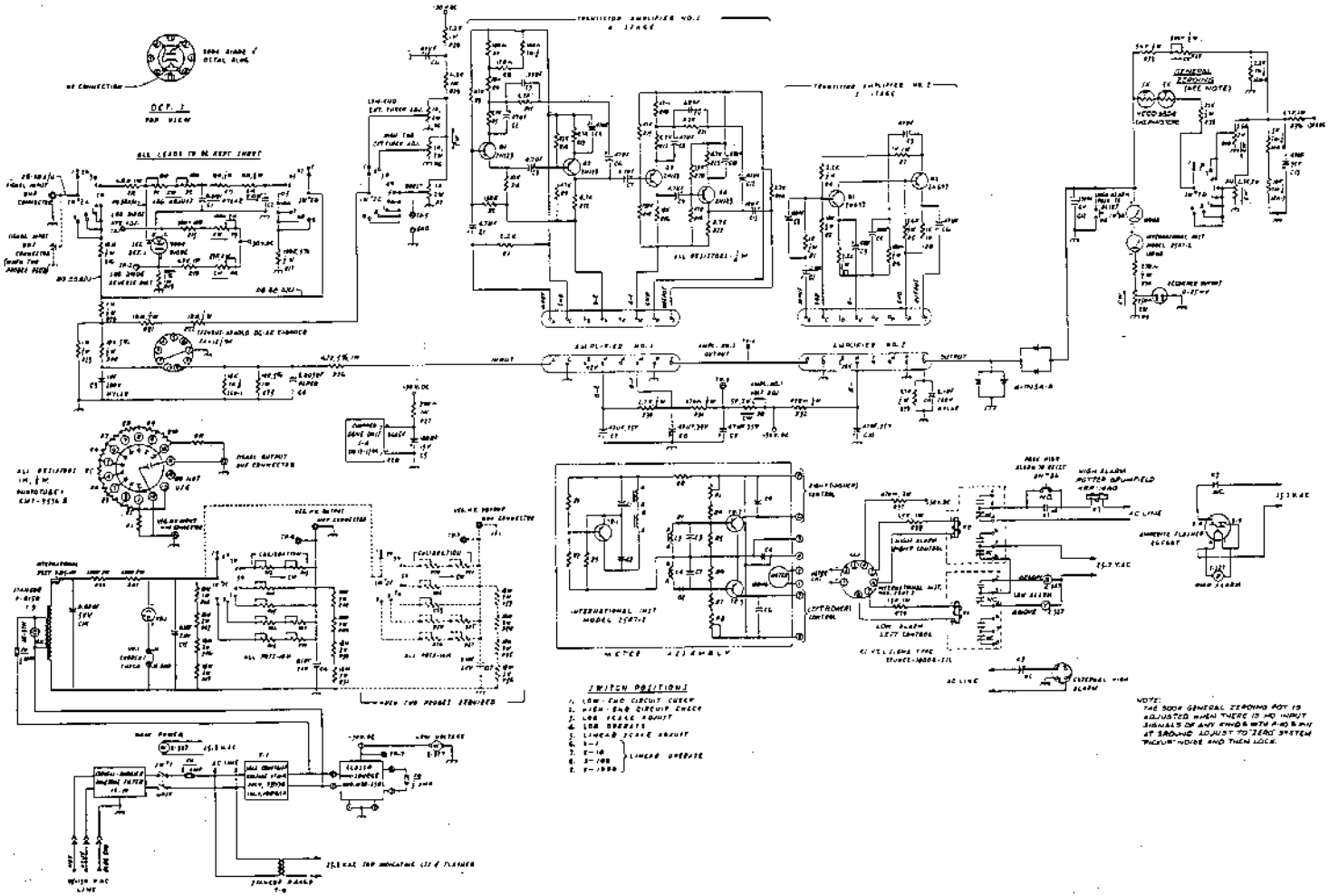

FIGURE 5.10

Mark II Combined Logarithmic
and Multirange Linear Response Area Radiation Monitor

employed, and 4 months of constant operation of the probe in a dose rate field to provide 5×10^{-6} amp of current showed that no degradation of performance occurred. In addition, the experimental logarithmic response instrument was operated 6 continuous months with no measureable change in performance.

Figure 5.11 is a photograph of a logarithmic response instrument and cable-connected detector probe which was calibrated to extend from 1 mr/hr to 500 r/hr, for a total of 5.5 decades, for a particular application. In addition, about 1.5 decades of scale overlapping was calibrated in at the automatic scale-change point to provide thorough, readable coverage in this zone. Except for meter scale variations and the multiposition selector switch, the combination logarithmic and linear response instrument is similar in appearance.

Development work was also carried out late in the year regarding a small specialized dose rate monitor suitable for use as a portable, hand-carried unit and as a line-operated monitor. A rechargeable battery is employed which can be trickle-charged from the line if fixed operation is desired. The instrument utilizes an EMI/US-9536-B phototube, or for higher gain though less stable operation, an RCA 6655-A phototube. A 2-in. x 2-in. cylinder of terphenyl-in-polyvinyltoluene is used as the scintillator. Only five transistors are used, with four forming a stable dc amplifier that controls a modified single transistor oscillator high voltage supply. Since the phototube gain varies with applied high voltage, the circuit being developed is such that the phototube anode output current is held nearly constant, as the dose rate increases, by control of the high voltage applied to the phototube. Tests to date indicate that an excellent logarithmic response, and corresponding meter reading, can be obtained over four decades with preliminary test coverage shown to be feasible from 1 mr/hr to 10 r/hr. Considerable circuit development work remains before final performance data can be obtained.

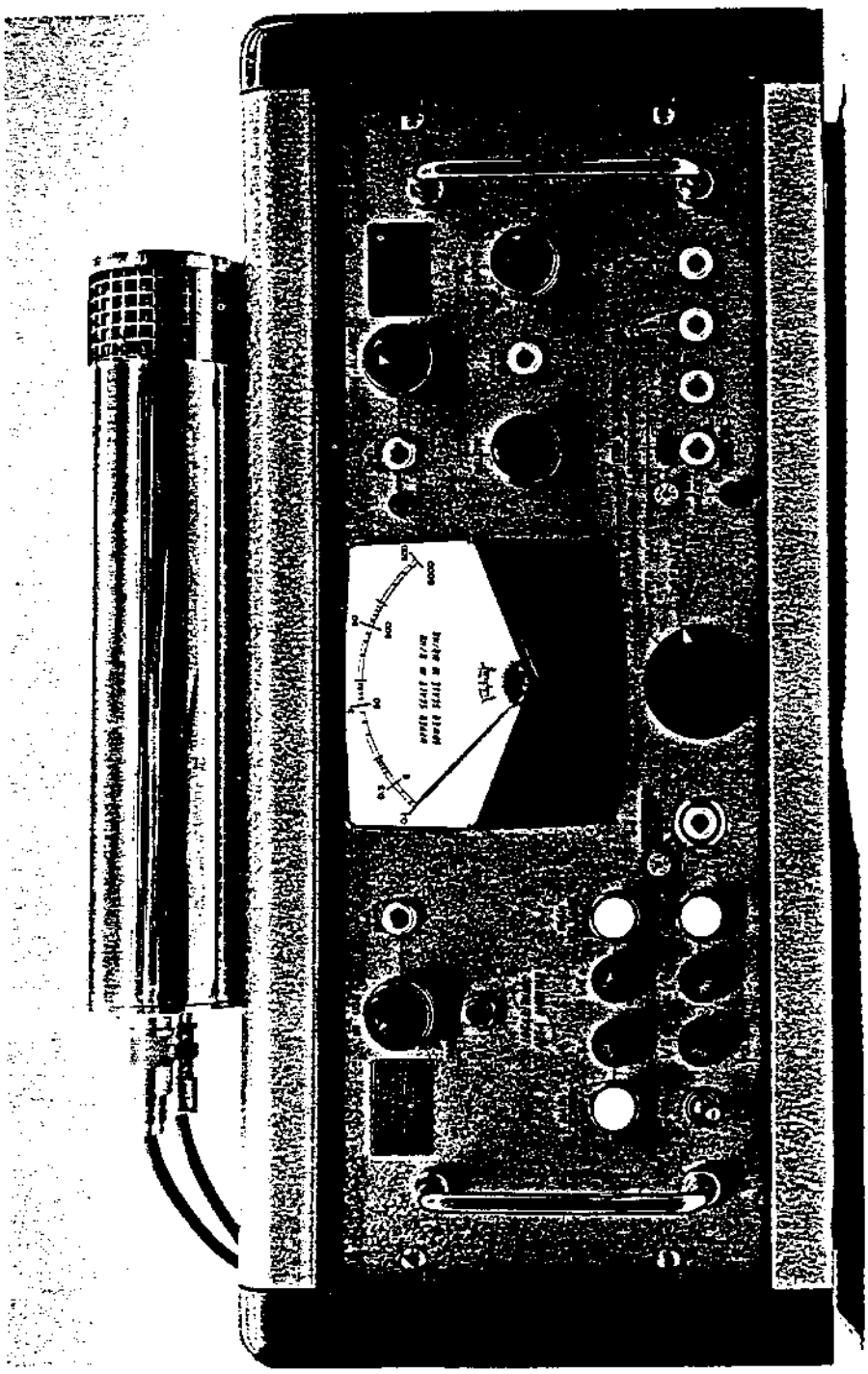

FIGURE 5.11
Mark III Scintillation Area Radiation Monitor

Solid State Scintillation Alpha Instrument - E. M. Sheen and W. G. Spear

Scintillation portable alpha survey instruments, termed "poppies," have been used successfully at Hanford since 1954.(5.17) These instruments use vacuum tube circuits, a multiplier phototube, and a light-shielded, ZnS scintillator. The instrument developed to replace the older units uses the same alpha detection probe but employs a solid state circuit to reduce operating costs through a substantial decrease in battery cost per hour of operation, reduction of maintenance costs, and improvement of reliability.

Figure 5.12 is a circuit diagram of the solid state scintillation alpha instrument excluding the transistorized high voltage supply which has been described previously.(5.18, 5.19)

Alpha particles which pass through the probe light shield of aluminized Mylar (0.9 mg/cm^2) and aluminum Dutch leaf, cause scintillations in the ZnS screen (about 10 mg/cm^2). The scintillation photons then cause photoelectrons to be emitted from the phototube cathode. Amplified output pulses from the anode are coupled to the input of the high input impedance amplifier, which employs transistors Q1 and Q2.

These form a feedback pair with the amount of negative feedback controlled by the 5 kohm potentiometer. The voltage gain can be varied as required. Feedback voltage pulses of negative polarity are developed across resistor R-19 and coupled to the junction of resistors R-20 and R-21. This voltage is approximately equal to the input voltage and raises the input impedance by bootstrap action.(5.20, 5.21) The input impedance is about 100 kohm in parallel with 50 pf. The amplifier output pulse from the collector of Q2 is coupled to the input of a monostable multivibrator, transistors Q3 and Q4. The Q3 output pulse, which is approximately 4 msec wide and 10v in amplitude, is coupled to headphones to aurally indicate the detected alpha particle. Circuit wave forms and quiescent voltages are also shown in Figure 5.12.

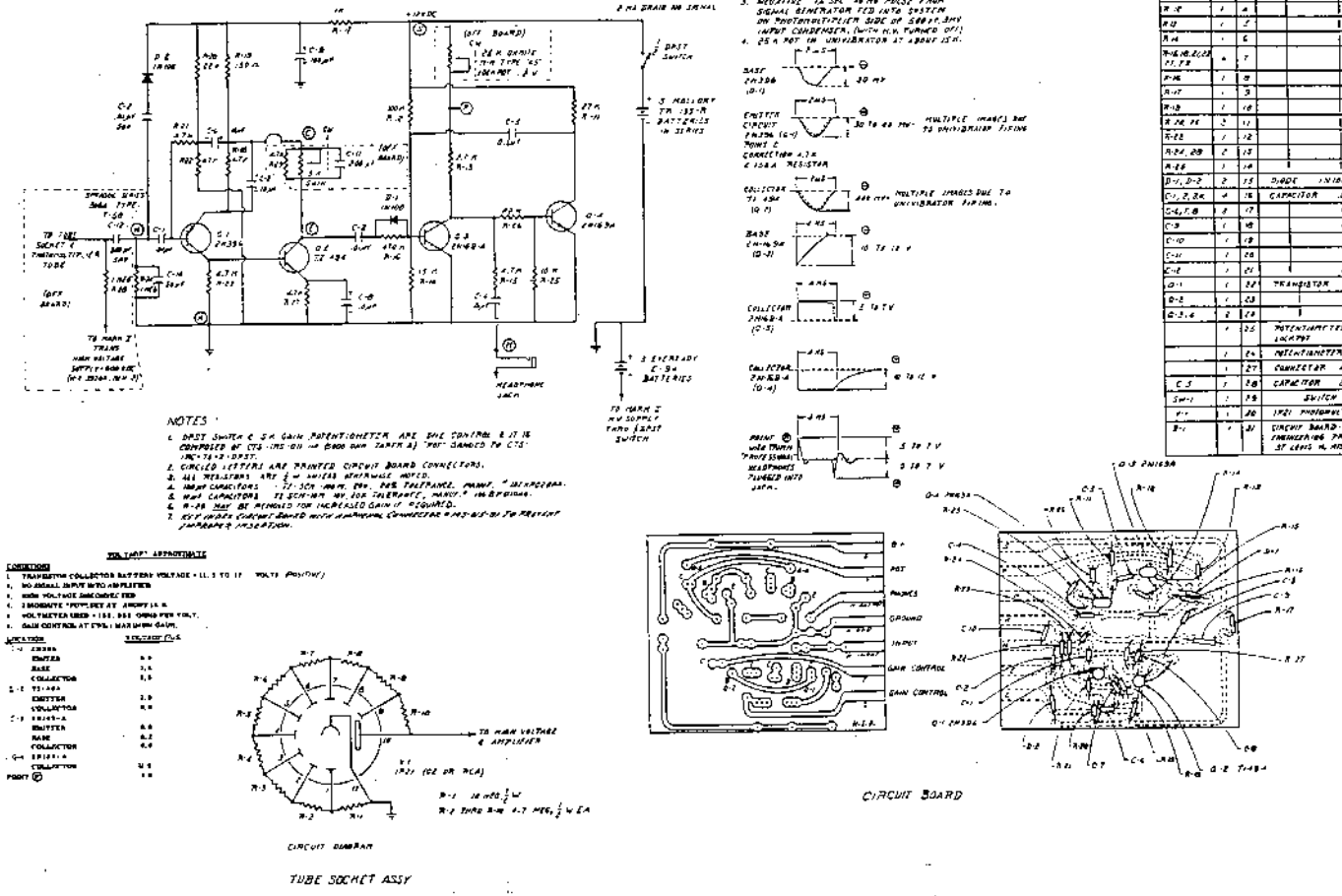

FIGURE 5.12

Solid State Scintillation Alpha Instrument

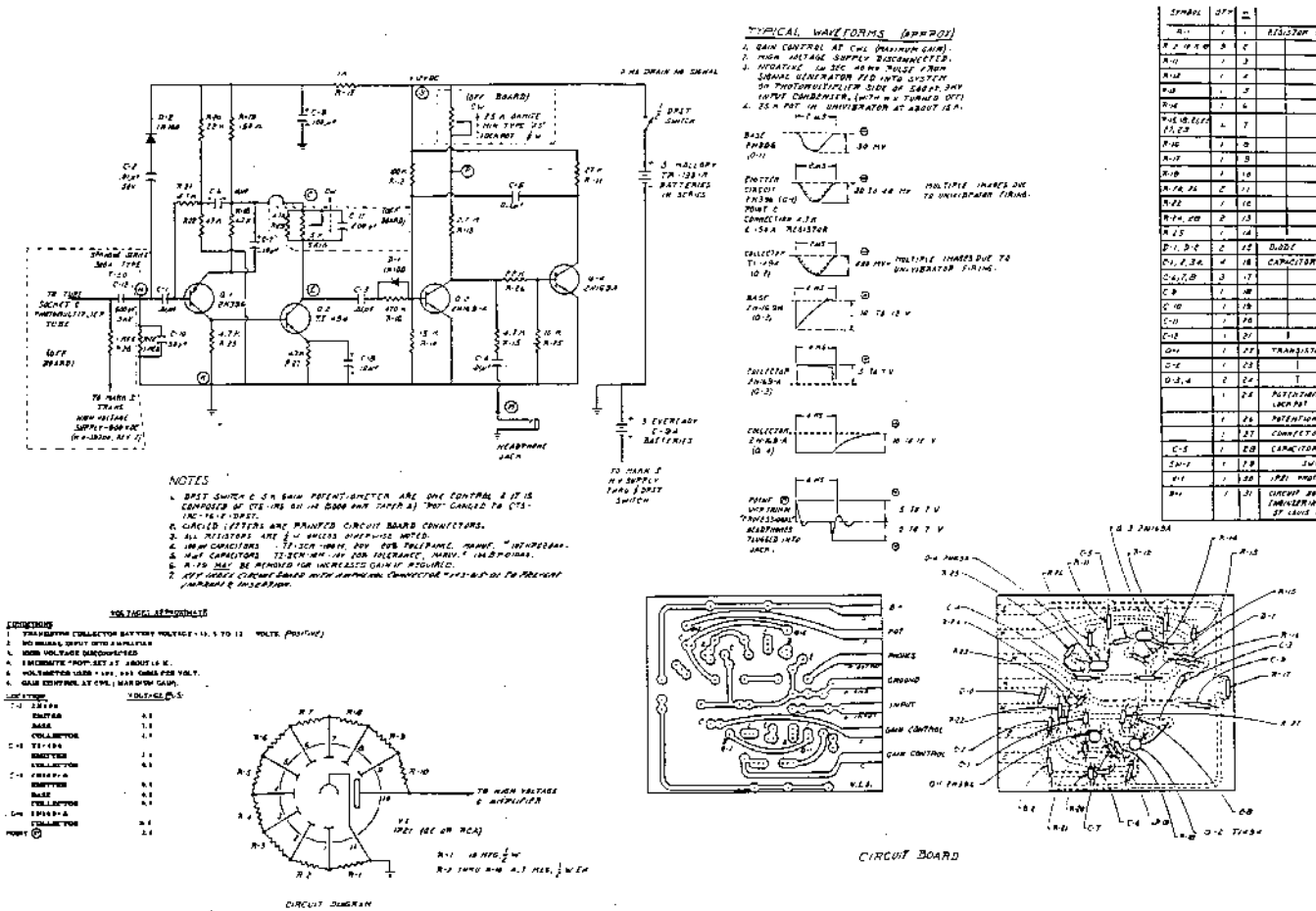

FIGURE 5.12

Solid State Scintillation Alpha Instrument

The developed and tested transistorized alpha instrument weighs 3.3 lb, has a 2-in. x 4-in. alpha-detecting sensitive probe area, and measures 3 in. x 6.8 in. x 4 in. The completed prototype is shown in Figure 5.13. The Pu^{239} alpha detection sensitivity was measured to be about 16% at probe center and 6% to 7% at the corners. The instrument was operated in Ra^{226} fields up to about 8 r/hr. By proper adjustment of the sensitivity control, it was possible to eliminate interference response due to gamma and still maintain an alpha counting efficiency of 12% in the center of the probe. In a fast neutron field of about 400 mrem/hr, with an accompanying gamma field of 80 mr/hr, proper adjustment of the sensitivity control resulted in a background of only 1 count/min and a counting efficiency to Pu^{239} alpha particles of 10% in the center of the probe. In tests, correct operation was obtained from 0 F to +120 F. The constant use battery life of both the old and the new instruments is 120 hr or 2¢/hr for the new unit versus 3.5¢/hr for the older instrument. Thirty of the new instruments have been purchased with fabrication by commercial manufacturers.

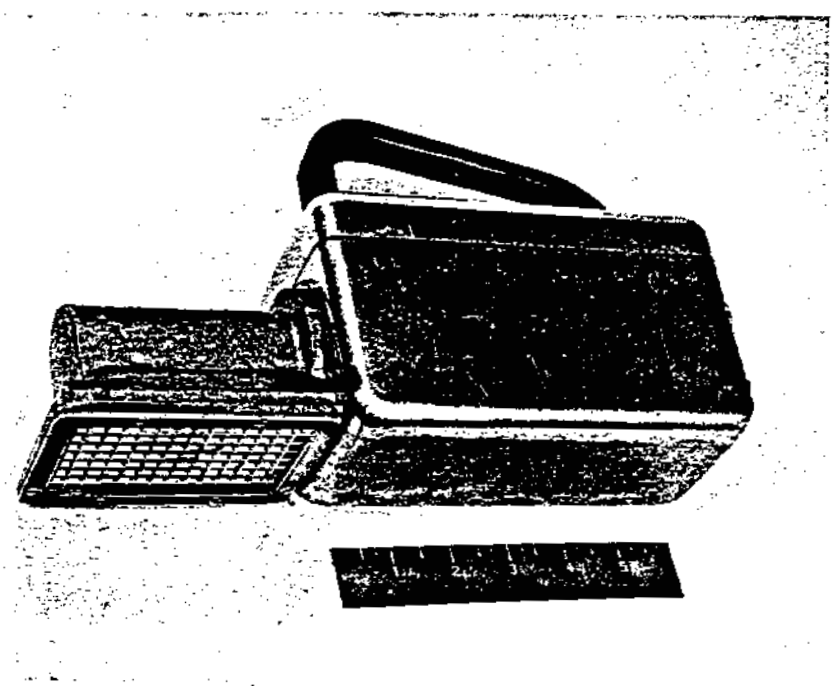

FIGURE 5.13
Solid State Scintillation Alpha Instrument

Dosimetry Instrumentation

Signaling Radiation Dosemeters * - D. P. Brown

Development continued regarding personally-carried, signaling radiation dosemeters which use a recharging type "pencil" ionization-chamber as a sensor and all solid state circuitry. Two basic types of units were experimentally fabricated and tested with both improved sensor action and more compact and versatile circuits. One dosemeter type provides an audible signal following accumulation of a specific gamma dose, and the second unit provides both visual indication of accumulated dose and preselected audible signaling as required.

A recharging-type ionization chamber [5.22] was used as a sensor in the development of signaling, miniature, gamma radiation dosemeters for personnel protection. Both platinum coated quartz fibers and solid platinum fibers of about 10μ diameter were used inside the chamber to recharge the center collector rod. Initially, the chamber is charged using an incorporated capacitor-type voltage supply. The charging fiber charges the center rod and then is repelled to an off-rod position. As the unit is exposed to gamma radiation, the charge gradually reduces until the fiber, once again, moves to recharge the rod. The resultant pulse, developed across a series resistor, is amplified to be used for signal circuit activation, binary advancement with light indication, and/or the driving of a miniature electromechanical register.

---

* A DOSEMETER is a single unit radiation sensor which monitors accumulated radiation and gives an audible or visual signal at a preselected dose, or which gives a continuous readout of accumulating dose.

Figure 5.14 shows the recharging sensor employed in the dosemeters. Battery B, shown as a battery, is in practice a Mylar foil capacitor of an extremely low leakage type, normally charged to about 250 vdc before the dosemeter is used. This capacitor acts as the chamber power supply. The center rod of the chamber can be either a quartz rod coated with conducting material, such as platinum or a graphite-water solution; or it can be a rod of conducting plastic, such as conducting Teflon. Considerable experimental work was carried out regarding the rod and the fiber material with indications apparent that a platinum fiber and a conducting Telfon center rod perform the best under constant use.

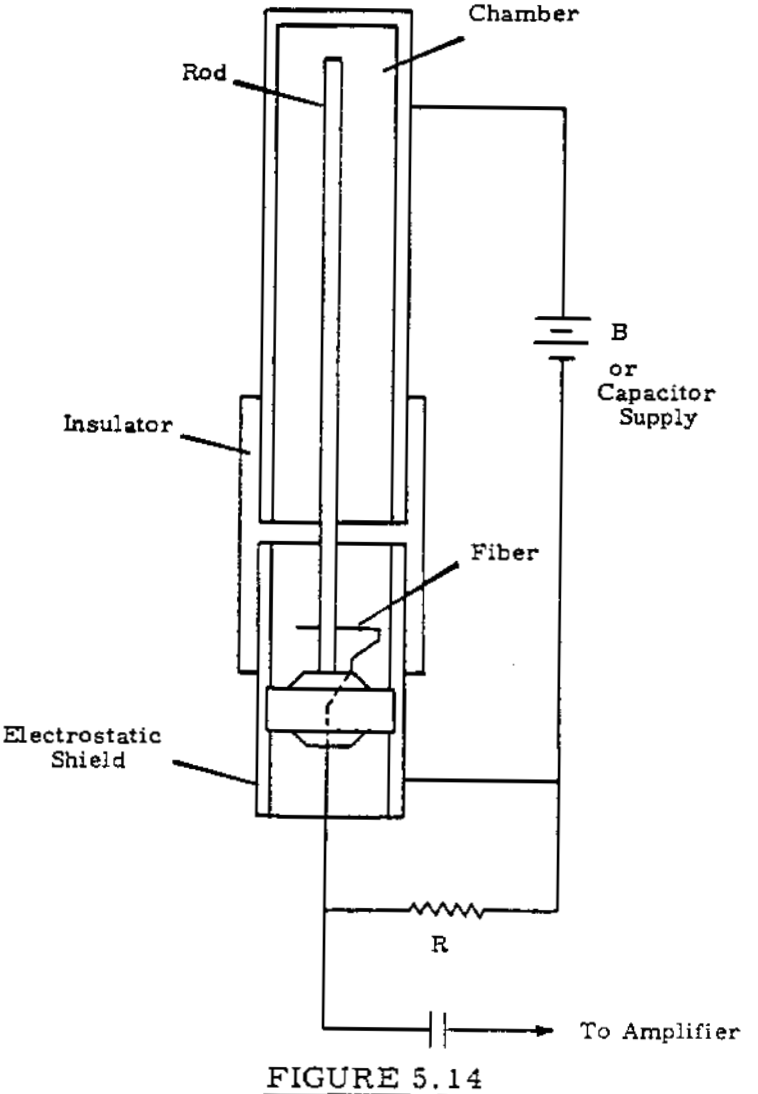

FIGURE 5.14
Recharging Ion Chamber

Figure 5.15 shows the simplified pocket dosemeter circuit which provides only an audible signal following one recharge cycle. In practice, this signal level is typically 50 mr; although, by fiber positioning and sizing, this level may be any point from 10 to 100 or more mr as desired for the particular use intended. Only a single 1.35 vdc mercury battery is necessary for circuit power. Dose accumulation signal level of 50 mr will provide repeatability within ± 5% or better.

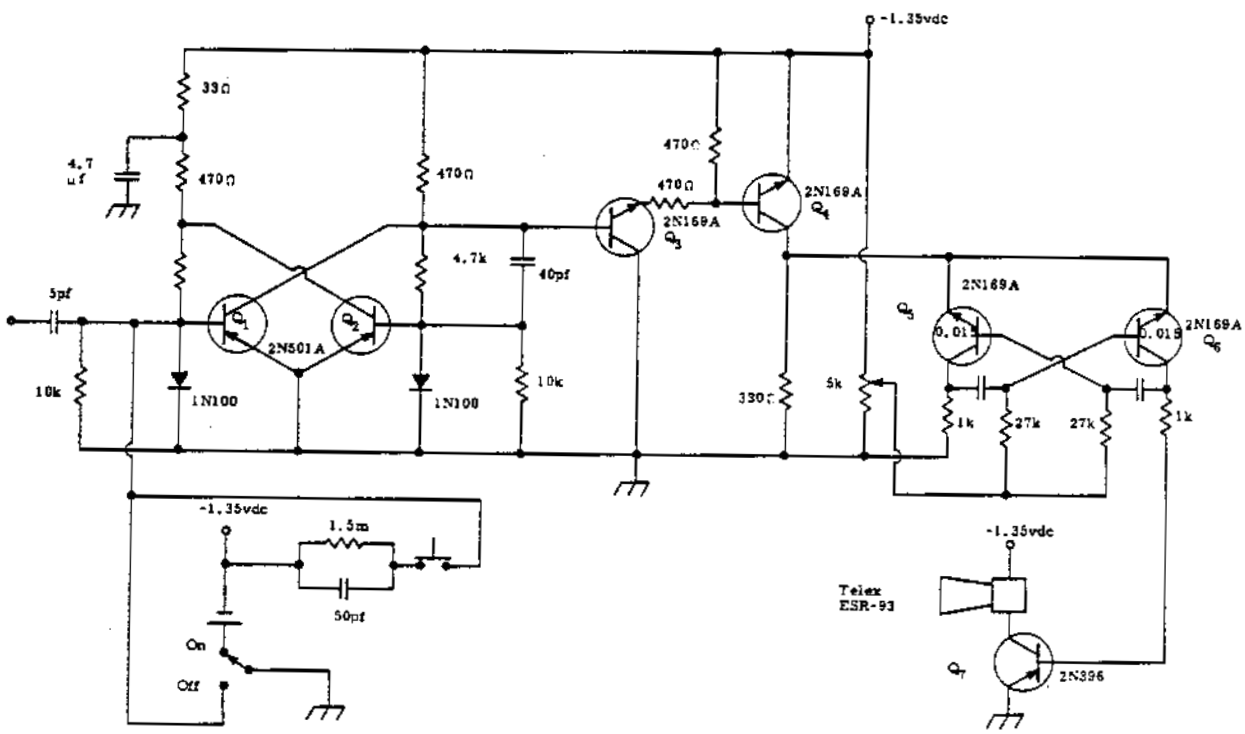

FIGURE 5.15
Circuit for Audible-Only Signaling Dosemeter

Figure 5.16 shows two circuits developed where visual indication of accumulated dose is desired. One circuit uses a miniature electromechanical register where each digit equates to a predetermined, by fiber size and placement, dose, typically 10 to 20 mr. Thus, each time the chamber is automatically recharged, the resultant pulse is amplified to advance the register one digit. The second circuit of Figure 5.16 uses subminiature binary circuits, which drive subminiature lights. In this circuit then, both a visual indication is obtained of increasing accumulated dose with, again, each digit equating to 10 or 20 mr or higher as desired. The audible signaling portion can be preselected to occur at any binary point as desired. Again, only a 1.35 vdc mercury battery is necessary for circuit power for 60 hr use.

In operation, the sensor capacitor voltage supply will operate the recharging circuit for at least 10 hr when the sensor is exposed to a dose rate of 15 r/hr; and, under tests, the sensor has been shown to be capable of correct operation at dose rates of 10 r/sec.

Figures 5.17 and 5.18 are photographs of two of the experimental prototype dosemeters which have been developed and tested. Figure 5.17 shows the single-point signal trip type which provides an audible signal; and Figure 5.18 shows the combination visual readout, using binaries, and preselected level signaling type.

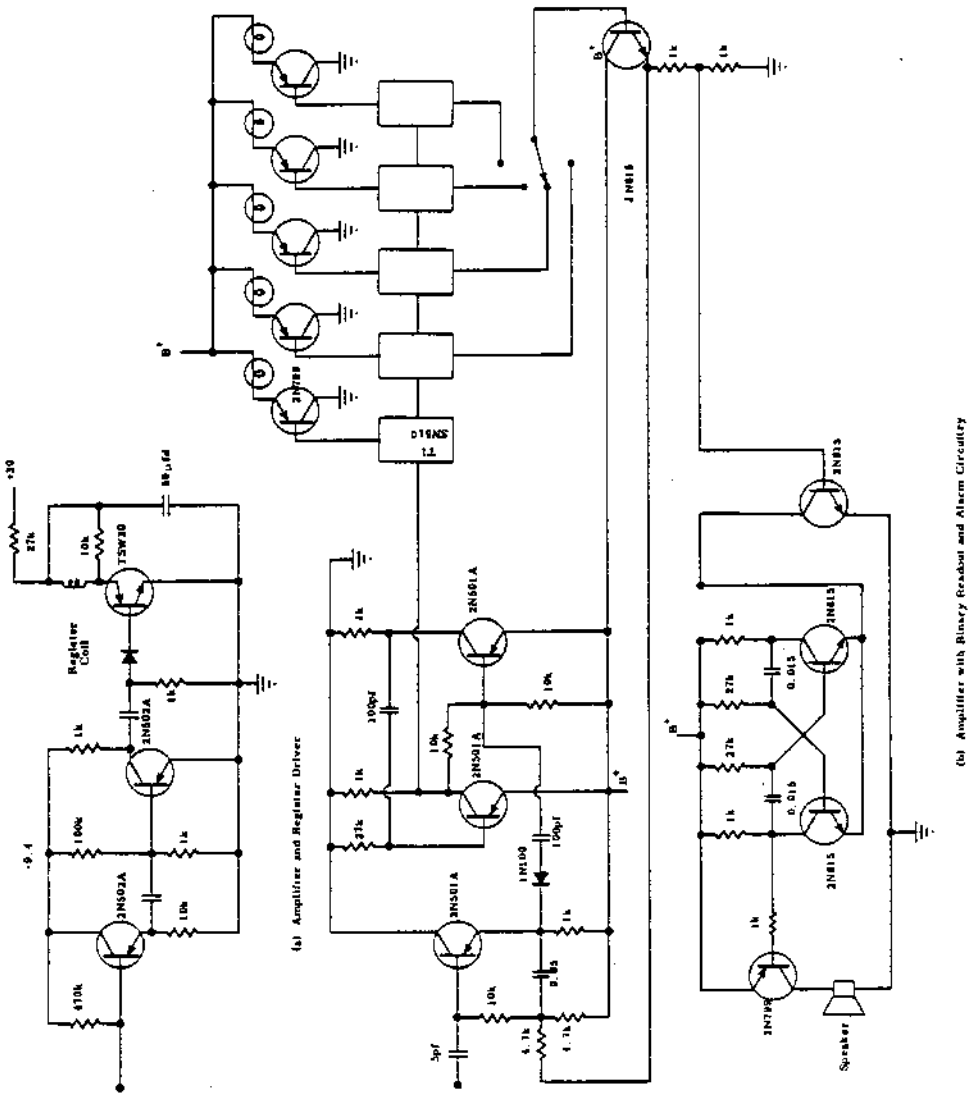

FIGURE 5.16
Circuits for Recharging-Type Dosemeters

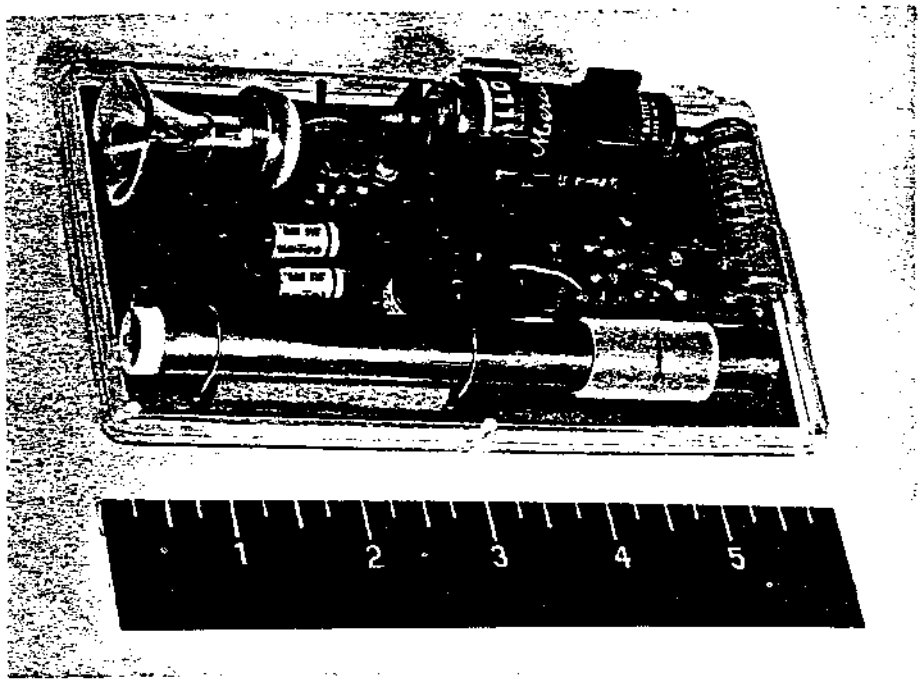

FIGURE 5.17
Signaling Radiation Dosemeter

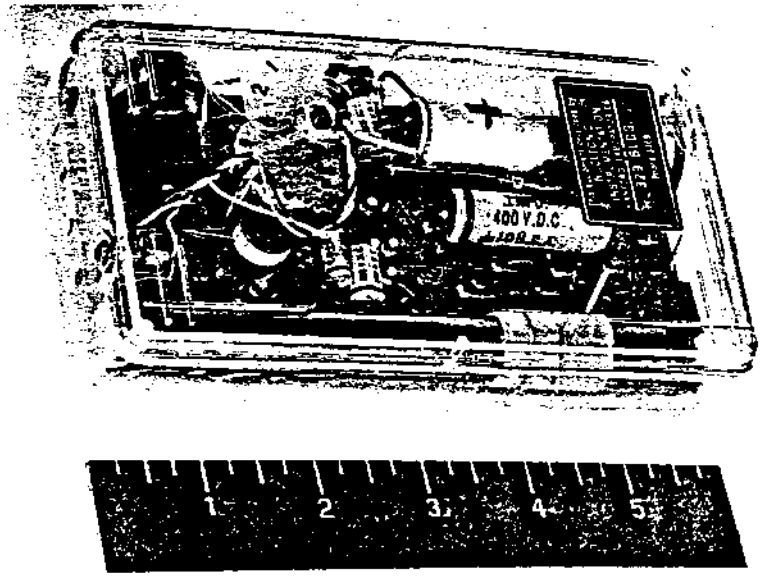

FIGURE 5.18
Indicating and Signaling Dosemeter

High Level Indicating Dosemeter - C. A. Ratcliffe and E. M. Sheen

Emergency conditions, such as criticality events, military situations, and civil defence, require the availability of simple, reliable dosemeters with a useful operational range from 5 to 100 r, perhaps higher. A dosemeter of a rugged nature was developed to meet these needs. The pocket-size instrument provides continuous visual readout of accumulated dose and selectable level audible signaling for dose levels from 5 to 100 r over a use period of 30 min or more.

A high-level dosemeter was developed for emergency use conditions as might occur during criticality. Preselected dose levels from about 5 to 100 r can be used to cause an audible signal at the particular level. In addition, a minature meter is included in the pocket-size dosemeter to provide a constant indication of the dose accumulated.

Figure 5.19 is a diagram of the dosemeter. In use, the ion chamber of 10 cc volume is charged to a particular voltage which corresponds to a known dose accumulation. This voltage is monitored on the included meter. The electrometer tube and associated solid-state circuits form a high impedance dc voltmeter. The incident gamma radiation discharges the ionization chamber and companion storage capacitor. As the point of discharge is reached which corresponds to the preset dose, the chamber-capacitor voltage will have decreased to the comparator trip circuit value. The trip circuit then operates, latching on, and activates the audible signaling device.

The capacity of the mercury batteries will permit about 100 hr of use. The leakage characteristics and electrometer tube characteristics are such that a 30 min use of the instrument equates to about 5 r. This determines the lowest level of possible operation of the instrument; however, the instrument can be recharged and re-used as desired.

Figure 5.20 is a photograph of one completed experimental phototype dosemeter.

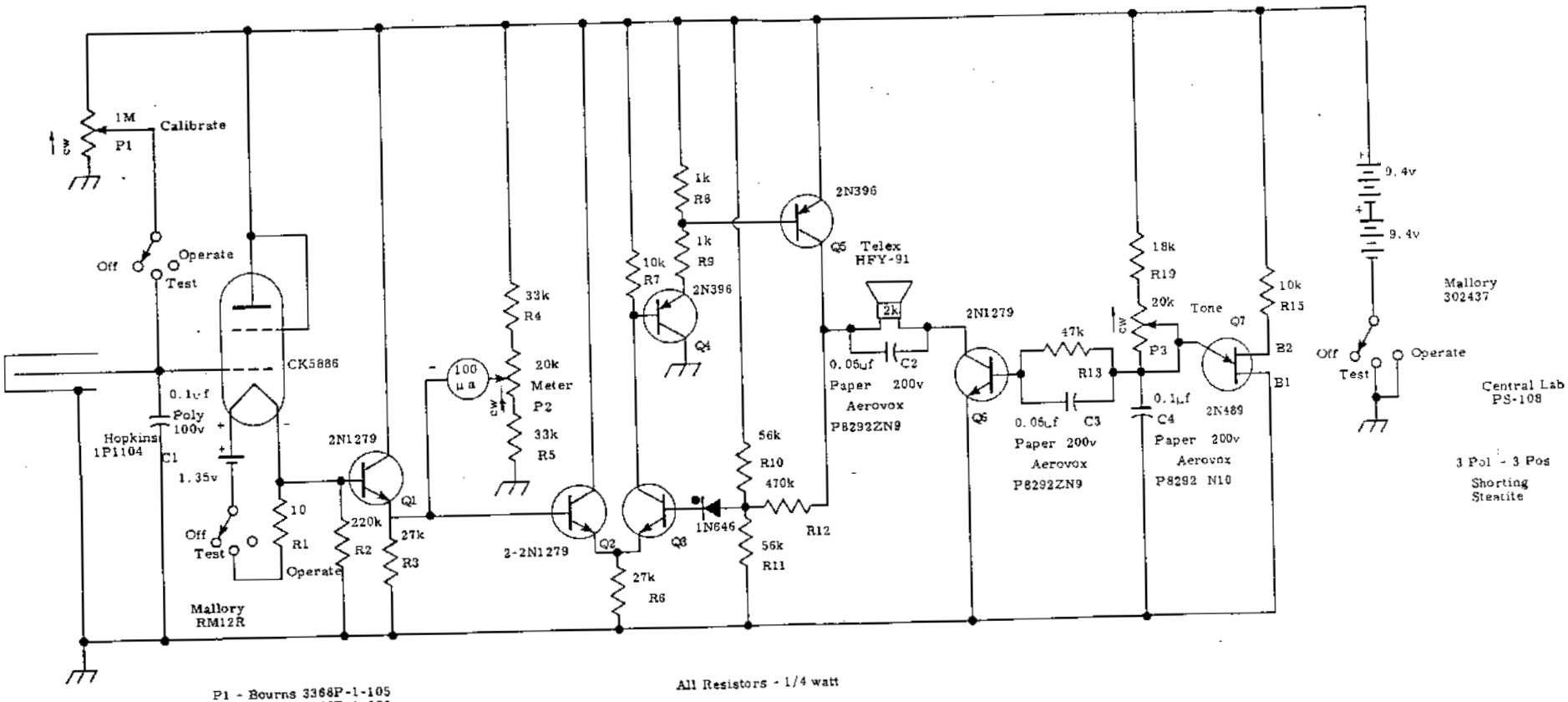

P1 - Bourns 3368P-1-105
P2 - Bourns 3368P-1-203
P3 - Bourns 3368P-1-203

All Resistors - 1/4 watt

FIGURE 5.19
High Level Dosemeter Circuit

FIGURE 5.20
High Level Indicating Dosemeter

A Technique for Measurement of Neutron Dose - G. F. Garlick

The conceived technique [5.23] measures the neutron flux at each energy and weights the obtained counts relative to their contribution to dose. This technique may be described as using a thermal energy neutron detector moderating material, for monitoring thermal-slow neutrons; using a resonance detector with moderating material for intermediate neutrons; and using a threshold fission detector for neutrons in the 0.5 to 10 Mev range. For each portion, a solid state device is used to detect the resultant charged particle. By electronically weighting the output pulses or counts from each detector, the desired dosimetry response curve may be matched to the desired degree of accuracy. Employing this technique, the ultimate device should be portable and of such a size to be worn on a belt clip. The experimental phases of the work have just commenced; the work to date has been of the theoretical-study nature.

With usual neutron dosimeters,* assumptions must be made of the neutron flux energy spectrum encountered. To obtain a true dosimeter, one can measure the neutron flux at each energy and weight the flux relative to its contribution to total dose. A theoretical study has been started regarding such a multiarray detection method.

The tissue dose from a specific energy neutron may be determined from the neutron dose curve obtainable.[5.24] In this technique, three individual solid state detectors are used in conjunction with hydrogenous moderating material to obtain neutron dose rate and dose readings.

---

* A DOSIMETER is a radiation sensor which only monitors accumulated radiation. The radiation information in a dosimeter must be extracted by an external method or instrumentation. (See footnote on page 5.28)

The three basic neutron detectors, which can comprise the experimental dosimeter-sensor, can be described as:

(1) Thermal—To detect thermal-to-slow neutrons, a solid state detector together with a Li^6 (or other thermal neutron sensitive) cover and a 1.5-in. radius hemisphere of polyethylene can be used.

(2) Intermediate—For detecting intermediate energy neutrons, a resonance detector can be used with approximately 1.5 in. polyethylene moderation. One possible detector would use a Rh^{103} foil over a lithium-diffused beta detector. To account for the 44 sec half-life of these betas, the counts may be converted to a voltage on a capacitance with a 44/0.693 sec RC time constant. The capacitor voltage could be sampled every second and the increase in voltage (above the normal decay profile) multiplied by 44/0.693. This increased voltage may be interpreted as intermediate neutrons counted and the dose contribution determined immediately at the sampling time.

(3) High Energy—For this detector it is desired to have a threshold interaction in the low Mev range with the neutron cross section remaining relatively constant from 1 to 10 Mev. Possible detecting elements are Am^{241} and Np^{237} to be used with a large-area solid state detector. The composite sensitivity of the entire device is essentially limited by this particular detector. For a direct reading dose rate device, the minimum reading would be about 100 mrem/hr. For an integrating dosemeter, the minimum resolution would be approximately 0.15 mrem.

To obtain the best match for the desired response curve the counts from each detector must be weighted and added into a count-rate-meter to provide a dose-rate measurement. Also, each detector indication may be counted with appropriate weighting factor in such a way that the neutron dose may be read directly from the counter dial.

The proposed dosimeter offers the possibility of a portable dose-rate meter or dosemeter to be carried on the person. The device should give dose rate indications of greater than 100 mrem/hr and dose indications at

levels above 0.15 mrem. The largest portion of the device will be the 1.5-in. radius hemisphere of moderating material. The additional associated counter and readout equipment can be miniaturized such that the device will be of a size to wear on a belt clip.

The studies to date have been of a theoretical nature and the experimental phases of the work have just commenced.

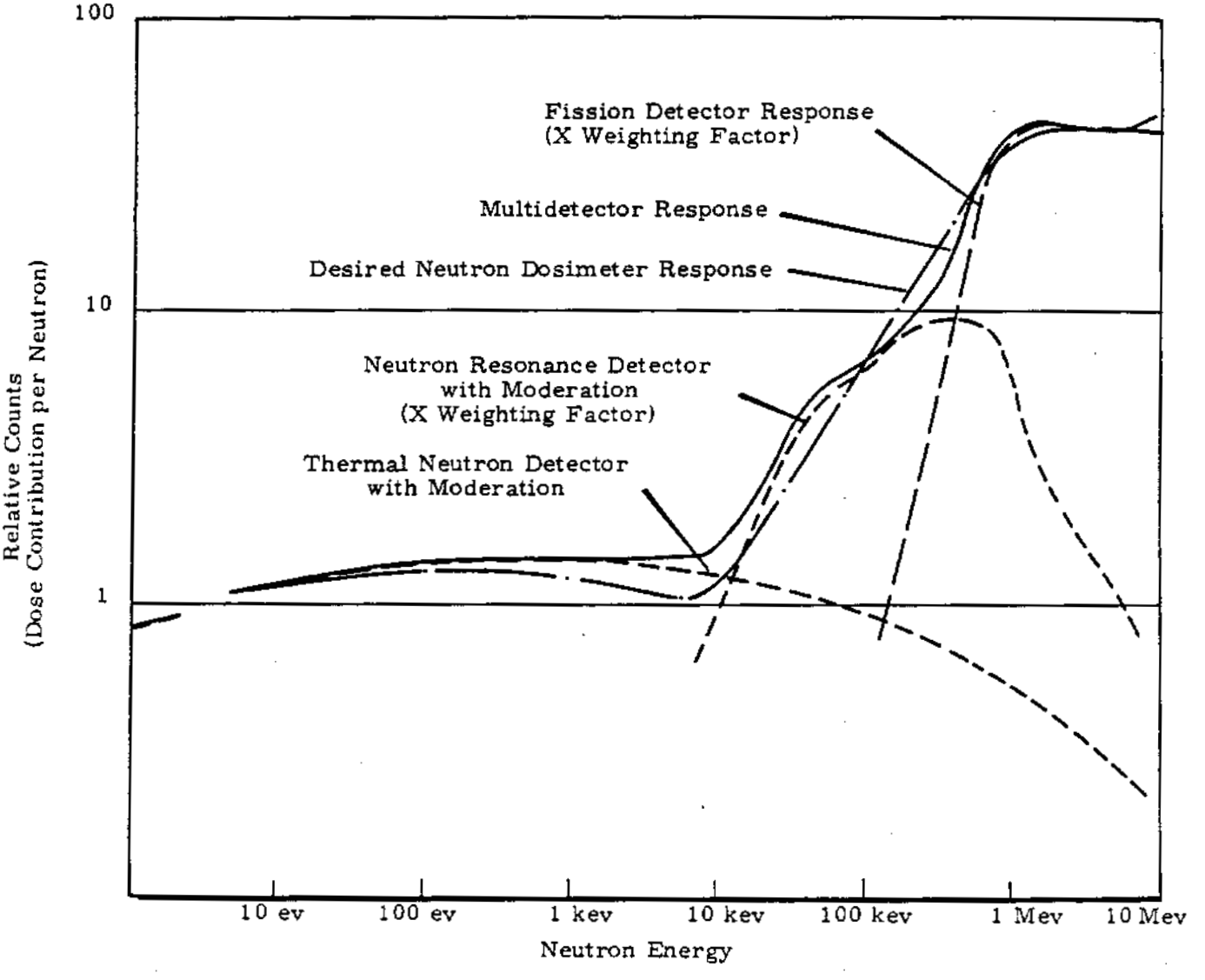

FIGURE 5.21

Relative Contribution to Dose Versus Neutron Energy

Radiation Detector Development

Alpha Monitor with Solid-State Detector[5.25] - E. M. Sheen

The developed alpha monitoring instrument uses a diffused junction silicon charged-particle detector which has a sensitive area of 2 cm^2. The detector, covered with a 0.9 mg/cm^2 protective aluminized Mylar light shield, produces 87 counts/min for a 520 dis/min Pu^{239} alpha source deposited over a 1 cm diameter area. With the detector in an 8 r/hr Ra gamma field, the externally-adjusted instrument produces approximately 70 counts/min from the same source. The background count rate is less than 1 count/min for both cases. The prototype, which weighs 12 oz, has a battery life of 30 to 40 hr, and it can employ two basic circuits for either diffused-junction or surface-barrier diode detector use.

Contaminated Air Monitoring Techniques

Alpha Energy Analysis Using CsI Detectors - D. P. Brown and M. O. Rankin

Detection of the Pu^{239} maximum permissible air concentration (MPC) of 2×10^{-12} μcuries/cm^3 is complicated by a varying background of natural alpha emitters. The air concentration of radon and thoron, in particular, varies considerably with atmospheric conditions. Since one MPC of airborne Pu^{239} is only 4.44×10^{-6} dis/min/cm^3, it is necessary to integrate the activity on a fixed filter to obtain adequate measurement sensitivity. Radon and thoron are also collected on the filter, and at times, their activity levels may accumulate to several hundred times the required detection level for Pu^{239}. Continuous monitors for airborne Pu^{239} have been developed,[5.26, 5.27] which will measure low level plutonium on the filter in the presence of radon and thoron activity. Studies are presently being conducted using a CsI detector and alpha energy analysis which should lead to a more sensitive and reliable continuous air monitor.

Radon was collected on millipore filter. The alpha spectrum of the collected radon was compared with the alpha spectrum from a plutonium source by using a CsI crystal and a multichannel analyzer. The radon C

peak was easily distinguishable but appeared in the same channel as the plutonium peak. Using these analyses as a guide, two single channel analyzer systems were set up. One analyzer was adjusted to view only the alpha peak from plutonium. Some counts due to radon appeared in this channel;therefore, the base line of the second analyzer was set just above the upper discriminator of the plutonium channel. The window width was adjusted until the counting rate due to radon in this channel was the same as the counting rate of the radon in the plutonium channel. Therefore, during routine monitoring of air, the ratio of radon in plutonium channel versus the radon in the other channel is equal to one. Plutonium deposition will change this ratio and can be used to trigger an alarm. The counting efficiency at the plutonium channel with the window was about 20% as measured with a Pu^{239} source. Initial studies indicate that a system of this type will have a sensitivity equating to about 5 MPC-hr.

Coincidence Counting for Plutonium Filter Contamination - M. O. Rankin

Many air sampling locations are used at Hanford and other sites where filters are exposed to 10 cfm flow rates for, typically, 24 hr. Following the exposure, the filters are collected for routine counting. The large number of such sampling locations precludes the establishment of continuous monitors (5.28, 5.29, 5.30, 5.31, 5.32) at each point. The present filter counting methods require a considerable waiting period to permit decay of the natural alpha emitters before the amount of plutonium can be determined. To circumvent this waiting period problem, an air filter measurement instrument, which uses coincidence counting techniques, has been developed to detect 1850 dis/min of plutonium in less than 2 min in the presence of 5000 dis/min of natural (radon and thoron) alpha activity on a standard 4-in. x 8-in. filter. The 1850 dis/min of plutonium is equivalent to the filter deposition obtained from a continuous air concentration of 2×10^{-12} $\mu c/cm^3$ existing for 25 hr with a filter flow rate of 10 cfm; thus, reliable measurement of the collected low level plutonium contamination can be made immediately following acquisition of the filter without waiting for the natural alpha emitters to decay.

The maximum permissible concentration of airborne plutonium, based on a 40-hr exposure week, is 2×10^{-12} $\mu c/cm^3$ (4.44×10^{-6} $dis/min/cm^3$ or 1.26×10^{-1} $dis/min/ft^3$) of air.[5.33, 5.34] To measure concentrations of this magnitude, it is necessary to integrate the airborne activity on a filter. During the sampling for airborne plutonium, concentrations of natural alpha emitters such as radon and thoron may increase to levels of 2×10^{-10} $\mu c/cm^3$. These two natural emitters and their daughter products have effective half-lives of 3.8 da and 10.6 hr, respectively, and are gases which are adsorbed on dust particles collected on the filter. In the maximum then, the deposited natural emitter amounts may be 100 times the deposited amounts for the maximum permissible concentrations of airborne plutonium. The decay chain of randon indicates that the total alpha activity due to radon can be deduced by measuring the rate of decay of Bi^{214} (Ra C) into Po^{214} (Ra C') and similarly, the total thoron alpha activity can be obtained from the decay rate of Bi^{212} (Th C) into Po^{212} (Th C'). These measurements can be obtained by using coincidence counting techniques since the beta emissions from both Bi^{214} and Bi^{212} are followed by alpha emissions from Po^{214} and Po^{212} in the relatively short average time intervals of 163 μ sec and 0.3 μsec, respectively. The alpha contribution from radon and thoron can then be determined through use of the relatively constant ratio of the stated coincidence events. The alpha activity from possible airborne plutonium can be determined by subtracting the measured radon thoron contribution from the measured total alpha activity on the air filter.

Figure 5.22 is a block diagram of the experimental instrumentation used to measure and record the number of coincidence events and the total alpha activity on the filters. The alpha and beta activity on a filter is detected with two 5-in. diameter scintillation detectors. After amplification, each beta pulse is shaped and is used to, in effect, open a gate for 200 μ sec. If an amplified alpha-caused pulse appears in the other channel while the gate is open, it is counted on a scaler as a coincidence event. All of the alpha-caused pulses are recorded on the alpha scaler.

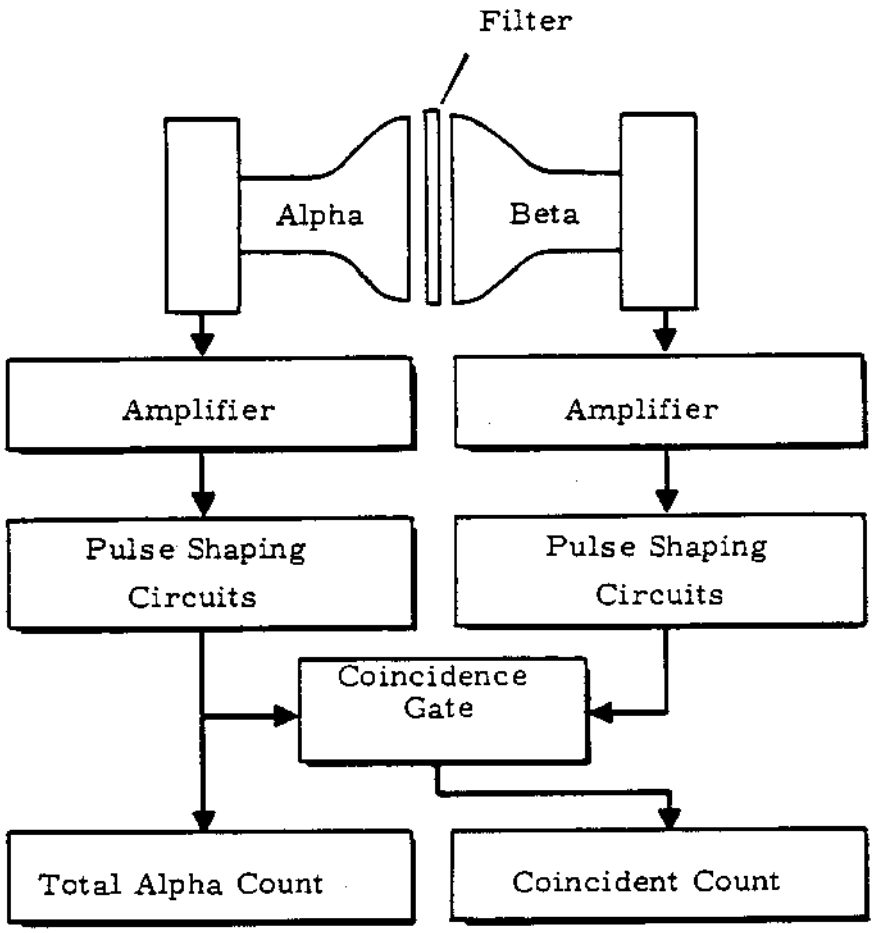

FIGURE 5.22

Plutonium Filter Contamination Counter

A control chart, Figure 5.23, relates the expected alpha, coincidence count, and the time after filter removal, and can be used to determine if there is plutonium contamination on the filter. The amount of plutonium can be estimated by subtracting the expected alpha from the total recorded alpha count. The expected alpha count is obtained by entering the graph with the recorded coincidence count and moving up to the appropriate range. By considering the elapsed time between filter removal from holder and the time of counting, only 250 counts/min or less due to plutonium contamination can pass undetected.

The complete details of the system are available in a report.[5.35] Operation of the prototype system has proven to be successful in field use at Hanford.

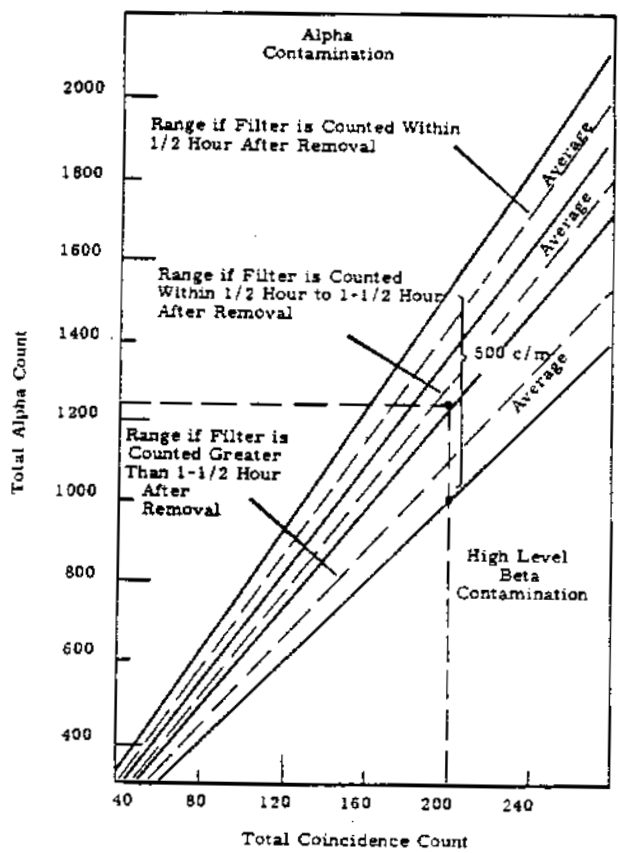

FIGURE 5.23
Total Alpha Versus Total Coincidence Count

Detection of Airborne Beryllium - W. L. Bunch and W. G. Spear

Beryllium is a highly toxic element which attacks the skin and muscous membranes of the body. An instrument is needed to determine the air concentrations of beryllium at facilities using the material. A study was made to determine if nuclear reactions could be employed to provide a unique and sensitive assay system. Both the $(\alpha, n\gamma)$ and the (γ, n) reactions can, in theory, be used to determine the amount of beryllium deposited on filter papers if appropriate radioactive sources can be obtained. Development was started on an experimental instrument that uses the alpha reaction to verify the study calculations.

The mucous membranes of the body, especially those forming the respiratory tract, are quite susceptible to attack by beryllium. Berylliosis, in either the acute or chronic form, has occurred in regions where beryllium or its salts have contaminated the air in concentrations greater than a few micrograms per cubic meter; therefore, a system is needed for determining the concentration and spatial distribution of beryllium as a function of time so adequate personnel protection measures can be taken. Pumps can be used to draw a specific volume of air through a filter paper on which the beryllium debris would be deposited. A unique and sensitive method of assaying these filters for beryllium is needed.

Beryllium undergoes two distinctive nuclear processes which provide potential methods of quantitatively analyzing filter paper deposits. One is the $Be^{9}(\alpha, n\gamma) \rightarrow C^{12}$ reaction in which both a high energy neutron and a distinctive high energy photon are emitted. By using a coincidence circuit, which requires the simultaneous detection of both the neutron and photon, the event is uniquely defined and background effects are virtually eliminated. It was calculated that a 2-curie alpha source would be required to detect microgram quantities of beryllium deposited on standard 2-in. diameter filter papers. Po^{210} is the only known high specific activity alpha emitter which could be utilized for such a source. Because of the associated radiation hazard, the source will be sealed to prevent contact with the filter paper and limit the

potential spread of contamination. Though necessary, the seal is undesirable since it degrades the energy of the alpha particles. The alpha system would also need to be enclosed in a gas-tight container for contamination control, because the source cover-seal would eventually fail under the continued alpha bombardment.

The other possible system would utilize the 1.69 Mev photons from Sb^{124} to cause the $Be^{9}(\gamma, n) \rightarrow Be^{8}$ reaction. Because of energy considerations, beryllium is the only known element which will emit neutrons when bombarded with these photons. It was calculated that an Sb^{124} source in excess of 100 curies would be required to detect fractional microgram quantities of beryllium deposited on the 2-in. diameter filter papers. Such a source would require at least 8 in. of lead shielding to permit operating personnel to remain near the system. The 60-day half-life of Sb^{124} is relatively short and detracts from the desirability of this technique.

Based on the completed theoretical study, design of an experimental $(\alpha, n\gamma)$ system was initiated to determine the sensitivity which can be achieved and to establish operating parameters and techniques which can be utilized.

REFERENCES

5.1 M. L. Barad and J. J. Fuquay. The Green Glow Diffusion Program, HW-71400 VOL1 and HW-71400 VOL2. January 1962.

5.2 M. O. Rankin. A Zinc Sulfide Particle Detector, HW-55917. May 1, 1958

5.3 J. D. Ludwick and R. W. Perkins. "Liquid Scintillation Techniques Applied to Counting Phosphorescence Emission," Anal. Chem., vol. 33, pp. 1230-1235. 1961.

5.4 S. Kinsman. Radiological Health Handbook, U. S. Department of Health, Education, and Welfare. September 1960.

5.5 Hanford Laboratories, General Electric Company. Radiation Protection Standards, HW-25457 REV. March 1960.

5.6 W. G. Spear. A Scintillation Transistorized Alpha-Beta-Gamma Hand and Shoe Counter, HW-60631. July 1959.

5.7 M. O. Rankin. Monitor for Mixed Fission Product Contamination on Face Masks, HW-67293. November 8, 1960.

5.8 W. G. Spear. Transistorized Line-Operated Radiation Detection-Instrumentation, HW-65553. January 1961.

5.9 E. M. Sheen. A Cable-Driving Pulse Preamplifier, HWIR-1481. 1962. (HW-73242)

5.10 D. P. Brown. A Logarithmic, Transistorized Count Rate Meter, HW-66899. October 14, 1960.

5.11 W. G. Spear. A Single Transistor High Voltage Supply, HW-38682. January 1, 1956.

5.12 W. G. Spear. Portable Radiation Instrumentation Standardization, HW-60404. September 1, 1959.

REFERENCES (Contd.)

5.13 J. J. Davidson. "Transistor AC Amplifier with High Input Impedance," Semiconductor Products, vol. 3, pp. 42-50. March, 1960.

5.14 D. D. Middlebrook and C. A. Mead. "Transistor AC and DC Amplifiers with High Input Impedance," Semiconductor Products, vol. 2, pp. 26-35 March 1959.

5.15 E. M. Sheen. Triggered Aural Tone Generators for Radiation Monitoring Instrumentation, HW-71359. November 1961.

5.16 R. A. R. Kent. Scintillation Alpha Detection Probes, HW-66837. September 12, 1960.

5.17 W. G. Spear. A Portable Scintillation-Type Alpha Survey Instrument, HW-30713. February 1, 1954.

5.18 W. G. Spear. A Single Transistor High Voltage Supply, HW-38682. January 1, 1956. (op. cit.)

5.19 W. G. Spear. Portable Radiation Instrumentation Standardization, HW-60404. September 1, 1959.

5.20 J. J. Davidson. "Transistor AC Amplifier with High Input Impedance," Semiconductor Products, vol. 3, pp. 42-50. March 1960. (op. cit.)

5.21 D. D. Middlebrook and C. A. Mead. "Transistor AC and DC Amplifiers with High Input Impedance," Semiconductor Products, vol. 2, pp. 26-35. March 1959. (op. cit.)

5.22 D. P. Brown and M. O. Rankin. Experimental Personnel Radiation Dosimeters, HW-SA-2590 A. August 1962. (See also Health Physics, vol. 8, p. 472.)

5.23 G. F. Garlick. A Technique for Measurement of Neutron Dose, HWIR-1611. November 1962.

5.24 National Bureau of Standards, Handbook 63, Protection Against Neutron Radiation Up to 30 Million Electron Volts, U. S. Department of Commerce, Washington, D. C. November 1957.

REFERENCES (Contd.)

5.25 E. M. Sheen. "Alpha Monitor with Solid-State Detector," Nuclear Instruments and Methods, vol. 17, pp. 140-144. October 1962. Voorburgwal, Amsterdam: North-Holland Publishing Company.

5.26 D. P. Brown, M. O. Rankin, C. D. Boyne, and W. G. Spear. A Coincidence Count Alpha Particulate Air Monitor, HW-75384. January 3, 1963.

5.27 M. O. Rankin. "Medium-Level Continuous Alpha -Air Monitor," Health Physics, vol. 4, pp. 293-298. May 1961.

5.28 D. P. Brown, M. O. Rankin, W. G. Spear, and C. D. Boyne. A Coincidence-Count Alpha-Particulate Air Monitor, HW-SA-2554. June 1962. (See also Health Physics, vol. 8, page 453. August 1962)

5.29 D. P. Brown, M. O. Rankin, C. D. Boyne, and W. G. Spear. A Coincidence-Count Alpha Particulate Air Monitor, HW-75384. January 3, 1963. (op. cit)

5.30 M. O. Rankin. "Medium-Level Continuous Alpha-Air Monitor," Health Physics, vol. 4, pp. 293-298. 1961. (op. cit)

5.31 G. Hinder and P. Iredale. The Detection of Airborne Plutonium Hazards, AERE-R-3783. January 1962.

5.32 C. L. Lindeken and W. A. Phillips. Plutonium Alpha Air Monitor Using a Solid State Detector, UCRL-6692. April 16, 1962.

5.33 Hanford Laboratories, General Electric Company. Radiation Protection Standards, HW-25457 REV. March 1960. (op. cit.)

5.34 National Bureau of Standards, Handbook 69, Maximum Permissible Body Burdens and Maximum Permissible Concentrations of Radionuclides in Air and in Water for Occupational Exposure, U. S. Department of Commerce, Washington, D. C. June 5, 1959.

5.35 M. O. Rankin. The Use of Coincidence Counting Techniques for Analyzing Low Level Plutonium Contamination on Filters, HW-75092. November 15, 1962.

INTERNAL DISTRIBUTION

Copy Number	
1	F. W. Albaugh
2	W. J. Bair
3	C. A. Bennett
4	O. E. Boston
5	L. K. Bustad
6	I. H. Dearnley
7	R. F. Foster
8	P. A. Fuqua
9	J. J. Fuquay
10	C. C. Gamertsfelder
11	P. F. Gast
12	J. K. Green
13	W. A. Haney
14	F. P. Hungate
15	E. R. Irish
16	W. E. Johnson
17	R. L. Junkins
18	A. R. Keene
19	H. A. Kornberg
20	M. Lewis
21	C. E. Linderoth
22	R. E. Nakatani
23 - 27	J. M. Nielsen
28	W. D. Norwood
29	R. F. Palmer
30	H. M. Parker
31	R. S. Paul
32	W. H. Reas
33	W. C. Roesch
34	L. C. Schwendiman
35	R. K. Sharp
36 - 37	W. G. Spear
38	A. J. Stevens
39	F. Swanberg
40	R. C. Thompson
41	M. T. Walling
42	W. K. Woods
43	D. C. Worlton
44 - 45	Biology Library
46	300 File
47	Record Center
48	Technical Publications
49 - 300	Extra

EXTERNAL DISTRIBUTION (SPECIAL)

Copy Number	
301	Advanced Technology Laboratories General Electric Company 1 River Road, Schenectady 5, N. Y. Attn: J. W. Healy - Consultant Technological Hazards
302 - 309	Atomic Energy Commission, Washington Division of Biology and Medicine Attn: N. F. Barr J. N. Wolfe S. A. Lough J. Z. Holland J. R. Totter W. D. Claus H. Hollister H. D. Bruner
310 - 311	duPont Company, Aiken Attn: W. B. Scott
312	duPont Company, Wilmington Attn: V. R. Thayer
313 - 314	G. E. Technical Data Center, Schenectady
315 - 316	Richland Operations Office Attn: K. L. Englund
317	Richland Operations Office Technical Information Library
318	Savannah River Operations Office Attn: K. K. Brown
319	U. S. Public Health Service Division of Health Mobilization Washington 25, D. C. Attn: J. J. Lang Acting Chief, Research Branch

Ptd.	Standard Distribution
4	ABERDEEN PROVING GROUND
1	AEROJET-GENERAL CORPORATION
	AEROJET-GENERAL NUCLEONICS
5	AERONAUTICAL SYSTEMS DIVISION
	AIR FORCE CAMBRIDGE RESEARCH LABORATORIES
1	AIR FORCE INSTITUTE OF TECHNOLOGY
2	AIR FORCE SPECIAL WEAPONS CENTER INSTITUTE
5	ARGONNE CANCER RESEARCH HOSPITAL
10	ARGONNE NATIONAL LABORATORY
1	ARMED FORCES INSTITUTE OF PATHOLOGY
1	ARMED FORCES RADIOBIOLOGY RESEARCH
4	ARMY CHEMICAL CENTER
1	ARMY CHEMICAL CENTER (TARAS)
1	ARMY CHEMICAL CORPS
1	ARMY ENVIRONMENTAL HYGIENE AGENCY
1	ARMY MEDICAL RESEARCH LABORATORY
1	ARMY SIGNAL RESEARCH AND DEVELOPMENT LABORATORY
2	ATOMIC BOMB CASUALTY COMMISSION
1	AEC SCIENTIFIC REPRESENTATIVE, FRANCE
1	AEC SCIENTIFIC REPRESENTATIVE, JAPAN
3	ATOMIC ENERGY COMMISSION, WASHINGTON
4	ATOMIC ENERGY OF CANADA LIMITED
3	ATOMICS INTERNATIONAL
2	BATTELLE MEMORIAL INSTITUTE
1	BIOSEARCH COMPANY
1	BORDEN CHEMICAL COMPANY
2	BROOKE ARMY MEDICAL CENTER
4	BROOKHAVEN NATIONAL LABORATORY
1	BUREAU OF MEDICINE AND SURGERY
1	BUREAU OF SHIPS (CODE 1500)
1	BUREAU OF YARDS AND DOCKS
1	CHICAGO PATENT GROUP
1	COLORADO STATE UNIVERSITY
1	COLUMBIA UNIVERSITY (ROSSI)
1	COMMITTEE ON THE EFFECTS OF ATOMIC RADIATION
3	DEFENCE RESEARCH MEMBER
1	DEFENSE ATOMIC SUPPORT AGENCY, WASHINGTON
2	DU PONT COMPANY, AIKEN
1	DU PONT COMPANY, WILMINGTON
1	EDGERTON, GERMESHAUSEN AND GRIER, INC., GOLETA
1	EDGERTON, GERMESHAUSEN AND GRIER, INC., LAS VEGAS
1	FRANKFORD ARSENAL
2	GENERAL DYNAMICS/FORT WORTH
2	GENERAL ELECTRIC COMPANY, CINCINNATI
1	GENERAL ELECTRIC COMPANY, PLEASANTON
	GOODYEAR ATOMIC CORPORATION
1	*HAZLETON NUCLEAR SCIENCE CORPORATION
1	HUGHES AIRCRAFT COMPANY
1	IOWA STATE UNIVERSITY
1	JOURNAL OF NUCLEAR MEDICINE
1	KNOLLS ATOMIC POWER LABORATORY
2	LOS ALAMOS SCIENTIFIC LABORATORY
1	LOVELACE FOUNDATION
1	MARTIN-MARIETTA CORPORATION
1	MASSACHUSETTS INSTITUTE OF TECHNOLOGY
1	MOUND LABORATORY
1	NATIONAL ACADEMY OF SCIENCES
2	NASA SCIENTIFIC AND TECHNICAL INFORMATION FACILITY
1	NATIONAL BUREAU OF STANDARDS
1	NATIONAL CANCER INSTITUTE
	NATIONAL INSTITUTES OF HEALTH
1	NATIONAL LEAD COMPANY OF OHIO
1	NATIONAL LIBRARY OF MEDICINE
1	NAVAL HOSPITAL
1	NAVAL MEDICAL RESEARCH INSTITUTE

Ptd.	Standard Distribution
1	NAVAL ORDNANCE LABORATORY
1	NAVAL POSTGRADUATE SCHOOL
2	NAVAL RADIOLOGICAL DEFENSE LABORATORY
1	NEW JERSEY STATE DEPARTMENT OF HEALTH
1	NEW YORK OPERATIONS OFFICE
1	NEW YORK UNIVERSITY (EISENBUD)
1	OFFICE OF ASSISTANT GENERAL COUNSEL FOR PATENTS (AEC)
10	OFFICE OF NAVAL RESEARCH
1	OFFICE OF NAVAL RESEARCH (CODE 422)
1	OFFICE OF THE CHIEF OF RESEARCH AND DEVELOPMENT
1	OFFICE OF THE SURGEON GENERAL
2	PHILLIPS PETROLEUM COMPANY (NRTS)
4	PRATT AND WHITNEY AIRCRAFT DIVISION
2	PUBLIC HEALTH SERVICE
	PUBLIC HEALTH SERVICE, CINCINNATI
1	PUBLIC HEALTH SERVICE, LAS VEGAS
	PUBLIC HEALTH SERVICE (LEE)
1	PUBLIC HEALTH SERVICE, MONTGOMERY
	PUBLIC HEALTH SERVICE, SAVANNAH
1	QUARTERMASTER RESEARCH AND ENGINEERING COMMAND
1	RAND CORPORATION
1	RESEARCH ANALYSIS CORPORATION
1	REYNOLDS ELECTRICAL AND ENGINEERING COMPANY, INC.
1	SANDIA CORPORATION, ALBUQUERQUE
2	SCHOOL OF AVIATION MEDICINE
1	SECOND AIR FORCE (SAC)
1	SOLON (LEONARD)
1	STRATEGIC AIR COMMAND
1	STRATEGIC AIR COMMAND (OS)
1	SURGEON GENERAL
1	UNION CARBIDE NUCLEAR COMPANY (ORGDP)
5	UNION CARBIDE NUCLEAR COMPANY (ORNL)
1	UNION CARBIDE NUCLEAR COMPANY (PADUCAH PLANT)
1	UNITED NUCLEAR CORPORATION (NDA)
1	U. S. GEOLOGICAL SURVEY, DENVER
1	U. S. GEOLOGICAL SURVEY, MENLO PARK
1	U. S. GEOLOGICAL SURVEY, NAVAL WEAPONS PLANT
1	U. S. GEOLOGICAL SURVEY, WASHINGTON
1	U. S. WEATHER BUREAU, WASHINGTON
3	UNIVERSITY OF CALIFORNIA, BERKELEY
1	UNIVERSITY OF CALIFORNIA, DAVIS
2	UNIVERSITY OF CALIFORNIA, LIVERMORE
1	UNIVERSITY OF CALIFORNIA, LOS ANGELES
1	UNIVERSITY OF CALIFORNIA, SAN FRANCISCO
1	UNIVERSITY OF CHICAGO, USAF RADIATION LABORATORY
1	UNIVERSITY OF HAWAII
1	UNIVERSITY OF PUERTO RICO
1	UNIVERSITY OF ROCHESTER
1	UNIVERSITY OF TENNESSEE
1	UNIVERSITY OF UTAH
1	UNIVERSITY OF WASHINGTON
1	WALTER REED ARMY MEDICAL CENTER
1	WAYNE STATE UNIVERSITY
4	WESTERN RESERVE UNIVERSITY
1	WESTINGHOUSE ELECTRIC CORPORATION
1	WESTINGHOUSE ELECTRIC CORPORATION (NASA)
325	DIVISION OF TECHNICAL INFORMATION EXTENSION
75†	OFFICE OF TECHNICAL SERVICES, WASHINGTON

*New listing or change in old listing.

†These copies should be shipped directly to the Office of Technical Services, Department of Commerce, Washington 25, D. C.